# APPLICATION OF AN ANALYTICAL SCALING METHOD TO BUILD TYPE WELLS FOR HORIZONTAL WELLS IN RESOURCE PLAYS

A Thesis

by

ROMAIN OLIVIER PHILIPPE MICHEL LEMOINE

Submitted to the Office of Graduate and Professional Studies of
Texas A&M University
in partial fulfillment of the requirements for the degree of

MASTER OF SCIENCE

| | |
|---|---|
| Chair of Committee, | W. John Lee |
| Committee Members, | Thomas A. Blasingame |
| | Marcelo Laprea-Bigott |
| Head of Department, | Jeff Spath |

December 2018

Major Subject: Petroleum Engineering

## ABSTRACT

The purpose of type wells is to portray the range of production profiles of a predetermined geological subset in a resource play. Most type well construction workflows rely on the creation of "average" profiles by simply averaging production for all wells in a given geological area, often a subset of a larger resource play. The production profile of empirical averaging cannot be directly associated with a set of reservoir and completion parameters. Relating to "Fetkovich's Field Type Curve" methodology published in 1987, we show that we can create more representative type wells if we average the wells that are scaled to a common "base well" with known completion and reservoir parameters. Scaling factors are determined by a fit of production data to an analytical solution developed for horizontal wells exhibiting transient linear flow followed by boundary-dominated flow. The scaling factors are influenced largely by matrix permeability, fracture length, fracture spacing, drawdown and lateral length. We use the distribution of permeability and fracture half-length found in the type curve diagnostic to forecast undrilled wells and wells with only short production histories.

Since the fit of production data depends on the geometrical shape of the type curve, we successfully demonstrate that the type curve applies to horizontal multi-fractured wells in known resource plays. We propose an original and integrated workflow based on our scaling methodology that includes the industry's current best practices to create type wells and characterize a geologically similar area with publically available data. Using this approach to scale production can dramatically increase the number of analogs and we demonstrate the application of the workflow with 126 wells from the Denton County in the Barnett shale. We observe that the scaling factors reduce the uncertainty of a typical well production for a given set of completion parameters, and provide a reliable tool to probabilistically forecast production. Furthermore, scaling time of underperforming wells in a group improves the durations of "known production" forecast. In conclusion, this analytically-based workflow provides reliable production forecasts and type wells with measured uncertainty. Because type wells are important tools for decision makers and engineers to determine economic feasibility of proposed development projects, more accurate type well construction has financial and strategic implications in the range of millions to billions of dollars.

# DEDICATION

This work is dedicated to my family and friends, for their support and without whom I wouldn't have had the motivation to carry this project until the end;

I also want to dedicate this work to the Unconventional Industry; may this workflow provide a reliable set of tools that improve reserve evaluation processes and contribute to a sustainable development of hydrocarbon resources;

Finally, I would also like to dedicate this work to the double degree program between Texas A&M and the IFP school in France, for the unique opportunity it gives to develop skills required to pursue a career in this industry

*"Geology is a science of observations that occur at multiple scales from planetary to microscopic, from different perspectives, and within varying context. Achieving an integrated, insightful interpretation/answer to a geologic problem requires thinking at different scales, seeing things from different perspectives, and understanding context. You should force yourself to do these three things when tackling a (…) reservoir problem."*

**J. Markhello**

*A + B, et voilà!*

**L. F. Albatar**

ACKNOWLEDGEMENTS

I would like to specifically thank the following for their contribution to this work:

Dr. W John Lee, chair of my advisory committee and mentor, for his unlimited guidance, precious support, his trust and for sharing his knowledge and experience;

Dr. Thomas A. Blasingame, member of my advisory committee, for his availability and his instrumental advice to help me complete this work;

Dr. Marcelo Laprea-Bigott, member of my advisory committee, for his unrestricted support and feedback in the preparation and of this work;

Randy Freeborn, Mark McLane and David Fulford, for sharing their experience and helping me understand the challenges in building type wells in resource plays;

# CONTRIBUTORS AND FUNDING SOURCES

## Contributors

This work was supported by a thesis committee consisting of Dr W. John Lee and Dr. Marcelo Laprea-Bigott of the Department of Petroleum Engineering and Dr. Thomas Blasingame of the Departments of Petroleum Engineering and Geology and Geophysics.

The data analyzed for Chapters IV to VI and Appendix J was provided by DrillingInfo© and the data analyzed in Appendix K was provided by Noble Energy.

All other work conducted for the thesis was completed by the student independently.

## Funding Sources

There are no outside funding contributions to acknowledge related to the research and compilation of this document

NOMENCLATURE

**Acronyms**

| | |
|---|---|
| BDF | Boundary dominated flow |
| BHP | Bottom-hole pressure |
| EUR | Estimated ultimate recovery |
| GSA | Geologic subset area |
| MFHW | Multi-fractured horizontal well |
| IP | Initial production |
| MBT | Material balance time |
| NPT | Non-productive time |
| NPV | Net present value |
| SRV | Stimulated reservoir volume |

**Field Variables**

| | |
|---|---|
| $c_t$ | Total compressibility, $psi^{-1}$ |
| DD | Drawdown, psi |
| $D_i$ | Arps' initial decline rate, $days^{-1}$ or $month^{-1}$ |
| $F_S$ | Fracture spacing, ft |
| $h$ | Net pay thickness, or reservoir height (Fig. 6), ft |
| $k$ | Reservoir permeability, md |
| $k_f$ | Fracture permeability, md |
| $L_w$ | Perforated lateral length, ft |
| $m(p)$ | Real gas pseudo-pressure, $psi^2/cp$ |
| $m_{sl}$ | Slope on reciprocal rate vs. square root of pseudo-time plot, $psi^2 day^{1/2}/cp/Mscf$ |
| $N_p$ | Cumulative production, MMscf |
| $N$ | Number of Wells |
| $n_f$ | Number of fractures or hydraulic stages |
| $p_i$ | Initial Reservoir Pressure, Psia |
| $p_{wf}$ | Bottom-hole pressure, Psia |

| | |
|---|---|
| $q_i$ | Arps' initial rate constant, Mscf/D or MMscf/month |
| $q_g$ | Single fracture gas flowrate, Mscf/D or MMscf/month |
| $q_t$ | Total gas flowrate, md |
| $t$ | Producing Time, days or months |
| $t_{elf}$ | Time at the end of linear flow, days or months |
| $\overline{t_{elf}}$ | Average time at the end of linear flow, days or months |
| $t_{MB}$ | MBT, days or months |
| $T$ | Reservoir temperature, $^{o}$R |
| $w$ | Fracture width, ft |
| $x_e$ | Reservoir half-length (Fig. 6), ft |
| $x_f$ | Fracture half-length in modified type curve, ft |
| $y_e$ | Reservoir half-width (Fig. 6), ft |
| $z$ | Gas deviation factor, dimensionless |

**Dimensionless variables**

| | |
|---|---|
| CSF | Dimensionless cumulative scaling factor |
| $F_{CD}$ | Dimensionless fracture conductivity |
| $q_D$ | Dimensionless rate |
| QM | Dimensionless rate match point |
| RSF | Dimensionless rate scaling factor |
| $t_{Dye}$ | Dimensionless time based on $y_e$ |
| $t_{DF_S}$ | Dimensionless time based on $F_S$ |
| TM | Dimensionless time match point |
| TSF | Dimensionless time scaling factor |

**Greek symbols**

| | |
|---|---|
| Δm(p) | Real gas pseudo-pressure drawdown, psi$^2$/cp |
| ε | Cumulative correction constant |
| μ | Viscosity, cp |
| φ | Porosity, fraction |

TABLE OF CONTENTS

LIST OF FIGURES

Page

LIST OF TABLES

Page

CHAPTER I

INTRODUCTION

## 1.1 Introduction

In the past 30 years, the price of petroleum commodities, tax incentives and technology have contributed to the development of extremely low permeability shale reservoir in North America. An historical landmark of this development was set in early 2000 by Mitchell Energy after commercially producing gas in the Barnett shales via hydraulically fractured horizontal wells (Bowker 2007). As of December 2017, shale gas production including the Marcellus, Bakken, Haynesville, and Eagle Ford accounts for more than 62% of the total production of natural gas in the US, as per the EIA (2018). **Fig. 1** illustrates the location of all the shale gas play in the United States.

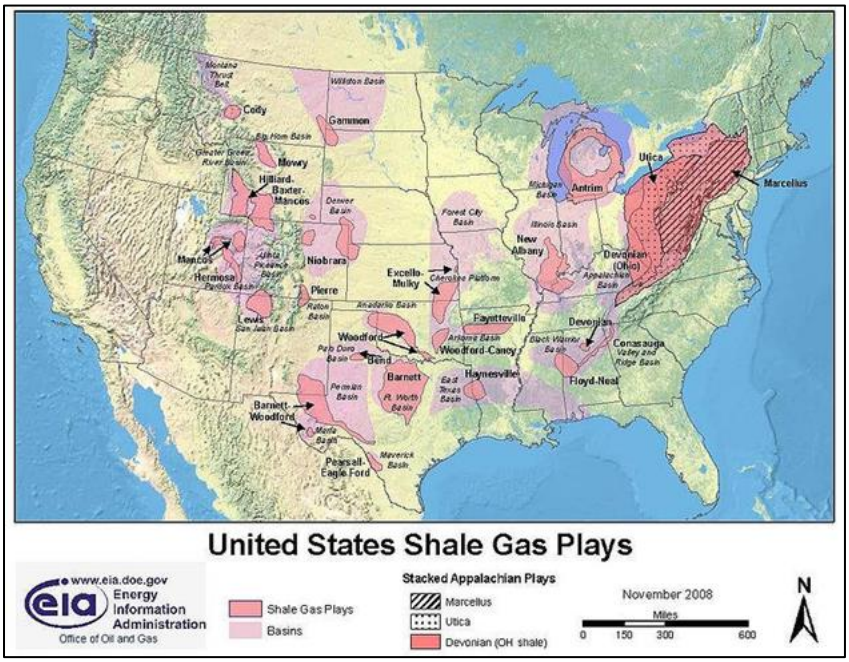


**Fig. 1—United States Shale Gas Plays reprinted from EIA, 2018.**

Production from unconventional shale gas reservoirs exhibit repeatable depletion patterns known as the "hockey stick" characterized by high initial rates with large decline rates at early time followed by significantly lower production rates over time. Shale gas resources are considered unconventional because they are continuous and heterogeneous accumulations spread over a large geographical area. Unconventional petroleum accumulations are independent of any trapping mechanism due to the ultra-low permeability (<0.1md) of the rock body which limits hydrodynamic processes and petroleum migration. The hydrocarbons are stored both in the matrix, the natural fractures and adsorpted in the organic matter (Hartman et al. 2011). Shale resources are commercially produced by drilling extended-reach horizontal wells. The laterals are stimulated with several hydraulic fracture stages that creates a preferential pathway between the matrix and the wellbore. The combination of large hydraulic fracture networks with the formation's heterogeneities results in uncertain fracture geometries and hydraulic properties. This uncertainty has limited the industry in its efforts to reliably match production and decline behavior of a shale gas well with analytical models or reservoir simulation. As a result, reserves estimates (EUR) and production forecasts of continuous accumulations have considerable uncertainty and usually rely on empirical or semi-empirical decline curve fitting methods such as those presented by Arps (1945), Ilk et al. (2008), Valko and Lee (2010), or Duong (2010). Curve fitting methods assume that a good fit of historical data to a decline equation will lead to a good forecast of future behavior. More sophisticated methods such as rate transient analysis allows us to characterize reservoirs and thus to forecast production without shutting in wells as in conventional pressure transient analysis. However, production data are usually of poor quality, and the lack of information about well downtime and bottom-hole pressure (BHP) limits the reliability of rate transient analysis.

To overcome the geologic uncertainty of the parameters governing the flow from shale reservoirs, the industry uses probabilistic methods to study the statistical behavior of key metrics such as EUR, initial production rates, peak rates or initial decline factors. SPEE Monograph 3 (2011) suggests that shale reservoirs can be characterized as resources plays if they exhibit a repeatable statistical distribution, usually lognormal. It also implies that offset well performance may not be a reliable predictor of performance of undeveloped locations. A common industry practice is to generate type wells (short for typical well production profiles) to portray the statistical range of production profiles of a given geological subset in a resource play. Most type well

construction workflows rely on the creation of "average" profiles by simply averaging production for all wells in the geographical area of interest.

## 1.2 Basic Concepts

### *1.2.1 Type Curve*

Since the development of resources plays, the terms "type wells" and "type curves" have been used to describe the typical well production profiles of a geologic area. Historically, the term "type curve" has long been used for a plot of dimensionless variables which displays the solution of an analytical model. Production decline type curves were developed by Fetkovich (1980) as a composite of an analytical solution of the flow in transient period with an empirical relationship for the later depletion stage. **Fig. 2** illustrates the two flow regions separated by an inflection point.

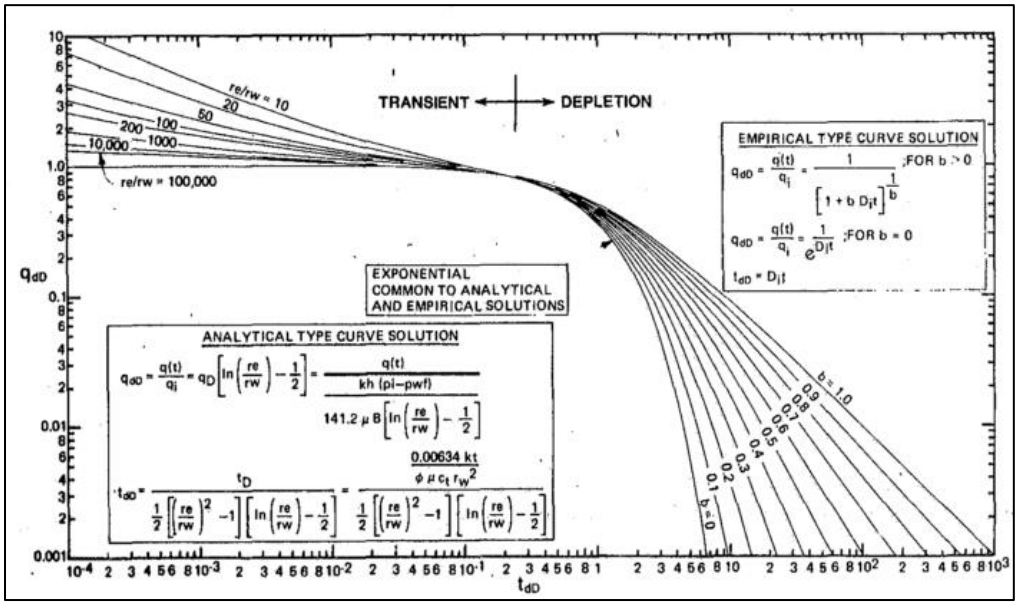


**Fig. 2—Composite type curve solution between an analytical model and empirical type curves, reprinted from Fetkovich, 1980.**

The overlay of the production data on the type curve allows us to estimate permeability, drainage area, and skin factor. Since 1980, many dimensionless production decline type curves

have been published as diagnostic tools for various reservoir types, geometries and flow characteristics. **Table 1** summarizes the major type curves available in the industry to perform production analysis.

| Author(s) (Year published) | Type curve |
|---|---|
| Fetkovich (1980) | Type Curve Approach for Decline Curve Analysis |
| Fetkovich et al. (1987) | Application of Decline Type Curve Analysis |
| Carter (1985) | Finite Radial and Linear-Gas Flow Systems Type Curves |
| Fraim and Wattenbarger (1987) | Type Curves for Gas Reservoirs Using Real Gas Pseudopressure and Normalized Time |
| Fraim et al. (1986) | Finite Conductivity Vertical Fracture Type Curves |
| Palacio and Blasingame (1993) | Type Curves for Gas Wells |
| Doublet et al. (1994) | Type Curves for Oil Wells |
| Cox et al. (1996) | Type Curves for Hydraulically Fracture Gas Wells |
| Wattenbarger et al. (1998) | Type Curves for Fractured Tight Gas Wells |
| Agarwal et al. (1999) | Type Curves for Radial and Vertically Fracture Wells |
| Chen and Teufel (2000) | Type Curves Including Early-Time Linear Flow for Tight Gas Wells |
| Marhaendrajana and Blasingame (2001) | Type Curves for Evaluating a Well in a Multiwell System |
| Camacho-V et al. (2005) | Decline Curve Behavior of Naturally Fractured Vuggy Carbonate Reservoirs |
| Araya and Ozkan (2002) | Type Curve Analysis for Vertical, Fractured, and Horizontal Wells |
| Pratikno et al. (2003) | Type Curves for a Well with a Finite Conductivity Vertical Fracture |

Table 1—Categorization of production decline type curve (modified after Currie 2010)

As the term “type curve” is sometimes used in the industry to describe a typical well production profile for a group of wells producing from the same resource play, we prefer the term “type well” to maintain consistent terminology with previous publications and long-standing definitions used in industry.

### *1.2.2 Type Well*

As opposed to type curves, type wells are dimensional plots characterizing the performance of a group of wells from resource plays based on the selected analogs. It is common to construct a type well using wells delimited by a chosen geologic area and filtered by the type of completions, operators or date of first production. In the industry, type wells are usually average rate-time profiles; however, they can also be profiles on the cumulative-time plot or simply a key metric

such as the estimated ultimate recovery (EUR), net present value (NPV), initial production rate or peak rate. Russell and Freeborn (2012) refer to a percentile type well as the production profile that achieves a certain percentile of a selected key metric. Because type wells are used to describe several attributes of typical production, **we explicitly mention the feature of the type well in this work, such as**: cumulative type well, type well profile, type well EUR, type well NPV. **Fig. 3** illustrate each kind of type well in red.

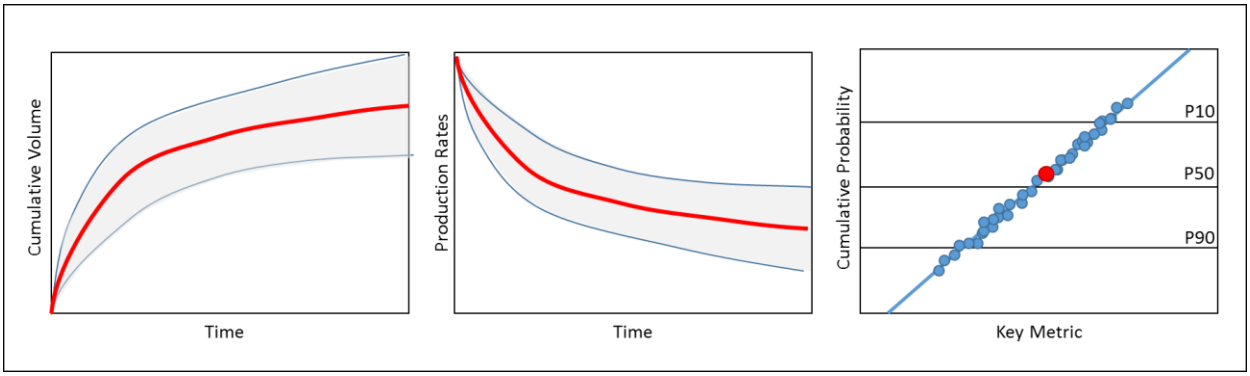


**Fig. 3—Left is the cumulative type well, center is a rate type well profile and right is a type well EUR, NPV or IP.**

In a resource play, the statistical distribution is important information to perform the analysis of well performances. Because of the uncertainty, a single value such as the mean is not sufficient to portray a range of possible outcomes. The SPEE encourages the use of a probabilistic metric such as the P10/P90 ratio to represent the variance of a sample around its mean. It is common to represent type well profiles and type well EURs with their P10, P50 and P90 percentile values. A P90 percentile is given by the reverse cumulative distribution function, which implies that there is a 90 percent chance that a random selection in the distribution will be greater or equal to that value.

Type wells are used to forecast the performance of wells with short production histories and undrilled wells because they can be represented by the typical outcomes of neighboring wells. For undeveloped projects, analogs can be used to infer the performance of a pilot well as long as certain criteria are satisfied. The comparison of type wells from different groups filtered by

completion design or regional extent allows us to quantify completion and operator performances or identify the presence of a "sweet spot" in the reservoir.

### 1.3 Statement of the Problem

Type wells have been used extensively for resource plays to determine the expected production from the typical behavior of analogs. However, there are few recommendations and no established guidelines or procedures to guide evaluators on how to construct type wells. Several methods and best practices were advocated by Fetkovich et al. (1987), Freeborn and Russell (2016) and Fulford et al. (2016), but most of the workflows implemented in commercial software packages remain flawed, non-transparent and limited.

Averaging production to build type wells does not properly account for different lateral lengths, completion designs and reservoir properties. Thus, evaluators are required to filter and sort analogous wells with similar properties to build a representative type well. This typically results in a large number of bins and a small number of wells in each bin. Type wells created with a restricted number of samples are most likely not representative of the population. To group more wells together, some authors have attempted to empirically normalize the production based on correlations. Rate normalization is not rigorous and varies based on the evaluator's experience. For instance, Freeborn and Russell (2016) suggests nonlinear scaling between initial production rates and lateral length due to the pressure drop in the wellbore.

Finally, production history allows us to diagnose reservoir and completion properties with rate transient analysis based on fundamental physics of fluid flow in porous media. Solving a reservoir problem requires us to understand and predict how fluid flows in space and **time**. The average of empirically normalized rate-time profiles does not address properly this multi-dimensional problem because it yields a synthetic profile that cannot be coupled with either specific reservoir or completion characteristics. As type wells are mostly used for investment decisions and time-value-of money analysis, they are limited because they currently do not account individually for reservoir, completion and geological uncertainties. Consequently, not addressing

properly the peculiar uncertainties of rate-time profiles can adversely impact the evaluation of a project and bias the outcome of a type well analysis. Because so many financial decisions are based on type wells in low-permeability reservoir development programs, more accurate type well construction can have financial implications in the range of millions to billions of dollars.

### 1.4 Objectives

We believe that production profiles should be scaled (or normalized) rigorously based on fundamental physical principles to increase the sample size and thus its statistical significance of the sample size. In addition, type wells should be created for a specific set of reservoir and completion properties. The objective of this work is to propose a rigorous scaling method which allows us to generate a type well for a given set of reservoir and completion properties. We define scaling factors by the fit of production data to modified analytical solutions from the commonly-used Wattenbarger type curve for horizontal wells exhibiting transient linear flow followed by boundary-dominated flow. We demonstrate that scaling factors are mathematically related to reservoir quality: matrix permeability, net pay thickness, completion quality, fracture half-length, fracture spacing, horizontal well lateral length, choke management practices, and drawdown. By rescaling all production profiles to a common reference or base well with specific properties, we are able to capture a typical production profile for wells located in a geological subset area (GSA). The typical profile can further be rescaled to forecast the production of wells with different properties. We also propose a methodology for use with shale gas wells, which can later be applied to other analytical models and types of fluids.

The following summarizes the methodology employed in the study:

- Define an analytical model adapted for horizontal multi-fractured wells (HMFW)
- Demonstrate the applicability of the analytical model to various shale gas plays
- Propose the “analytical scaling method” as a coherent and rigorous approach to scale production profiles
- Recommend a workflow for best practices to generate type wells, with a focus on publically available data
- Demonstrate the workflow in a full-scale case study
- Propose a new outlier detection tool tailored for publically available data

# CHAPTER II

# LITERATURE REVIEW

In this review, we will present some practices currently used to construct type wells along with integrated workflows published by several authors. The first part of the review focuses on the selection and treatment of production data used to create a type well production profiles. The second part of this chapter presents six type well workflows that were reviewed for this research.

## 2.1 Production Data Selection and Treatment

### *2.1.1 Data selection and limitations*

To construct representative type wells, the analog wells selected must satisfy certain criteria to perform the analysis. Several criteria reviewed for this work were selected from Miller et al. (2017), McLane and Gouveia (2015), SPEE (2016), and Russell and Freeborn (2012) are presented in **Table 2**.

| |
|---|
| Geological Unit, GSA, Lithology |
| Reservoir Pressure, Well Depth |
| Porosity-Thickness |
| PVT, Condensate yield |
| Completion Design – Fracture Treatment |
| Well Density, Well Design, Well Location |
| Artificial Lift Design |

Table 2—Criteria for type well selection

For most analysis, and based on the data available, there is a tradeoff between the criteria and the number of wells selected wells. SPEE Monograph 3 (2011) states the minimum number of samples required as a function of the P10/P90 ratio of the EUR distribution and the maturity of the play in tables 2.1 and 3.3. The maturity of a field determines how representative the curves used to predict future performance will be and the P10/P90 ratio indicates the variability in the

expected results. Typically, low risk projects have a ratio of 2 to 4 whereas a higher risk (uncertainty) is associated with a ratio in the range of 10 to 25.

Well production data can limit the accuracy of the analysis because they are usually considered low resolution/low frequency. Authors recommend that we carefully review the source of the information and understand the limitations of the data used for the analysis. Compared to publically available monthly produced volumes, the use of daily rates and pressure data can significantly improve the results of a production analysis workflow. Mattar et al. (2006) identified several issues such as the allocation of produced volumes, the variation of pressures, change in operating conditions, the limitations of the multiphase flow meters, and the frequency of measurements. These sources of errors generate artifacts, also known as outliers or noise that increase the range of uncertainty in the results of an analysis. To overcome the adverse effect of artifacts in the analysis, Chaudhary and Lee (2016a) and Holdaway (2014) presented supervised and unsupervised procedures to identify outliers.

### *2.1.2 Time Shifting*

Since wells are not all drilled at the same time and may have experienced downtime or shut-in periods, the data must be corrected in order to illustrate the real depletion pattern of the reservoir. Freeborn et al. (2012) recommended that we shift production profiles for all wells to the time of first production or peak rate in the case of a significant ramp-up period. Furthermore, Groulx (2015) recommended that cumulative volumes and production rates be plotted as a function of the producing time by removing the well downtime. We note, however, that production time as opposed to calendar time will impact economic calculations as downtime is not considered.

### *2.1.3 Rate normalization*

Since most wells experience different drawdowns over time, the production rate should also be normalized for pressure variations in addition to time corrections. Pressure normalization allows us to improve the identification of flow regimes and the actual depletion pattern of the stimulated reservoir volume as recommended by Fetkovich et al. (1987). Most of the DCA and analytical models assume constant BHP; thus, if rates are not corrected for pressure variations, the

forecast can be compromised. Chaudhary and Lee (2016b) and Lacayo and Lee (2014) proposed methodologies to normalize rate and improve the reliability of forecasting methods. An example of daily pressure normalized rate is presented in Appendix K.

For type well construction purposes, rate normalization is a practice that is currently applied to wells with different lateral lengths and completion designs. The question was addressed analytically and numerically by Yu and Gouveia (2015) to identify relationships between recovery factor and of the number of fractures, drainage area (lateral length multiplied by well spacing) and the lateral length of a tight gas well. The authors found from a sensitivity study that the stimulated lateral length is linearly proportional to the final recovery. Furthermore, they acknowledged that the number of stages as well as the drainage area affects the recovery when the matrix permeability is extremely low. Overall, Yu and Gouveia recommended an integrated workflow for wells in a rock body for which the permeability ranges from 0.1 to 0.01mD. They rescale the initial production and the EUR based on the correlation between EUR and the stimulated lateral length. Several authors, including Miller et al. (2107) referred to this technique.

Freeborn and Russell (2016) normalize ("scale") rate-time profiles based on three parameters: the number of fractures, the initial production decline rate, and initial production rate. The effect of each parameter is determined by semi-empirical correlations, and expressed as a multiplier. The multiplier for number of fractures is simply the ratio of the number of fractures in target and analog wells, which implies a linear correlation. The initial production decline multiplier is based on an empirical correlation of production decline with lateral length. Finally, the initial production multiplier is a ratio derived from an analytical expression for the time to reach fracture interference in a linear flow system as a proxy for the permeability-thickness product for a well. The product of the three multipliers provides an overall scaling methodology that can be used to diagnose the well characteristics. However, the empirical nature of the multipliers and the non-uniqueness of the methodology limits the reliability of the normalization.

## 2.2 Review of Type Well Construction Workflows

The time slice method is widely used in the petroleum industry to generate type well profiles because of its simplicity. After the production profiles of a group of wells selected for a type well construction have been time shifted and rate normalized, the average, median, P10 and

P90 rates are recorded at every time interval. This sequence of rates yields a synthetic profile over time. Freeborn et al. (2012) reported many concerns about this workflow. The type well rate must be based on an average rate from the total number of wells used in the analysis; otherwise, it creates a survivor bias that can skew the data towards the wells with longer production histories. To address this problem, Groulx (2015) recommends that we limit the type well construction by using a sample size cutoff. However, for wells with short production histories, the type well production profile can be limited in duration. Russell and Freeborn (2013) demonstrated that forecasting production based on a single average type well does not provide a reliable forecast for the group of wells. Freeborn et al. (2012) recommends that we average the forecasted production of each well. They also demonstrate that the percentiles type wells produced by the time slice method cannot be associated with a type well EUR or type well initial production (IP) since there is no direct correlation between the EUR and the IP.

McLane and Gouveia (2015) proposed an alternative methodology to estimate a type well EUR based on the aggregation principle and the central limit theorem. As resources play are statistical by nature, the aggregation principle allows us to estimate the range of confidence of achieving a specific type well percentile as a function of the distribution of analog wells, the sample size and the target number of wells to be drilled. This methodology allows us to quantify the uncertainty of a project and can further be used to validate the choice of analogs with a sequential aggregation plot. However, this method does not provide guidance to help us to generate a type well production profile over time.

Freeborn and Russell (2016) suggested a methodology to create probabilistic type wells based on an aggregated distribution of EURs for a specified number of wells. By using Monte Carlo simulation for a sample of EUR distributions for analog wells, the rate vs time profiles are weighted based on a the relative frequency of the random selection. By defining a target percentile, the weighted average of all the profiles yields an estimation of the percentile type well profile. Other metrics such as NPV, payout time and IP can also be used to create probabilistic type wells.

Xiong et al. (2017) proposed a modified hyperbolic type well construction profile calibrated using numerical simulation. Xiong claimed that the workflow proposed takes advantage of the different approaches to reserves estimation based empirical DCA, analytical and numerical simulations. The objective is to create a type curve for a GSA based on a numerical model to consistently forecast the production of wells from the same GSA. They first select a well profile that is close to the P50 rates from a group of profiles generated with a numerical simulator and calibrated with real data. The model is built upon the range of uncertainty of all the input parameters, such as PVT data, porosity, permeability and fracture geometry. They then parametrize the selected well with a multi-segment Arps model. Each segment of the model represents a flow regime, identified based on the characteristic shape on a diagnostic plot. Each segment is then fitted with a set of "b" and "D" parameters.

Fulford et al. (2016) presented a semi empirically parametrized type well profile based on an alternative decline curve presented by Fulford and Blasingame (2013) that parametrizes the evolution of the Arp's "b" factor during the producing life of a horizontal well in infinite acting linear flow followed by boundary dominated flow. By fitting each production data with a Bayesian revision algorithm, the authors generate a 30 year forecast to estimate the well EUR. The parametrized type well is generated by averaging the constant of the transient hyperbolic model, assuming a linear relationship between EUR and the model parameters. Fulford et al. (2016) suggested a similar methodology to create percentile type wells by averaging the parameters of the wells that reached a target EUR. The averaged transient hyperbolic model's parameters are then used to generate the probabilistic type well profile.

Finally, Fetkovich et al. (1987) presented with the original development of dimensionless type curves a method to capture the typical decline of a conventional field. Since the production of each well matches the geometrical shape of a depletion type curve, the overlay of several log rate and log time profiles on each other allows us to delineate a common depletion pattern. Fetkovich et al. (1987) referred to this technique as a field type curve, which the authors also refer to an "average well." The overlay of the data allows us to create, with a certain range of accuracy, a log-log type well that can be fitted with a decline equation. A field type curve was developed for

the Monterey fields in California. It demonstrates that, by combining the short history of an individual well with the field type curve, we can forecast production of the individual well. Fig. 4 illustrates the overlay of different fields from the same formation in California. By estimating the fluid and rock properties, well spacing and operating pressure, Fetkovich et al. developed a field type curve for production at constant-wellbore pressure

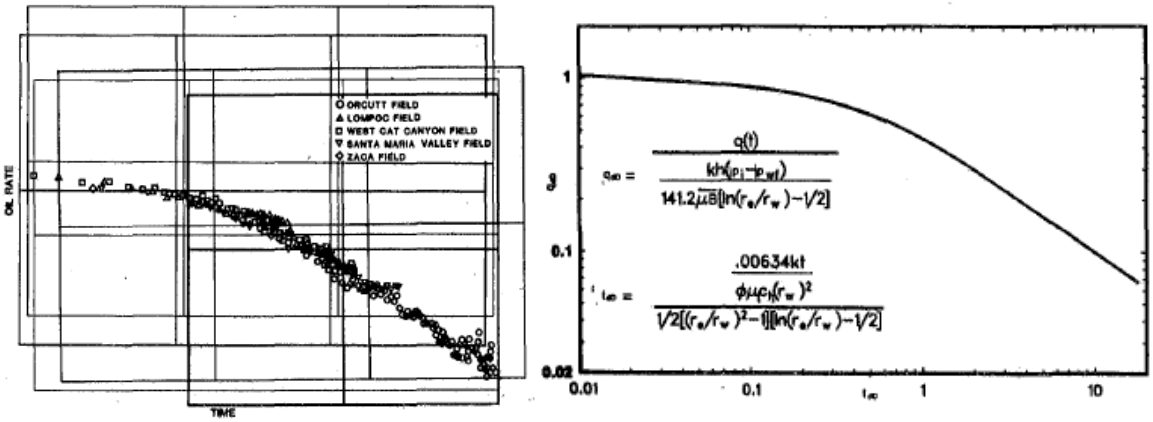


**Fig. 4—Left: overlay of five different production profiles. Right: field type curve for the Monterey Field, reprinted from Fetkovich et al., 1987.**

The authors acknowledged that the field type curve for this example is similar to a harmonic decline stem with a Apr's "b" factor of 1. Based on this typical production profile, the difference in productivities of each well and relative position on the overlay used for reservoir characterization and forecasting.

### 2.3 Material Balance Time and Type Curve Analysis

Because Fetkovich (1980) presented the dimensionless solution of rate-time relationships for constant bottom hole pressure and constant operating conditions, the application of the methodology to real production data was limited by the assumption of constant flowing pressure

conditions throughout a well's life. Palacio and Blasingame (1993) developed a superposition time function they called "material balance time." It enables the match of a variable pressure/rate history of a single phase flow on the Fetkovich Type curves with a b=1 stem once the flow regime is boundary dominated. The MBT for liquid flow at a given time is the ratio of cumulative produced volume to the flow rate. The authors also proposed a formulation for compressible fluid flow as an equivalent slightly-compressible liquid flow that corrects for pressure-dependent fluid properties; they called this modified time function material balance pseudo-time. Because the material balance pseudo-time requires the integration of fluid properties over time, Clarkson (2013) suggested that this time function can be a good first approximation for the production analysis of unconventional gas wells. Agarwal et al. (1998) demonstrated that the use of MBT converts a constant pressure depletion solution to a constant rate solution. Use of MBT forces data in BDF to follow a harmonic decline trend, but it does not provide the same rigorous results during transient flow as we obtain using ordinary time.

Using MBT can limit the accuracy of rate transient analysis and type curve analysis due to the presence of noise and outliers in the data, (Agnia et al. 2012). Invalid production data can adversely impact the diagnosis of flow regimes when rates are plotted against MBT. The authors demonstrated that unusually small flow rates will align on a line characterized by a negative unit slope line. **Fig. 5** (left) illustrates an example from SPEE Monograph 4 (2016). The red points were detected as outliers. Fig. 5 (right) shows the position of these points on a log-log rate-MBT plot.

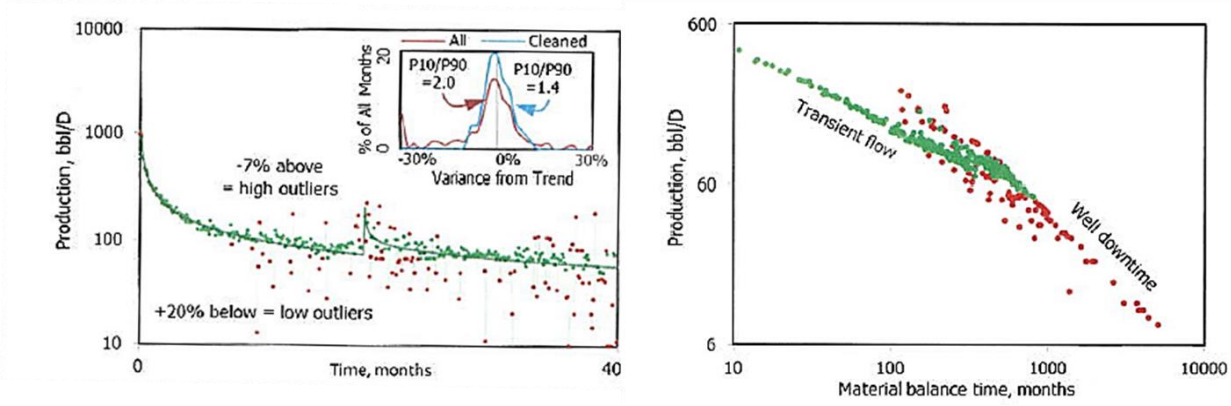


**Fig. 5—MBT outlier impact on log-log diagnostic plot, reprinted from SPEE, 2016.**

This example demonstrates how outliers can portray a fictitious BDF regime. Such errors can lead to a significant reduction in the apparent hydrocarbons in place. Supplementing outlier removal techniques cited in section 2.1.1, Agnia et al. (2012) proposed a specific workflow to identify outlier and noisy data when MBT is used in an analysis.

# CHAPTER III

# DEVELOPMENT OF THE ANALYTICAL MODEL

## 3.1 Original Analytical Model for Vertical Wells with Single Vertical Fracture in Tight Reservoirs

Wattenbarger et al. (1998) published an analytical solution for the linear flow under constant rate and constant BHP conditions. The authors observed extended periods of transient linear flow in these low permeability reservoirs. Therefore, they proposed a theoretical model with a vertical well placed in the center of a rectangular and homogenous reservoir bounded by no-flow boundaries. One of the cases studied by the authors was a vertical well with a vertical fracture which extends to the drainage boundaries of the reservoir. **Fig. 6** illustrates the model geometry from a top view. The constant $y_e$ represents the distance from the fracture to the drainage boundary, $x_f$ is the fracture half-length and $x_e$ is the distance from the well to the drainage boundary along the fracture plane. For clarity, Fig. 6 shows the model in three dimensions, and illustrates the position of the fracture plane in blue relative to the no flow boundaries in red.

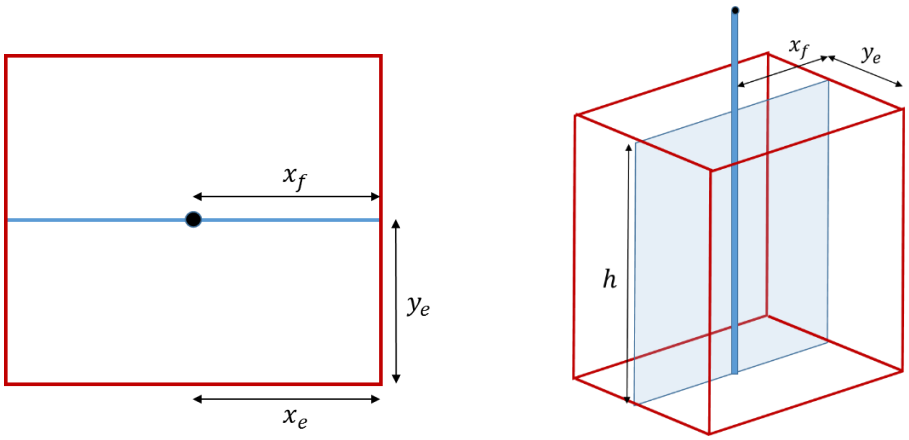


**Fig. 6—Analytical model geometry, left is a top view and right is in 3 dimensions**

The model presented in Fig. 6 assumes homogenous matrix permeability, porosity and compressibility. Furthermore, the fracture and the wellbore are infinitely conductive, which assumes a dimensionless fracture conductivity, $F_{CD}$, greater than 100. $F_{CD}$ is the ratio of the fracture permeability- fracture width product to the matrix permeability- fracture half-length product as shown in Eq. 1.

$$F_{CD} = \frac{k_f w}{k x_f} \tag{1}$$

Because the fracture extends to the boundaries of the reservoir, fluid flows in a linear pattern from the matrix towards the fracture. Wattenbarger et al. (1998) published the solution for two inner boundary conditions, constant rate and constant BHP, and closed reservoir outer boundary condition for both liquid and further adapted the solution to gas systems with the real gas pseudo-pressure developed by Al-Hussainy et al. (1966). In this work, we only present the gas solution, but the principles presented also apply to liquid flow. Eqs. 2 and 3 describe the relationship between the dimensionless rate $q_D$ and dimensionless time $t_{Dye}$ and the physical properties of the analytical model illustrated by Fig. 6 for a tight gas reservoir. Eq. 4 details the real gas pseudo-pressure given used in Eq. 2.

$$\frac{1}{q_D} = \frac{kh\left[m(p_i) - m(p_{wf})\right]}{1424 q_g T} \tag{2}$$

$$t_{Dye} = \frac{0.00633kt}{(\emptyset \mu c_t)_i y_e^2} \tag{3}$$

$$m(p) = 2\int_{p_o}^{p} \frac{p}{z\mu} dp \tag{4}$$

**Fig. 7** plots the both constant rate and constant BHP solutions for closed linear reservoirs. Based on Agarwal et al.'s findings (1998), MBT can replace real time in Eq. 3 to transform the graph for constant BHP production to a graph for constant rate production.

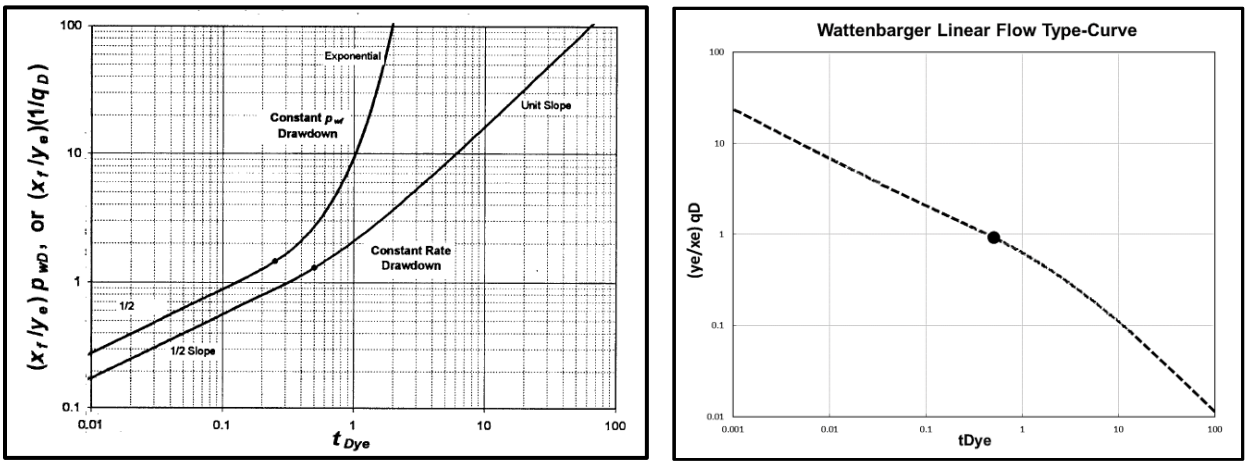


**Fig. 7—Constant rate and constant BHP solutions for closed linear reservoirs, reprinted from Wattenbarger et al., 1998.**

As displayed in Fig. 7Fig. 7—Constant rate and constant BHP solutions for closed linear reservoirs, reprinted from Wattenbarger et al., 1998, the constant rate drawdown solution can be characterized by a half slope in the linear transient period until a dimensionless time of 0.5 marked with a black dot. Following this time, a transition period occurs for one log cycle to a dimensionless time of 5 indicating the start of BDF by following a unit slope line, just as in the Arps harmonic decline model. As for other type curves, the graphical match of actual production data to the dimensionless type curve allows us to identify flow regimes and estimate unknown parameters. Eqs. 2 and 3 can be rearranged to define a rate match point $QM$ and a time match point $TM$ as shown in Eqs. 5 and 6.

$$QM = {\left(\frac{y_e}{x_e}\right) q_D}\Big/{q_g} = \left(\frac{y_e}{x_e}\right)\frac{1424 q_g T}{kh\left[m(p_i) - m(p_{wf})\right]} \tag{5}$$

$$TM = {t_{Dye}}\Big/{t_{mb}} = \frac{0.00633k}{(\emptyset \mu c_t)_i y_e^2} \tag{6}$$

A match of the pressure normalized rate versus MBT on the dimensionless type curve similar to Fig. 7 allows us to solve for two unknown parameters of Eqs. 6 and 7.

### 3.2 Modified Analytical Model for HMFW

The analytical model described by Wattenbarger et al. (1998) applies strictly only to vertical wells with a single vertical fracture; however, most of the wells currently drilled in ultra-low permeability reservoirs are horizontal with multiple stimulation treatments. Therefore, we modified Wattenbarger et al.'s model to accommodate for the completion geometry and the number of hydraulic fracture stages in modern horizontal wells. **Fig. 8** compares the modified geometry to that in Fig. 6. In Fig. 8, the red lines represent the extent of the closed reservoir boundaries and the blue plane represents the fracture which is perpendicular to the wellbore.

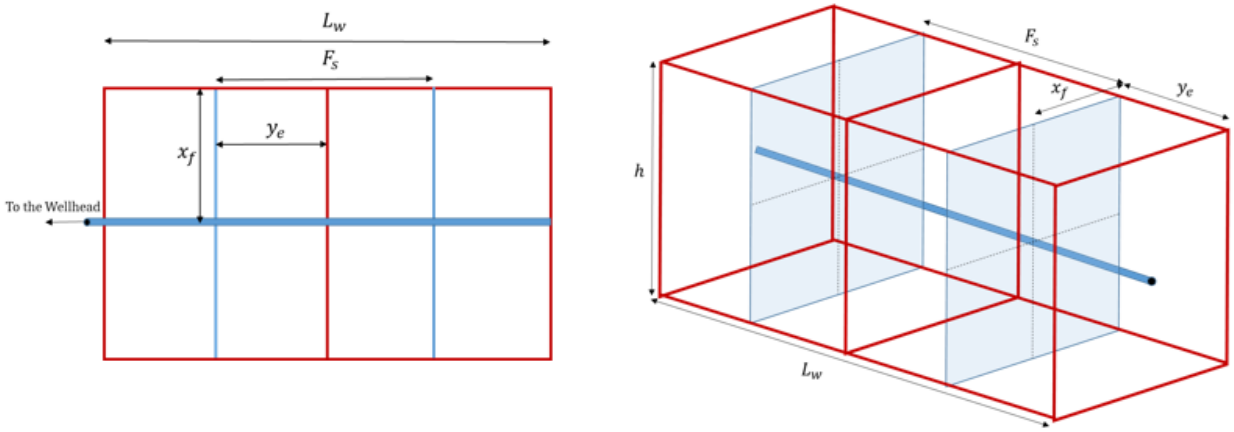


**Fig. 8—Modified analytical model for multi-fractured horizontal wells, left shows a top view and the right shows a 3D view.**

By assuming the same fracture half-length $x_f$ for each fracture stage and constant fracture spacing, $F_s$ (twice the constant $y_e$), the analytical model presented in Fig. 6 can be used as an element of symmetry that can be duplicated for a given number of stages. Fig. 8 shows a modified model with two adjacent fracture stages along the horizontal well. We introduce the parameter $q_t$ for total flow rate, which is the sum of the flow rates from all the fractures. Because the fractures

are identical, we assume that each fracture stage will produce the same rate as we neglect the pressure drop in the fracture and the wellbore. Furthermore, the number of fractures can be expressed as the total lateral length $L_w$ divided by the distance between of fracture stages $F_s$. Based on these relationships, we introduced the total flow rate $q_t$ in Eq. 7 and the distance from fracture to the boundary $y_e$ in Eq. 8.

$$Q_t = n_f * q_g = \frac{L_w}{F_s} * q_g \tag{7}$$

$$y_e = \frac{F_s}{2} \tag{8}$$

As demonstrated in Appendix 1, Eqs. 2 and 3 can be modified based on Eqs. 7 and 8 to characterize the dimensionless solution of the modified analytical model. Eqs. 9 and 10 summarize the development presented in Appendix A where the solution is expressed in terms of the fracture spacing $F_s$, the fracture half-length $x_f$, the total flow rate $q_t$ and the length of the completed horizontal section of the well $L_w$.

$$\left(\frac{F_s}{x_f}\right) q_D = \left(\frac{{F_s}^2}{x_f}\right) \frac{1424\, T q_t}{khL_w\left[m(p_i) - m(p_{wf})\right]} \tag{9}$$

$$t_{DF_s} = \frac{0.02532kt}{(\emptyset \mu c_t)_i F_s^2} \tag{10}$$

**Fig. 9** illustrates the modified type curve for the dimensionless variables defined in Eqs. 9 and 10. Since the fracture spacing is twice the distance $y_e$, the type curve generated from the modified model differs from the original as detailed in Appendix A. As the flow in the matrix is linear towards the fractures, the same diagnostic characteristics of transient and BDF regimes appear in the modified type curve shown in Fig. 9

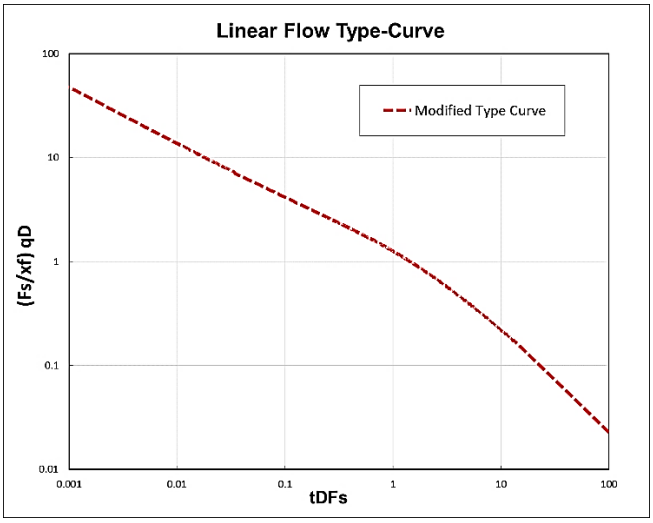


**Fig. 9—Modified dimensionless type curve.**

As with the original type curve presented by Wattenbarger et al. (1998), production data can be matched on the type curve to identify flow regimes and estimate unknown parameters such as permeability and fracture half length. The match points for the modified type curve are given by Eqs. 11 and 12, which are rearrangements of Eqs. 9 and 10.

$$QM = \frac{\left(\frac{F_s}{x_f}\right) q_D}{q_t} = \left(\frac{F_s^{\,2}}{k}\right) \frac{1424\, T}{x_f h L_w \left[m(p_i) - m(p_{wf})\right]} \tag{11}$$

$$TM = \frac{t_{DF_s}}{t_{mb}} = \left(\frac{k}{F_s^2}\right) \frac{0.02532}{(\emptyset \mu c_t)_i} \tag{12}$$

As for Eq. 6, the time match point in Eq. 12 is also expressed as a function of MBT. **Fig. 10** shows an example of a production data in red, matched on the dimensionless type curve in black, before the match on the left and after the match on the right. The value for the rate match point QM and time match point TM are given by the arrows pointing to the axes. The upper axis represents the material balance time (days), and the right arrow points towards the pressure-normalized rate. The lower arrow points towards the dimensionless time axis and the left arrow points towards the dimensionless rate axis. This graphical example illustrates how match points

can be determined to solve for permeability and the fracture half-length in Eqs. 11 and 12 if the other parameters are known.

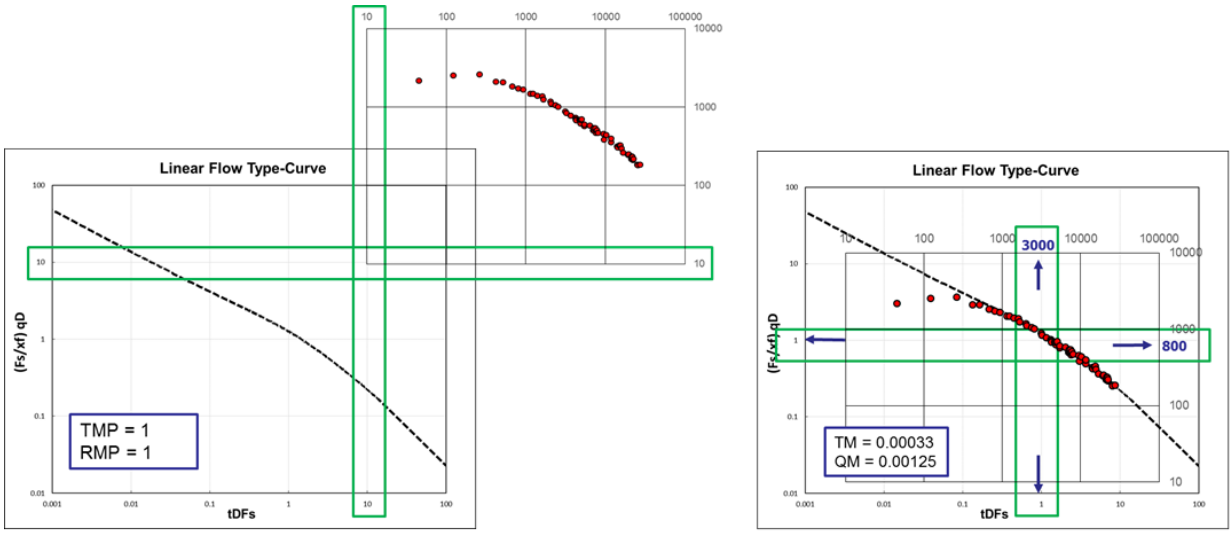


**Fig. 10—Production diagnostic on modified type curve prior shifting (left) and fitted (right).**

As demonstrated in Eqs. 11 and 12, the modified type curve is directly related to the number of fracture stages since the dimensionless variables include lateral length and fracture spacing. Therefore, Fig. 9 can characterize any horizontal well with multiple fracture if the production data can be matched. As the model is built on the assumption of a homogeneous matrix where stimulated reservoir volume (SRV) is defined by the fracture dimensions, we are neglecting flow from the unstimulated matrix outside the SRV. Therefore, calculating the fracture half-length allows us to directly estimate the SRV which is defined by the geometrical assumptions of the model and the match of the production data on the boundary dominated flow section of the type curve. Similarly, permeability found in the rate or time match point represents only an idealized permeability of this homogeneous rock.

### 3.3 Application to Various Shale Oil and Gas Plays in the US, Canada and Argentina

To validate the suitability of the modified type curve for linear flow presented in the previous section to shale reservoirs, we conducted a scoping study of wells in various developed

fields to determine whether their production histories display the characteristic geometrical shapes of the type curve. The oldest horizontal wells from the Barnett, Fayetteville, Marcellus, Haynesville, Eagle ford, Utica, Montney, Niobrara, Bakken and Vaca Muerta shale reservoirs were selected because they are the most likely to be in BDF. **Table 3** summarizes the ten plays we analyzed. All the US-based production information was provided by DrillingInfo as of April 2018. The reservoir search name in the first column defines the search filter under the production tab. The second column displays the total number of horizontal gas wells reported under the given reservoir name. Column three indicates the maximum number of months of the well which has produced for the longest time. Columns four and five display the filters chosen arbitrarily to reduce the number of wells downloaded for the analysis, as indicated in column six. Finally, column seven shows the number of wells chosen for display in **Figs. 11 to 21**.

| 1 | 2 | 3 | 4 | 5 | 6 | 7 |
|---|---|---|---|---|---|---|
| Reservoir Search Name | Total Number of Horizontal Wells | Maximum Number of Month Produced | Minimum Number of Month Produced Selected | Maximum Number of Month Produced Selected | Number of Wells Downloaded | Number of Wells Displayed |
| BARNETT SHALE GAS | 16424 | 308 | 170 | 200 | 68 | 24 |
| FAYETTEVILLE GAS | 5386 | 154 | 90 | 90 | 78 | 29 |
| MARCELLUS SHALE GAS | 7459 | 134 | 96 | 100 | 66 | 23 |
| HAYNESVILLE SHALE GAS | 3097 | 125 | 110 | 120 | 41 | 25 |
| EAGLE FORD SHALE GAS | 950 | 109 | 90 | 100 | 50 | 32 |
| EAGLE FORD SHALE OIL | 2904 | 120 | 84 | 110 | 88 | 28 |
| UTICA SHALE GAS | 145 | 61 | 25 | 61 | 43 | 33 |
| MONTNEY SHALE* | N/A | N/A | N/A | N/A | 45 | 25 |
| NIOBRARA OIL | 3570 | 115 | 80 | 100 | 90 | 33 |
| BAKKEN SHALE OIL | 2281 | N/A | 122 | 130 | 246 | 19 |
| VACA MUERTA GAS* | N/A | 77 | 12 | 77 | 153 | 47 |

*Well Information not retrieved from Drilling Info

Table 3—Shale gas play sampling information

For each resource play, we prepared a log-log plot of monthly produced volume vs. MBT., To diagnose flow regimes, pressure-normalized rates should be plotted vs. material balance time to identify flow regimes. However, we had access only to publically reported monthly production

volumes, so we assumed a constant operating bottom hole pressure for each well. Because some of the wells have a very long production history, we observed discontinuities in the some of the rate profiles. We believe that the discontinuities can be caused by a re-stimulations, well interferences, drastic change in bottom-hole pressure or the change of artificial lift system. Only wells with a continuous decline and a limited number of outliers were selected and displayed on Figs. 11 to 21**.** Since each well has a different production behavior, diagnostic lines were added on each figure to highlight the slopes. The green line characterized by a negative unit slope is the diagnostic shape for BDF whereas the orange line characterized by a negative half slope is the diagnostic shape for linear transient flow. We used the overlay technique described by Fetkovich et al. (1987) to develop a field type well by shifting the profiles onto each other based on geometrical similarities. The right plots in Figs. 11 to 21 demonstrate that all the shale plays have similar field type curves, and all exhibit transient linear flow followed by BDF.

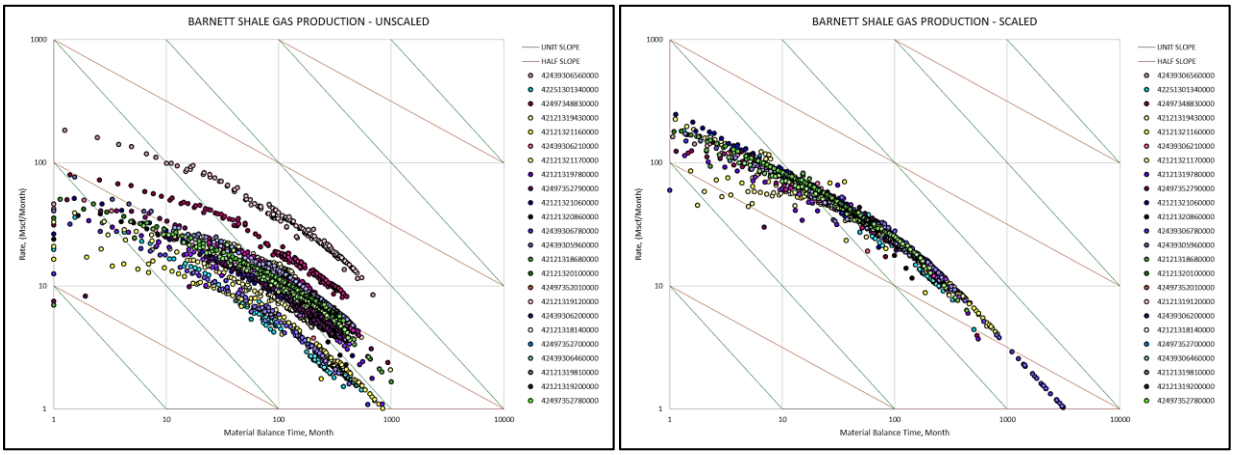


**Fig. 11—Left: unscaled Barnett shale gas production. Right: Barnett type well production profile.**

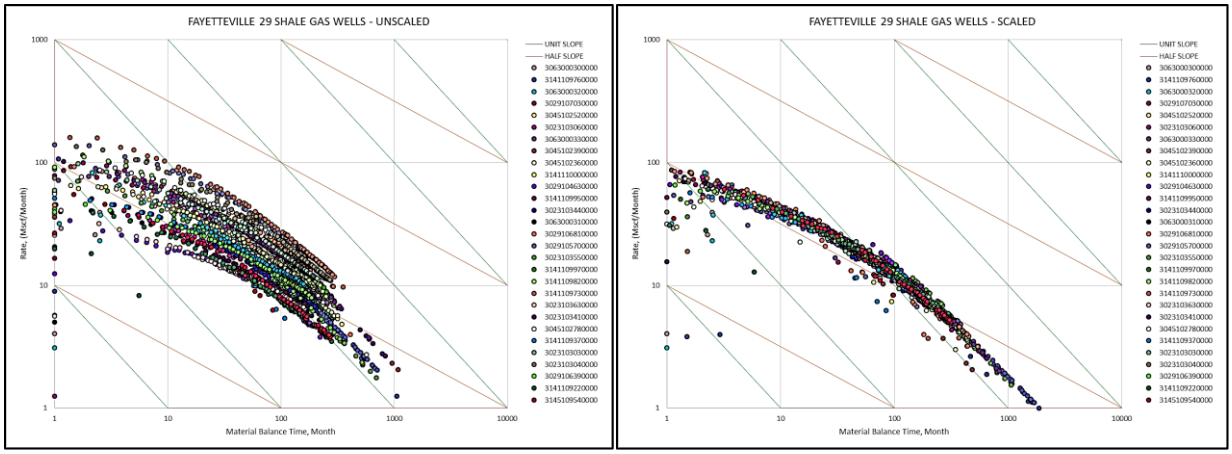


**Fig. 12—Left: unscaled Fayetteville shale gas production. Right: Fayetteville type well production profile.**

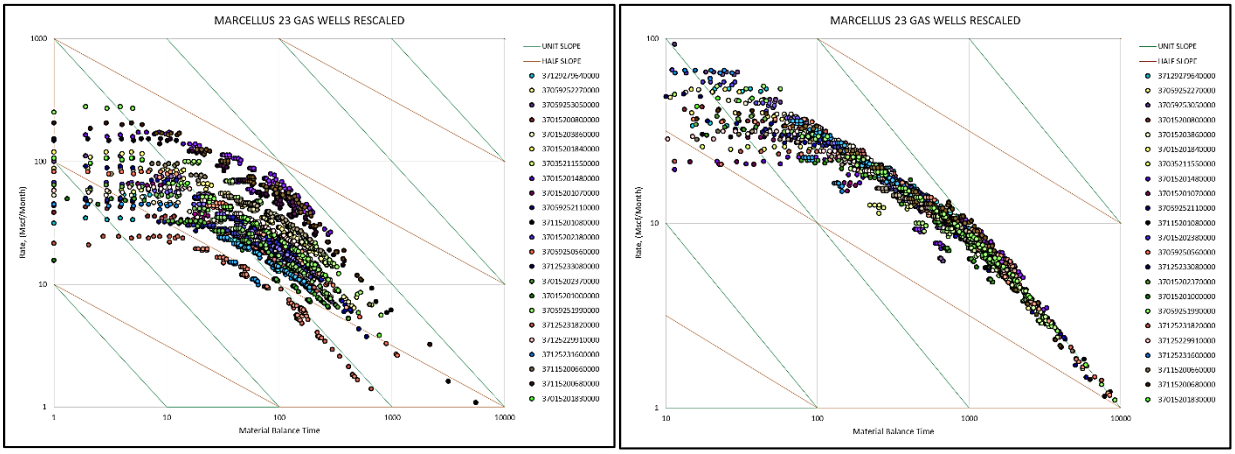


**Fig. 13—Left: unscaled Marcellus shale gas production. Right: Marcellus type well production profile.**

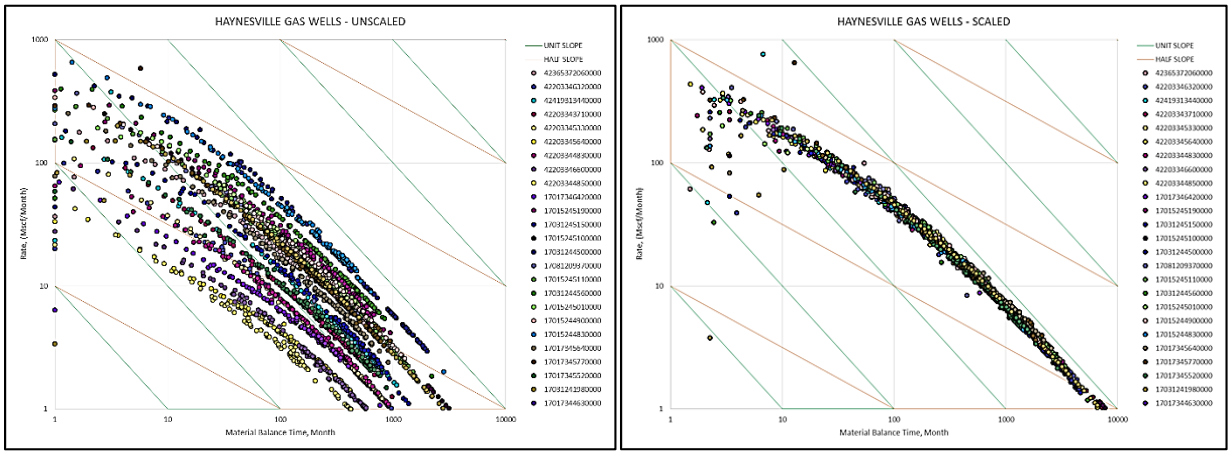


**Fig. 14—Left: unscaled Haynesville shale gas production. Right: Haynesville type well production profile.**

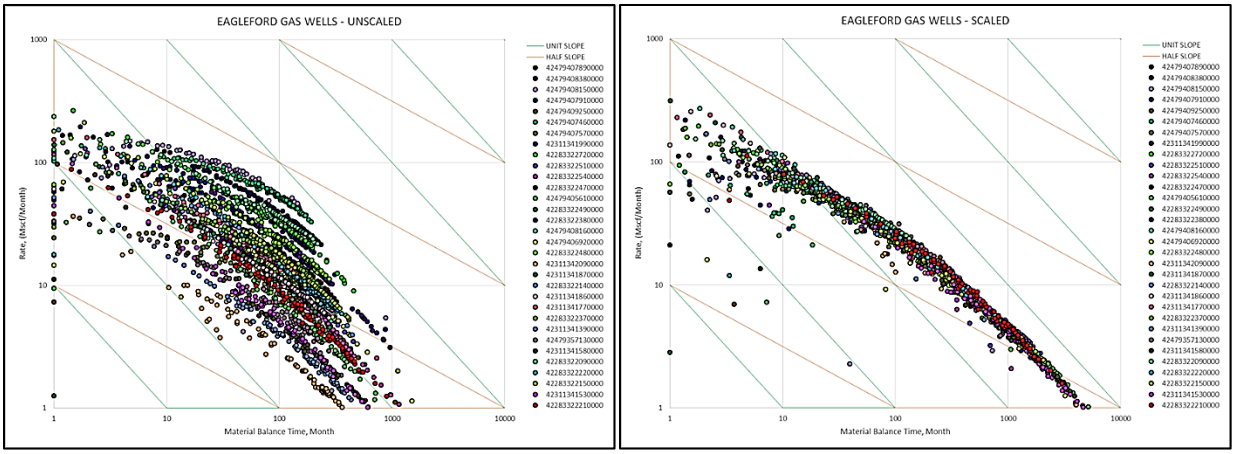


**Fig. 15—Left: unscaled Eagle ford shale gas production. Right: Eagle ford type well production profile.**

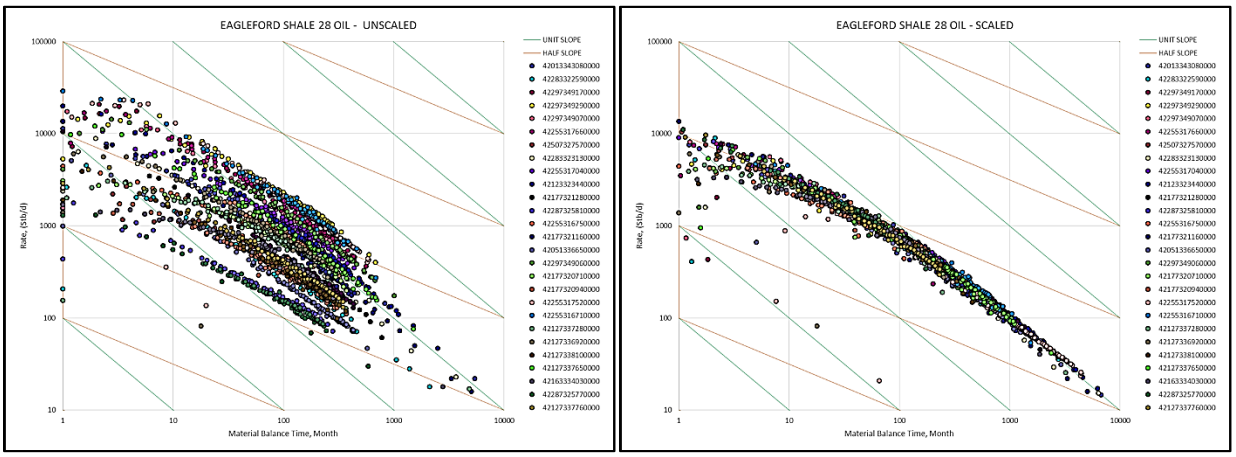


**Fig. 16—Left: unscaled Eagle ford shale oil production. Right: Eagle ford type well production profile.**

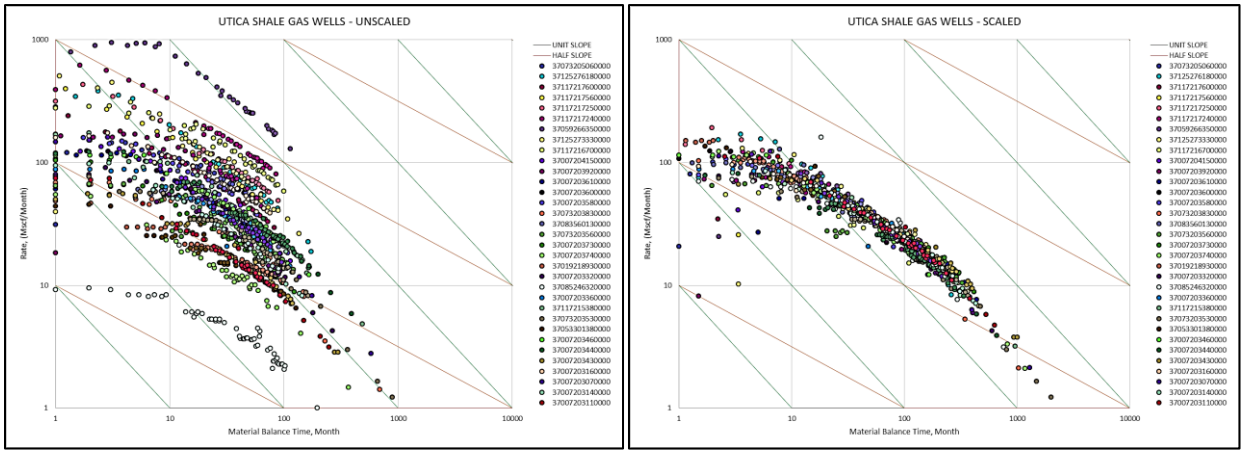


**Fig. 17—left: unscaled Utica shale gas production. Right: Utica type well production profile.**

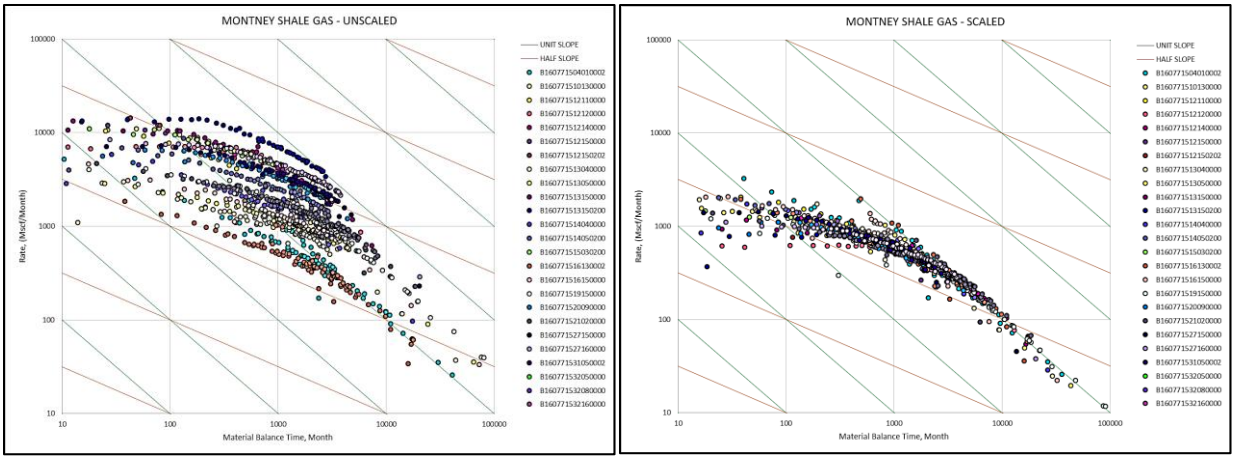


**Fig. 18—Left: unscaled Montney shale gas production. Right: Montney type well production profiles**.

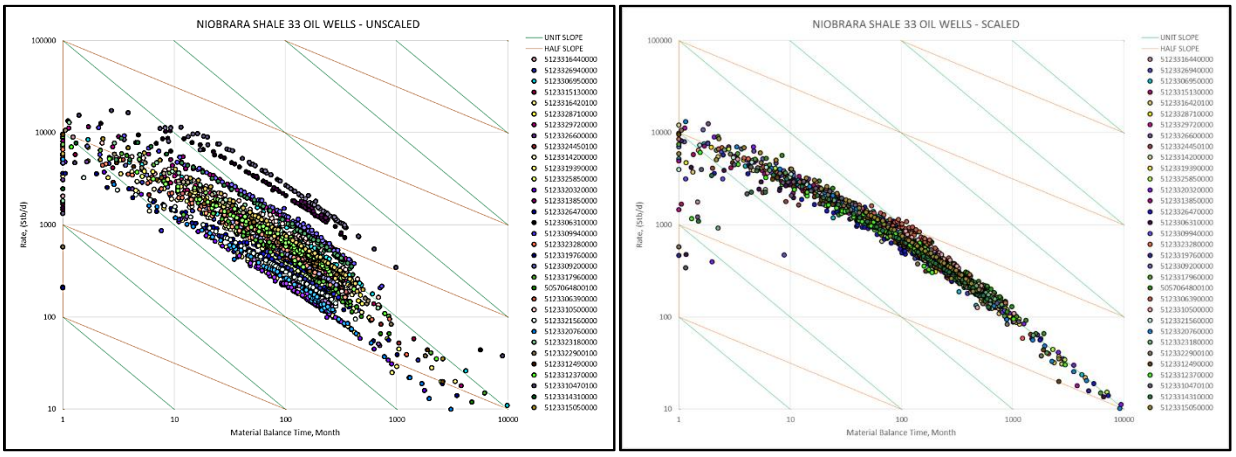


**Fig. 19—Left: unscaled Niobrara shale oil production. Right: Niobrara type well production profiles.**

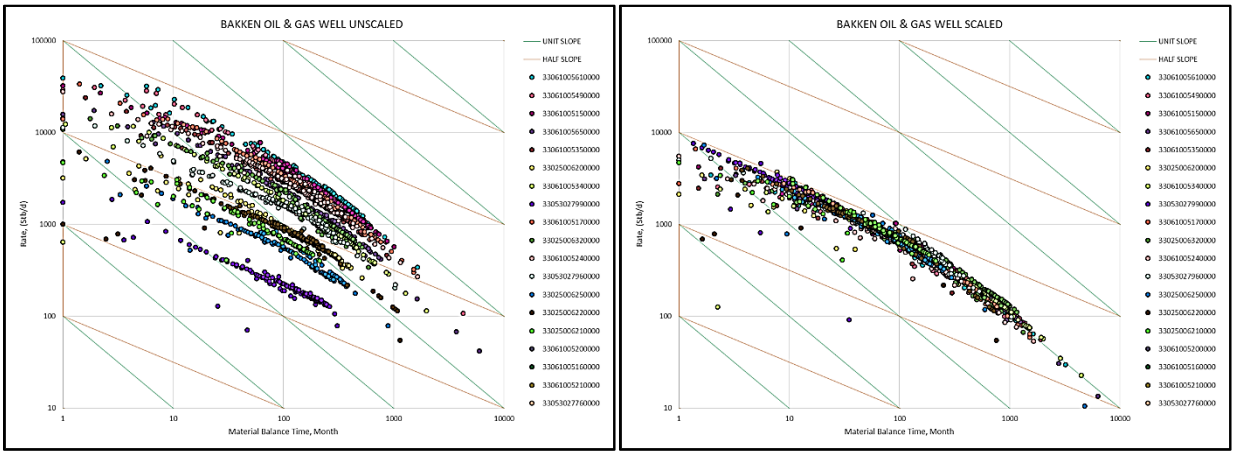


**Fig. 20—Left: unscaled Bakken shale oil production. Right: Bakken type well production profiles**.

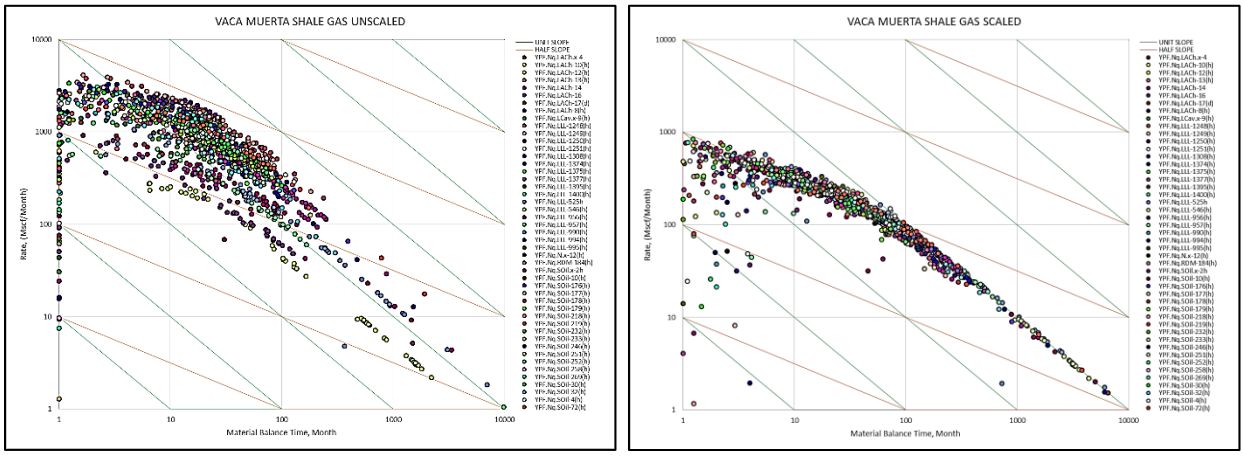


**Fig. 21—left: unscaled Vaca Muerta shale gas production. Right: Vaca Muerta type well production profile.**

These results validate the assumption that we can use the modified type curve to estimate the properties of the reservoir and the completions.

# CHAPTER IV

# DEVELOPMENT OF THE ANALYTICAL SCALING METHOD

## 4.1 Analytical Scaling Definition

The field type curve for the eight different resources plays discussed in Chapter 3 were created by shifting log-log rate-time plots horizontally and vertically until they matched a standard, uniform set of conditions. This shifting is equivalent to multiplying both rate and time by multiplication factors which differ from well to well and which results in the production data plots being "scaled" to the standard or uniform conditions. We refer to these multipliers as scaling factors. In this regard, both illustrations in Fig. 10 present the rate and time match points given by Eqs. 11 and 12 as scaling factors because they represent the vertical and horizontal displacement of the production data relative to the type curve. Since the rate and time match points are functions of the analytical model parameters, we further refer to this shifting methodology as "analytical scaling." Fetkovich et al. (1987) presented an overlay of different production profiles from similar fields with a common drive mechanism on a log-log plot to represent the similar behavior of these reservoirs. Since the field type curve matches a known analytical solution, the vertical and horizontal displacement of the profiles relative to one another simply reflects the difference in parameters of the analytical model. For instance, by correlating Fig. 4 and the analytical model of Fig. 2, the authors interpreted the shift on the rate axis as a difference in permeability-thickness product. Similarly, the shift on the time axis reflect the differences in both the permeability and effective wellbore radius. In a like manner, Figs. 11 to 21 demonstrate that the production profiles of shale reservoirs follow the characteristic shape of an analytical solution for linear flow. Therefore, the objective of this chapter is to demonstrate rigorously the relationships between the linear flow analytical model parameters and the scaling factors required to match production profiles generated analytically to a reference profile.

To conduct this analysis, the *hybrid horizontal multifrac model* in the IHS Harmony RTA software was used to generate production profiles of hypothetical gas wells.

**Table 4** summarizes the input parameters chosen to define the reference profile, which, in this chapter, we also refer to as the base-case scenario. In this simulation, only hydrocarbons located between fractures flowed in the fractures and thus into the well.

| Model Parameter (Unit) | Value |
|---|---|
| **Analytical Model Properties** | |
| Initial Reservoir Pressure (Psia) | 5000 |
| Fracture Half Length (ft) | 330 |
| Lateral Length (ft) | 7500 |
| Fracture Conductivity | 1.0E+06 |
| Fracture Skin | 0 |
| Number of Fractures | 50 |
| Matrix Permeability (nD) | 3.9 |
| Distance from Fracture to Permeability Boundary (ft) | 75 |
| Net Pay (ft) | 100 |
| Total Porosity (%) | 5 |
| Gas Saturation (%) | 60 |
| Water Saturation (%) | 40 |
| Formation Compressibility (psi-1) | 6.48E-06 |
| Reservoir Length (ft) | 7500 |
| Reservoir Width (ft) | 330 |
| Reservoir Temperature (F) | 170 |
| Well Radius (ft) | 0.35 |
| Sand Face Pressure Pressure (Psia) | 500 |
| Terminal Rate (MMscf/D) | 0.005 |
| Fracture Conductivity (Dimensionless) | 1.0E+06 |
| Fracture Skin | 0 |
| **PVT Properties** | |
| PVT Correlation | B.W.R (Table) - default |
| Viscosity Correlation | Carr et al. - default |
| Gas Type | Dry gas |
| Separator Gas Gravity | 0.65 |
| Carbon Dioxide Content (%) | 0 |
| Hydrogen Sulfide Content (%) | 0 |
| Nitrogen Content (%) | 0 |
| Gas Critical Temperature (R ) | 374 |
| Gas Critical Pressure (psia) | 670.91 |
| Water General Correlation | Meehan - Default |
| Water Gravity | 1 |
| Water Salinity (ppm) | 35000 |
| Irreducible Water Saturation (%) | 40 |

Table 4—Base case analytical model parameters.

**Fig. 22** is a top view of the model's schematic. The yellow vertical diamonds are vertical fractures, the dotted lines represent the no-flow boundaries caused by fracture interference. Finally, the black line is the outer limit of the SRV and the horizontal yellow line is the horizontal wellbore.

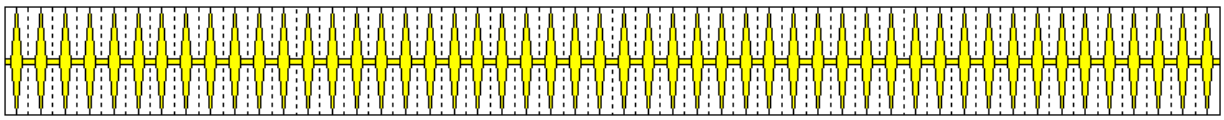

**Fig. 22—Hybrid horizontal multi-fractured well schematic.**

The choice of the hybrid model was based on its ability to incorporate pressure-dependent properties in pseudo time. Using pseudo time allows us to reduce inaccuracies of analytical models when modeling unconventional gas wells with low permeability, geomechanical reservoir effects or large pressure drawdown. For a single phase gas, the hybrid model reduces significantly the computational time to the level of an analytical model while providing the accuracy of a numerical model (IHS 2014). Adsorption, geomechanical effects and changing skin effects were not included in the analysis in order to focus the analysis of the simulation results on the analytical model parameters.

### 4.2 Scaling Factor Relationship with the Modified Analytical Model Parameters

The following section will present the scaling relationships of the permeability, net-pay thickness, fracture spacing, fracture half-length, lateral length, and drawdown. Other properties from the analytical model such as the compressibility, porosity or viscosity can also be studied; however, we assumed them constant as the wells located in the same GSA would have similar properties. Different simulations were generated to perform a sensitivity study for each parameter, as presented in **Table 5**.

| Parameter (Unit) | Base Case | Case 1 | Case 2 | Case 3 | Case 4 |
|---|---|---|---|---|---|
| Permeability (nD) | 3.9 | 1.95 | 2.73 | 5.07 | 7.8 |
| Fracture Spacing (ft) | 150 | 250 | 187.5 | 100 | 75 |
| Fracture Half Length (ft) | 330 | 150 | 240 | 420 | 510 |
| Lateral Length* (ft) | 7500 | 3000 | 4500 | 9000 | 12000 |
| Net Pay Thickness (ft) | 100 | 25 | 50 | 150 | 200 |
| Pressure | 500 | 250 | 1000 | 1500 | 2000 |
| Drawdown (psi^2/cp) | 1.43E+09 | 1.45E+09 | 1.37E+09 | 1.27E+09 | 1.14E+09 |

*Change in Lateral length does not impact fracture spacing, thus the number of fracture is modified such that the fracture spacing remains constant.

Table 5—Parameters used in analytical model parameter sensitivity study.

As displayed in Table 5, the drawdown is the difference between the pseudo-pressure at the initial reservoir pressure and the sand face pseudo-pressure. The pseudo-pressures are calculated from spreadsheet published by Guo et al. (2007), which integrates numerically Eq. 4. As shown in Table 5, the base case BHP is 500 psia and the BHPs in cases 1 to 4 are 250, 1000, 1500 and 2000 psia.

Since the analytical model generates similar rate-MBT profiles on log-log plots, we simply overlaid case 1 to 4 profiles onto the base case profile. The time and rate scaling factors are identified on **Figs. 23 to 46** by the acronyms TSF and RSF. The scaling factors were found by trial and error using an optimization algorithm programmed with Solver in VBA. The profiles were first shifted horizontally by changing the TSF until the profiles reached a parallel position. Then the profile was shifted vertically by changing the RSF in order to overlay the base case. The TSF and RSF are displayed on the right plots in Figs. 23 to 46 and also summarized in **Table 6** to Table 11.

As we conducted the scaling on the log-log plot of the rate versus MBT, we also matched the log-log plot of rate vs. time and the Cartesian plot of cumulative production vs. time. A cumulative scaling factor (CSF) was used instead of a RSF on the cumulative plots to shift the profiles vertically. The results presented in the following sub-sections demonstrate the scaling factor relationships for each property. Furthermore, we demonstrate that the scaling factors are proportionally related to the analytical model parameters.

### *4.2.1 Permeability*

Figs 23 to 25 show the results of the sensitivity study of the four cases with different permeabilities. By visually inspecting Fig. 23 we recognize that all the production profiles generated analytically, can be rescaled to match the base case scenario since they present the same characteristic shape with a negative half slope transient period followed by the negative unit slope.

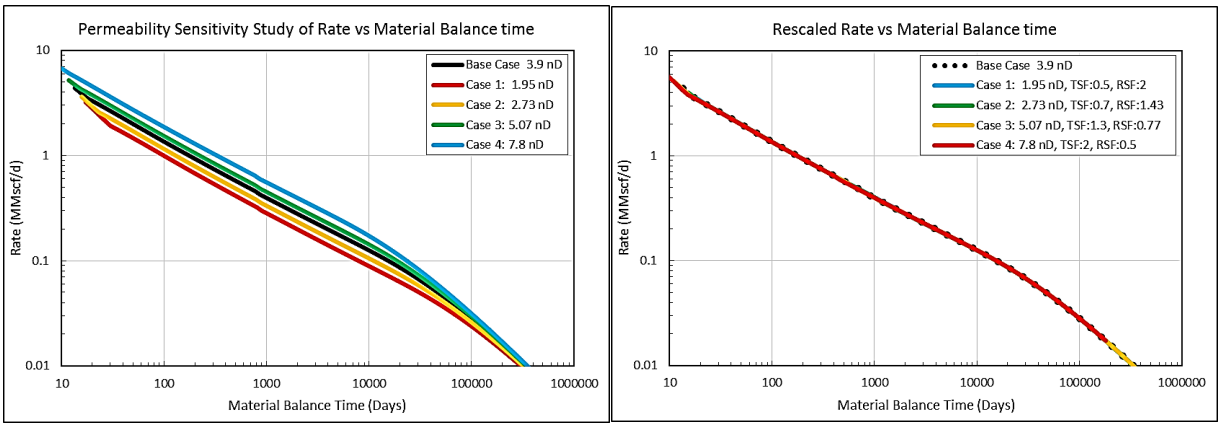


**Fig. 23—Left: permeability rate MBT profiles. Right: scaled rate MBT profiles.**

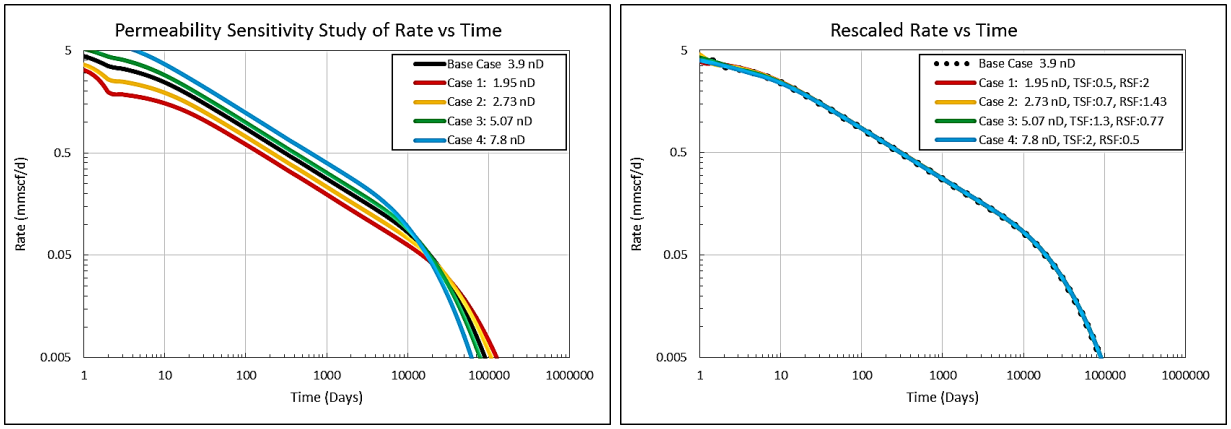


**Fig. 24—Left: permeability rate time profiles. Right: scaled rate time profiles.**

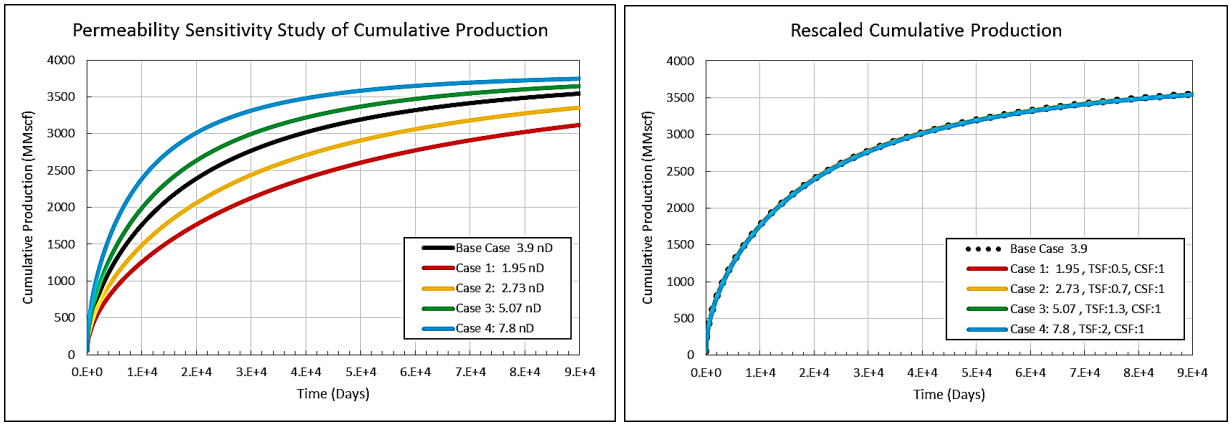


**Fig. 25—Left: permeability cumulative profiles. Right: scaled cumulative profiles.**

A summary of the scaling factors given on the previous figures is presented in Table 6.

| Plot | Rate vs. MBT Plot | | Rate vs. Time Plot | | Cumulative vs. Time Plot | |
|---|---|---|---|---|---|---|
| Scaling factor | Time | Rate | Time | Rate | Time | Cumulative |
| Base Case: 3.9 nD | 1 | 1 | 1 | 1 | 1 | 1 |
| Case 1: 1.95 nD | 0.5 | 2 | 0.5 | 2 | 0.5 | 1 |
| Case 2: 2.73 nD | 0.7 | 1.43 | 0.7 | 1.43 | 0.7 | 1 |
| Case 3: 5.07 nD | 1.3 | 0.77 | 1.3 | 0.77 | 1.3 | 1 |
| Case 4: 7.80 nD | 2 | 0.5 | 2 | 0.5 | 2 | 1 |

Table 6—Scaling factors of the permeability sensitivity study.

We observe that the TSF and the RSF are inversely proportional and directly correlated to the difference in permeability. The relationship can be described by Eq. 13 where $k$ is the permeability of the profile that is rescaled to match the base case profile, which has the reference permeability $k_{ref}$. Because the TSF and RSF are inversely proportional, a change in permeability will shift the curve on a negative unit slope on the log-log plot of rate versus MBT as shown in Fig. 23.

$$TSF_k = \frac{1}{RSF_k} = \frac{k}{k_{ref}} \tag{13}$$

Further observations of the cumulative scaling factors entail that the cumulative profile do not require to be rescaled vertically. In other words, changing the permeability of the analytical model will only impact the time required to produce a given cumulative volume, thus doubling the permeability would reduce the time by a factor of two.

### *4.2.2 Fracture Spacing*

Figs. 26 to 28 show the sensitivity study of the four cases with different fracture spacing. As for the permeability, visually inspecting Fig. 23 shows that all the production profiles generated analytically can be rescaled to match the base case scenario since they present the same characteristic shape with a negative half slope period followed by a negative unit slope.

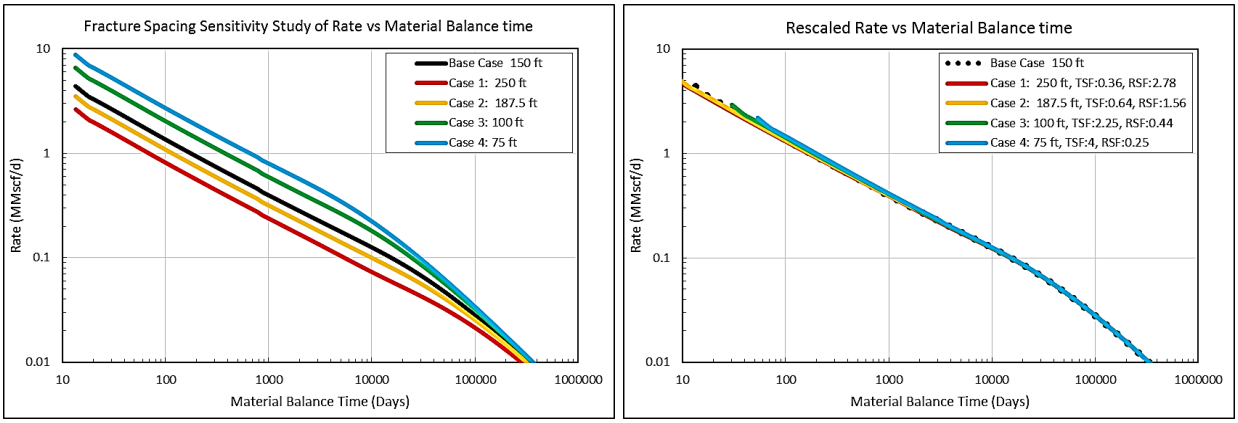


**Fig. 26—Left: fracture spacing rate MBT profiles. Right: scaled rate MBT profiles.**

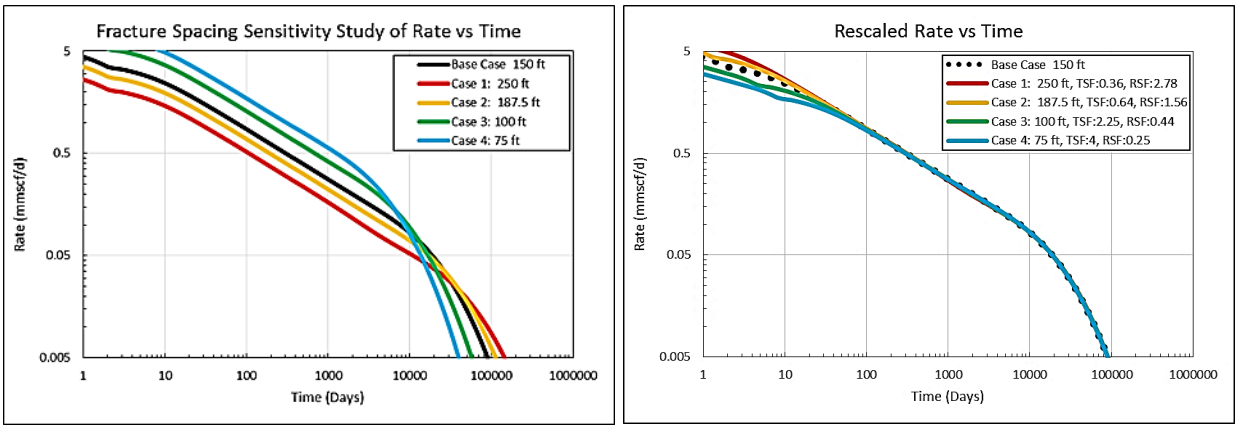


**Fig. 27—Left: Fracture spacing rate-time profiles. Right: scaled rate-time profiles.**

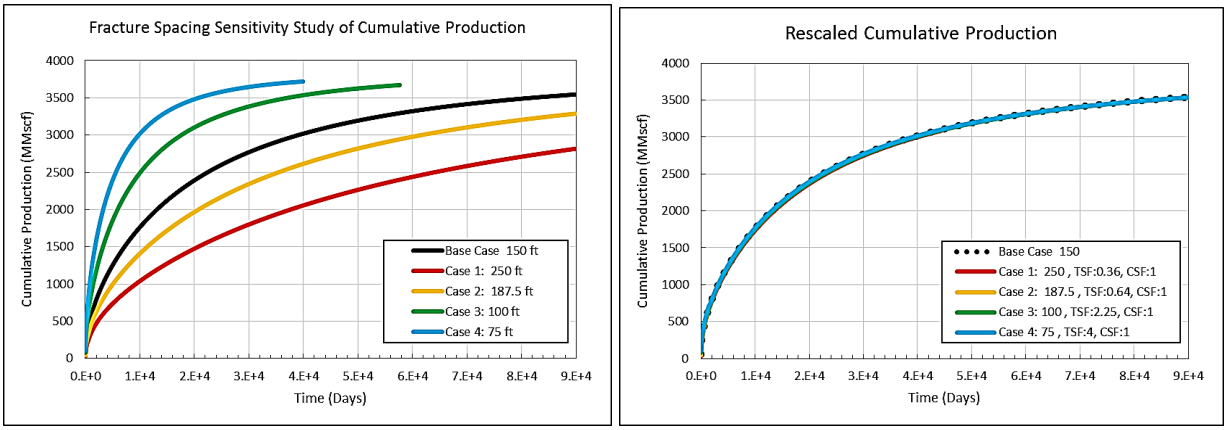


**Fig. 28—Left: fracture spacing cumulative profiles. Right: scaled cumulative profiles.**

A summary of the scaling factors given on the previous figures is presented in Table 7.

| Plot | Rate vs. MBT Plot | | Rate vs. Time Plot | | Cumulative vs. Time Plot | |
|---|---|---|---|---|---|---|
| Scaling factor | Time | Rate | Time | Rate | Time | Cumulative |
| Base Case 150 ft | 1 | 1 | 1 | 1 | 1 | 1 |
| Case 1: 250 ft | 0.36 | 2.78 | 0.36 | 2.78 | 0.36 | 1 |
| Case 2: 187.5 ft | 0.64 | 1.56 | 0.64 | 1.56 | 0.64 | 1 |
| Case 3: 100 ft | 2.25 | 0.44 | 2.25 | 0.44 | 2.25 | 1 |
| Case 4: 75 ft | 4 | 0.25 | 4 | 0.25 | 4 | 1 |

Table 7—Scaling factors of the fracture spacing sensitivity study.

As for the permeability relationship, we observe that the TSF and the RSF presented in Table 7 are inversely proportional and directly correlated to the difference in fracture spacing squared. The relationship can be described by Eq. (14) where $F_s$ is the fracture spacing of the profile that is rescaled to match the base case profile, which has the reference spacing $F_{s,ref}$. Because the TSF and RSF are inversely proportional, a change in fracture spacing between two identical wells will shift the curve on a negative unit slope on the rate-MBT log-log plot as shown in Fig. 23.

$$TSF_{FS} = \frac{1}{RSF_{FS}} = \left(\frac{F_{s,ref}}{F_s}\right)^2 \tag{14}$$

Further observation of the cumulative scaling factors leads us to conclude that the cumulative profiles do not need to be rescaled vertically for a change in fracture spacing. *Changes in fracture spacing impact only the time required to produce a given cumulative volume.*

### *4.2.3 Fracture Half Length*

Figs. 29 to 31 show the sensitivity study of the four cases with different fracture half length. Fig. 29 shows that all the production profiles are parallel and can be rescaled by shifting the curve on the vertical axis.

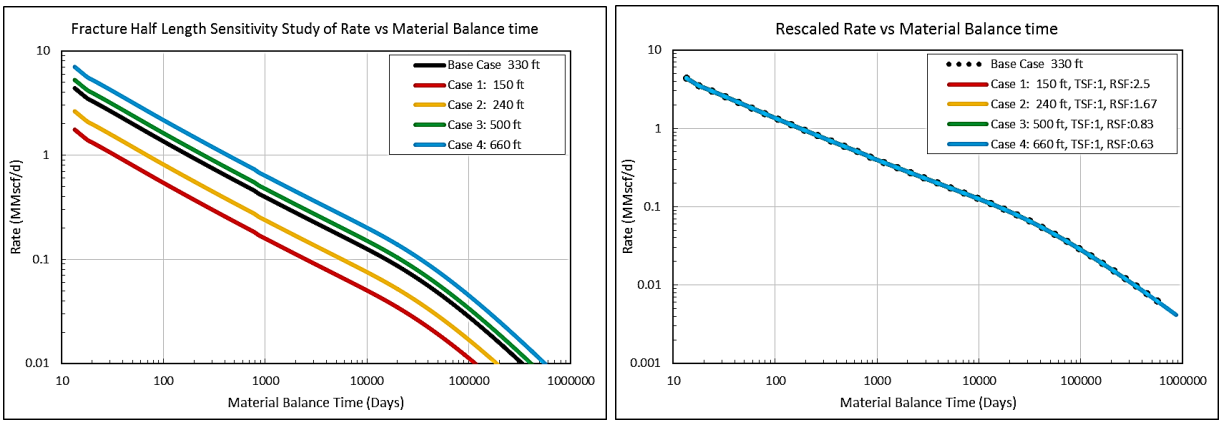


**Fig. 29—Left: fracture half-length rate MBT profiles. Right: scaled rate MBT profiles.**

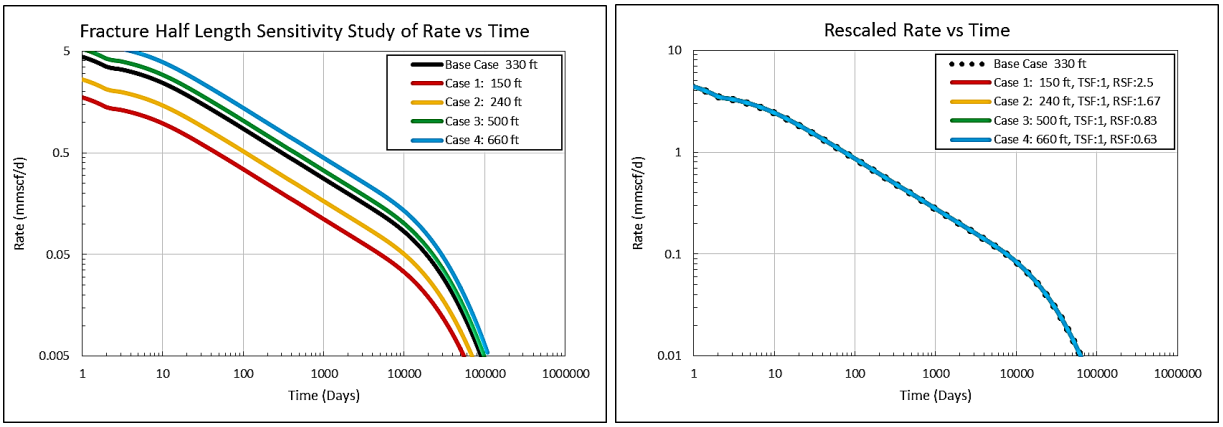


**Fig. 30—Left: fracture half-length rate time profiles. Right: scaled rate time profiles.**

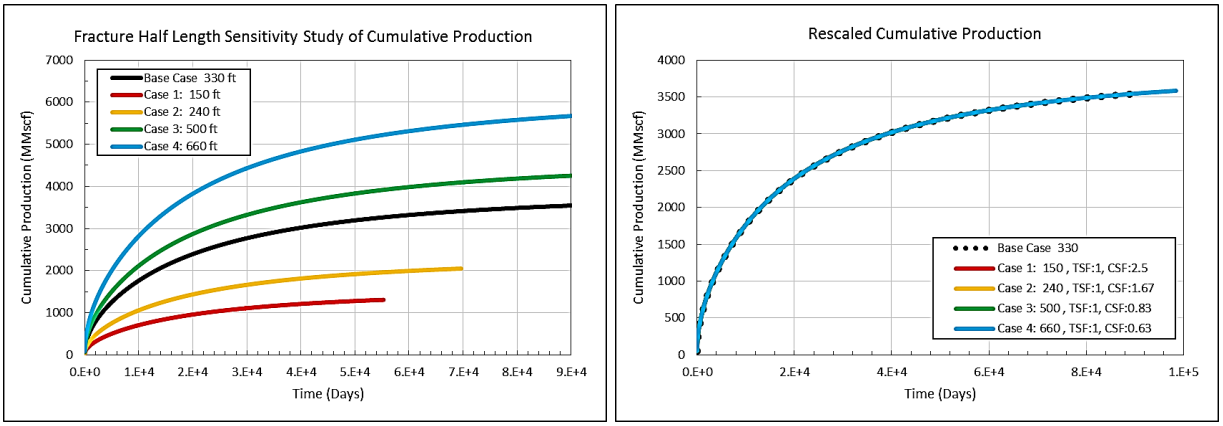


**Fig. 31—Left: fracture half-length cumulative profiles. Right: scaled cumulative profiles.**

A summary of the scaling factors given on the previous figures is presented in Table 8.

| Plot | Rate vs. MBT Plot | | Rate vs. Time Plot | | Cumulative vs. Time Plot | |
|---|---|---|---|---|---|---|
| Scaling factor | Time | Rate | Time | Rate | Time | Cumulative |
| Base Case 330 ft | 1 | 1 | 1 | 1 | 1 | 1 |
| Case 1: 150 ft | 1 | 2.5 | 1 | 2.5 | 1 | 2.5 |
| Case 2: 240 ft | 1 | 1.67 | 1 | 1.67 | 1 | 1.67 |
| Case 3: 500 ft | 1 | 0.83 | 1 | 0.83 | 1 | 0.83 |
| Case 4: 660 ft | 1 | 0.63 | 1 | 0.63 | 1 | 0.63 |

Table 8—Scaling factors of the fracture half-length sensitivity study.

As opposed to the permeability and fracture spacing relationships, we observe that a change in fracture half-length does not require a time shift since the TSF is always equal to 1. However, we find that the RSF presented in Table 8 are directly correlated to the difference in fracture half length. The relationship can be described by Eq. 15 where $x_f$ is the fracture half length of the profile that is rescaled to match the base case profile, which has the reference half-length $x_{f,ref}$. Because a change in fracture half-length results only in a change of RSF and CSF, a change in fracture half-length between two identical wells would only shift the curve vertically on the log-log plot of rate versus MBT as shown in Fig. 29. Further observations on the cumulative profile shows that the recovery is proportional to the change in fracture half-length for the same producing time.

$$RSF_{xf} = CSF_{xf} = \frac{x_{f\,ref}}{x_f} \tag{15}$$

### *4.2.4 Lateral Length*

Figs. 32 to 34 show the sensitivity study of the four cases with different well lateral lengths, while fracture spacing remains constant. To keep the fracture spacing constant, the number of fractures calculated with Eq.7 allows us to account for the change in lateral length. As for the fracture half-length, Fig. 32 shows that all the production profiles are parallel and can be rescaled by shifting the curve vertically.

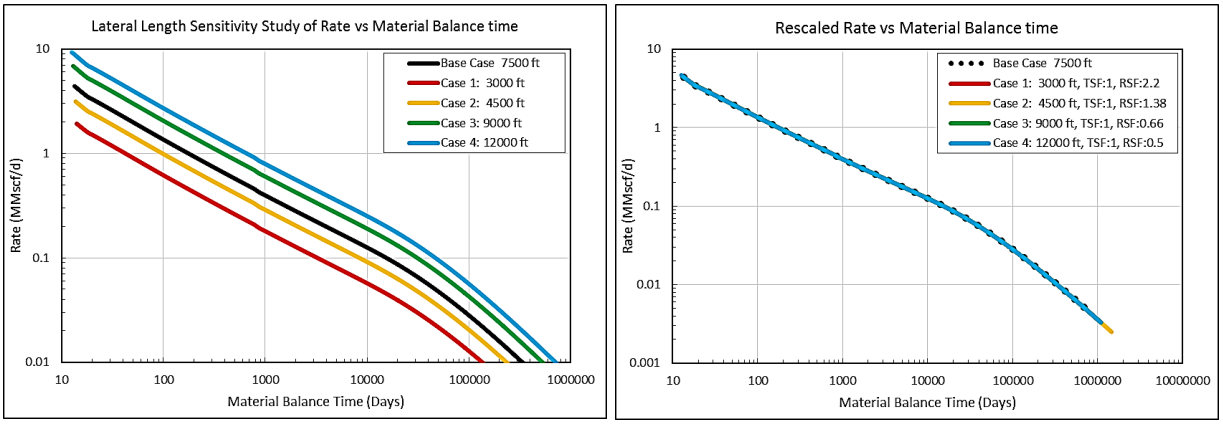


**Fig. 32—Left: lateral length rate MBT profiles. Right: scaled rate MBT profiles.**

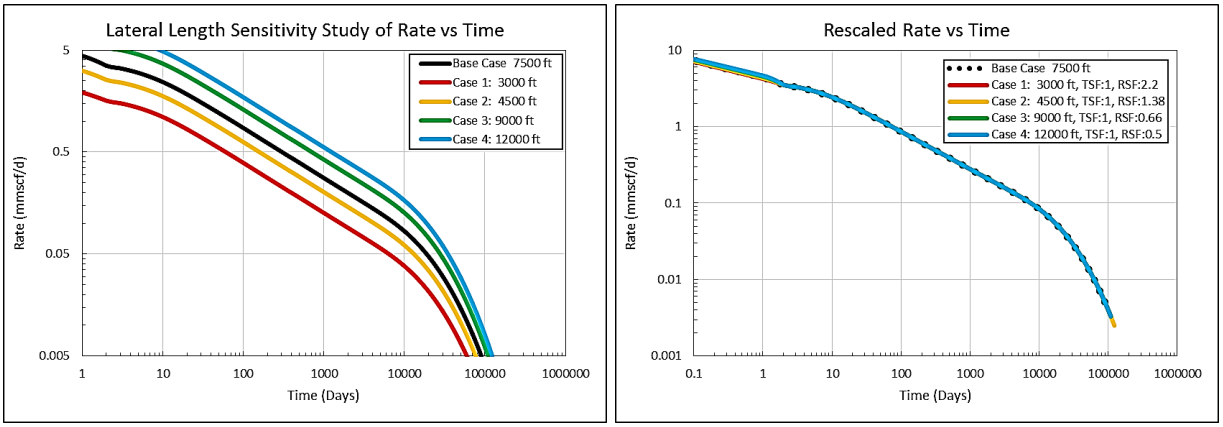


**Fig. 33—Left: lateral length rate time profiles. Right: scaled rate time profiles.**

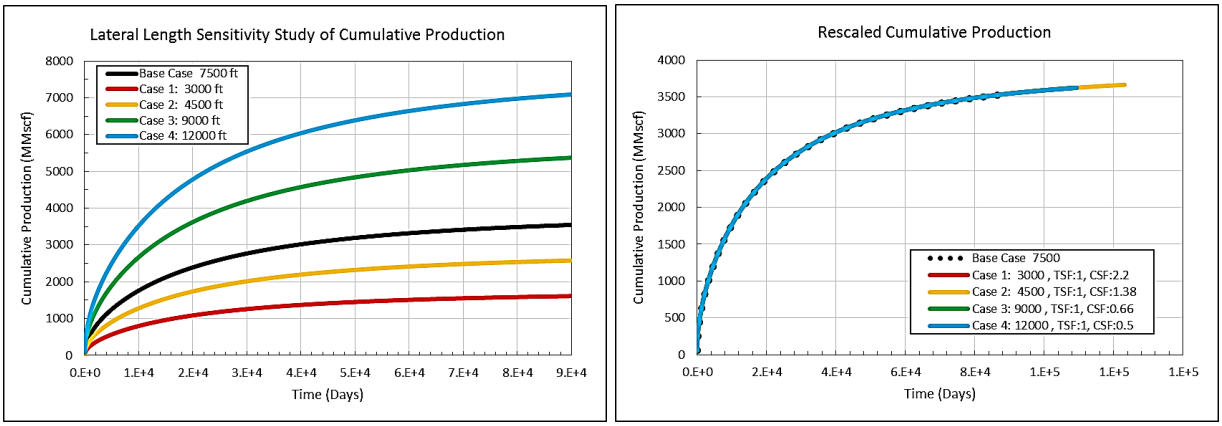


**Fig. 34—Left: lateral length cumulative profiles. Right: scaled cumulative profiles.**

A summary of the scaling factors given on the previous figures is presented in Table 9.

| Plot | Rate vs. MBT Plot | | Rate vs. Time Plot | | Cumulative vs. Time Plot | |
|---|---|---|---|---|---|---|
| Scaling factor | Time | Rate | Time | Rate | Time | Cumulative |
| Base Case 7500 ft | 1 | 1 | 1 | 1 | 1 | 1 |
| Case 1: 3000 ft | 1 | 2.2 | 1 | 2.2 | 1 | 2.2 |
| Case 2: 4500 ft | 1 | 1.38 | 1 | 1.38 | 1 | 1.38 |
| Case 3: 9000 ft | 1 | 0.66 | 1 | 0.66 | 1 | 0.66 |
| Case 4: 12000 ft | 1 | 0.5 | 1 | 0.5 | 1 | 0.5 |

Table 9—Scaling factors of the lateral length sensitivity study.

Similar to the effect of fracture half length, we observe that a change in lateral length does not require a time shift since the TSF is always equal to 1. However, we find that the RSF presented in Table 9 are directly correlated to the difference in lateral length. The relationship can be described by Eq. 16 where $L$ is the lateral length of the profile that is rescaled to match the base case profile, which has the reference lateral length $L_{ref}$. Because a change in lateral length results only in a change of RSF and CSF, a change in lateral length between two identical wells would only shift the curve vertically on the log-log plot of rate versus MBT as shown in Fig. 32. Further observations on the cumulative profile shows that the EUR is proportional to the change in fracture lateral length because it is one of the parameters that governs the total SRV as shown in Fig. 8.

$$RSF_L = CSF_L = \frac{L_{ref}}{L} \tag{16}$$

### *4.2.5 Net-Pay Thickness*

Figs. 35 to 37 show the sensitivity study of the four cases with different net-pay thicknesses. As for the results of the fracture half-length and the lateral length studies presented previously, Fig. 35 shows that all the production profiles are parallel and can be rescaled by shifting the curve on the vertical axis.

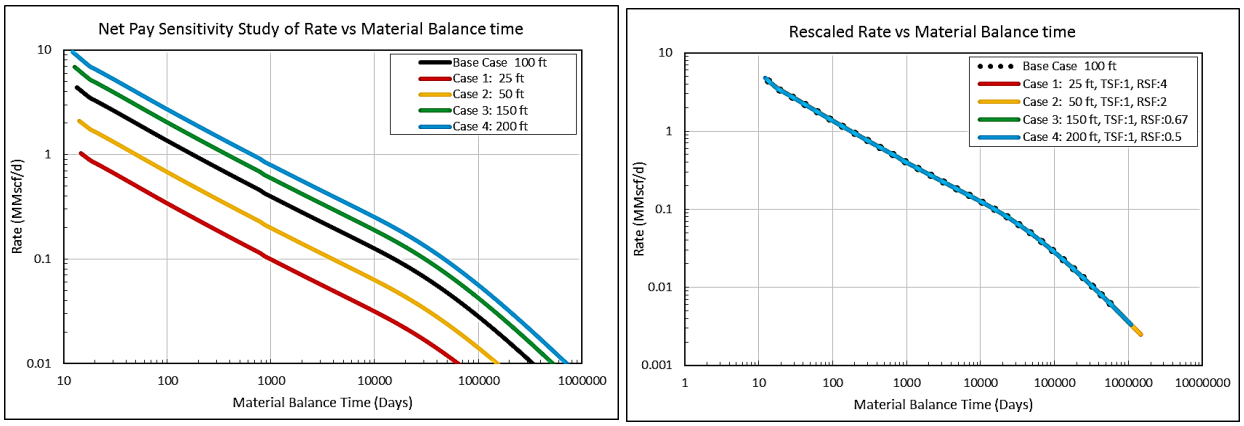


**Fig. 35—Left: net pay rate MBT profiles. Right: scaled rate MBT profiles.**

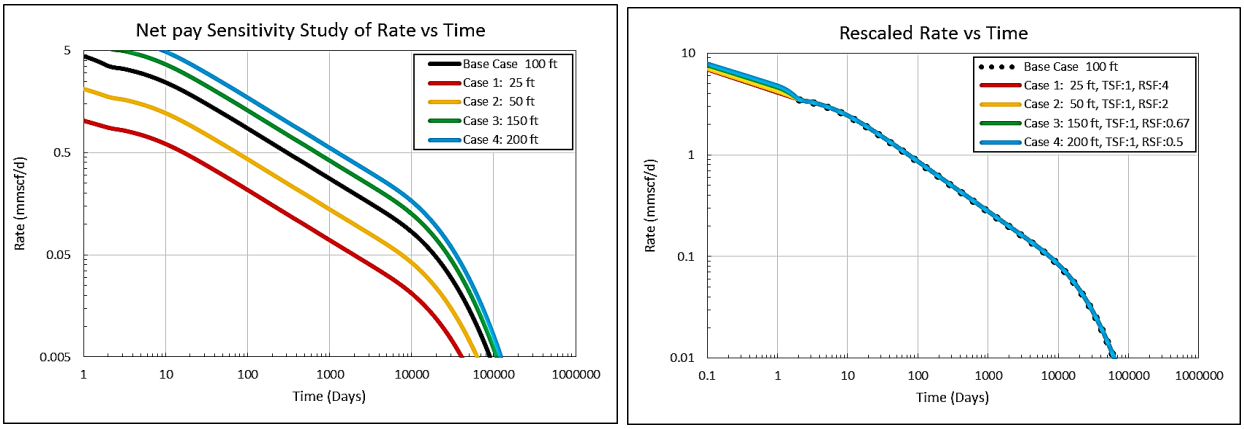


**Fig. 36—Left: net pay rate time profiles. Right: scaled rate time profiles.**

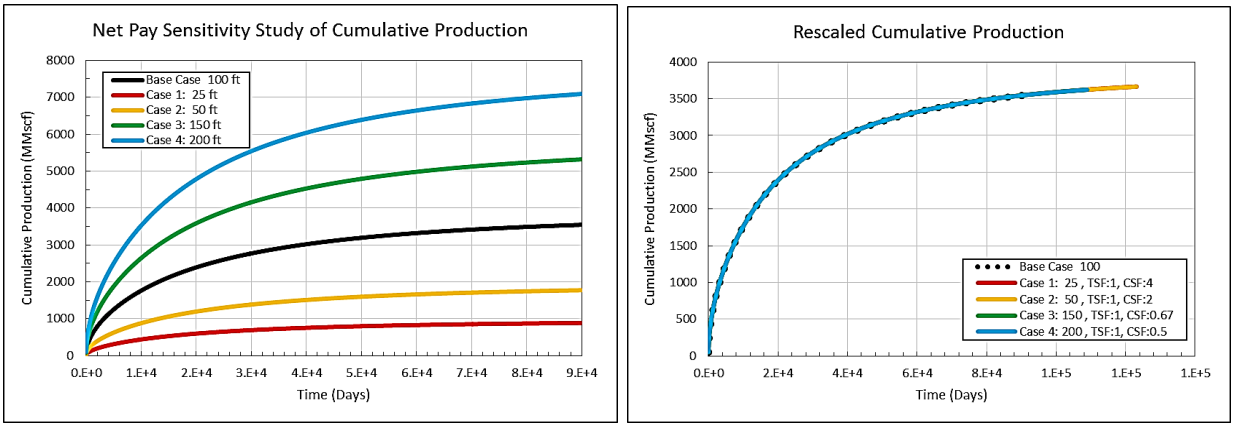


**Fig. 37—Left: net pay cumulative profiles. Right: scaled cumulative profiles.**

A summary of the scaling factors given on the previous figures is presented in Table 10.

| Plot | Rate vs. MBT Plot | | Rate vs. Time Plot | | Cumulative vs. Time Plot | |
|---|---|---|---|---|---|---|
| Scaling factor | Time | Rate | Time | Rate | Time | Cumulative |
| Base Case 100 ft | 1 | 1 | 1 | 1 | 1 | 1 |
| Case 1: 25 ft | 1 | 4 | 1 | 4 | 1 | 4 |
| Case 2: 50 ft | 1 | 2 | 1 | 2 | 1 | 2 |
| Case 3: 150 ft | 1 | 0.67 | 1 | 0.67 | 1 | 0.67 |
| Case 4: 200 ft | 1 | 0.5 | 1 | 0.5 | 1 | 0.5 |

Table 10—Scaling factors of the net pay sensitivity study.

Similar to the results of the fracture half-length and the lateral length studies, we observe that a change in net pay does not require a time shift since the TSF is always equal to 1. However, we find that the RSF presented in Table 9 are directly correlated to the difference in net pay thickness. The relationship is described by Eq. 17 where $h$ is the net pay of the profile that is rescaled to match the base case profile, which has the reference lateral length $h_{ref}$. Because a change in lateral length results only in a change of RSF and CSF, a change in net pay thickness between two identical wells would only shift the curve vertically on the log-log plot of rate versus MBT as shown in Fig. 35. Further observations of the cumulative profile shows that the EUR is proportional to the change in net pay because it is one of the parameters that governs the total stimulated matrix volume as shown in Fig. 8.

$$RSF_L = CSF_L = \frac{h_{ref}}{h} \tag{17}$$

### *4.2.6 Drawdown*

As opposed to the other parameters presented in the previous subsections, the pseudo-pressure changes with time since it is integrated from a low base pressure to the average reservoir pressure as shown in Eq. 4. As presented by Aziz et al. (1976), the pseudo-pressure in transient flow must be calculated using the initial reservoir pressure while the average reservoir pressure should be used in BDF. Since the average reservoir pressure changes over time during BDF, it directly impacts the pseudo-pressure calculation. Anderson and Mattar (2007) present the pseudo-time function as a semi-analytical technique that requires a material balance analysis and an approximation of the distance of investigation. Because such analysis is commonly not possible without pressure data and with only monthly reported production volumes, we propose a conservative scaling relationship for the transient period only. Until the transient reaches all the boundaries of the reservoir, some parts of the reservoir are still at initial reservoir pressure. Therefore, we assume that the average reservoir pressure remains equal to the initial reservoir pressure until the end of the transient flow regime. Black arrows in Figs. 35 to 37 point to the approximate time at which the transient linear flow regime ends. Figs. 41 to 43 are identical to Figs. 38 to 40 but show only the transient flow regime.

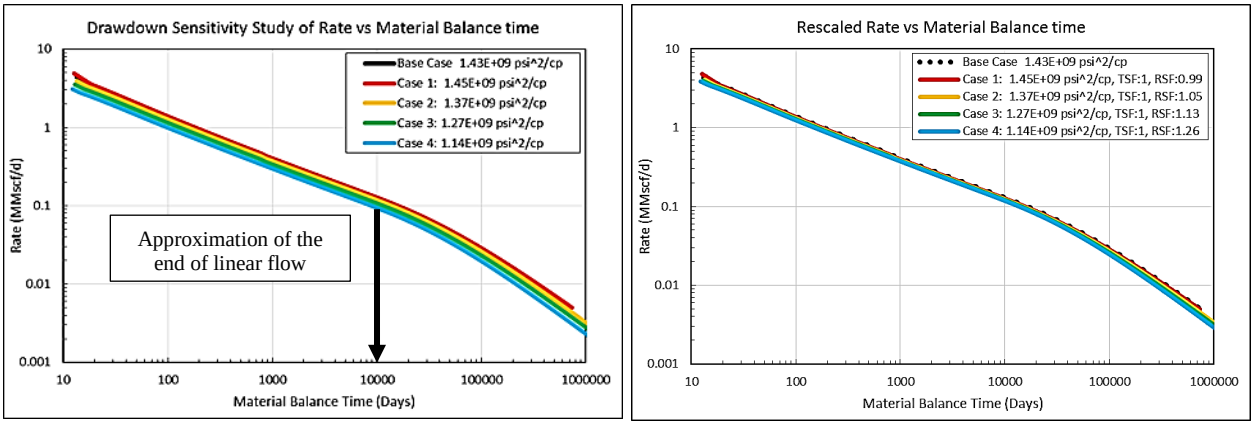


**Fig. 38—Left: drawdown rate MBT profiles. Right: scaled rate MBT profiles.**

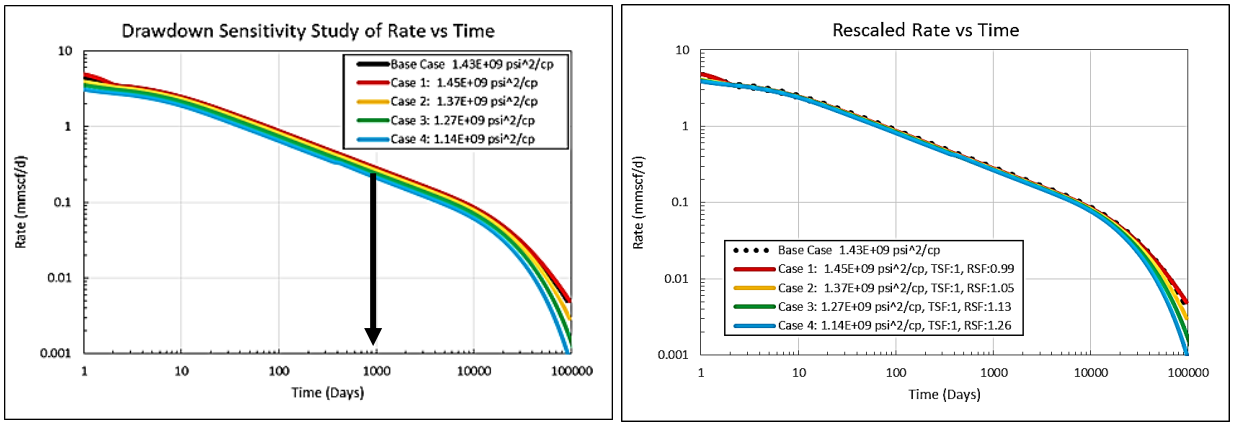


**Fig. 39—Left: drawdown rate time profiles. Right: scaled rate time profiles.**

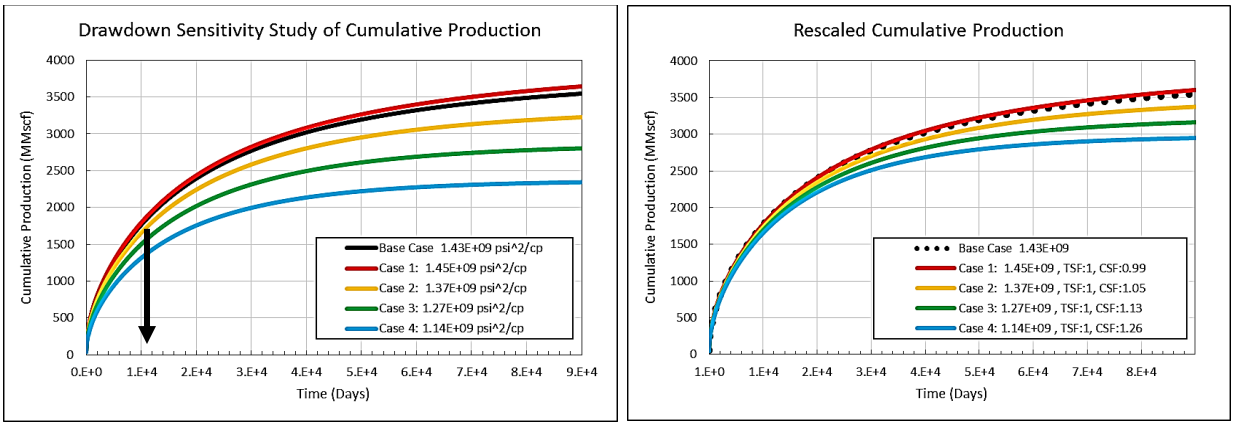


**Fig. 40—Left: drawdown cumulative profiles. Right: scaled cumulative profiles.**

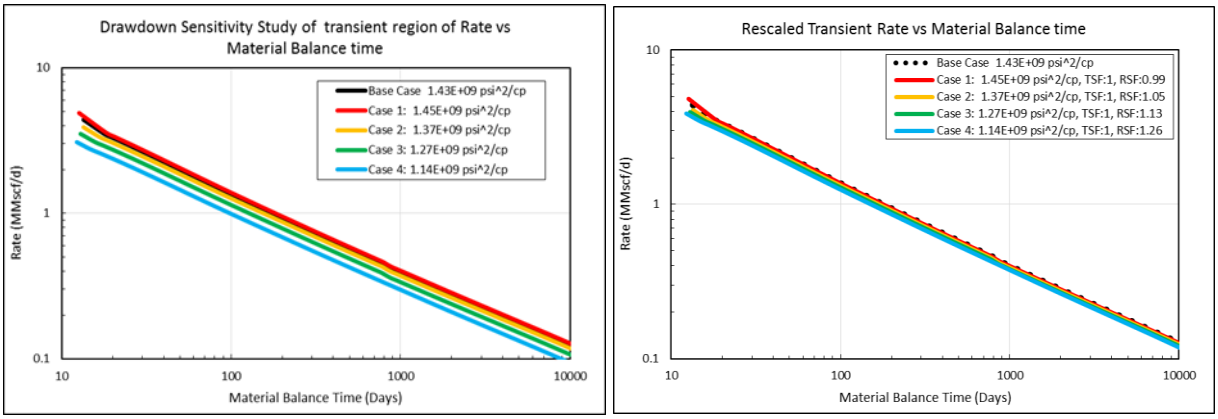


**Fig. 41—Left: transient drawdown rate MBT profiles. Right: scaled rate MBT profiles.**

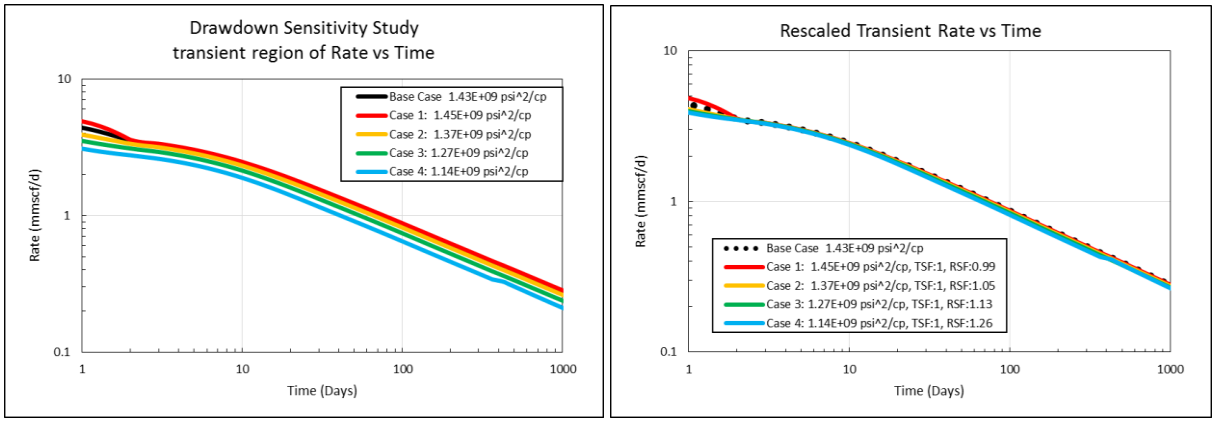


**Fig. 42—Left: transient drawdown rate time profiles. Right: scaled rate time profiles.**

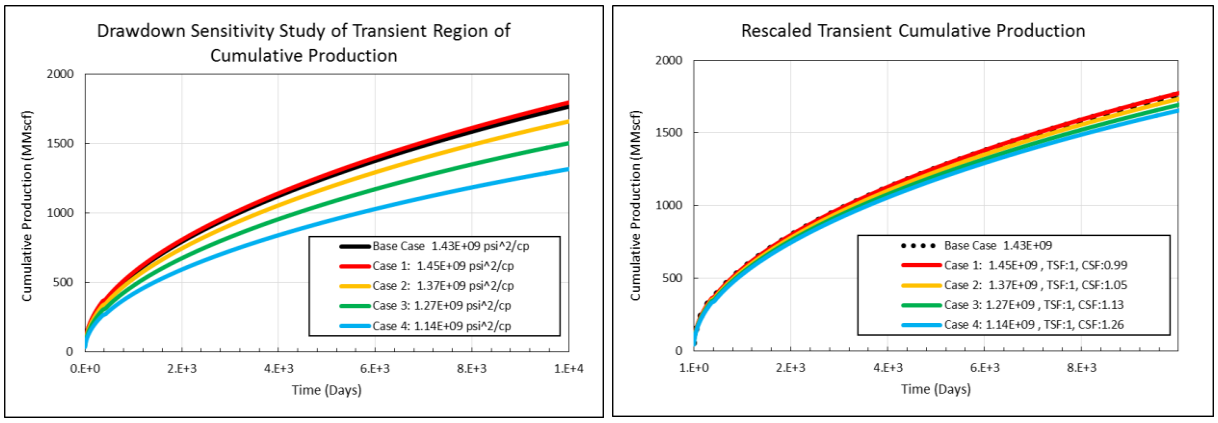


**Fig. 43—Left: transient drawdown cumulative profiles. Right: scaled cumulative profiles.**

Fig. 41 shows that the profiles are parallel to each other at early time; therefore, we rescaled the profiles only vertically based on the ratio of pseudo-pressure drawdown shown in Eq. 18. The right plots of Figs. 41 to 43 demonstrate that the proposed scaling factor relationship for the difference in drawdown allows us to rescale approximately the production profiles. However, Fig. 43 shows that the profiles do not match exactly although the scaling significantly reduces the divergence of the cumulative profiles. This behavior may be caused by the pseudo-pressure calculation method with a material-balance average reservoir pressure used in the analytical model. Nevertheless, the following equation summarizes the scaling factor relationship for drawdown.

$$RSF_{DD} = \frac{DD_{ref}}{DD} \tag{18}$$

A summary of the scaling factors given on the previous figures is presented in Table 11

| Plot | Rate vs. MBT Plot | | Rate vs. Time Plot | | Cumulative vs. Time Plot | |
|---|---|---|---|---|---|---|
| Scaling factor | Time | Rate | Time | Rate | Time | Cumulative |
| Base Case 1.43E+09 psi^2/cp | 1 | 1 | 1 | 1 | 1 | 1 |
| Case 1: 1.45E+09 psi^2/cp | 1 | 0.99 | 1 | 0.99 | 1 | 0.99 |
| Case 2: 1.37E+09 psi^2/cp | 1 | 1.05 | 1 | 1.05 | 1 | 1.05 |
| Case 3: 1.27E+09 psi^2/cp | 1 | 1.13 | 1 | 1.13 | 1 | 1.13 |
| Case 4: 1.14E+09 psi^2/cp | 1 | 1.26 | 1 | 1.26 | 1 | 1.26 |

Table 11—Scaling factors of the drawdown sensitivity study.

### *4.2.7 Summary of Analytical Scaling Factors*

Scaling factors were correlated to differences in permeability, net pay thickness fracture spacing, fracture half-length, and lateral length. A scaling relationship was proposed for the transient region only because it cannot properly account for the change in average reservoir pressure in BDF. **Table 12** summarizes Eq. 13 to 18 for the rate-time and cumulative-time scaling factor relationships. The equations presented below allow us to scale a production profile onto any reference production profile based on known parameters.

| | Rate-Time | | Cumulative-Time | |
|---|---|---|---|---|
| Parameters | TSF | RSF | TSF | CSF |
| Permeability | $\frac{k}{k_{ref}}$ | $\frac{k_{ref}}{k}$ | $\frac{k}{k_{ref}}$ | 1 |
| Fracture Spacing | $\left(\frac{F_{s,ref}}{F_s}\right)^2$ | $\left(\frac{F_s}{F_{s,ref}}\right)^2$ | $\left(\frac{F_{s,ref}}{F_s}\right)^2$ | 1 |
| Fracture Half Length | 1 | $\frac{x_{f_{ref}}}{x_f}$ | 1 | $\frac{x_{f_{ref}}}{x_f}$ |
| Lateral Length | 1 | $\frac{L_{ref}}{L}$ | 1 | $\frac{L_{ref}}{L}$ |
| Net Pay Thickness | 1 | $\frac{h_{ref}}{h}$ | 1 | $\frac{h_{ref}}{h}$ |
| Drawdown* | 1 | $\frac{DD_{ref}}{DD}$ | 1 | $\frac{DD_{ref}}{DD}$ |

*Scaling relationship approximatively valid for transient linear flow

Table 12—Analytical scaling factors relationships.

Several observations can be made from the summary of the results in Table 12 because it addresses fundamental relationships of flow in porous media. By investigating the cumulative-time scaling factors, we can identify two groups of parameters. The first group is "depletion" parameters, permeability and the fracture spacing, which control the rate at which the reservoir depletes with time. The relationship of those parameters is consistent with the distance of investigation given by Eq. 19, which is a modified version of Eq. 3 from Wattenbarger et al. (1998). Since the dimensionless time at which the transient flow regime ends is equal to 0.25 for a constant BHP, the time at which the transient is affected by the boundary can be expressed in days as a function of the permeability and the distance to the permeability boundary:

$$t = \frac{0.25 * (\emptyset \mu c_t)_i * y_e^2}{0.00633 * k} \tag{19}$$

Hence, an increase in fracture spacing increases the distance from the fracture to the no-flow boundary and therefore increases the duration of the transient flow regime by a factor of $y_e^2$, which is consistent with the scaling factor relationship recorded in Table 12. The same principle applies to the effect of permeability: an increase in permeability will reduce the duration of transient flow. The reason why the TSF and the RSF are inversely proportional can be explained with Eqs. 9 or 12 in which the ratio $F_s^2/k$ is also present. Hence, an increase in rate can be correlated to either an increase in permeability or a decrease in fracture spacing at any dimensionless rate. This observation is intuitive; a decrease in fracture spacing means an increase in the number of fractures for a fixed lateral length.

The second group consists of fracture half length, lateral length and net pay, all of which affect SRV as Eq. 20 indicates:

$$V = 2 * x_f * L * h \tag{20}$$

Furthermore, because those parameters are present only in Eq. 11 for the rate match point and not in Eq. 12 for the time match point, they rescale only the rate or cumulative profiles. As demonstrated in Appendix B, if the match points were used in to match an actual profile instead of the type curve, the rate match point and the time match point will reflect the product of scaling

factors given different reservoir and completion properties. The following example will demonstrate the multiplicative properties of the time and rate scaling factors. A synthetic production profile, case 5, was created with different fracture and matrix properties to analyze the scaling factors required to overlay it on the base case profile. **Table 13** summarizes the model parameters.

| Parameters (Units) | Base Case | Case 5 |
|---|---|---|
| Permeability (nD) | 3.9 | 2.73 |
| Fracture Spacing (ft) | 150 | 114 |
| Fracture Half Length (ft) | 330 | 420 |
| Lateral Length* (ft) | 7500 | 8500 |
| Net Pay Thickness (ft) | 100 | 90 |
| Drawdown (psi^2/cp) | 1.43E+09 | 1.43E+09 |

Table 13—Summary of multi-parameter scaling study

We applied the same scaling methodology based on the VBA algorithm to match the production profiles on the various plots displayed in Figs. 44 to 46. The TSF for the rate-time profile is 1.212, the RSF is 0.636, and the CSF is 0.77.

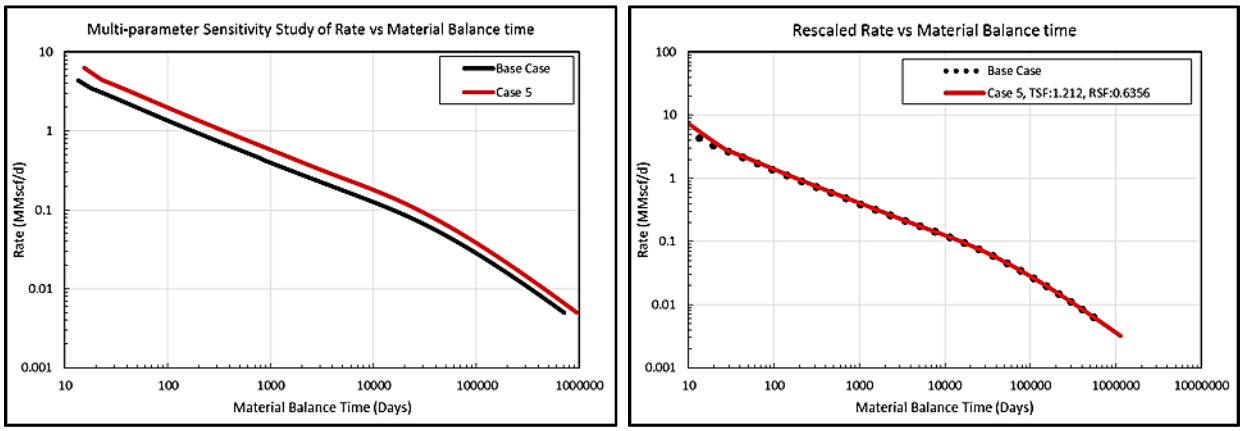


**Fig. 44—Left: multi-parameter rate MBT profiles. Right: scaled rate MBT profiles.**

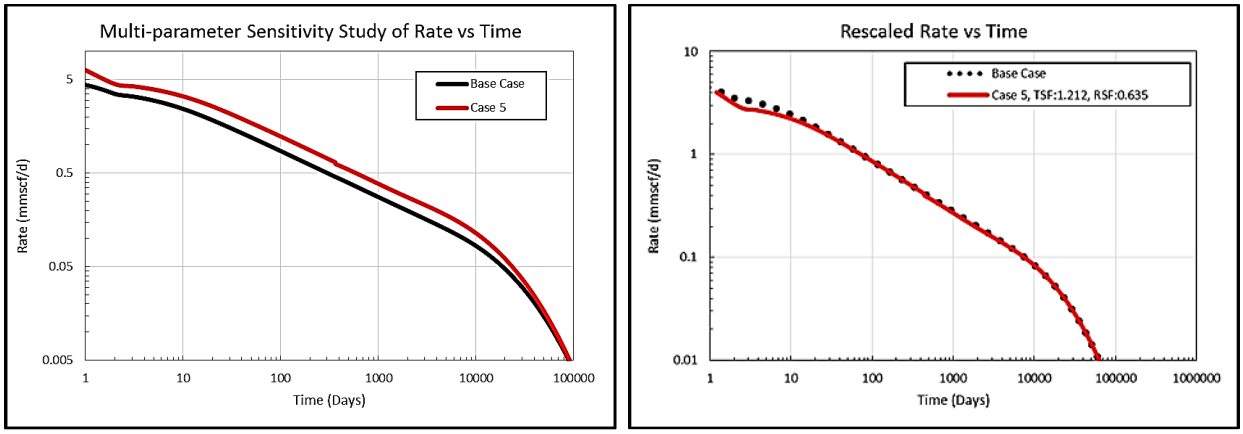


**Fig. 45—Left: multi-parameter rate time profiles. Right: scaled rate time profiles.**

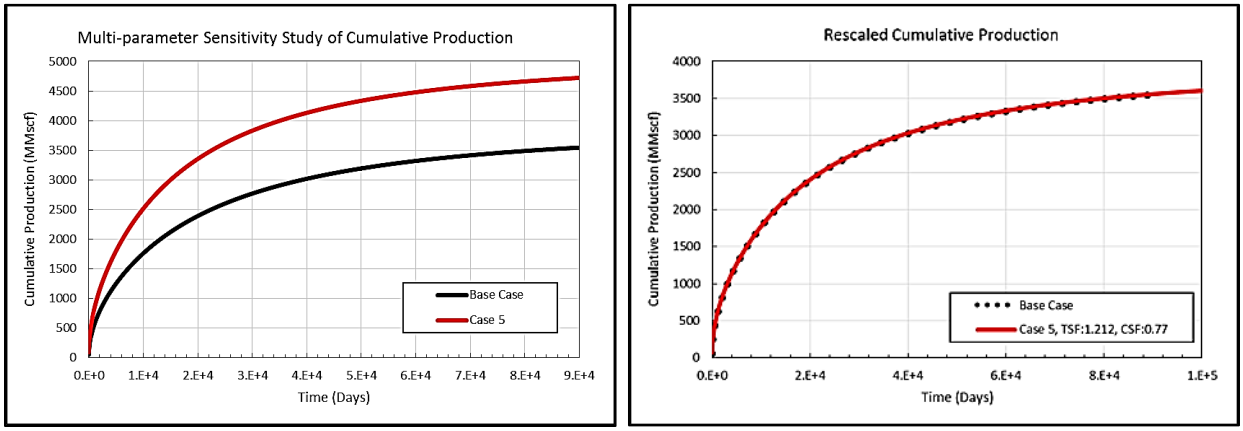


**Fig. 46—Left: multi-parameter cumulative profiles. Right: scaled cumulative profiles.**

We found that the scaling factors presented in Figs. 44 to 46 are directly related to the product of the scaling factors of Table 12 and are presented in **Table 14**. In summary, the final scaling factors are the products of each individual parameter scaling factors.

| | Rate-Time | | Cumulative-Time | |
|---|---|---|---|---|
| Parameters | TSF | RSF | TSF | CSF |
| Permeability | 0.70 | 1.43 | 0.70 | 1.00 |
| Fracture Spacing | 1.73 | 0.58 | 1.73 | 1.00 |
| Fracture Half Length | 1.00 | 0.79 | 1.00 | 0.79 |
| Lateral Length | 1.00 | 0.88 | 1.00 | 0.88 |
| Net Pay Thickness | 1.00 | 1.11 | 1.00 | 1.11 |
| Drawdown* | 1.00 | 1.00 | 1.00 | 1.00 |
| Scaling Factor Product | 1.212 | 0.636 | 1.212 | 0.770 |

Table 14—Multi-parameter scaling factor calculation.

The production profiles for different models can be rescaled based on the differences in individual parameters. Appendix B summarizes the relationships we found in this study, and demonstrates that the match points required to overlay two rate-time profiles are the products of the scaling factor relationships given in Table 12. Since the dimensionless equations are applicable only to the rate-time profile, our study also provides insight into the relationships of scaling factors for the cumulative-time profile. The composite scaling factor relations can thus be described by Eqs. 21 to 23.

$$RSF = RSF_{F_s} * RSF_k * RSF_L * RSF_h * RSF_{x_f} * RSF_{DD} \quad (21)$$

$$TSF = TSF_{F_s} * TSF_k \quad (22)$$

$$CSF = RSF_L * RSF_h * RSF_{x_f} * RSF_{DD} \quad (23)$$

Recalling the need to understand the physical properties of a reservoir and how they affect the depletion in space and time, our observations based on the cumulative profile are that permeability and the fracture spacing govern the time required to deplete a reservoir. Logically, the size of the SRV governs the quantity of fluids we expect to recover. A complicating factor is that the drawdown between the sand face pressure and the average reservoir pressure changes over time after transient flow ends. The diagnostic plots in Figs. 23 to 46 display rate-time and cumulative-time profiles, and they are not corrected for changes in drawdown with time. This observation is important because most analyses that are conducted with monthly produced

volumes and publically reported data cannot be corrected reliably changes in average reservoir pressure. Therefore, we conclude that under the same drawdown, the profiles can be rescaled for permeability, fracture half length, spacing, lateral length and net pay. Since most wells have different sand face pressures and initial pressures due to different depths and the associated pressure gradients, production profiles should be scalable for the drawdown during transient flow. We expect deviations from the scaling relationship during BDF due to changes in average reservoir pressure.

Finally, scaling factors are applicable to the transient period only for two reasons. The first is the fact that the fit of a production profile on a rate-MBT unit-slope decline provides no information about the decline characteristics on a log-log rate-time plot during BDF, for which the b factor can vary from 0 to 1. Second, because drawdown is affected by changes in average reservoir pressure, once a well is in BDF, we can expect large variations in calculated pseudo-pressure differences.

### 4.3 Application of Scaling Factors in Type Well Construction

Using the analytical model described in previous sections, production profiles can be rescaled based on the properties diagnosed with the type curve. The objective of this section is to demonstrate how scaling factors are used to reflect typical production behavior. A limited database containing stage spacing for a small number of wells was available for the Marcellus, Fayetteville, Haynesville and Barnett shale plays. We selected ten wells from each play which displayed BDF and which had relatively smooth and continuous production profiles. Using the procedure described in section 3.2, we estimated the permeability and fracture half-length from the known fracture spacing, gas gravity, lateral length and well depth by matching the modified type curve. Other parameters such as the porosity, pressure gradient, gas saturation, reservoir temperature were taken from Jarvie (2012). Using the known and estimated properties, we then calculated scaling factors to rescale the production profiles to a hypothetical well defined by the average values of each parameter. Given that the BHP data was not accessible, we assumed a similar drawdown for all the Haynesville and the Marcellus wells and estimated it to be 0.1 $p_i$ for the Eagle Ford and Barnett wells.

### *4.3.1 Haynesville Shale Gas Example*

The Haynesville shale is located across eastern Texas and northern Louisiana. It produces thermogenic gas at typical depths of 10,500 to 13,500 ft and has an estimated pressure gradient of 0.8 psi/ft. The Haynesville shale has a reported gas content of 100-330 scf/ton;, 25% of the gas is adsorbed while the rest is free gas in a gas-filled porosity of 6% (Jarvie 2012). To estimate the permeability and fracture half length of the ten profiles presented in **Table 15**, an average net pay thickness of 150 ft was assumed based on an estimated gross thickness of 200 ft. The pseudo-pressure drawdown was estimated to be 3.21E+09 $psi^2/cp$ for an initial reservoir pressure of 9600 psia and a BHP of 500 psia, given a gas gravity of 0.6 and no impurities in the gas. Finally, an average porosity of 8.3% and a reservoir temperature of 825 R were also used in the calculations to estimate permeability and fracture half-length with Eqs. 11 and 12. Table 15 summarizes the results of the analysis in which the wells 1 to 10 were matched to the modified type curve. Columns 8 and 9 in Table 15 present the time and rate match points. These match points were used with Eqs. 11 and 12 to estimate permeability and fracture half length. The last two columns present scaling factors to fit the production profile to a well with lateral length of 5235 ft, fracture spacing of 185 ft and a permeability of 512nD. The ten wells studied have permeabilities ranging from of 330 to 700nD, which is similar to the average permeability of 350 nD reported by Jarvie (2012).

| Well # | API# | Lateral Length | Stage Number | Fs (ft) | xf (ft) | k (nD) | TM | QM | TSF | RSF | CSF |
|---|---|---|---|---|---|---|---|---|---|---|---|
| 1 | 4234733290 | 5345 | 20 | 267 | 175 | 706 | 0.00218 | 0.000132 | 1.05 | 0.99 | 1.04 |
| 2 | 4234733300 | 5437 | 25 | 217 | 230 | 332 | 0.001549 | 0.000139 | 0.75 | 1.04 | 0.78 |
| 3 | 4234733294 | 5513 | 26 | 212 | 263 | 366 | 0.001793 | 0.000104 | 0.87 | 0.77 | 0.67 |
| 4 | 4234733304 | 6023 | 25 | 241 | 188 | 428 | 0.001626 | 0.000146 | 0.79 | 1.09 | 0.86 |
| 5 | 4240530480 | 5929 | 25 | 237 | 244 | 415 | 0.001626 | 0.000114 | 0.79 | 0.85 | 0.67 |
| 6 | 4234733305 | 5225 | 24 | 218 | 188 | 425 | 0.001977 | 0.000139 | 0.96 | 1.04 | 1.00 |
| 7 | 4234733271 | 4540 | 19 | 239 | 133 | 622 | 0.002403 | 0.000186 | 1.16 | 1.39 | 1.61 |
| 8 | 4234733269 | 4655 | 19 | 245 | 117 | 687 | 0.002523 | 0.000195 | 1.22 | 1.46 | 1.78 |
| 9 | 4234733267 | 5040 | 21 | 240 | 125 | 659 | 0.002523 | 0.000169 | 1.22 | 1.26 | 1.54 |
| 10 | 4234733268 | 4641 | 21 | 221 | 192 | 483 | 0.00218 | 0.000139 | 1.05 | 1.04 | 1.09 |
| ref | N/A | 5235 | N/A | 233 | 185 | 512 | N/A | N/A | 1.00 | 1.00 | 1.00 |

Table 15—Haynesville shale gas scaling parameters.

**Figs. 47 to 49** show the original production data on the left and the rescaled profiles on the right based on the scaling factors presented in Table 15.

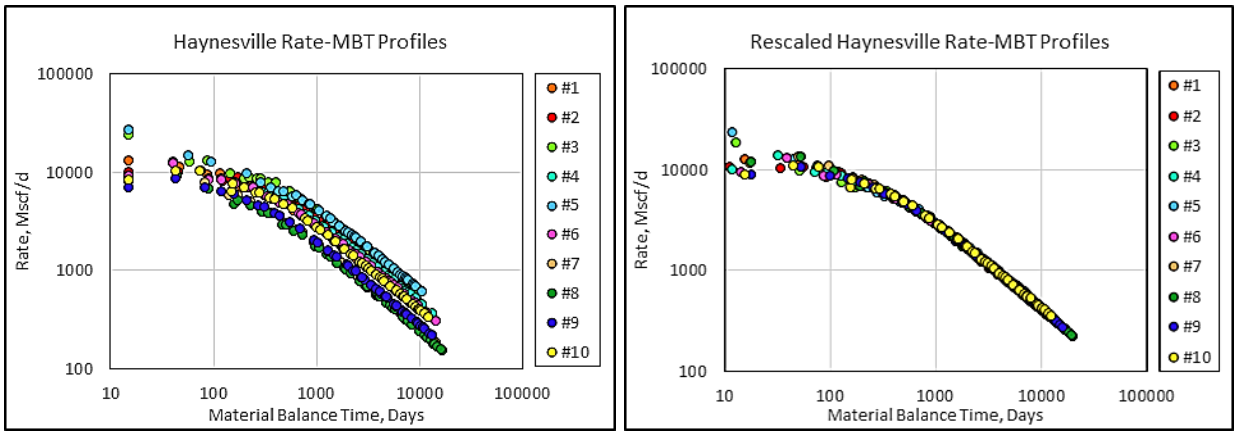


**Fig. 47—Left: Haynesville rate-MBT profiles. Right: scaled rate-MBT profiles.**

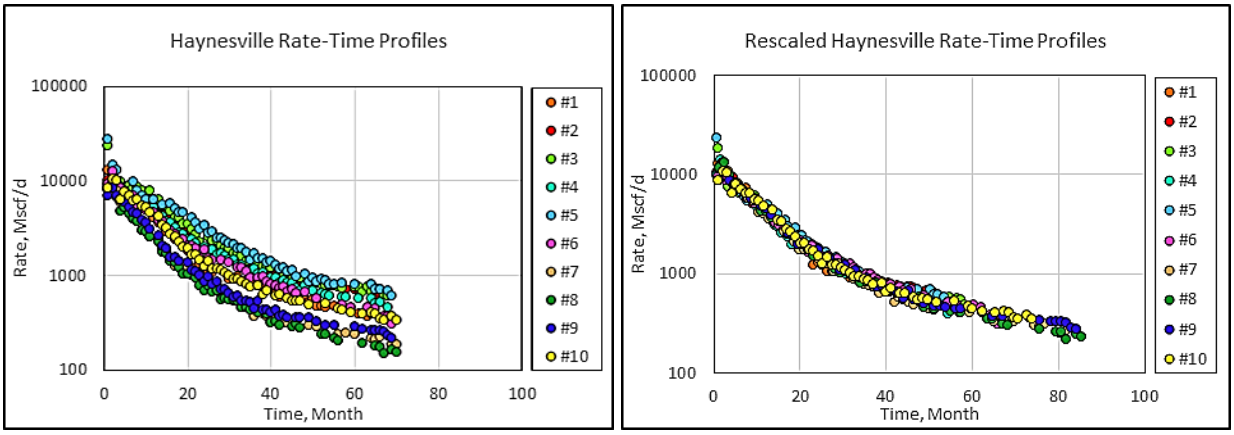


**Fig. 48—Left: Haynesville rate-time profiles. Right: scaled rate-time profiles.**

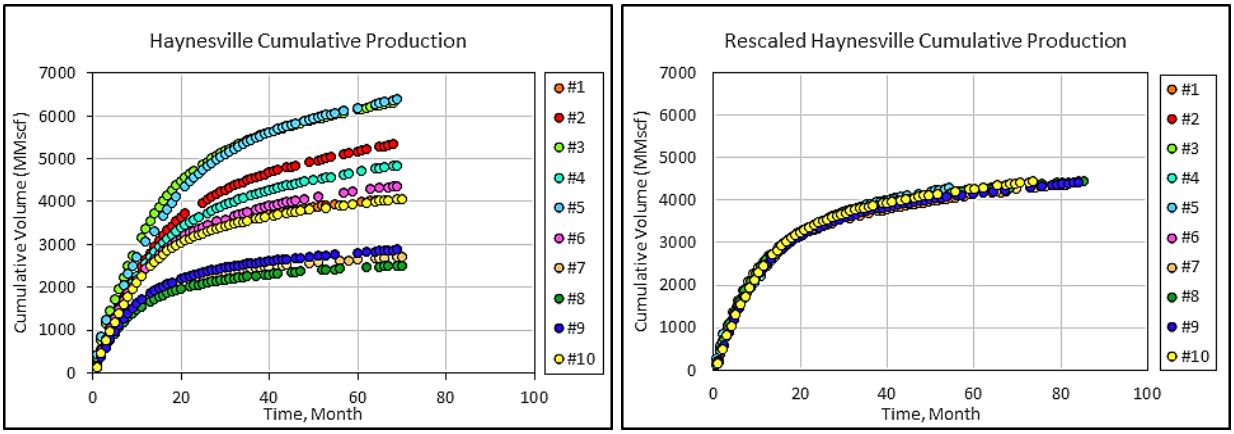


**Fig. 49—Left: Haynesville cumulative production profiles. Right: scaled cumulative production profiles.**

After rescaling the production profiles of the Haynesville shale, we see in Figs. 47 to 49 that all show the same typical production profiles at different scales.

### *4.3.2 Eagle Ford Shale Gas Example*

The Eagle Ford shale formation, the source rock of the Austin chalk located across southern Texas, was deposited in the Cretaceous period. The gas is thermogenic; typical depths of the gas window range from 6,000 to 13,000 ft with an estimated pressure gradient of 0.52 psi/ft. The Eagle Ford shale has a reported gas content of 200-220 scf/ton, where 25% of the gas is adsorbed while the rest is free gas in a gas-filled porosity of 4.5% (Jarvie 2012). To estimate the permeability and fracture half length of the ten profiles presented in **Table 16**, an average net pay thickness of 200 ft was assumed based on an estimated maximum gross thickness of 300 ft. In this example, the pseudo-pressure drawdown was calculated based on the pressure gradient and the true vertical depth of the well. The range of depth varies from 9,600 ft to 12,700 ft, and an operating BHP of 500 psia was used for the drawdown calculation, given an average gas gravity of 0.72 and no impurities in the gas. Finally, an average porosity of 4.5% and a reservoir temperature of 770$^{o}$ R were also used to estimate permeability and fracture half-length with Eqs. 11 and 12. Table 16 summarizes the results of the analysis in which wells 1 to 10 were matched with the modified type curve. Columns 10 and 11 in Table 16 present time and rate match points which were used to estimate permeability and fracture half length. The last two columns are scaling factors used to fit

the production profiles to a "reference" well with lateral length 5654 ft, fracture stage spacing of 329 ft, fracture half-length of 48 ft and permeability 792 nD. The ten wells studied have permeabilities ranging from 478 to 1,574 nD, which is consistent with the average range of permeability of 700 to 3,000 nD reported by Jarvie (2012).

| Well No. | API No. | Well Depth (ft) | Drawdown ($psi^2/cp$) | Lateral Length | Stages | $F_s$ (ft) | $x_f$ (ft) | k (nd) | TM | QM | TSF | RSF | CSF |
|---|---|---|---|---|---|---|---|---|---|---|---|---|---|
| 1 | 4225532531 | 12073 | 1.61E+09 | 6385 | 18 | 355 | 58 | 830 | 0.001 | 0.0007 | 0.90 | 0.98 | 0.88 |
| 2 | 4225532344 | 12427 | 1.68E+09 | 5606 | 17 | 330 | 87 | 697 | 0.001 | 0.0005 | 0.88 | 0.73 | 0.64 |
| 3 | 4225532534 | 10718 | 1.33E+09 | 5369 | 16 | 336 | 36 | 1574 | 0.0018 | 0.0008 | 1.50 | 1.31 | 1.97 |
| 4 | 4225532571 | 12134 | 1.62E+09 | 6158 | 18 | 342 | 39 | 732 | 0.0009 | 0.0011 | 0.85 | 1.59 | 1.35 |
| 5 | 4225532324 | 12517 | 1.70E+09 | 5800 | 17 | 341 | 76 | 672 | 0.0009 | 0.0006 | 0.79 | 0.89 | 0.70 |
| 6 | 4231134741 | 12061 | 1.61E+09 | 5050 | 17 | 297 | 43 | 642 | 0.001 | 0.0011 | 0.99 | 1.51 | 1.49 |
| 7 | 4247941577 | 9654 | 1.12E+09 | 5650 | 19 | 297 | 40 | 973 | 0.0013 | 0.001 | 1.30 | 1.51 | 1.96 |
| 8 | 4229735011 | 12502 | 1.70E+09 | 5716 | 17 | 336 | 70 | 1014 | 0.0013 | 0.0004 | 1.23 | 0.63 | 0.77 |
| 9 | 4225531867 | 12757 | 1.75E+09 | 5671 | 16 | 354 | 70 | 785 | 0.001 | 0.0006 | 0.85 | 0.89 | 0.76 |
| 10 | 4225531798 | 12506 | 1.70E+09 | 5134 | 17 | 302 | 56 | 478 | 0.0008 | 0.0011 | 0.72 | 1.51 | 1.09 |
| ref | N/A | N/A | 1.68E+09 | 5653.9 | 17 | 329 | 58 | 792 | N/A | N/A | 1 | 1 | 1 |

Table 16—Eagle Ford shale gas scaling parameters.

**Figs. 50 to 52** show the original production data on the left and the rescaled profiles on the right based on the scaling factors presented in Table 16. The profiles on the rate-MBT plots rescale to a common shape, although the decline is not as smooth because of outliers. We can see that well 7 has a profile at late times slightly different from the other wells. On average, the onset for boundary dominated flow occur at 1000 MBT days. Fig. 51 shows the rescaled profiles on semi-log rate-time plots. Wells 7 and 3 are outperforming the overage of the rescaled wells, which is also confirmed on Fig. 52.

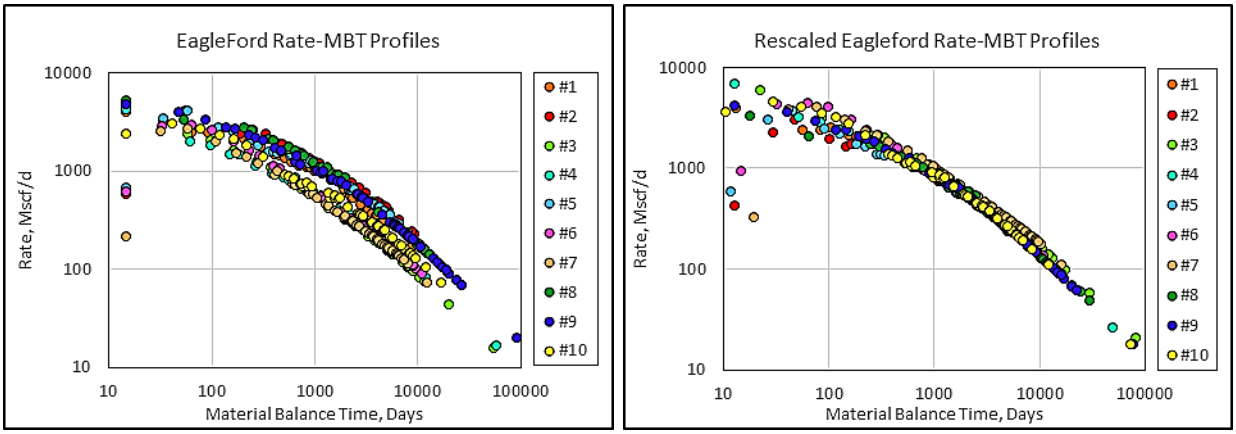


**Fig. 50—Left: Eagle Ford rate-MBT profiles. Right: scaled rate-MBT profiles.**

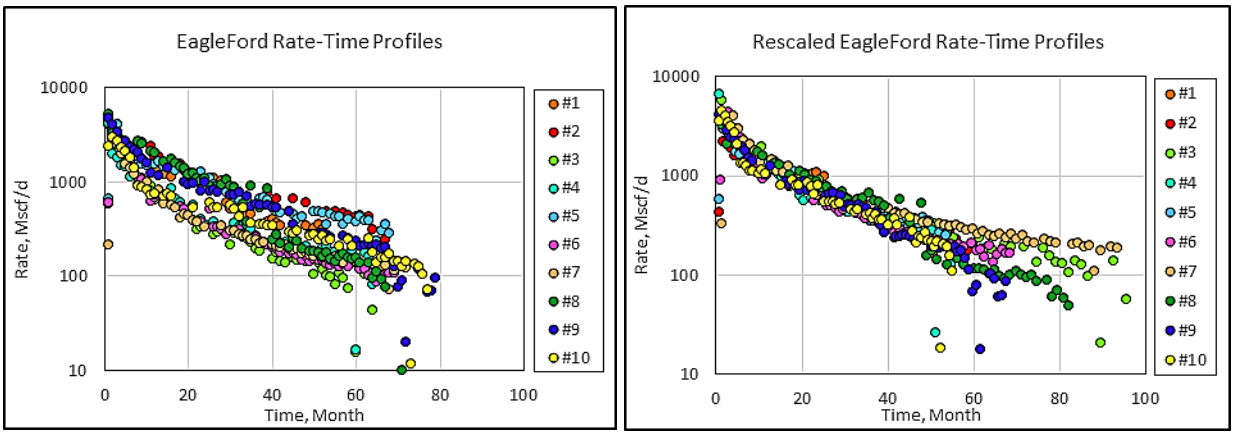


**Fig. 51—Left: Eagle Ford rate-time profiles. Right: scaled rate-time profiles.**

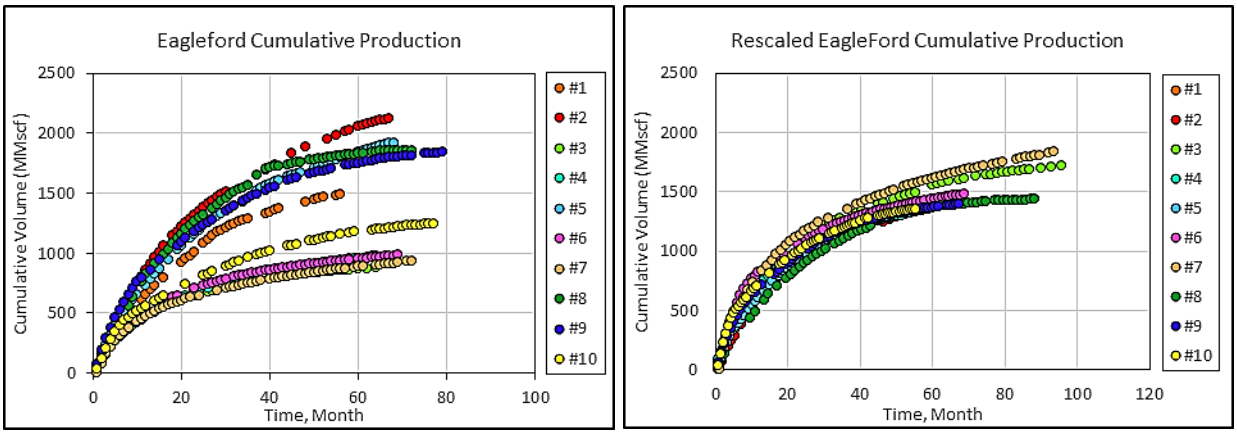


**Fig. 52—Left: Eagle Ford cumulative production profiles. Right: scaled cumulative production profiles.**

We can provide several reasons that might explain the different behavior of wells 3 and 7 compared to the other rescaled profiles. First, the depths of wells 3 (10,770 ft) and 7 (9,600 ft) are shallower than the depths of the other wells, which average of 12,300 ft. Also, the BHP history is unknown, and variable BHP can certainly affect flow regime identification because the rates are not corrected for drawdown. Furthermore, assuming a BHP of 500 psi for all wells may bias the analysis. For well 7, the pseudo-pressure drawdown assumed is 50% lower than for the average well reported in Table 16. Hence, rescaling the entire profile by multiplying the cumulative production by 1.5 can be a source of error because the drawdown scaling factor was demonstrated to be a valid approximation only for wells in transient flow. This argument may explain why the rescaled profiles of wells 3 and 7 appear to be outliers in Fig. 52.

The relationships predicted by our scaling factor theory are observable in the data. For instance, well 8 (dark green on the left plot of Fig. 52) shows a different trend after 37 months of production compared to well 2 (red). As both wells have similar vertical depth, lateral length and fracture spacing, well 2 was diagnosed to have a smaller permeability and a larger fracture half-length than well 8. Hence, for approximately the same period of production of about 70 months, well 8 is in a more advanced stage of depletion than well 2 which has a larger stimulated area and a smaller permeability. This explains why well 8 has a time scaling factor of 1.23 greater than well 2 which has a time scaling factor of 0.88.

### *4.3.3 Marcellus Shale Gas Example*

The Marcellus shale gas formation is located in the Appalachian basin which was deposited during the Devonian period. The gas is thermogenic and is found at depths ranging from 4,000 to 8,500 ft, with an estimated pressure gradient of 0.61 psi/ft. The Marcellus shale has a reported gas content of 60-150 scf/ton; 45% of the gas is adsorbed while the rest is free gas in gas-filled porosity of 4% (Jarvie 2012). To estimate the permeability and fracture half length of the ten profiles presented in Table 17, an average net pay thickness of 200 ft was assumed based on a maximum estimated gross thickness of 350 ft. The pseudo-pressure drawdown was estimated to be 1.68E+09 $psi^2/cp$ for an average vertical depth of 7850 ft, an initial reservoir pressure of 4788.5 psia and a BHP of 500 psia, given a gas gravity of 0.6 and no impurities in the gas. An average porosity of 8% and a reservoir temperature of $750^o$ R were also used in the calculations to estimate permeability and

fracture half-length with the Eqs. 11 and 12. **Table 17** summarizes the results of the analysis in which wells 1 to 10 were matched to the modified type curve. Time and rate match points, provided in columns 8 and 9, were used with Eqs. 11 and 12 to estimate permeability and fracture half length. The two right-most columns are the scaling factors calculated to fit the production profile of a hypothetical well with lateral length 4606 ft, fracture spacing 248 ft, a fracture half-length 409 ft and permeability 245 nD, all approximate average properties for the 10-well data set. The ten wells have permeabilities ranging from of 87 to 368 nD, greater than the average permeability of 70 nD reported by Jarvie (2012). The fact that almost 45% of the gas is adsorbed might affect the estimation of the permeability with our analytical model. As adsorption is outside of the scope of this research, further studies should be carried out to estimate the impact of adsorption on the scaling factors.

| Well No. | API No. | Lateral Length | Stages | $F_s$ (ft) | $x_f$ (ft) | k (nd) | TM | QM | TSF | RSF | CSF |
|---|---|---|---|---|---|---|---|---|---|---|---|
| 1 | 3708120346 | 5198 | 18 | 289 | 340 | 293 | 0.00050 | 0.00037 | 0.89 | 1.17 | 1.04 |
| 2 | 3705925582 | 3742 | 25 | 150 | 473 | 87 | 0.00056 | 0.00033 | 0.98 | 1.06 | 1.04 |
| 3 | 3703521234 | 6366 | 17 | 374 | 237 | 345 | 0.00036 | 0.00060 | 0.62 | 1.96 | 1.22 |
| 4 | 3711721120 | 5102 | 17 | 300 | 330 | 204 | 0.00033 | 0.00060 | 0.58 | 1.90 | 1.09 |
| 5 | 3712524354 | 2639 | 17 | 155 | 307 | 176 | 0.00105 | 0.00039 | 1.85 | 1.22 | 2.27 |
| 6 | 3711721121 | 4999 | 17 | 294 | 390 | 216 | 0.00036 | 0.00047 | 0.63 | 1.49 | 0.94 |
| 7 | 3713120078 | 4594 | 20 | 230 | 597 | 368 | 0.00100 | 0.00012 | 1.77 | 0.38 | 0.67 |
| 8 | 3711520362 | 3902 | 16 | 244 | 738 | 209 | 0.00050 | 0.00023 | 0.89 | 0.72 | 0.64 |
| 9 | 3705925387 | 4778 | 16 | 299 | 304 | 329 | 0.00053 | 0.00043 | 0.94 | 1.35 | 1.26 |
| 10 | 3705925910 | 4742 | 32 | 148 | 373 | 226 | 0.00148 | 0.00013 | 2.61 | 0.40 | 1.04 |
| ref | N/A | 4606 | 20 | 248 | 409 | 245 | N/A | N/A | 1.00 | 1.00 | 1.00 |

Table 17—Marcellus shale gas scaling parameters.

**Figs. 52 to 53** show the original production data on the left and the rescaled profiles on the right based on the scaling factors presented in Table 17.

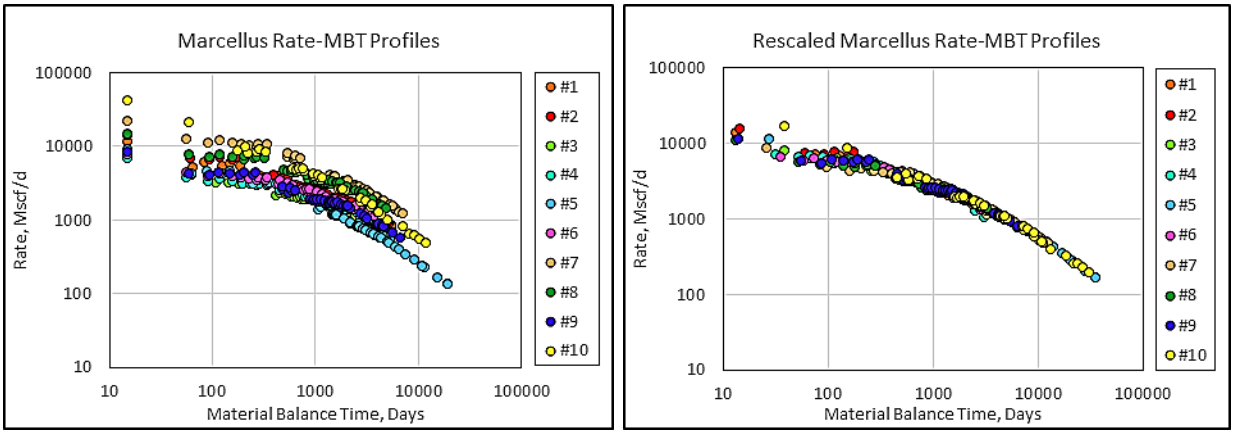


**Fig. 53—Left: Marcellus rate-MBT profiles. Right: scaled rate-MBT profiles.**

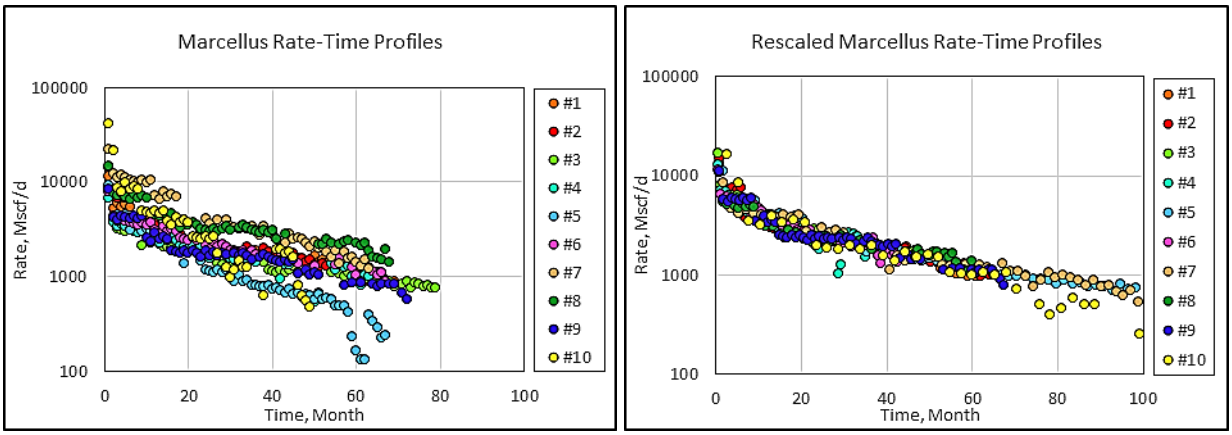


**Fig. 54—Left: Marcellus rate-time profiles. Right: scaled rate-time profiles.**

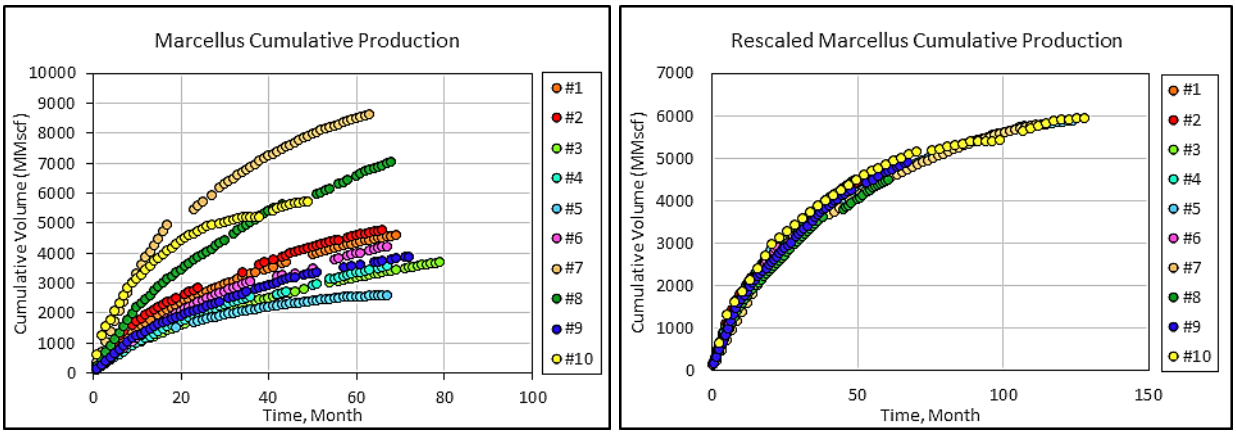


**Fig. 55—Left: Marcellus cumulative production profiles. Right: scaled cumulative production profiles.**

Figs. 53 to 55 illustrate the application of the scaling methodology to a common well profile. With the rate-MBT profiles matched as on the modified type curve, we notice that the rate-time data also align on a similar trend, despite the noise in the production profiles. Looking more closely to well 9 (dark blue on the left plot of Fig. 54), we notice that the rates are almost constant for several months for the first 30 month of production. This most likely indicates that the operator was managing the choke or the artificial lift system to maintain production and avoid decline in rate. Such operating practices can limit the interpretation of flow regimes if the rates are not corrected by the drawdown. The same effect is observable in well 10 (yellow). However, despite the noise on the rate-time profile, Fig. 55 shows that the cumulative profiles rescale to a similar production profile. As for the Eagle Ford, some observations can be made on the scaling factors. First of all, the range of lateral length varies from 2639 ft to 6366 ft and the fracture half-length varies from 237 to 738 ft. Since the net pay thickness is assumed to be the same for all the wells, the lateral length and the fracture half-length are the two governing parameters that define the total stimulated volume. Wells 7 and 8 have the largest SRV's of the well set, determined by comparing the product of lateral lengths and fracture half lengths for all wells. Since they are rescaled to a well dimension that has a smaller stimulated volume, the CSF reflects the reduction in cumulative production due to rescaling. Similarly, well 5 (blue) has the smallest lateral length and a smaller fracture half-length than the well to which it is rescaled, so the CSF reflects the increase in cumulative required to match the reference stimulated volume. The "depletion" parameters correction, governed by the ratio $k/F_s^2$, is given by the time scaling factor. Table 17 shows that wells 5 and 10, (blue and yellow on the plots) have small fracture spacing and average permeability. This intuitively indicates that the SRV will deplete faster.

### *4.3.4 Barnett Shale Gas Example*

The Barnett shale gas formation, located in the Fort Worth basin in Texas, was deposited in the Mississippian period. This thermogenic gas is produced from depths ranging 6,500 to 8,500 ft, with a pressure gradient of 0.48 psi/ft. The Barnett shale has a reported gas content of 300-350 scf/ton, with 55% of the gas adsorbed and the rest free gas in a gas-filled porosity of 5% (Jarvie 2012). To estimate the permeability and fracture half length of the ten profiles presented in **Table 18**, we assumed an average net pay thickness of 200 ft based on a maximum estimated gross

thickness of 350ft. The pseudo-pressure drawdown was calculated based on the reported vertical depth of each well to obtain the initial reservoir pressure and a BHP of 500psia, given a gas gravity of 0.6 and no impurities in the gas. An average porosity of 6% and a reservoir temperature of 660$^{o}$ R were also used in the calculations to solve for permeability and fracture half-length with the Eqs. 11 and 12. Table 18 summarizes the results of the analysis in which wells 1 to 10 were matched to the modified type curve. Columns 10 and 11 summarize the time and rate match points which were used with Eqs. 11 and 12 to estimate permeability and fracture half length. The last two columns present the scaling factors to scale to fit the production profile of a theoretical well with these average properties: lateral length, 3965 ft; a fracture spacing, 235 ft, a fracture half-length, 397 ft, and permeability 483 nD. For ten wells studied have permeabilities ranging from 298 to 1012 nD, which is larger than the average permeability of 50 nD reported by Jarvie (2012). Since 55% of the total gas is adsorbed in the Barnett shale, desorption could account for an apparent increase in permeability.

| Well No. | API No. | Depth (ft) | Drawdown ($psi^2/cp$) | Lateral Length (ft) | Stage Number | $F_s$ (ft) | $x_f$ (ft) | k (nd) | TM | QM | TSF | RSF | CSF |
|---|---|---|---|---|---|---|---|---|---|---|---|---|---|
| 1 | 4212133970 | 8474 | 8.36E+08 | 5149 | 13 | 396 | 227 | 471 | 0.00040 | 0.00080 | 0.97 | 0.77 | 0.75 |
| 2 | 4212134172 | 8178 | 7.89E+08 | 2094 | 6 | 349 | 419 | 316 | 0.00035 | 0.00131 | 0.84 | 1.26 | 1.06 |
| 3 | 4212134169 | 8272 | 8.03E+08 | 3925 | 10 | 393 | 309 | 298 | 0.00026 | 0.00125 | 0.63 | 1.20 | 0.75 |
| 4 | 4212134163 | 7783 | 7.27E+08 | 3903 | 10 | 390 | 379 | 325 | 0.00029 | 0.00102 | 0.69 | 0.99 | 0.68 |
| 5 | 4212134170 | 8341 | 8.15E+08 | 5129 | 13 | 395 | 192 | 658 | 0.00057 | 0.00069 | 1.37 | 0.67 | 0.91 |
| 6 | 4212134198 | 8095 | 7.75E+08 | 3079 | 8 | 385 | 170 | 332 | 0.00030 | 0.00259 | 0.73 | 2.49 | 1.81 |
| 7 | 4212134177 | 8491 | 8.39E+08 | 3064 | 8 | 383 | 270 | 329 | 0.00030 | 0.00151 | 0.73 | 1.46 | 1.06 |
| 8 | 421213402 | 7813 | 7.31E+08 | 4539 | 11 | 413 | 148 | 1012 | 0.00080 | 0.00080 | 1.93 | 0.77 | 1.49 |
| 9 | 4212133939 | 8112 | 7.78E+08 | 5379 | 12 | 448 | 71 | 673 | 0.00045 | 0.00235 | 1.09 | 2.27 | 2.46 |
| 10 | 4212133878 | 7921 | 7.48E+08 | 2799 | 7 | 400 | 208 | 403 | 0.00034 | 0.00214 | 0.82 | 2.06 | 1.68 |
| ref | N/A | N/A | 7.84E+08 | 3906 | 10 | 395 | 239 | 482 | N/A | N/A | 1 | 1 | 1 |

Table 18—Barnett shale gas scaling parameters.

**Figs. 56 to 58** show the original production data on the left and the rescaled profiles on the right based on the scaling factors presented in Table 18. As for the other plays presented in this

section, the wells used in the Barnett shale were rescaled to a common profile. Despite the noise caused by outliers and the poor quality of the data, the rate-MBT profiles were rescaled to a common depletion profile in late time. The early time variation on the profiles could be adjusted if pressure histories were available.

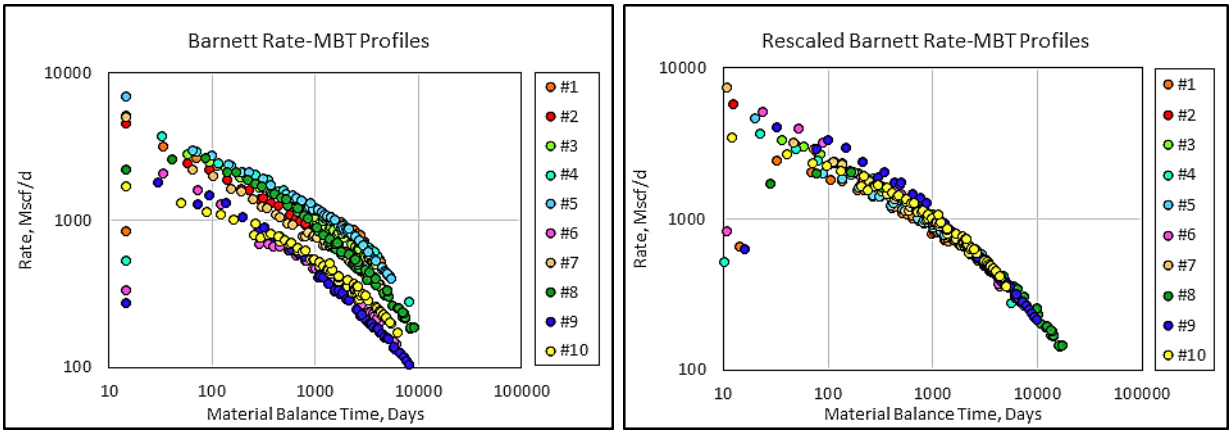


**Fig. 56—Left: Barnett rate-MBT profiles. Right: scaled rate-MBT profiles.**

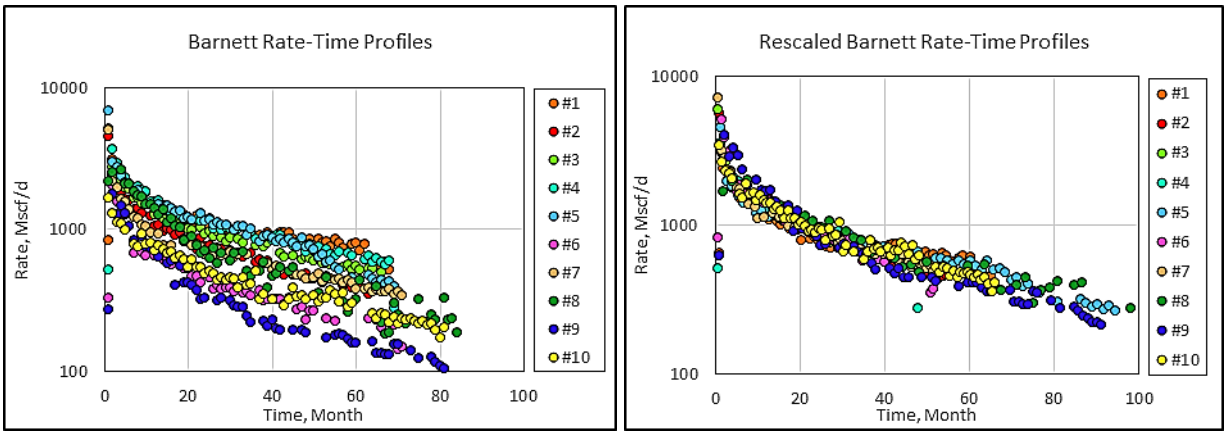


**Fig. 57—Left: Barnett rate-time profiles. Right: scaled rate-time profiles.**

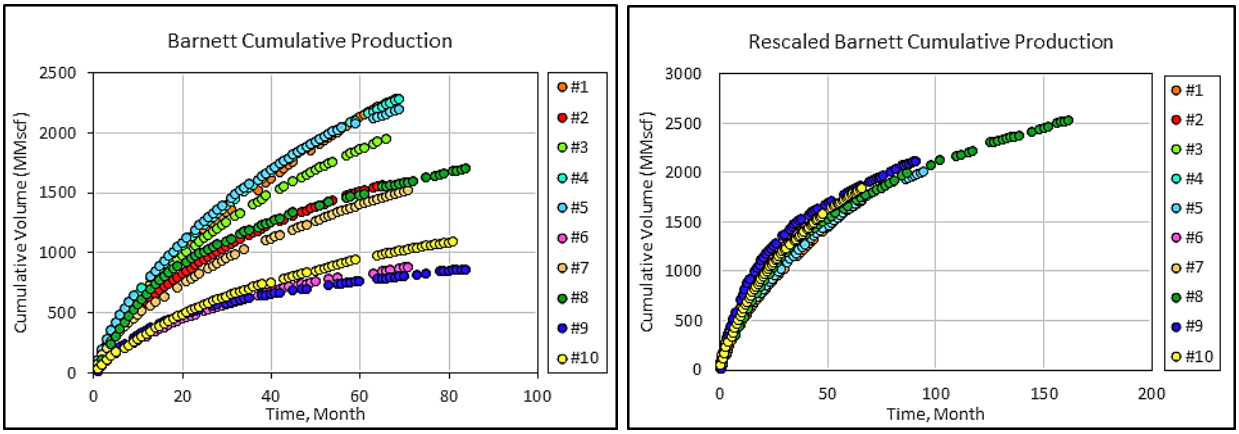


**Fig. 58—Left: Barnett cumulative production profiles. Right: scaled cumulative production profiles.**

As for the other example, the scaling of the Barnett profiles is consistent with the parameters diagnosed from the type curve match. Well 8 (dark green) has a high TSF due to its high permeability. Hence, compared to other wells, Well 8 is in a much more advanced state of BDF depletion, which is why none of the cumulative profiles can be rescaled this same production time in Fig. 58.

### *4.3.5 Summary of Shale Gas Examples*

Ten wells that reached BDF in four shale-gas resource plays were studied and rescaled to a set of common parameters based on their known and diagnosed properties found with matches on the modified type curve. The monthly produced data, lateral length, stage spacing, and pseudo-pressure were based on data from DrillingInfo or estimated. Estimated values of permeability were compared to those reported by Jarvie (2012). We found that the Haynesville and the Eagle Ford permeability were in the same range given by Jarvie (2012) while the Marcellus and Barnett Shales permeabilities were larger than those reported by Jarvie. Desorption in shales with greater amounts of adsorption could account for some of the differences. Ambrose et al. (2010) suggested that the organic matter in which the gas is adsorbed represents the majority of the porosity in the rock. While it has no direct impact on permeability and fracture half length, using the free-gas porosity

may understate the effective porosity that should have been used in the analytical model. This could impact the estimated permeability and fracture half-length. In the scaling parameters, porosity would change only the time match point interpretation. At a given set of match points, a larger porosity would lead to a larger estimated permeability. A larger permeability would lead to smaller fracture half-length estimate from the rate match point interpretation. Thus, desorption could impact both permeability and fracture half-length estimates. More research could help us understand the impact of desorption on reservoir properties estimated from production data.

Furthermore, based on the available true vertical depth data, the initial reservoir pressure of the Eagle Ford and the Barnett wells was estimated to determine drawdown, and a BHP equal to 0.1 $p_i$ was assumed. In contrast, we assumed an average drawdown for the Haynesville and the Marcellus shales since the wells had similar depths. We assumed a BHP of 500 psi for all wells and calculated $m(p)$ from the reservoir temperature, initial reservoir pressure and the gas gravity with an automated spreadsheet developed by Guo et al. (2007). As the drawdown scaling seems to match all the profiles, the two wells located at shallower depths did not align properly. The discrepancy is attributed to either the assumed drawdown, or the effect of changing average reservoir pressure during BDF.

The examples were consistent with the fundamental relationships between the scaling factors and the parameters used to rescale the profiles. Indeed, other things being equal, wells with either larger permeability or smaller stage spacing would be expected to have a larger initial rate and a shorter transient period. Such wells would be rescaled with a large TSF compared to underperforming wells since they deplete faster. Similarly, the parameters correlated to the stimulated volume, lateral length, net-pay thickness and fracture half-length correlated with the observed shapes of the cumulative production plots. Given the same depletion parameters, a larger stimulated volume would yield larger cumulative production. Finally, as the rate is the derivative of cumulative production at a given time, the RSF is a combination of the CSF and the TSF. Differences in scaling factors in the rate-time profile and the cumulative-time profile can be explained by the fact that the cumulative production is the integral of the rate over time. Assuming that a hyperbolic decline curve can fit at least one section of the curve, parameters in the decline curve equations should be related to the scaling factors. In Appendix C, we show that, if the Arps' decline model fits a profile, then the CSF and TSF are respectively multiples of the cumulative

production and time. We also find that the CSF divided by the TSF yields the RSF. The derivation demonstrates that the scaling factors are independent of the Arps hyperbolic b factor. Therefore, this relationship holds also for exponential decline (b=0) and harmonic decline (b=1).

Extending the observations in Chapter 3 where we rescaled production profiles of each resource play onto a similar profile, we matched the profiles in this Chapter based on theoretical physical relationships. This work demonstrates that an "effective" permeability and "effective" fracture half-length can be calculated to estimate the depletion parameter and the stimulated volume, *which dictate the scale of a common production profile.* It also demonstrates how publicly reported data can be used to determine a SRV and effective permeability. In conclusion, scaling factors are the results of an analytical model match and allow us to efficiently normalize the production.

### 4.4 Scaling Factor Application for Reservoir Diagnostic

A major focus of this research is to show that analytical scaling factors are a tool that can improve the characterization of a typical profile in a GSA. As demonstrated in Appendix C, they can also be used in decline models, which in turn can be used to diagnose reservoir and completion properties. This process, which can be regarded as a "reverse engineering approach," shows that the initial rate initial decline rate parameters in Arps decline models are directly related to the scaling factors when we rescale a production profile. This section opens the discussion on this kind of application and does not intend to provide a full description of the applications and limitations. The derivations presented in Appendix D were prepared to show how the TSF and the RSF can be decoupled from the rate and time variables and be related to the parameters in the Arps decline models. In the harmonic decline model, two new constants can be expressed as functions of $q_i$ and $D_i$. In summary, we demonstrate that the scaling factors initially defined as a combination of properties such as permeability, fracture half-length, etc. are also functions of initial rate and initial decline rate in Arps decline models, *assuming that the decline model fits the observed production data*. The time scaling factor is directly related to the ratio of decline rates while the rate scaling factor is related to the ratio of initial rates. Cumulative production scaling factors are related to the reservoir volume parameters and the drawdown, and also to the ratio of the initial rate to the initial decline rate.

Theoretically, these relationships can be used to estimate the relative differences in permeabilities and SRV's between two wells by fitting cumulative production data. If the fit of the transient data were always reliable and consistent in different wells in a GSA, the scaling factors could provide a methodology to estimate unconventional well performance in the transient flow regime. Indeed, because the hyperbolic equation with b equal to 2 is theoretically supposed to fit the transient linear flow regime of any well, we can find values of qi and Di for each well. Comparing a given well to a reference well would allow us to calculate scaling factors which should allow us to estimate unknown properties. Because the TSF depends only on differences in fracture spacing and permeability, if fracture spacing is known, the difference in permeability can be calculated. The same procedure applies for the CSF: assuming that differences in drawdown, net pay thickness and lateral length are known, differences in fracture half-length can also be calculated. **Fig. 59** illustrates 3 wells plotted on an $N_p$-1/q diagnostic plot. This plot, developed in Appendix H, is a straight-line diagnostic tool we can use to identify the segment of the production history that is in transient linear flow. We can rescale the $N_p$-(1/q) profiles with the original scaling factors from the type curve match to transform the transient regions on different wells to similar profiles.

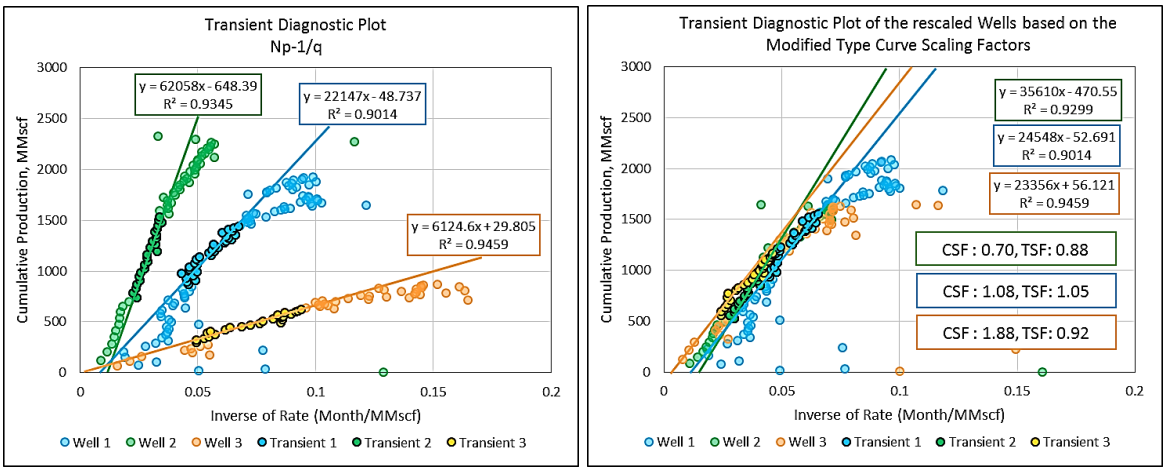


**Fig. 59—Study of the application of the scaling factors on a transient flow regime diagnostic plot.**

As this process is implemented, we can see the impact of scaling factors on the diagnostic plot. However, the slope and the intercept of the lines that fit the transient segments are approximations based on the points selected as "transient," and rescaling them does not overlay them properly. The inverse process was attempted but was unsuccessful. The calculation of the scaling factors from the decline curve coefficients overstates the differences in properties because the fits of the curves are not accurate enough. Hence, this methodology is not practical but could theoretically be applied with perfect fits.

Other potential applications include estimation in the change of reservoir and completion parameters of a wells in the transient flow regime after a workover operation, long shut-in periods or other external events that can cause a change in effective permeability or fracture half length. This requires that the well remain in transient flow regime after the event to compare the parameters of the hyperbolic equation with a b factor of two.

In summary, we demonstrated theoretically that the scaling factors previously defined as the functions of properties such as permeability and fracture half-length are also functions of Arps decline model parameters initial rate and the initial decline rate, assuming that the Arps model fits the data. These results are related to the idea that a multi-segment decline model, such as the modified Arps hyperbolic model, can parametrize a dimensionless rate-time profile, which is the cornerstone of the scaling factor methodology. *Finally, this demonstration also introduces the perspective that initial rates and decline rates in Arps' empirical decline models can be related to analytical scaling factors, and therefore physical properties.* The main limitation of this methodology is our inability to *fit* production data uniquely, due to outliers and multiple pairs of initial rates and decline rates that can provide acceptable fits.

# CHAPTER V

# TYPE WELL CONSTRUCTION AND PRODUCTION FORECASTING WORKFLOW

The analytical scaling methodology was demonstrated to reliably rescale production profiles of horizontal multi-fractured wells flowing in boundary dominated flow given an interpreted value of permeability and fracture half length. The relationship given by the scaling factors in Table 12 can be used to normalize production data and build representative type wells. As demonstrated for four field examples, production profiles of wells in a GSA characterize a common reservoir behavior as they are rescaled to a reference profile under the assumption of constant operating conditions. This methodology can improve type well construction because it allows us to group more wells into relatively few bins that would otherwise be separated into different bins. The objective of this chapter is to present a new workflow to construct type wells by characterizing the typical profile of the wells in a GSA. We will also demonstrate how the production profiles of a GSA can be used to forecast undrilled wells or wells flowing in transient flow regime by using their permeability and fracture half-length distributions. **Fig. 60** illustrates the complete workflow presented in this chapter. The color code presented on Fig. 60 details the organization of this chapter. Section 5.1 describes how to approach the data from a GSA using steps 1-4. It includes recommendations on how to analyze and validate production data before proceed into later steps. Based on the assumption that most horizontal multi-fractured wells follow the behavior of the modified analytical model, we suggest organizing production profiles into three categories. The first category is wells that are producing in BDF; the second, wells still in transient flow, and last for wells with discontinuous profiles, unstable declines or untypical shapes on rate-MBT diagnostic plots. A specific course of action is recommended for each group. Section 5.2 discusses the steps required to build a base-case profile from wells in BDF to forecast production. Section 5.3 summarizes the process to forecast production for wells still in transient flow. Section 5.4 explains how to develop a probabilistic model to forecast production for undrilled wells, and section 5.5 provides comments about wells that cannot be studied with the modified analytical model. Chapter 6 presents a case study based on Barnett Shale wells in Denton County as an application of the workflow presented in Chapter 5.

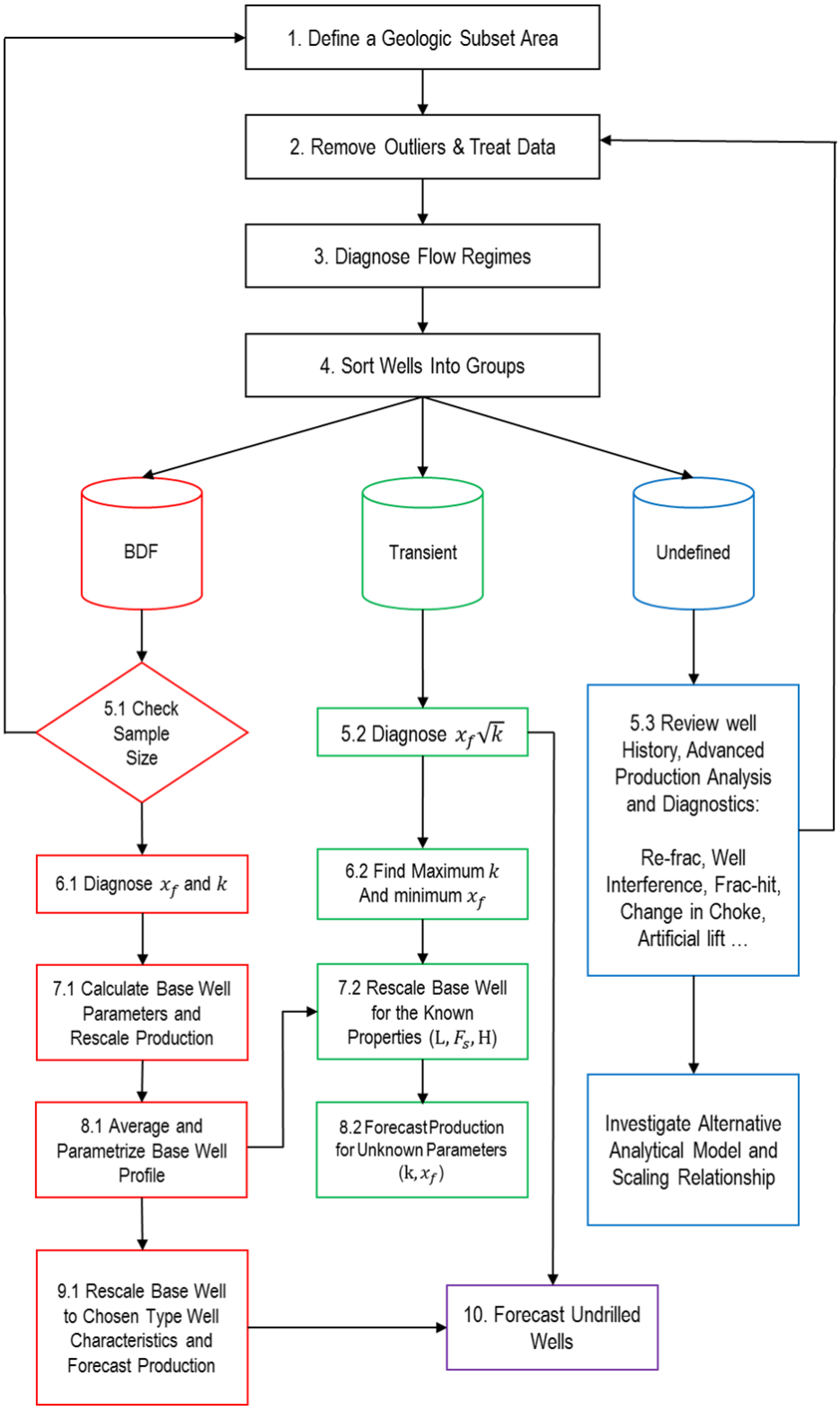


**Fig. 60—Analytical type well construction workflow and forecasting methodology.**

### 5.1 Geologic Subset Area Definition and Data Validation

In all this work, we limit our consideration to wells that have been producing for a significant time under constant operating conditions; only these wells are useful in creating a representative typical well production profile or type well for a GSA. The steps of the workflow presented in this section address the current limitations of sample size in type well construction methods presented in the literature. To reduce the statistical uncertainty caused by small sample size, wells with similar characteristics demonstrated by similar curve shapes on log-log rate-MBT plots are included in the same bin. Step 1 to 4 on Fig. 60 are summarized in the following list:

1. Define a study area large enough to include a statistically significant number of wells producing in the same geologic subset area (GSA)
2. Remove outliers from the production profiles and validate their production history.
3. Identify the flow regimes of each well based on a log-log rate-MBT diagnostic plot
4. Separate the wells into 3 groups:
    4.1. Wells in BDF
    4.2. Wells in the transient flow regime
    4.3. Well with undefined flow regimes and discontinuous production history

To implement the first step, we recommend that evaluators assess the amount of production data available for the study. We assume that only publicly reported produced volumes and limited well data are available for step 1. The advantage in developing a workflow to create type wells based on publically available volumes is to benefit from potentially larger data sets to characterize a GSA. Still, because we assume constant operating pressure, we recommend the use of higher frequency rate and pressure data when available as they can significantly improve flow regime diagnosis and improve permeability and stimulated volume estimations from matches with the modified type curve. We encourage analysts to understand the limitations of publically reported data and recommend using more complete and accurate data when it is available. Only horizontal wells should be selected for analysis. Section 2.1 provides more information about the data selection process and the number of wells required to conduct the study.

For step 2, several methods can be used to validate the production data, as section 2.1.1 discusses. An outlier detection tool, such as the methodology presented in Appendix E, is essential. This outlier detection tool allows us to identify misleading data points on a production profile. Based on this methodology, the ramp-up periods seen in some shale wells should be discarded for matching the modified type curve because it does not represent the reservoir behavior but rather fracture clean-up or choke management practices.

Step 3 differentiates production profiles by the nature of their flow regimes on a log-log rate-MBT plot. **Fig. 61** illustrates the geometrical characteristics of transient linear flow and BDF regimes.

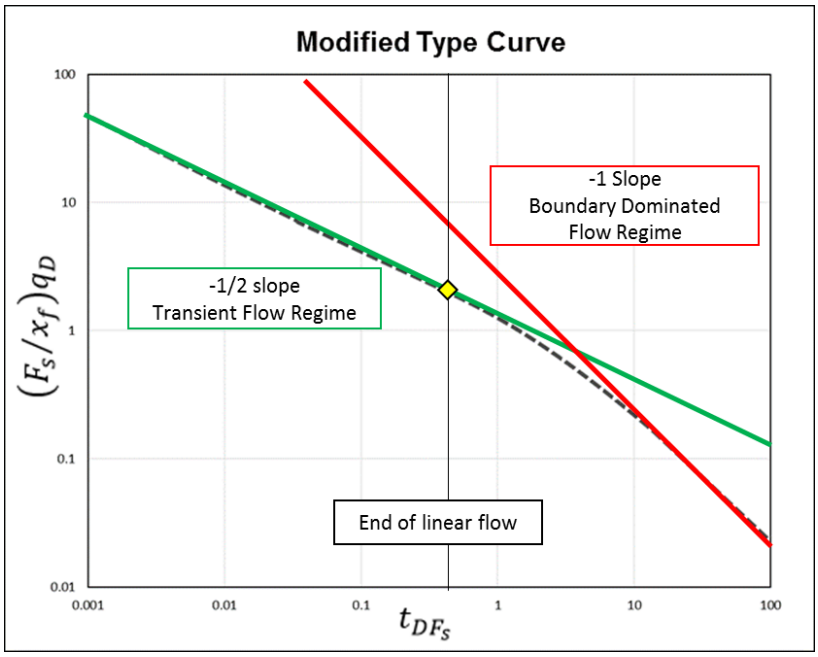


**Fig. 61—Modified type curve diagnostic plot**

Most of the wells presented in this work display different behavior at early time as displayed on Figs. 11 to 21. Flow regime analysis of early time usually requires high frequency data as well as pressure history to normalize the rate for changing pressure drawdown. As we assume that the pressure data is unavailable, we neglect the initial production trend because we

cannot differentiate between the variation in pressure, choke management and the presence of a transient bilinear flow regime.

**Fig. 62** illustrates the three types of production profiles as guidance to group wells. The green lines have negative unit slopes (BDF) whereas the orange lines have negative half slopes (transient linear flow).

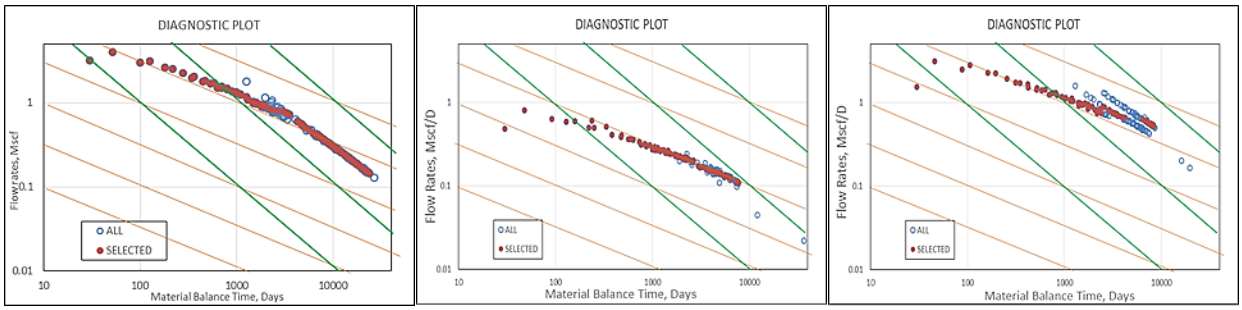


**Fig. 62—Flow regime diagnostic groups, BDF (left), transient flow (middle) undefined flow (right).**

The production history of wells like those on the right plot of Fig. 59 does not allow us to identify a continuous change of flow regimes. Trying to fit this data to the modified type curve would not provide a unique and reliable estimation of permeability or fracture half length.

### 5.2 Type Well Construction Workflow with Wells in Boundary Dominated Flow

We demonstrated in Chapter 4 that most shale gas wells producing under constant operating conditions in the resources we analyzed exhibit a transient linear flow region followed by a boundary dominated flow region, manifested by a negative half slope followed by a negative unit slope. In the section 5.1, we recommended a workflow that uses this characteristic behavior to bin wells into groups. For the bin containing the wells flowing in BDF, step 5.1 of our workflow recommends that we review the sample size. Indeed, depending on the amount of data available and the maturity of the play, the size of the GSA can often be modified to include a statistically sufficient number of BDF wells, with minima spelled out in Table 2.1 of SPEE Monograph 3 (2011).

Step 6.1 recommends that we then match the production profiles of the wells flowing in BDF on the modified type curve. We use TM and QM from the match to estimate an permeability and a fracture half-length from Eqs. 11 and 12. If net-pay thickness and operating BHP information are not available, we can assume realistic and informed values for all wells. For example, we might estimate the drawdown to be 0.1 $p_i$.

The properties estimated in step 6.1 allow us to normalize the production profiles to a theoretical reference or base well, using the analytical scaling factors proposed in Chapter 4. In step 7.1, we can define the parameters of the base well as the average of the parameters of the group of wells in BD; e.g., we could choose the base well permeability to be the average of the permeabilities of all the wells in BDF; this procedure can be followed for all the scaling parameters. The calculated scaling factors are then used to scale the production profiles for all wells and thus normalize the wells to the same reference parameters as in section 4.3.

Step 8.1 suggests that we calculate the average of the scaled production profiles to define the typical production profile of the "base well". This averaging methodology is similar to the time slice method described in the literature review and can be applied to rate-time and cumulative-time profiles. Since we average data points that have been scaled for time, we generate the average profile as a by averaging the data present in every slice. When most production profiles have been scaled to common reference conditions, applying the time slice method will significantly reduce the survivor bias in the results. Freeborn et al. (2012) recommended that wells should be forecasted to a common well life to avoid survivor bias. However, we suggest that only actual production data be averaged instead of using a combination of the history and forecast because most of the profiles will scale to a common trend. Since most forecasting methods rely on semi-empirical relationships, a long-term forecast could bias the average production profile. Percentile type wells can be created at this step if the rescaled production profiles have significantly different trends, but we believe that this procedure is too complicated to be included in the scaling process. It may be necessary, however, if the scaled production trends are do not follow similar production trends.

Step 9.1 allows us to build a type well by rescaling the base well profile to set of reservoir and completion properties based that we choose, using appropriate scaling factors. The discrete base well profile generated with the time slice method can be rescaled, but the profile can also be parametrized with a multi-segment decline model and rescaled. As only known production can be

rescaled, the different segments in the decline trend can be fitted with any decline model we choose (especially with composite parametrization, presented in Section 5.2.1) to forecast the longer-term production with different b factors. While we forecast the average profile, we believe this method is acceptable because the profiles have been normalized to common reference conditions.

To summarize, type wells constructed using our recommendations are simply rescaled base well profiles for a selected set of completion and reservoir parameters. The base well, from which we scale, is also intrinsically a type well that reflects the reference values of parameters (perhaps the average values of properties for wells in BDF).

### *5.2.1 Composite Parametrization Method for Type Wells*

We investigated a parameterization of the average production profile in this study. Our proposed method *is basically an empirical curve fitting exercise*, in which we attempt to reproduce the flow regimes that characterize the typical production profile of a multi-fractured horizontal well. We parametrize the average production history with a two-segment decline model such as *the modified Arps hyperbolic model*. We will refer to the procedure as *composite parametrization* because of the formulation of the cumulative production equation with a constant ε that accounts for the ramp-up period. The first segment should fit the transient region and the second segment should fit the BDF region. While the methodology's primary purpose is to fit data, it has some limitations which we will discuss. Nevertheless, applying composite parameterization to the reference production profile allows us to use scaling factors to rescale the profile to chosen type well characteristics. Indeed, based on the difference in reservoir or completion parameters, we are able to rescale the decline model of the composite parametrization with the scaling factors as demonstrated in Appendix C.

The first segment of the composite parametrization should be fitted with a hyperbolic decline model with a b value such that it fits as many points as possible with the single decline model. The most likely Arps b value for transient linear flow is 2 because the production of multi-fractured horizontal wells follows a half slope line on the log-log rate-MBT plot. However, publically reported production data are not corrected for the change in BHP. A half-slope line does not always fit the production profile for a significant period of time before it starts to transition

to BDF. In theory, we observe a half slope on the rate-MBT plot only after BHP is stabilized and when fracture damage does not affect the slope of the plot. We have observed that b = 1 often provides a good fit of production data that appear to be in transient flow. Therefore, we present two parametrization options in Appendices G and H. In both cases, fitting the transient section with *a single decline curve segment* allows us to rescale this segment efficiently with scaling factors as demonstrated in Appendix C. In either case, we use a cumulative production correction factor, $\epsilon$, in the parametrization to correct the cumulative production profile for the deviation of rates from the equation that provides the best fit of early transient data. Appendices G and H present diagnostic plots that can guide us in the choice of the method to use. When a hyperbolic equation with b=2 fits most of the transient data, the data should fall on a straight line on an $N_p$ vs.1/q plot as the examples in Appendix H demonstrates. When b = 1 provides the best fit, the procedure is similar as the example in Appendix G demonstrates. In this phase of the study, we used the methodology presented in Appendix G with b=1. Eqs. 24 and 25 summarize how the Arps decline model with b = 1 is modified to fit the transient section of averaged cumulative profile with a correction factor $\epsilon$. Appendices G and H also present methodologies to determine $q_i$, $D_i$ and the correction factor $\epsilon$ based on diagnostic plots.

$$N_P(t) = \frac{q_i}{D_i}\left[\ln\left(t + \frac{1}{D_i}\right) - \epsilon \ln\left(\frac{1}{D_i}\right)\right] \tag{24}$$

$$N_P(t) = \frac{q_i}{D_i}\left[\sqrt{1 + 2D_i t} - \epsilon\right] \tag{25}$$

To separate the end of linear flow and BDF segment, the time at the end of linear flow can be used as an intersection point. The time at the end of linear flow can be identified graphically after we generate the reference rate-MBT profiles from the reference rate-time and cumulative-time profiles computed previously. The time at which the reference profile deviates from the half slope is when we should switch to the second segment. An alternative way to estimate the time linear flow ends is to calculate the average of the all the scaled times of linear flow using Eq. 26.

$$\overline{t_{elf}} = \frac{\sum_{i=1}^{N}\left(TSF_i * t_{elf_i}\right)}{N} \tag{26}$$

The end of linear flow is given by the Rate-MBT data point that lies the closest to the dimensionless time of 0.5 on the modified type curve as shown by the yellow diamond on Fig. 61. Wattenbarger identified this point as the location on the curve where the slope changes from a negative half slope towards a negative unit slope. Because the data overlaid on the type curve is the Rate-MBT plot, the MBT should be converted to real time. As the MBT is a superposition function, several points may lie on the same MBT if the data is noisy. An average of those points should provide a good estimate of the actual time at the end of linear flow.

The second segment that characterizes the depletion flow regime is created using a principle similar to that Fetkovich (1980) used to develop his production type curve (Fig. 2). The second segment starts based on the rate, decline and cumulative production computed at the time at the end of linear flow from the previous segment. Those parameters are found based on the equations of Appendix I and used to generate different depletion stems with b values varying from 0 to 1. **Fig. 63** shows a typical composite parametrization curve where the first segment is the plotted as plain black line, the second segments are colored differently based on the b factor, and the yellow diamond indicates the end of linear flow. Maintaining the different depletion stems on the second segment allow us to determine the b factor that applies to the reference production profile. Since the second segment of the composite model depends on the time at the end of linear flow, each type well may have a different depletion stem. For instance, **Fig. 64** shows a type well forecast with the time at the end of linear flow half that in Fig. 63 to show the difference in the second segments. We can see that there is a larger expected range of cumulative production at 200 months on Fig. 64 than on Fig. 63. Hence, wells that reach the end of linear flow sooner have a wider range of depletion stems.

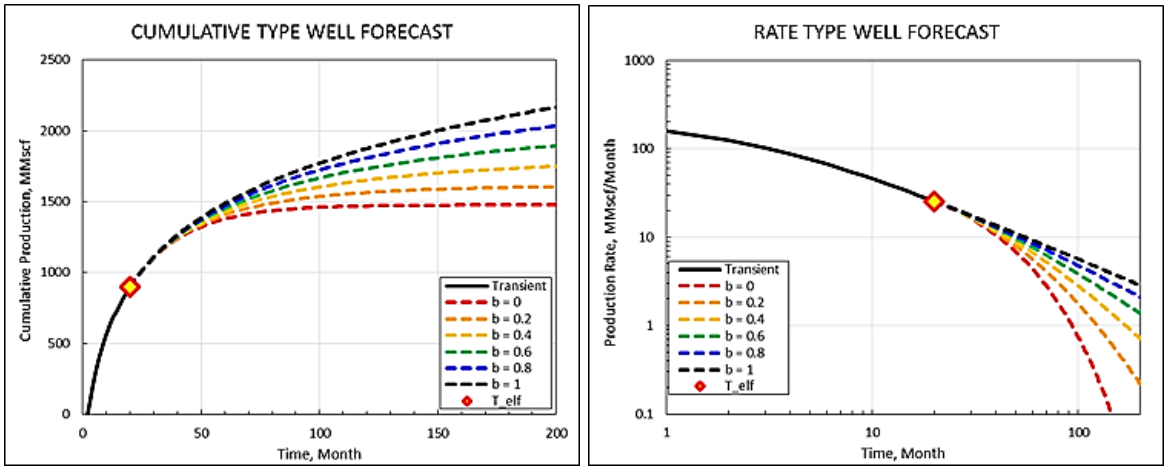


**Fig. 63—Composite parametrization used to forecast type wells and diagnose BDF behavior: $q_i$= 220 MMscf/mo, $D_i$ = 0.38 1/mo, $t_{elf}$ = 20 mo.**

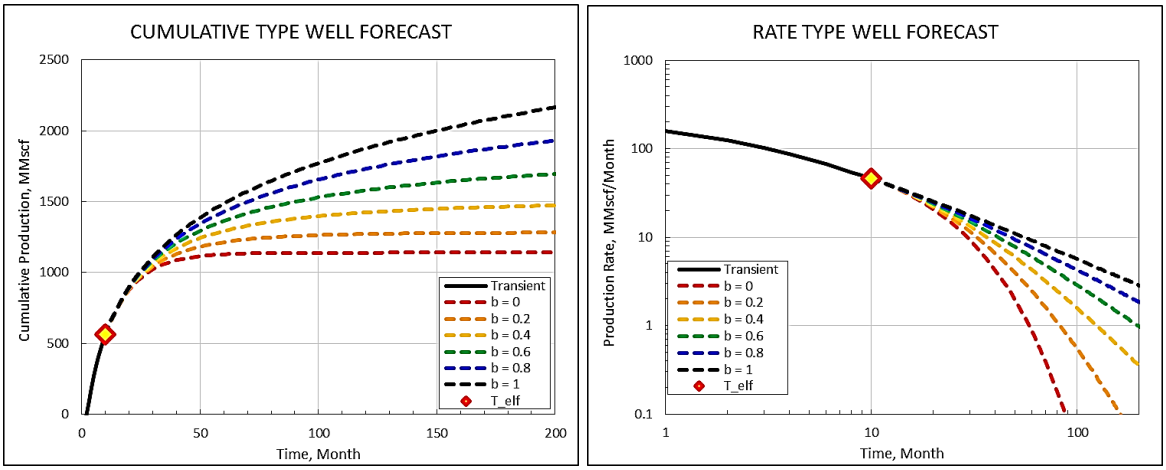


**Fig. 64—Composite parametrization used to forecast type wells and diagnose BDF behavior: $q_i$= 220 MMscf/mo, $D_i$ = 0.38 1/mo, $t_{elf}$ = 10 mo.**

The subsections 5.2.1.1 through 5.2.1.4 show how composite parametrization can be applied to the four examples presented in section 4.3. The transient segment was parametrized with the methodology presented in Appendices G and H and composite parametrization was used to characterize the late time behavior of each GSA.

#### 5.2.1.1. Composite Parametrization Example in the Haynesville Shale

The transient section of the reference cumulative-time profile shown in Fig. 66 was used to determine the decline parameters in Eq. 25. From Fig. 47, we estimated an average time of end of linear flow to be 5 to 8 months. Both parametrization methods are used for the transient section. In both cases, **Fig. 62** indicates that Arps decline models with either b =1 or 2 fit the data.

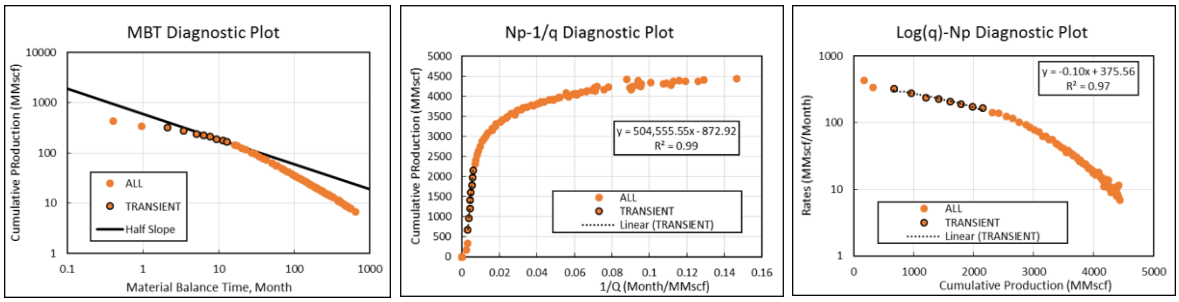


**Fig. 65—Haynesville transient diagnostic plots**

**Fig. 66** presents the composite parametrization of the Haynesville type well for this specific GSA with both a transient segment with b = 1 or 2.

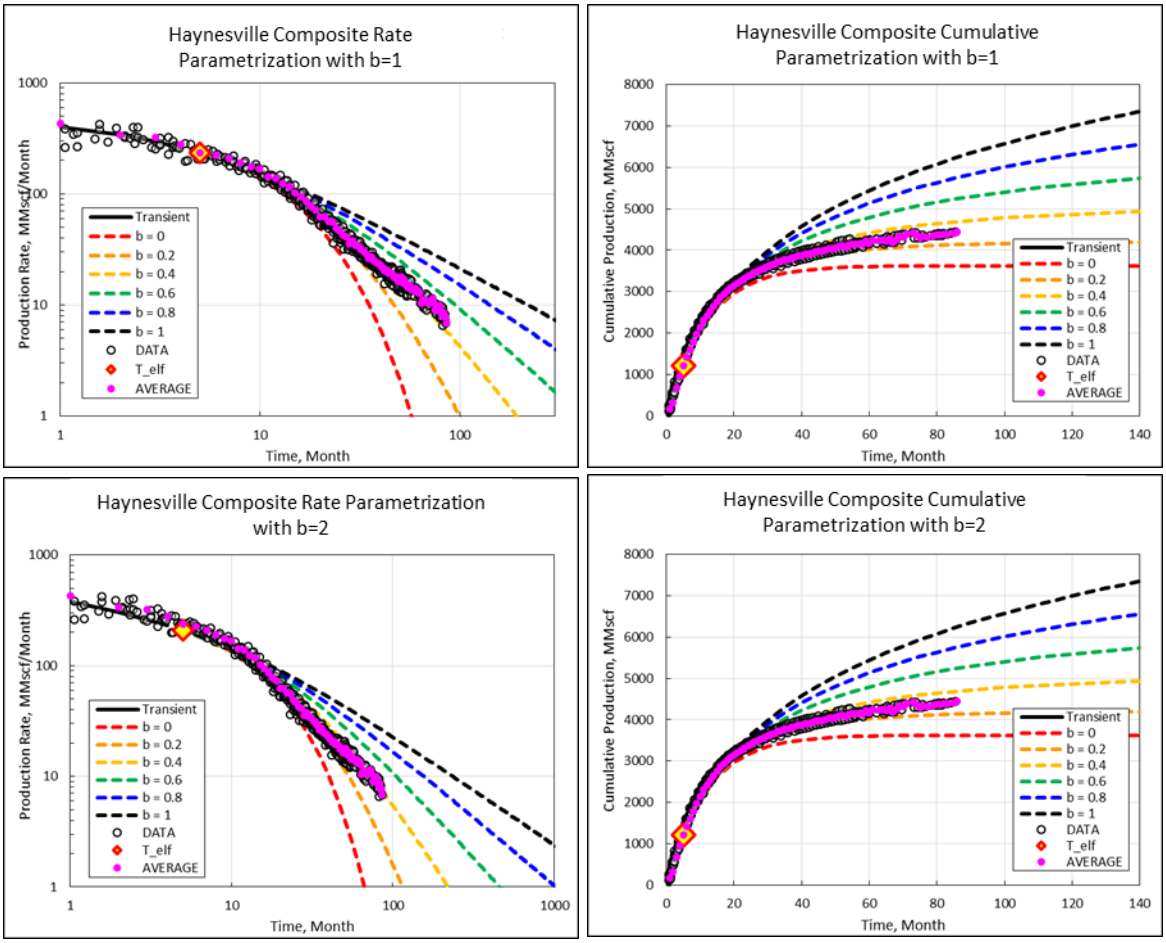


**Fig. 66—Haynesville composite parametrization used to forecast Haynesville type wells and diagnose BDF. Upper plots show the case with b = 1, where $q_i$= 486 MMscf/mo, $D_i$ = 0.21 $mo^{-1}$, $t_{elf}$ = 5 mo and $\epsilon$ = 1.11. The lower plot shows the case with b=2 where $q_i$= 578 MMscf/mo, $D_i$ = 0.66 $month^{-1}$, $t_{elf}$ = 5 mo and $\epsilon$ = 1.37.**

Fig. 66 shows that b = 1 fits the transient data better than b = 2 at early times. We see that the BDF follows decline stems of 0.3 and 0.4 for the two cases. Both methodologies essentially agree since the transient segment is very short and an approximation of the parameters was possible from the diagnostic plots of Fig. 65.

### 5.2.1.2. Composite Parametrization Example in the Eagle Ford Shale

**Fig. 67** presents the transient diagnostic plots. From Fig. 50, we estimated an average end time of linear flow of 15 Months. It appears that both transient parametrization methods can be used to fit the transient data because we can linearize the transient section of the production profile.

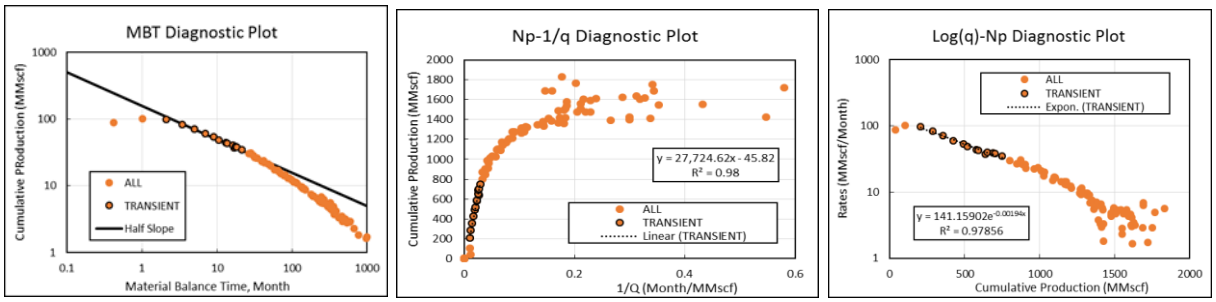


**Fig. 67—Eagle Ford transient diagnostic plots.**

**Fig. 68** presents the parametrization of the scaled production data. The results presented in section 4.3.2 indicated that two of the wells in this data set were not properly scaled, probably due to differences in depths and estimated drawdowns. Fig. 68 shows that those two wells have an impact on the averaged profile, especially at late times. The deviation from the group at later times illustrate the survivor bias that was mentioned by several authors as detailed in the literature review, section 2.2. An investigation of both parametrization methods shows that the parametrization with b = 1 works better than with b = 2 for BDF, while the two outliers shown by the red arrow on Fig. 68 lead to an overestimation of the typical production for this reference well. Finally, the orange arrow shows that parametrization with b = 2 does not provide a good fit of the data. Since fitting with b = 0 leads to an overestimate of production, we prefer the parametrization with b = 1 for the transient flow and b = 0.2 for BDF.

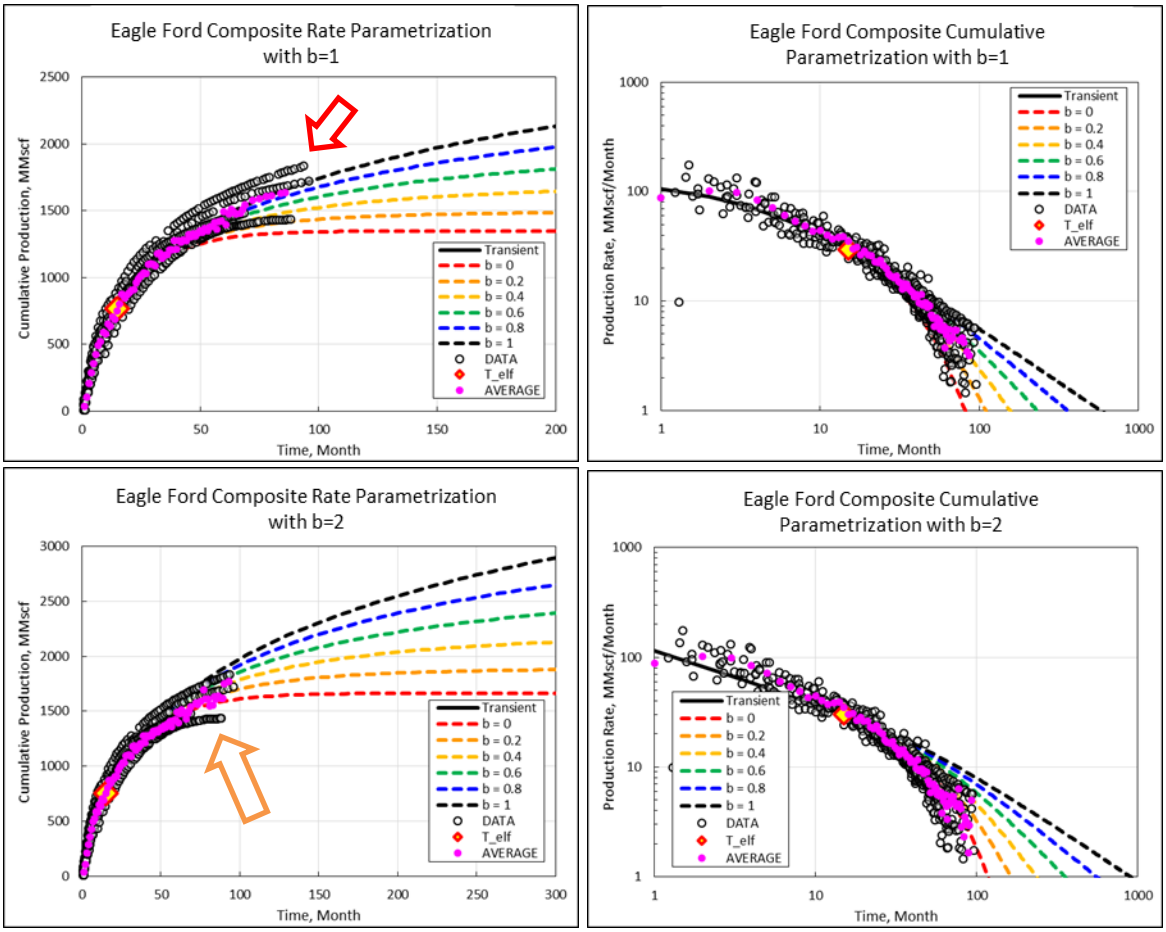


**Fig. 68—Eagle Ford composite parametrization used to forecast type well production and diagnose BDF. The upper plots show the b = 1 case where $q_i$= 129MMscf/mo, $D_i$ = 0.22 $mo^{-1}$, $t_{elf}$ = 15 mo and $\epsilon$ = 1.09. The lower plot is the case b=2, where $q_i$= 605MMscf/mo, $D_i$ = 13.2 $mo^{-1}$, $t_{elf}$ = 15 mo and $\epsilon$ = 3.52.**

In this example, we observed that the Eagle Ford transient production can be fitted with b = 1 and the BDF can be fit with b = 0.2. The log(q)-$N_p$ diagnostic plot in Fig. 67 also demonstrates that the linear fit of the transient data also fits the early section of BDF approximately.

### 5.2.1.3. Composite Parametrization Example in the Marcellus Shale

The transient section of the averaged production profile shown on **Fig. 69** was used to estimate the decline parameters of the parametrization of Eqs. 24 and 25. From the data in Fig. 53, we estimated the average end time of end of linear flow to be 35 months.

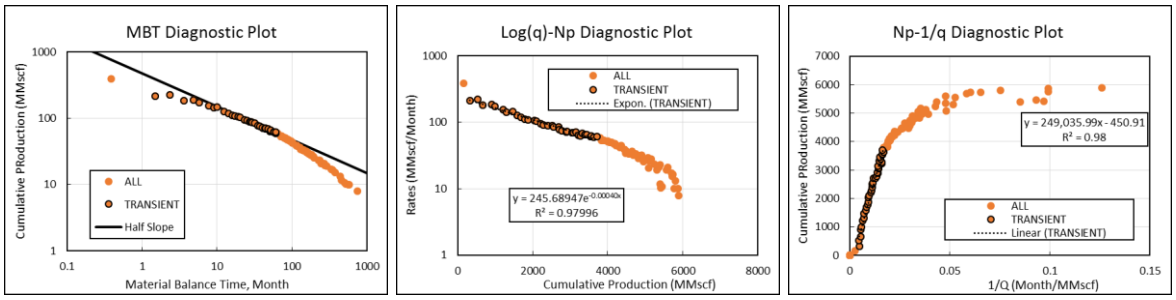


**Fig. 69—Marcellus transient diagnostic plots**

Since Fig. 69 shows that either parametrization method could lead to accurate results, they were used. We present both parametrization on **Fig. 70**.

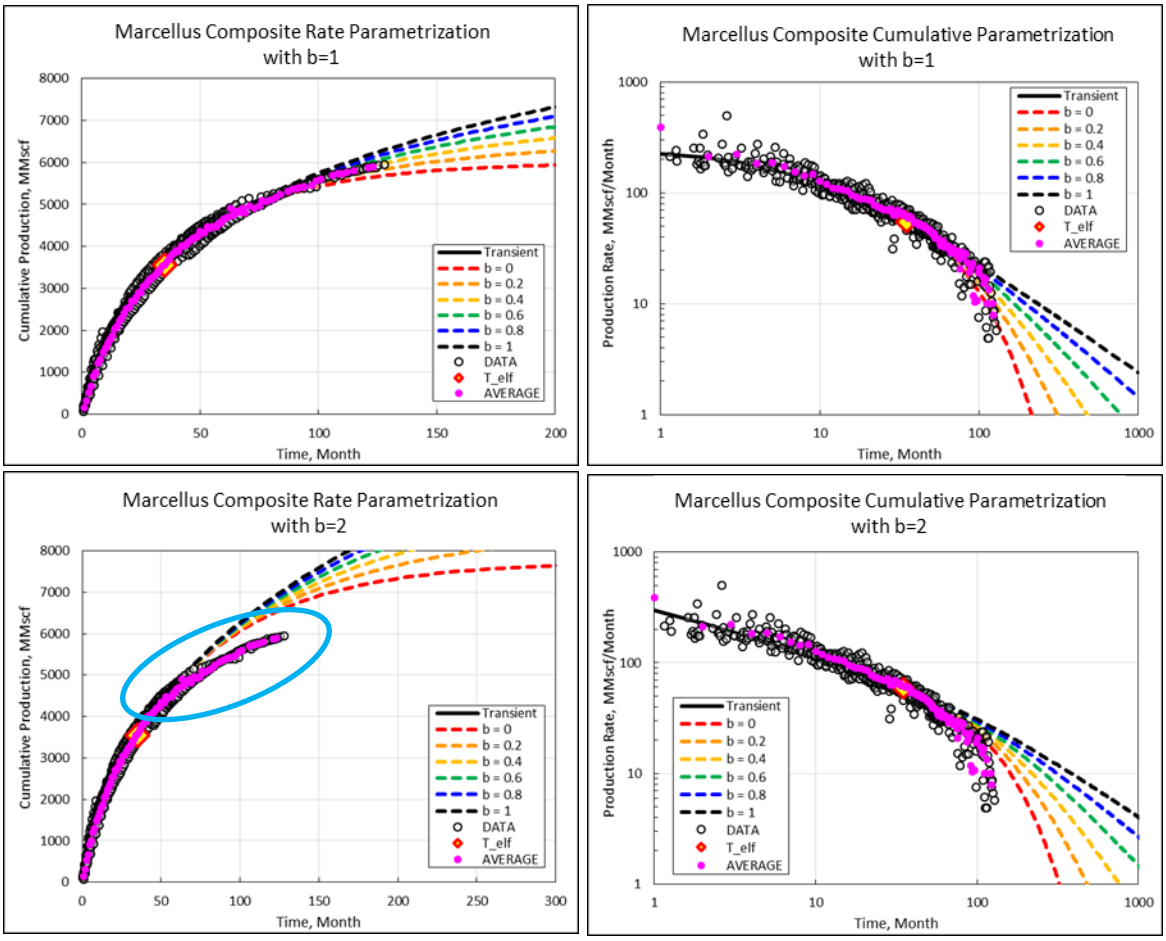


**Fig. 70—Marcellus composite parametrization used to forecast type wells and diagnose BDF. The upper plots show the case with b = 1 where $q_i$= 248.3 MMscf/mo, $D_i$ = 0.102 /mo$^{-1}$, $t_{elf}$ = 35 month and $\epsilon$ = 1.025. The lower plot shows the case b=2 where $q_i$= 550 MMscf/mo, $D_i$ = 1.216 mo$^{-1}$, $t_{elf}$ = 35 mo and $\epsilon$ = 1.46.**

Fits with b = 1 parametrize the depletion of the Marcellus type well more accurately than b = 2 because none of the decline stems of the b =2 model follow the production trend after the end of linear flow. The diagnostic decline stems of the second section do not provide many indications about appropriate values of b factor during BDF. Based on the longest producing well, it seems that it matches a hyperbolic depletion stem where b = 0.4. However, this observation is valid only for this specific well. As Fig. 63 and Fig. 64 demonstrate, it is difficult to estimate b factor because of the small differences in the depletion stems. **Fig. 71** compares the results of the two methods, and we conclude that b =1 provides a better fit.

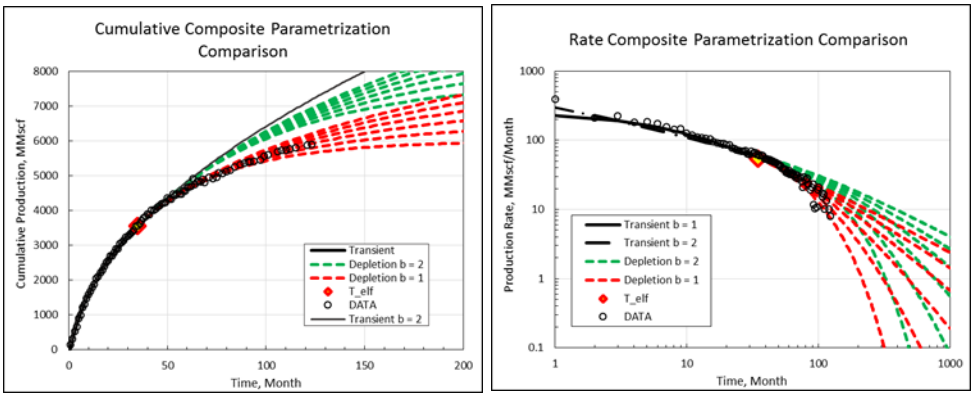


**Fig. 71—Marcellus composite parametrization comparison**

### 5.2.1.4. Composite Parametrization Example in the Barnett Shale

The transient section of the averaged rate-MBT profile shown in **Fig. 72** was used to diagnose the transient region and the associated parameters for Eq. 24 and 25. In Fig. 56, we find an average time of end of linear flow of 35 Months.

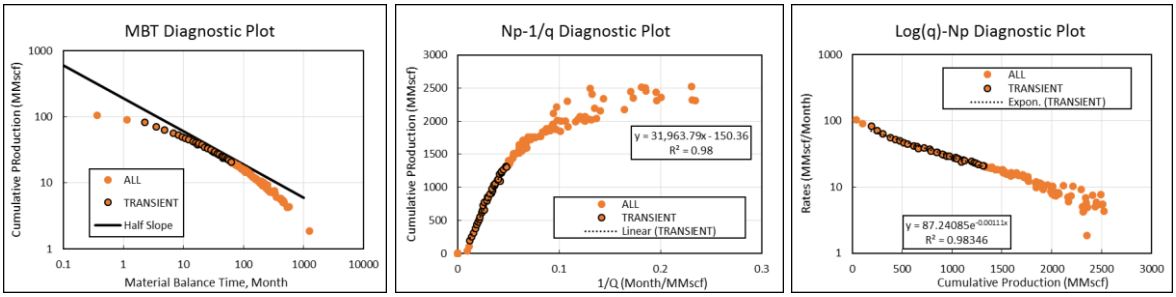


**Fig. 72—Barnett transient diagnostic plots.**

Since Fig. 72 shows that either parametrization method could be used, is the results from both are presented in **Fig. 73**.

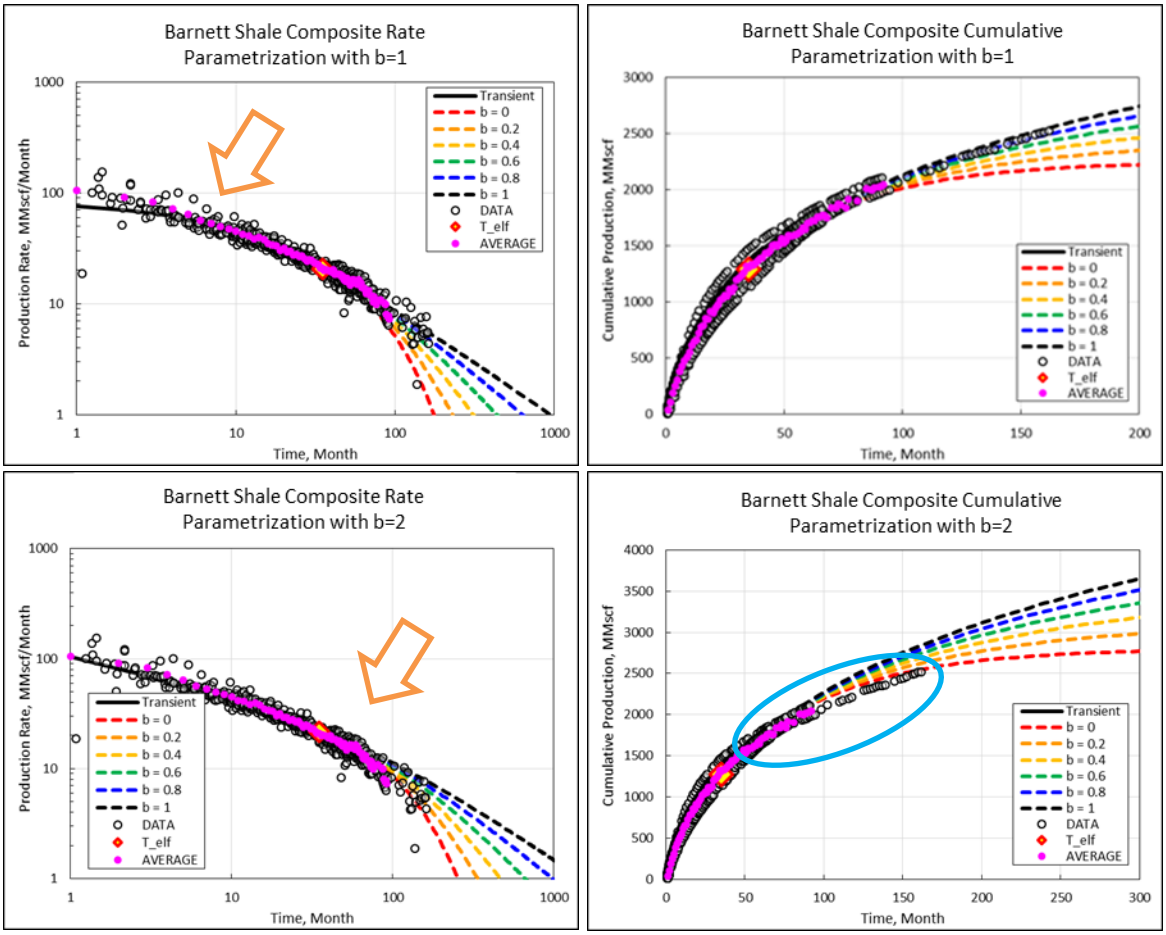


**Fig. 73—Barnett composite parametrization used to forecast type wells and diagnose BDF. The upper plots show the harmonic case where $q_i$= 82 MMscf/mo, $D_i$ = 0.086 $mo^{-1}$, $t_{elf}$ = 35 mo and $\epsilon$ = 1.014. The lower plot shows the hyperbolic case b=2 where $q_i$= 176 MMscf/month, $D_i$ = 0.94 $mo^{-1}$, $t_{elf}$ =35 mo and $\epsilon$ = 1.36**

Comparing both parametrization methods, we can see that the fit with b = 2 is better than the fit with b = 1, as shown with the orange arrow on Fig. 72. However, the depletion stems of the hyperbolic segments are above the scaled production, as shown by the blue circle. Finally, the fit of transient data with b =1 leads to a much better BDF b-stem match of 0.8. As the b = 1 parametrization fits the production profile better, **Fig. 74** confirms this result. Comparing both parametric equations, it appears that the depletion stems from the b = 2 transient data fit are much higher than the depletion stems from the b = 1 transient data fits. Because both equations shift at the same time at the end of linear flow, the parameters calculated with the equations presented in Appendix I influence the depletions stems.

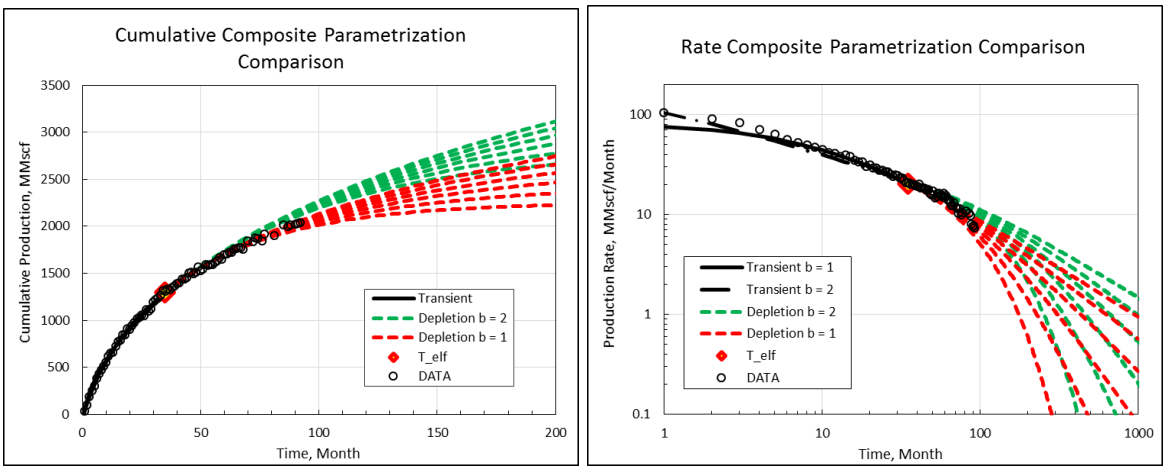


**Fig. 74—Composite parametrization comparison for the Barnett shale example.**

While the objective of using the composite parametrization is to fit the data, the fits of transient data with b = 1 lead to better fits of BDF data. Also, linear regression fits of transient data in Fig. 72, fit most of data in BDF as well.

#### 5.2.1.5. Composite Parametrization of Shale Gas Examples Summary

To summarize the four examples, we observe that the composite parametrization with b=1 and a value of epsilon greater than 1 generally provide a better fit, if not equal, compared to the fit with a b=2. The depletion stems depends on the parameters calculated in Appendix I. The equation of the depletion stems were developed empirically and some modification to those equation may improve the fit.

Finally, we observed that most of the transient data plotted on a straight line on the Log(q)-Np plot. Because a straight line on the Log(q)-Np indicates that a b=1 can fit the production data, it validates the good fit we observed, expect for the Haynesville that has a very short transient period and a sharp transition in boundary dominated flow. **Fig. 75** present the data of the plays to compare their behavior. As previously mentioned, we see that a straight line could fit more than

half of the total production history. While this observation may be an isolated result, it encourages to use a b=1 when fitting the transient section of publicly available data.

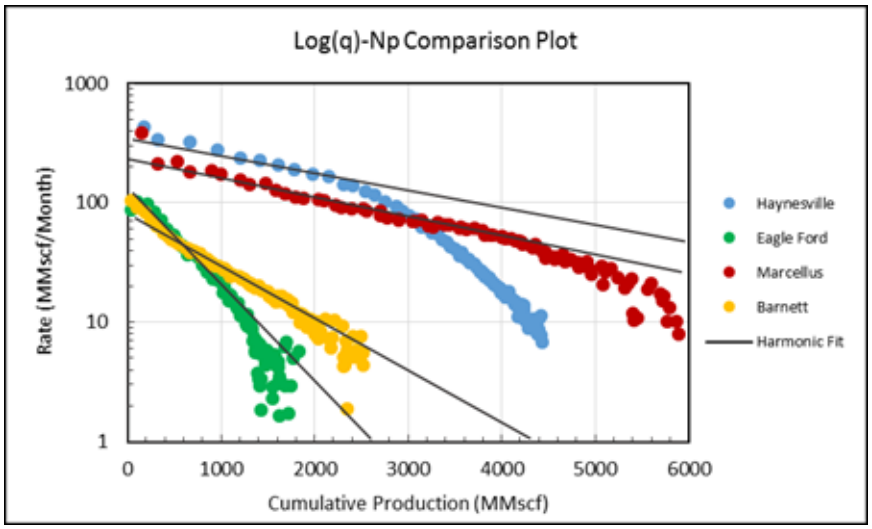


**Fig. 75—Log(q)-Np comparison plot of the type well for each play**

Finally, the b factors of the second segment should not be directly compared to Fetckovitch's depletion stems since the depletion stems of the composite parametrization depends on the approximate fit of the transient segment. Nevertheless, the Haynesville type well has an excellent fit with a b factor of 0.4 since it has such a large production history. Inversely, the Barnett and the Marcellus shale did not have enough time producing in BDF to distinguish a specific b factor on the stems. So based on the limited information, it seems that the Barnett follows a b of 0.8 while the Marcellus follows a b of 0.4. Such wells do not provide enough information to forecast the group, and different b factors should be used. Finally, the noisy data of the Eagle Ford also reduced our ability to accurately determine a b factor. Discarding the shallower wells, it seems that the depletion varies between a b of 0.2 to 0.4.

This small sample of each shale gas play seems coherent with Fetkovich's recommendations of using b = 0.4 to 0.5 for gas wells in BDF. A study with older wells should be done to validate our observations.

In summary, the composite parametrization can play a key role in type well construction. After rescaling the production profiles with the scaling factors, the group of wells should show a common reservoir behavior as we observed that the rates converge to the same profile. We suggest to generate the typical profile by averaging the scaled profiles with the time slice method. We also recall that survivor bias may impact the behavior of the profile at late time. The composite parametrization allows to fit the averaged profile with two hyperbolic segments and the switch between the two segments occurs at the end of linear flow. It appears that a decline with a b smaller than two of the transient section provides a better result for publicly available data. But a b value of 2 is theoretically recommended based on the transient flow regime characteristics. We encourage to try both as the objective is to fit as many points as possible. Since the depletion stems may be used to forecast future production, but we recommend to use at least a range of b factors to characterize this uncertainty.

### 5.3 Production Forecasting for Wells Producing in Transient Flow Regime

We use the base case profile generated in the section 5.2 to forecast the production of wells in transient flow regime. As instructed by Fig. 60, the base well profile is rescaled to set of permeability and fracture half length. Because both of those properties are unknown, we use the transient flow regime section of the profile to estimate the $x_f\sqrt{k}$ product. We relate this product to the performance of the well because we estimate one property based on the assumption of the other. To estimate this value, Wattenbarger et al. (1998) demonstrated that the half slope on the log-log diagnostic plot is equivalent to a straight line on the $\frac{\Delta m(p)}{q}$ vs. $\sqrt{t}$ plot for a constant pressure case. Appendix F details the derivation of the $x_f\sqrt{k}$ product for the modified analytical model presented in Chapter 3, which is summarized by Eq. 25.

$$x_f\sqrt{k} = f_{cp}\frac{315.5F_s}{hL_w m_{sl}}\frac{T}{\sqrt{(\mu\emptyset c_t)_i}} \tag{24}$$

The constant $m_{sl}$ is the slope of the line going through the points in transient linear flow on the $\sqrt{t}$ plot. **Fig. 76** presents the correct procedure to estimate $x_f\sqrt{k}$. Only the points colored in

blue should be fitted to find $m_{sl}$. The points in red are discarded because they do not fall on the negative half slope as shown on the diagnostic plot. For this research, we assume that the $x_f\sqrt{k}$ product theoretically remains constant throughout the life of the well because we also assume a constant operating condition and change of properties with time.

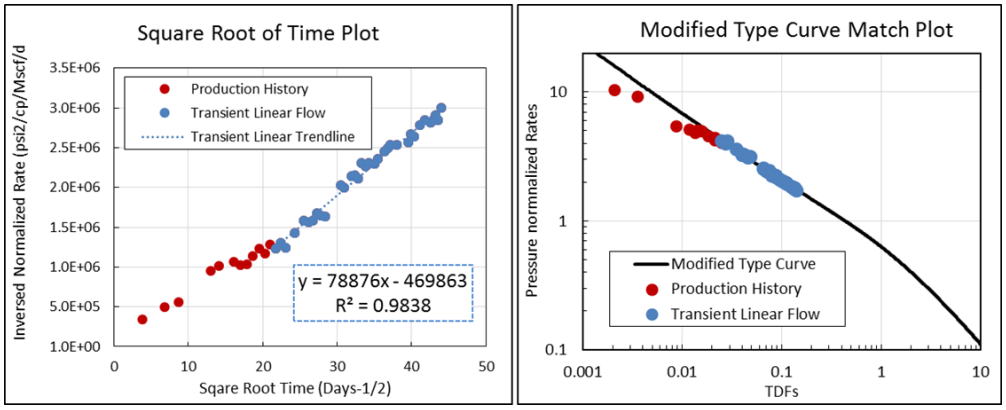


**Fig. 76—Example of the procedure to estimate $m_{sl}$. Left: square root time plot; right: modified type curve match plot.**

Based on the calculation of $x_f\sqrt{k}$ from the $\sqrt{t}$ plot, we estimate the maximum permeability and minimum fracture half-length with the modified type curve. Wattenbarger et al. (1998) suggested that the end of linear flow occurs at a dimensionless time of 0.5 for the constant rate case and 0.25 for the constant pressure case. Since the MBT converts a constant pressure solution to a constant rate solution, we match the latest point of the production to the dimensionless time of 0.5 as displayed on **Fig. 77**. This fit provides the most conservative estimation of permeability and fracture half-length because it implies that the future production would occur in boundary dominated flow. It also defines the smallest size of the SRV and forecasts a greater production decline. Solving Eq. 11 and 12 with the associated TM and QM yields the maximum effective permeability and minimum fracture spacing. The left plot of Fig. 77 shows that the profile can be matched on multiple locations of the type curve, which also implies multiple forecasts.

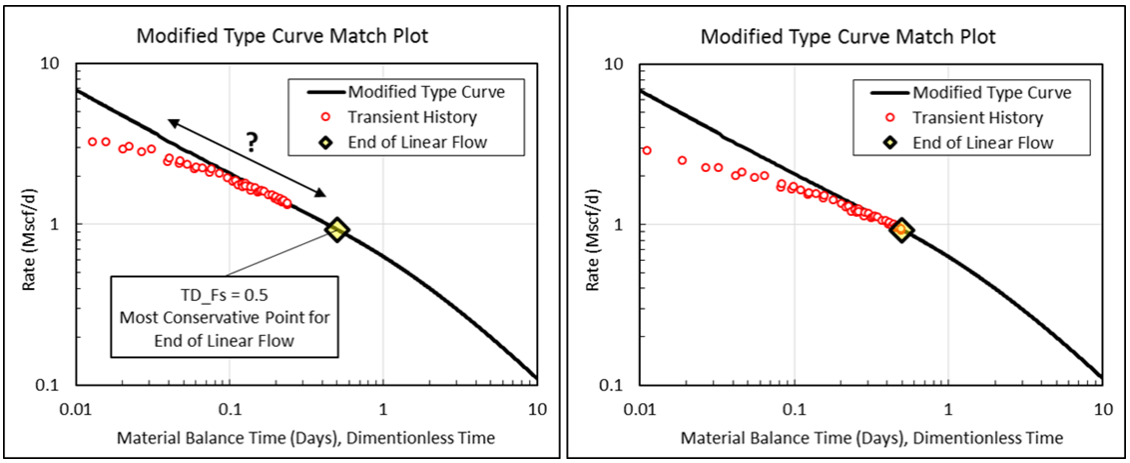


**Fig. 77—Conservative estimation of permeability and fracture half-length on modified type curve match plot**

To illustrate the change in permeability and fracture half-length based on how the data fits the type curve, **Fig. 78** shows the four different matches on the modified type curve. The pink match corresponds the most conservative fit as shown on the right plot of Fig. 77. Case 2 to 4 are matches that fit the data at different locations on the type curve. The right plot of Fig. 78 shows a cross plot of the permeability and fracture half-length. As expected, the pink circle has the highest permeability and the lowest fracture half-length since it is the most conservative case. Furthermore, the power trend line applied to the results confirms the relationship between the permeability and the fracture half-length. In this example, the $x_f\sqrt{k}$ is equal to 6.7. A cross-plot of the permeability and the fracture half-length is an alternative method to determine $x_f\sqrt{k}$.

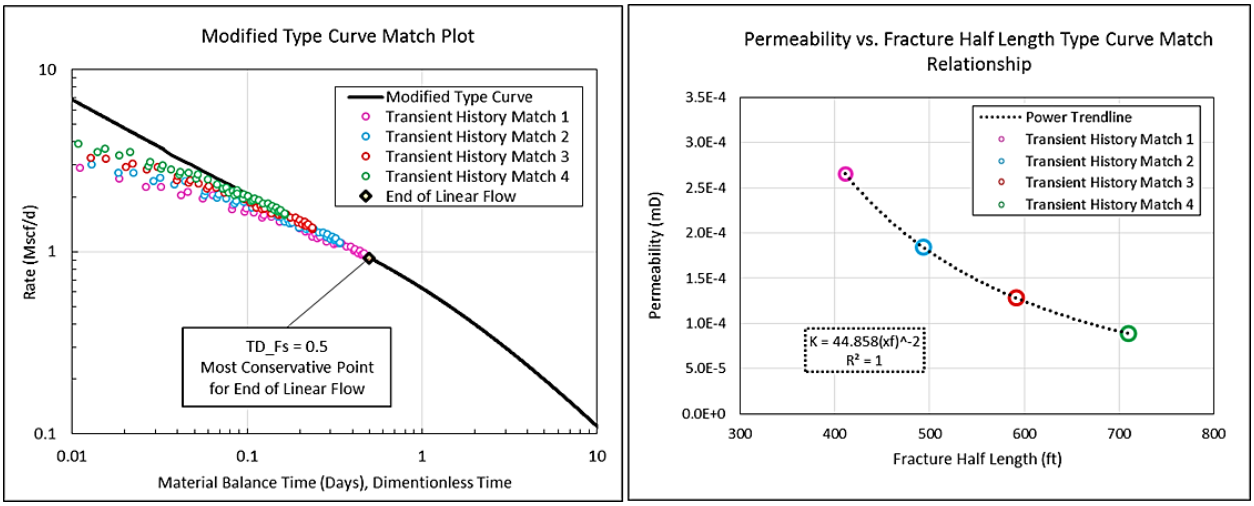


**Fig. 78—Permeability and fracture half-length relationship (right) for different matches of transient data on the modified type curve (left).**

We implement step 7.2 and 8.2 of the workflow by first rescaling the base case profile to the known properties: the lateral length, fracture spacing and net-pay thickness. Then, the most conservative guess of the permeability and the fracture half-length are used to generate the most conservative forecast. Given the uncertain duration of the transient flow regime, we also recommend to probabilistically forecast the production using a realistic distribution of the permeability (or fracture half-length), such as the truncated distributions of the previously estimated properties in BDF. The distribution should be truncated by either the maximum permeability of the minimum fracture half length. Otherwise, it would mean that our well would already be flowing in BDF. It is most likely that the maximum permeability will truncate a significant portion of the original permeability distribution since most of the wells in BDF are likely to have higher permeability or at least denser stage spacing. Finally, only one distribution should be sampled since the other parameter can be calculated with $x_f\sqrt{k}$. Hence, for a known $x_f\sqrt{k}$, sampling a value of permeability would automatically provide a value for the fracture half-length. This procedure takes advantage of the functional relationship given by $x_f\sqrt{k}$ to forecast production of wells in transient flow regimes as we are able to rescale independently for each estimated property.

## 5.4 Production Forecasting for Undrilled Wells

Forecasting undrilled wells with the analytical scaling method provide both a deterministic and probabilistic estimation. The scaling factors provide a reliable tool to normalize base well and forecast the production of a specific completion design, such as lateral length, stage spacing and expected drawdown for the life of the well. A deterministic forecast is provided by scaling with the average value of permeability, fracture half-length and net pay thickness of the base well. However, using a mean value does not quantify the range of uncertainty for the unknown parameters. Given the estimated distributions of reservoir and completion properties, we recommend to build probabilistic forecasts of undrilled well from the base case profile and the scaling factors generated by a Monte Carlo simulation. This method is very similar to the procedure used to estimate reserves in the conventional industry because it use the information that characterizes the reservoir

As shown on Fig. 60, different kinds of input variables can be used to rescale the base well profile. Using only the specific distribution of the wells in boundary dominated flow can limit the range of expected production. As most of the wells with short production history are in transient flow regime, the distribution of $x_f\sqrt{k}$ can also be used to model dependencies between the permeability and fracture half length. Furthermore, publicly reported inputs such as the proppant concentration, the proppant size, stimulation fluid volume, cluster spacing, choke size, formation thickness, gas gravity or the minimum distance to the nearest neighbor or total vertical depth may be studied with a regression analysis to find correlations, if causation are possible, with the permeability and the fracture half-length. Ignoring such correlation in a Monte Carlo model can distort and over-estimate the uncertainty. We suggest to set up a Monte Carlo model with correlation between variables. The mathematical model used in the Monte Carlo simulation relies solely on the scaling factors and the parametric equation of the base well profile. From them, we have the ability to compute a rate or a cumulative volume at any time and for any set of properties.

Because the IP or the EUR are variables that were previously used to normalize in the literature, we constructed **Table 19** to clarify the list of input and output parameters of our model. We refer to the scalable parameters as primary input parameters because they are the ones used to rescale the base production profile. The secondary parameters are other inputs, such as the completion designs, that cannot be scaled directly but can be used indirectly by identifying

correlations with primary inputs via regression analysis. Finally, the primary output of the model are RSF, TSF and CSF. They allow to rescale the parametrized profile and calculate the secondary output such as the initial rates and cumulative production at any time. In any case we recommend to normalize for the initial rate, IP or EUR because those parameters theoretically only reflect the effect of the primary variables.

| Primary Input Variable | Secondary Input Variables | Primary Output Variables | Secondary Output Variables |
|---|---|---|---|
| Lateral length | $x_f\sqrt{k}$ | TSF | Initial rate |
| Stage spacing | Proppant concentration | RSF | Time at end of linear flow |
| Net-Pay thickness | Stimulation fluid volume | CSF | EUR |
| Fracture half-length | Cluster spacing | | IP(30) |
| Permeability | Gas gravity | | IP(60) |
| Base-case Profile(s) | Well depth | | IP(180) |
| "b" Factor Forecast | Formation thickness | | |
| | Net/gross | | |
| | Distance to the closest neighboring well | | |

Table 19—Monte Carlo variable definition to forecast undrilled wells.

The primary inputs variables have already been presented as the scaling factors of Chapter 4. If we forecast for a specific well/completion design, other inputs such as secondary variables of Table 19 can be used to run the model. It requires that dependencies between the secondary input variables and the primary variable can be identified, such as a correlation between the fracture half-length and the volume of stimulation fluid. Wright (2015) recommends to practice good engineering judgement while determining the correlation between a dependent and an independent variable, only if we believe that there is a causation. Regression analysis should be applied to the variables of the wells in the GSA to identify and validate dependencies based on a large number of sample. A conservative methodology would be to anticipate causation between input parameters and prevent unrealistic correlations.

We demonstrated that the scaling factors allows to rescale the production profiles based on the diagnostic of the parameters in the dimensionless equations. Hence, the analytical scaling and

the relationships presented in Table 12 provide the direct correlations between the primary inputs and the secondary output variables based on fundamental fluid flow principles. While some empirical correlations between EUR or initial production and for instance lateral length or stage spacing were presented by some authors (Voneiff et al. 2014), we believe that they are conditioned by the theory provided in the analytical scaling factors. We believe that the added value for the industry lies in the correlations between the primary and the secondary inputs variables. Understanding those correlation will narrow the uncertainty when forecasting production, and thus the EUR. For instance, given a large data set of wells with similar fracture spacing and lateral length, a potential correlation between the stimulation designs could allow the construction of a specific distribution of permeability and fracture half-length. All in all, the outcome of this methodology inherently depends on the confidence in the input variables and their dependencies. To build representative forecasts, several distribution and correlations should be tested in order to study the sensitivity of each parameters. As it will be illustrated in Chapter 6 with the example of an undrilled well with specific design parameters, the cumulative production can be generated for different dependencies between the uncertain variables. Finally, tools like the sequential aggregation plot allows to test each distribution and validate the most reliable model in order to forecast production.

### 5.5 Wells with Undefined Flow Regimes

The wells classified under undefined flow regimes can be more or less a great percentage of the full dataset depending on the quality of the reported volumes and their production history. Several factors can prohibit a good match between the production history and the modified type curve. The first limiting factor is a major change in operating conditions after workovers, such as a change in artificial lift, a re-stimulation treatment in this well or its neighbors. Those changes directly impact the estimated “effective” permeability and fracture half-length parameters assuming that the rest of the parameters would remain constant. Such changes are usually visible on all the diagnostic plots and create discontinuities in the production history on diagnostic plots. Two examples of changes in operating conditions are presented in Appendix K colored multi-segments plotted on the MBT diagnostic plot. Similarly, the following example illustrated by **Fig.**

**79** shows two common cases encountered when trying to diagnose the reservoir and completion properties of MFHW. A change in operating conditions were highlighted by the color difference, the blue color shows the first segment and the red shows the second segment. In the first case, the production profile is discontinued after 110 months, which leads to a sudden change of slope on the MBT plot and the square-root of time plot. The production of the second segment seems to be flowing in boundary dominated flow as per the slope on the MBT plot. Based on this sudden change, it is possible to match the MBT plot to the type curve; however, because the segments are discontinuous, we would diagnose a permeability and a fracture half-length that may not be representative of either the properties of the first or the second segment. The same issue arises for the second example where it appears that the second segment is shifted up on the MBT.

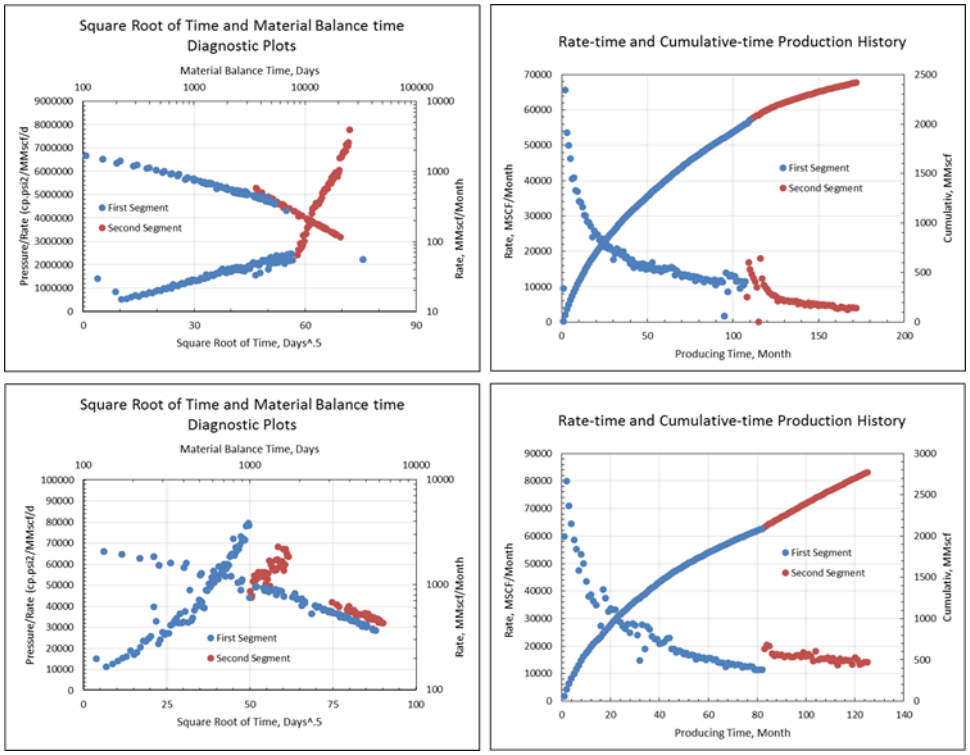


**Fig. 79—Two examples of change in operating conditions of two shale gas wells, top is 4212133100 and the bottom one is 4212131843.**

As opposed to the first example, the second example has greater rates and the cumulative production then increases to a higher rate than usual. Some speculations can be made on what happened for both examples, but the logic of the analytical scaling factors gives some clues if only the first segment is diagnosed. Some difficulties may arise because there could be multiple matches on the material-balance time plot, which may not provide a unique value of permeability. If enough production data is available, we recommend to match a section that continuously fit both flow regimes, however, it may only be used to estimate previous performance.

Other issues such as outliers and time shifting to producing time from calendar times are factors that can affect the diagnostic, and the user of the type curve is recommended to understand the limitations, which are addressed in Chapter 2. Furthermore, using pressure data will improve the flow regime diagnostic as it gives the ability to rescale for the drawdown with time, which circumvent a major uncertainty when dealing with public data. Finally, the last case that could happen, despite it was not encountered when fitting the data to the modified type curve, is the possibility of a different slopes on the MBT plot, even after correcting for changing BHP. As the slope is the main indicator of the flow regimes (bilinear, linear, BDF and elliptical), it is possible that the assumption of linear flow between fracture may not be applicable in a certain GSA based on the hydraulic fracture treatment and the nature of the formation. Different type curves exist for other flow geometries and can provide scaling relationships as it was demonstrated in Appendix B.

In summary, publicly reported data are the main focus of this work and it provides challenges due to the reporting quality and the frequency of the data. However, it appears to be sufficient to identify flow regimes and characterize the performance of a well with the estimated properties of a simplified analytical model. We recommend to use as much knowledge on the production practices of the wells studied to understand and interpret flow regimes, and subsequently the reservoir and completion properties. While the shale gas wells demonstrated a good fit against the modified type curve in chapter 3, many factors affect the production history during the life of the well and can create some discontinuities that limit the identification of flow regimes.

# CHAPTER VI

# CASE STUDY – DENTON COUNTY BARNETT SHALE GAS

This chapter was prepared to present the main applications of the workflow presented in Chapter 5. The chapter is separated into different sections, the first one introduces the Geologic Subset Area based on the data available for the study. The second section will present the work performed to generate a base well profile from the wells diagnosed with boundary dominated flow. The base well will be compared to the type wells generated with the time slice method to show the main advantages of this method. The following section will present how the base well can be used to forecast the production of other wells based on their current production history. The fourth section presents a forecasting example of an undrilled well based on a probabilistic method. Finally, the fifth section illustrates how the parametrization of the production can provide some information about the difference in permeability and fracture half-length of wells flowing in transient flow regime with a certain range of certainty. As this case study treats gas wells, other case studies are presented in Appendices J and K to demonstrate the application of the analytical scaling-factors to oil and condensate multi-fracture horizontal wells. As predicted in Chapter 3, since most of the profiles of MFHW fit the type curve, we are able to estimate the unknown properties of the modified analytical model and rescale the profiles to build type wells.

## 6.1 Geologic Subset Area Dataset Presentation

This case study was performed on horizontal wells producing exclusively natural gas from the Barnett formation in the Denton County, Texas as shown in blue on **Fig. 80**. The Barnett shale formation was deposited in the Mississippian period and is composed of two units, the upper and lower units separated by the Forestburg limestone. The structural features in the Denton County are the Muenster Arch in delimiting the northern extent of the Barnett shale and the Mineral Wells – Newark East fault system crossing in the South-West to the North-East section of the formation. The Barnett shale is deeper and thicker in the Denton County than the other counties. The wells in the Mississippian Barnett shale formation produce mainly gas and a small fraction of condensate. The first vertical wells drilled in the Denton County was put in production in 1985 and the first

horizontal well was put on production in 2003. As of May 2018, there are 1355 reported vertical wells, 1729 horizontal wells and 183 deviated or undefined wells. The total number of currently active horizontal wells is 1315 and vertical wells is 1319. The total historical production of the Denton County is 1088 BCF of gas and the contribution from the horizontal well is only 196 BCF, which represents only 18% of the historical cumulative production. Since the methodology presented in Chapter 5 is more accurate with stage spacing information, we were limited to a smaller data set, composed of 179 wells which define the Denton County GSA. **Fig. 81** shows the Denton county GSA delimited by the dotted green line. The map also illustrates the horizontal well density with their respective wellbore trajectories. The dark blue color define the wells with stage spacing information. We can see an uneven well density in the Denton county GSA, with an average of 2.45 square miles per well. In order to reduce the geologic uncertainty, we reduced the GSA to a smaller area as illustrated on Fig. 81. This GSA was chosen for the high well density with 654, and because it contains 100 wells with stage spacing information. The case study area represents a total surface area of 110 square miles with a density of 1.1 sq. mile/well whereas the total Denton county GSA represents 440 square miles with a well density of 2.45 sq. mile/well.

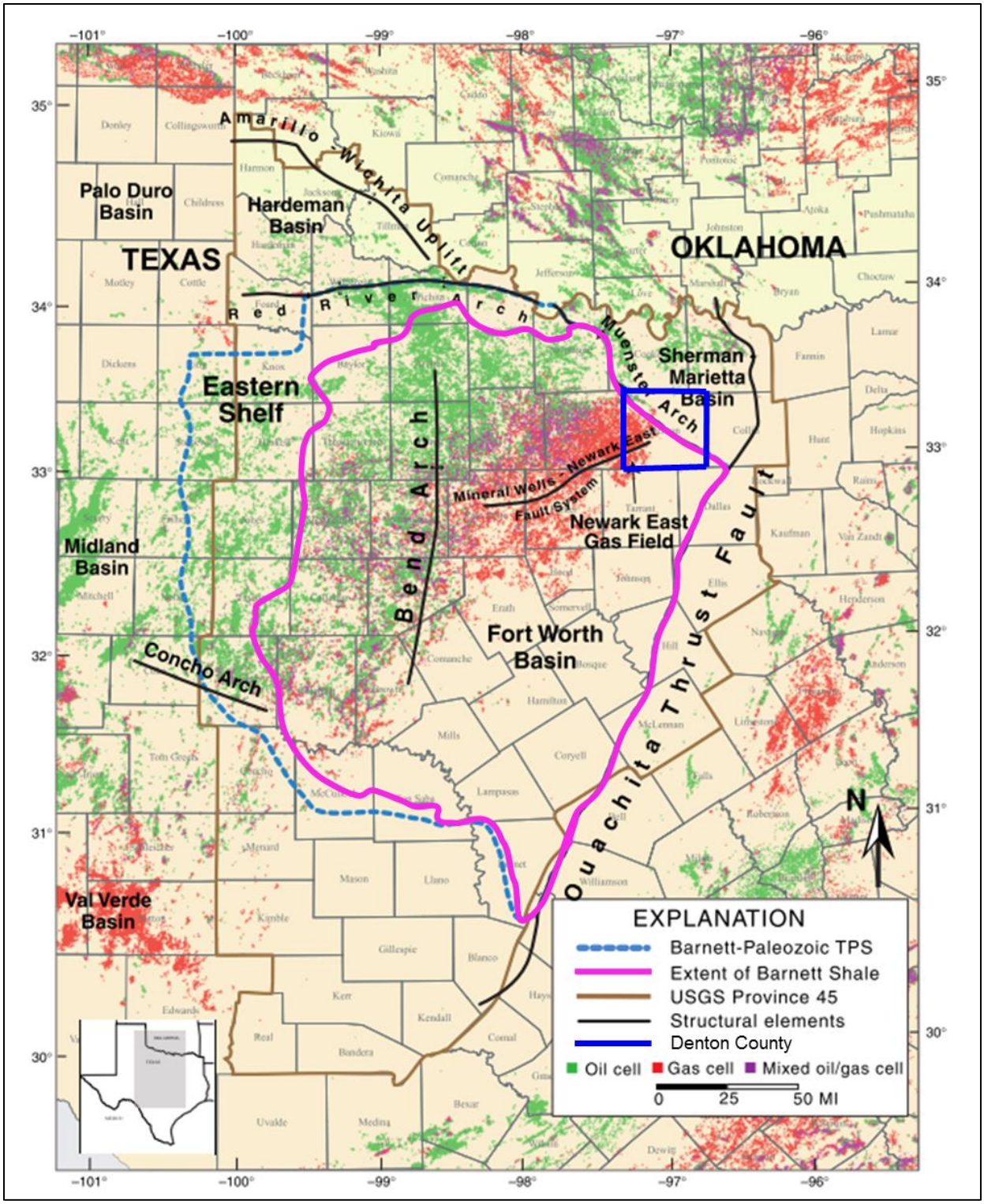


**Fig. 80—Maps showing Oil-, gas- and mix oil-and-gas-production cells reprinted and modified from Pollastro 2007, with the geographic extent of the Barnett Shale, its major structural elements, the location of the Denton County; cells are equal to 0.25 mi$^2$.**

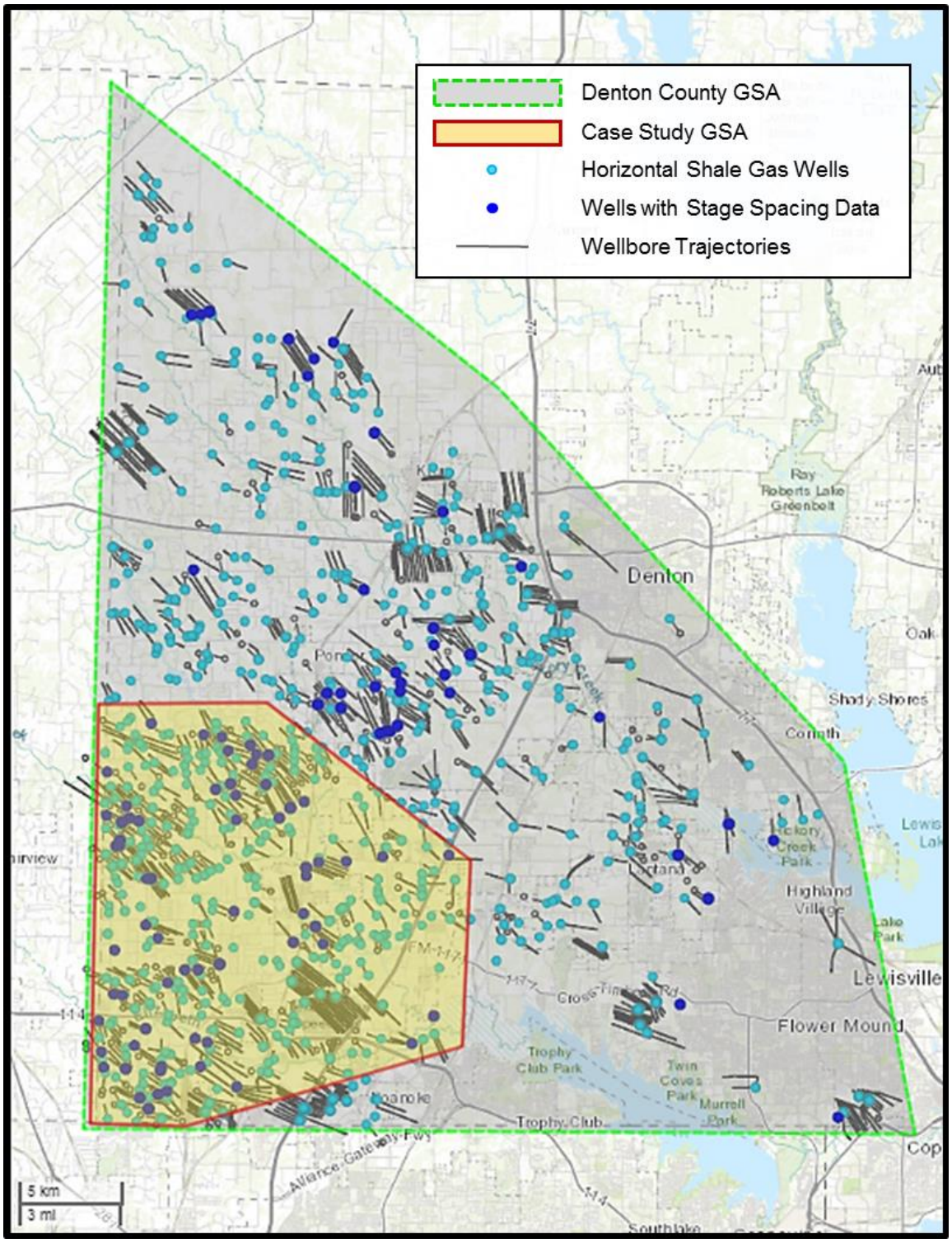


**Fig. 81—Map of Denton County horizontal wells distribution in the case study GSA.**

Based on the defined GSA, the production data was treated according to step 2 to 4 as described in Fig. 60. The production from each well in the Denton County GSA and the Case Study GSA were organized into the three different groups based on the flow regime diagnostic on the rate-MBT plot. There was a total number of 28 wells in BDF, 34 wells in transient and 38 wells with discontinuous production history in the case study GSA as presented on **Fig. 82**. Overall, the dataset of horizontal wells with stage spacing in the Denton County GSA accounts for 55 wells in boundary dominated flow, 71 wells with a transient flow regime and 53 wells with discontinuous profiles.

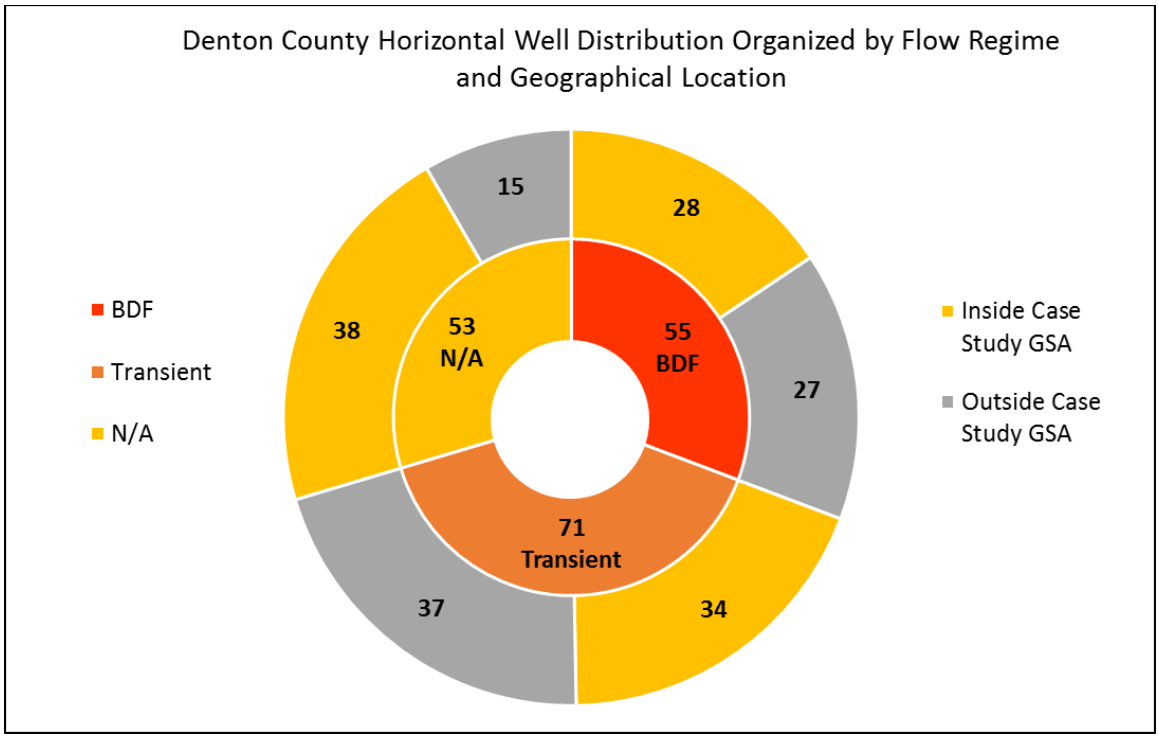


**Fig. 82—Distribution of wells from the Denton county GSA organized by flow regimes and geographical location.**

**Fig. 83** shows the spacial distribution of the well in BDF in green compared to the remaining wells in transient or undefined flow regime in dark blue. Luckily, we see that the wells in BDF are homogeneously spread over the GSA, and we avoid a potential geographical bias.

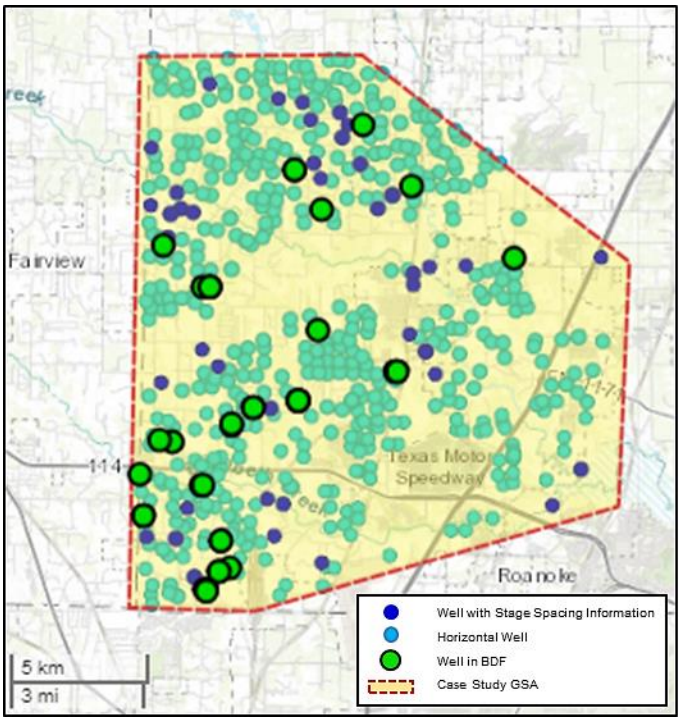


**Fig. 83—Map showing the well distribution by type in the case study GSA.**

The 28 wells in BDF selected in the case study GSA are plotted on the semi-log plot rate-time and Cartesian cumulative-time plot as shown on **Fig. 84**. We observe that there is a diverse range of productivity in the BDF group. The outliers detected by the technique presented in Appendix E are not shown on Fig. 84, which explains the gap in the cumulative and rate-time profiles. Assuming that a sample of 28 wells is statically sufficient to conduct the analysis, the next step requires to estimate the permeability and fracture half-length with the modified type curve.

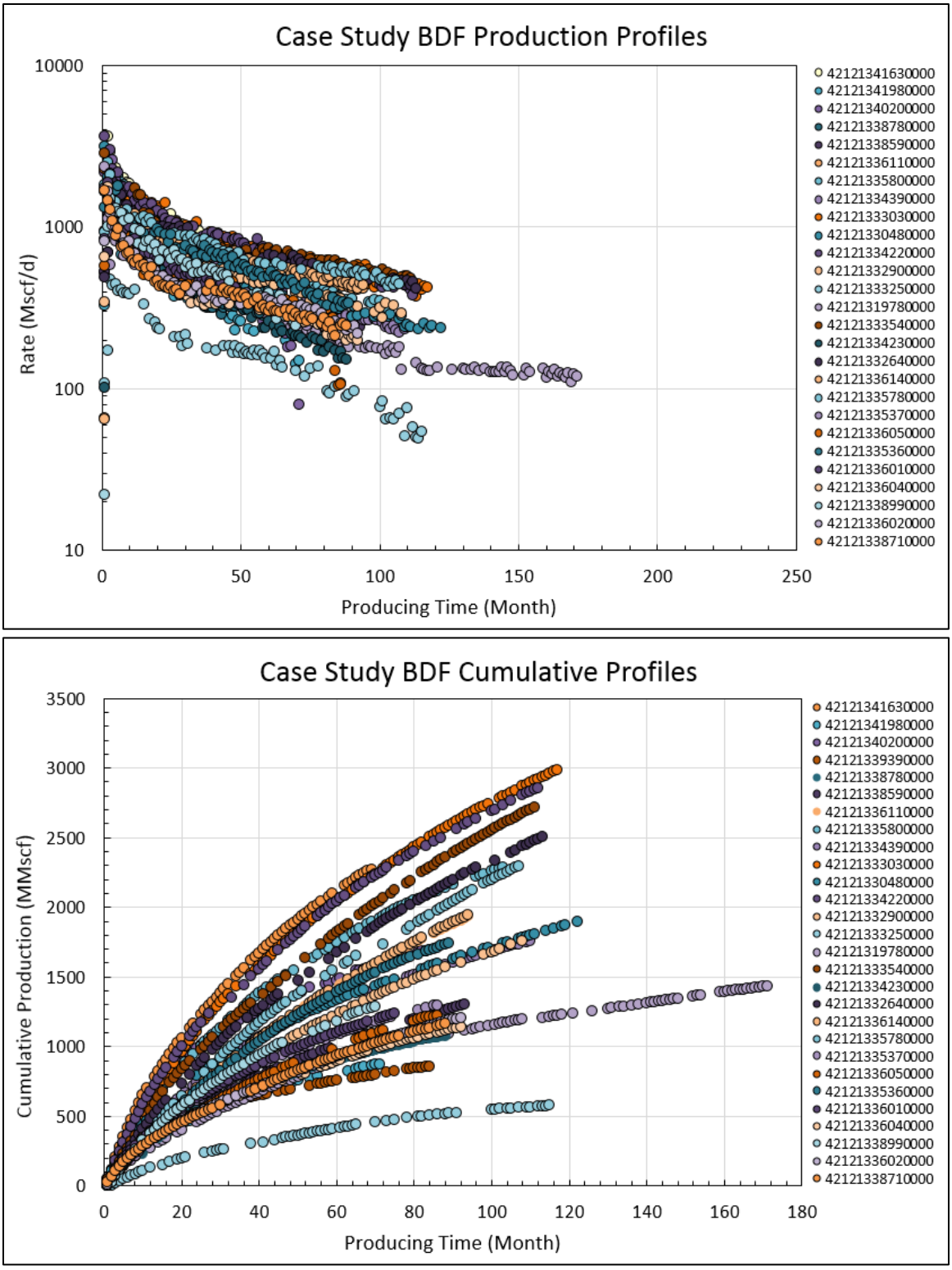


**Fig. 84—Barnett shale case study; BDF wells rate-time profiles (top) and cumulative-time profiles (bottom).**

## 6.2 Base Well Construction and Validation

As for the analysis conducted in section 4.3 for the Barnett shale, an average reservoir temperature of 660 Rankine was used. We calculated the flowing pressure equal to $0.1p_i$ and the initial reservoir pressure was calculated based on the true vertical depth of the lateral multiplied to a pressure gradient of 0.44 psi/ft. Since the gas gravity was provided in the data set as shown in Table 20, the pseudo pressure drawdown was calculated for each case with the spreadsheet equations assuming no impurities in the gas. Finally, we assumed a constant net pay thickness of 200ft for each well because we could not quantify the total thickness of the producing formation for each well or the equivalent vertical extent of the fracture treatment. The value of 200ft was used for the theoretical fracture height (net pay thickness) as per Fig. 8. As already mentioned in chapter 4, the result of the fracture half-length is proportional to the net pay thickness, so using the same value for all the wells will normalize the calculated fracture half-length.

**Table 20** presents the results of the match on the modified type curve and **Fig. 85** illustrates the results presented in the table. Based on the shape of the distributions and the size of the sample, we see that the permeability and the fracture half-length appear to fit a lognormal distribution.

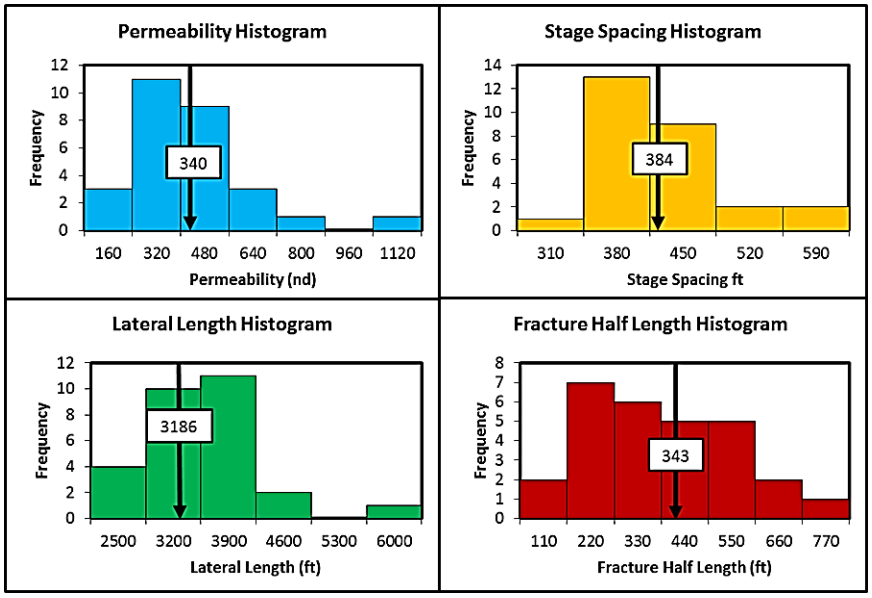


**Fig. 85—Distribution and average of the major reservoir and completion parameters of the 28 wells in BDF from the case study GSA.**

| Well API No | First Prod. | Lateral L. | Stage Number | Fracture Spacing | Well Depth | Net Pay | Proppant Loading | Frac Fluid | Initial Pressure | Flowing Pressure | Gas S. Gravity | P.P. Drawdown | TM | QM | $x_f$ | K | $T_{elf}$ |
|---|---|---|---|---|---|---|---|---|---|---|---|---|---|---|---|---|---|
| $10^{-4}$ | MM-YY | (ft) | | (ft) | (ft) | (ft) | (lbs) | (bbls) | (psia) | (psia) | | (psia^2/cp) | $10^{-3}$ | $10^{-3}$ | (ft) | (nD) | (Days) |
| 4212133325 | Apr-08 | 3642 | 10 | 364.2 | 7322 | 200 | 4.5E+06 | 2.2E+05 | 3221.7 | 322.2 | 0.61 | 6.5E+08 | 0.48 | 3.65 | 75.38 | 474.2 | 26 |
| 4212133290 | Dec-08 | 3399 | 9 | 377.7 | 7476 | 200 | 7.9E+06 | 4.3E+05 | 3289.4 | 328.9 | 0.61 | 6.7E+08 | 0.16 | 2.24 | 390.06 | 166.0 | 70 |
| 4212133536 | May-09 | 3154 | 8 | 394.3 | 7522 | 200 | 8.4E+06 | 1.6E+05 | 3309.7 | 331.0 | 0.61 | 6.8E+08 | 0.34 | 1.31 | 326.03 | 394.9 | 39 |
| 4212133537 | Mar-09 | 3454 | 9 | 383.8 | 7570 | 200 | 4.6E+06 | 1.9E+05 | 3330.8 | 333.1 | 0.61 | 6.9E+08 | 0.33 | 1.84 | 219.70 | 356.4 | 34 |
| 4212133578 | Mar-09 | 2784 | 8 | 348.0 | 7433 | 200 | 2.0E+06 | 1.9E+05 | 3270.5 | 327.1 | 0.6 | 6.7E+08 | 0.20 | 1.38 | 613.88 | 179.9 | 56 |
| 4212133354 | Nov-08 | 3279 | 9 | 364.3 | 6599 | 200 | 7.8E+06 | 3.8E+05 | 2903.6 | 290.4 | 0.6 | 5.4E+08 | 0.20 | 1.25 | 705.43 | 197.2 | 60 |
| 4212133899 | Jun-10 | 2049 | 6 | 341.5 | 7409 | 200 | 2.2E+06 | 8.6E+04 | 3260.0 | 326.0 | 0.61 | 6.6E+08 | 0.36 | 1.59 | 403.39 | 311.1 | 32 |
| 4212133303 | May-08 | 3329 | 9 | 369.9 | 7375 | 200 | 4.4E+06 | 2.0E+05 | 3245.0 | 324.5 | 0.61 | 6.6E+08 | 0.19 | 1.25 | 601.95 | 193.6 | 52 |
| 4212133859 | May-10 | 2939 | 8 | 367.4 | 7438 | 200 | 2.6E+06 | 1.2E+05 | 3272.7 | 327.3 | 0.62 | 6.7E+08 | 0.23 | 2.35 | 293.00 | 232.1 | 45 |
| 4212133611 | Apr-10 | 3192 | 10 | 319.2 | 7402 | 200 | 2.9E+06 | 1.1E+05 | 3256.9 | 325.7 | 0.6 | 6.6E+08 | 0.17 | 1.76 | 489.15 | 130.8 | 69 |
| 4212133580 | May-09 | 3204 | 9 | 356.0 | 7335 | 200 | 6.0E+06 | 3.0E+05 | 3227.4 | 322.7 | 0.6 | 6.5E+08 | 0.27 | 1.25 | 449.04 | 252.3 | 40 |
| 4212133439 | Nov-08 | 2860 | 8 | 357.5 | 7544 | 200 | 1.4E+06 | 1.6E+05 | 3319.4 | 331.9 | 0.61 | 6.9E+08 | 0.34 | 1.44 | 324.44 | 324.7 | 36 |
| 4212133605 | Jul-09 | 2814 | 7 | 402.0 | 7293 | 200 | 1.6E+06 | 1.7E+05 | 3208.9 | 320.9 | 0.62 | 6.5E+08 | 0.25 | 2.13 | 316.35 | 306.4 | 45 |
| 4212133614 | Apr-10 | 3466 | 11 | 315.1 | 7353 | 200 | 3.0E+06 | 1.2E+05 | 3235.3 | 323.5 | 0.6 | 6.6E+08 | 0.16 | 1.76 | 478.48 | 121.3 | 70 |
| 4212133602 | Jun-10 | 3421 | 6 | 570.2 | 7843 | 200 | 1.5E+06 | 8.3E+04 | 3450.9 | 345.1 | 0.62 | 7.3E+08 | 0.24 | 2.35 | 219.50 | 587.0 | 44 |
| 4212133048 | Nov-07 | 2151 | 5 | 430.2 | 7976 | 200 | 1.9E+06 | 8.1E+04 | 3509.4 | 350.9 | 0.6 | 7.5E+08 | 0.28 | 1.59 | 433.61 | 386.9 | 37 |
| 4212133422 | Oct-08 | 3619 | 10 | 361.9 | 7738 | 200 | 3.5E+06 | 3.8E+05 | 3404.7 | 340.5 | 0.6 | 7.2E+08 | 0.21 | 1.19 | 486.65 | 204.3 | 52 |
| 4212133604 | Jun-10 | 3051 | 6 | 508.5 | 7922 | 200 | 1.5E+06 | 8.3E+04 | 3485.7 | 348.6 | 0.62 | 7.4E+08 | 0.27 | 2.35 | 219.67 | 514.8 | 36 |
| 4212131978 | Sep-03 | 1821 | 20 | 91.1 | 7912 | 200 | 3.4E+05 | 4.3E+04 | 3481.3 | 348.1 | 0.65 | 7.4E+08 | 0.27 | 2.47 | 351.20 | 16.5 | 45 |
| 4212133878 | Jul-10 | 2799 | 7 | 399.9 | 7921 | 200 | 1.4E+06 | 9.0E+04 | 3485.2 | 348.5 | 0.62 | 7.4E+08 | 0.34 | 2.14 | 208.25 | 402.6 | 34 |
| 4212133871 | Oct-10 | 2603 | 9 | 289.2 | 7637 | 200 | 1.4E+06 | 7.4E+04 | 3360.3 | 336.0 | 0.61 | 7.0E+08 | 0.27 | 2.25 | 289.16 | 165.0 | 45 |
| 4212133601 | Jun-10 | 3296 | 6 | 549.3 | 7875 | 200 | 1.5E+06 | 8.2E+04 | 3465.0 | 346.5 | 0.62 | 7.4E+08 | 0.27 | 2.03 | 237.63 | 600.8 | 38 |
| 4212133423 | Sep-08 | 2464 | 7 | 352.0 | 7794 | 200 | 7.4E+06 | 6.2E+05 | 3429.4 | 342.9 | 0.6 | 7.2E+08 | 0.41 | 1.94 | 219.03 | 382.7 | 26 |
| 4212133264 | Sep-08 | 3514 | 7 | 502.0 | 8029 | 200 | 1.6E+07 | 8.9E+05 | 3532.8 | 353.3 | 0.64 | 7.6E+08 | 0.15 | 1.59 | 494.85 | 279.4 | 73 |
| 4212134163 | Mar-12 | 3903 | 10 | 390.3 | 7783 | 200 | 3.6E+06 | 1.6E+05 | 3424.5 | 342.5 | 0.61 | 7.2E+08 | 0.29 | 1.02 | 378.91 | 325.0 | 39 |
| 4212134198 | Mar-12 | 3079 | 8 | 384.9 | 8095 | 200 | 1.9E+06 | 9.7E+04 | 3561.8 | 356.2 | 0.62 | 7.7E+08 | 0.30 | 2.59 | 169.74 | 331.8 | 30 |
| 4212134020 | Feb-11 | 4539 | 11 | 412.6 | 7813 | 200 | 5.8E+06 | 2.6E+05 | 3437.7 | 343.8 | 0.6 | 7.3E+08 | 0.80 | 0.80 | 148.43 | 1012.1 | 15 |
| 4212133939 | Feb-11 | 5379 | 12 | 448.3 | 8112 | 200 | 3.5E+06 | 1.8E+05 | 3569.3 | 356.9 | 0.63 | 7.7E+08 | 0.73 | 1.67 | 61.49 | 1097 | 16 |
| Base Well | - | 3186 | - | 384.0 | - | 200 | - | - | - | - | - | 7.0E+08 | - | - | 343.36 | 340.1 | - |

Table 20—Summary of the wells in BDF from the case study GSA in the Barnett shale.

The plots of **Fig. 86** shows the production of the 28 wells in boundary dominated flow before and after being rescaled to the base well properties presented in the last row of Table 20. **Table 21** presents the cumulative, rate, and time scaling factors calculated for all the wells. The scaling factors rescale the rate profiles on the MBT plot on a single trend, especially during the late time, as expected from the previous development presented in section 4.3.

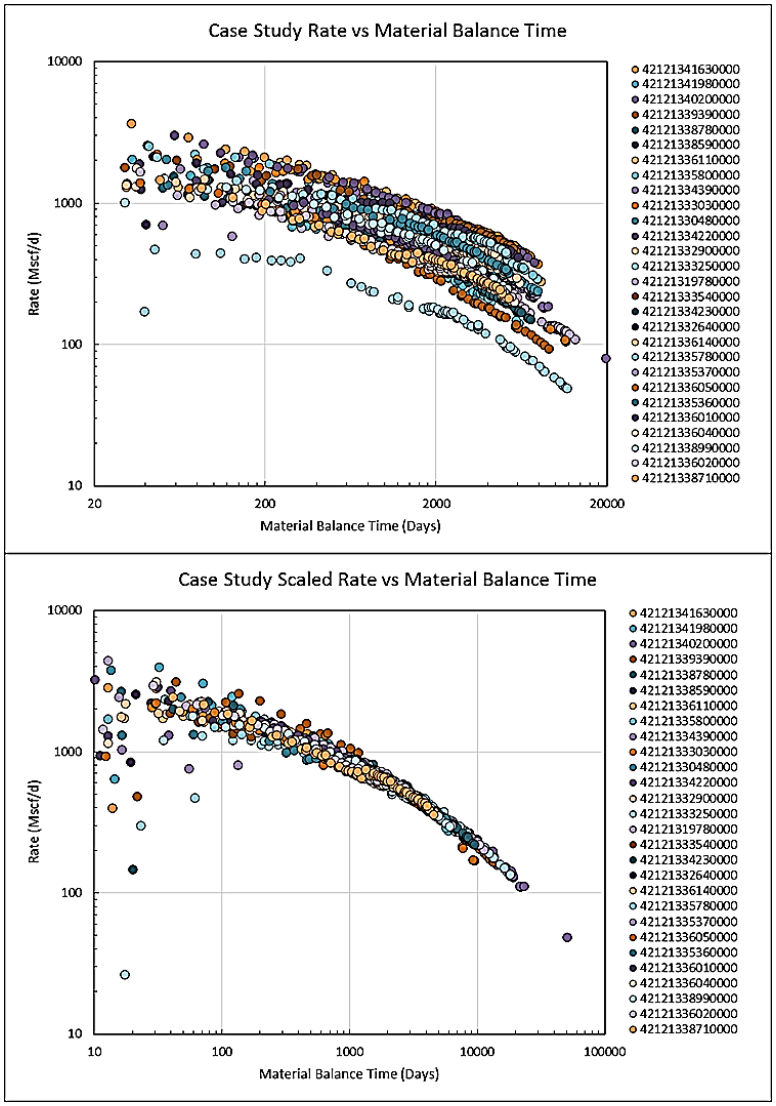


**Fig. 86—Original and rescaled production on the rate-MBT plot of the 28 wells in BDF from the case study GSA.**

| Well API # | Permeability | | Lateral Length | | Fracture Half Length | | Fracture Spacing | | Pseudo-Drawdown | | Rate-Time | | Cumulative-Time | |
|---|---|---|---|---|---|---|---|---|---|---|---|---|---|---|
| | TSF | RSF | TSF | RSF | TSF | RSF | TSF | RSF | TSF | RSF | TSF | RSF | TSF | CSF |
| 4212133325 | 1.39 | 0.72 | 1.00 | 0.84 | 1.00 | 4.56 | 1.11 | 0.90 | 1.00 | 1.10 | 1.55 | 2.74 | 1.55 | 4.24 |
| 4212133290 | 0.49 | 2.05 | 1.00 | 0.91 | 1.00 | 0.88 | 1.03 | 0.97 | 1.00 | 1.06 | 0.50 | 1.68 | 0.50 | 0.85 |
| 4212133536 | 1.16 | 0.86 | 1.00 | 0.98 | 1.00 | 1.05 | 0.95 | 1.05 | 1.00 | 1.05 | 1.10 | 0.98 | 1.10 | 1.08 |
| 4212133537 | 1.05 | 0.95 | 1.00 | 0.89 | 1.00 | 1.56 | 1.00 | 1.00 | 1.00 | 1.04 | 1.05 | 1.38 | 1.05 | 1.45 |
| 4212133578 | 0.53 | 1.89 | 1.00 | 1.11 | 1.00 | 0.56 | 1.22 | 0.82 | 1.00 | 1.07 | 0.64 | 1.03 | 0.64 | 0.66 |
| 4212133354 | 0.58 | 1.72 | 1.00 | 0.94 | 1.00 | 0.49 | 1.11 | 0.90 | 1.00 | 1.32 | 0.64 | 0.94 | 0.64 | 0.60 |
| 4212133899 | 0.91 | 1.09 | 1.00 | 1.50 | 1.00 | 0.85 | 1.26 | 0.79 | 1.00 | 1.08 | 1.16 | 1.19 | 1.16 | 1.38 |
| 4212133303 | 0.57 | 1.76 | 1.00 | 0.92 | 1.00 | 0.57 | 1.08 | 0.93 | 1.00 | 1.09 | 0.61 | 0.94 | 0.61 | 0.57 |
| 4212133859 | 0.68 | 1.47 | 1.00 | 1.05 | 1.00 | 1.17 | 1.09 | 0.92 | 1.00 | 1.07 | 0.75 | 1.76 | 0.75 | 1.32 |
| 4212133611 | 0.38 | 2.60 | 1.00 | 0.96 | 1.00 | 0.70 | 1.45 | 0.69 | 1.00 | 1.08 | 0.56 | 1.32 | 0.56 | 0.73 |
| 4212133580 | 0.74 | 1.35 | 1.00 | 0.96 | 1.00 | 0.76 | 1.16 | 0.86 | 1.00 | 1.10 | 0.86 | 0.94 | 0.86 | 0.81 |
| 4212133439 | 0.95 | 1.05 | 1.00 | 1.08 | 1.00 | 1.06 | 1.15 | 0.87 | 1.00 | 1.05 | 1.10 | 1.08 | 1.10 | 1.19 |
| 4212133605 | 0.90 | 1.11 | 1.00 | 1.09 | 1.00 | 1.09 | 0.91 | 1.10 | 1.00 | 1.11 | 0.82 | 1.60 | 0.82 | 1.32 |
| 4212133614 | 0.36 | 2.80 | 1.00 | 0.89 | 1.00 | 0.72 | 1.48 | 0.67 | 1.00 | 1.09 | 0.53 | 1.32 | 0.53 | 0.70 |
| 4212133602 | 1.73 | 0.58 | 1.00 | 0.90 | 1.00 | 1.56 | 0.45 | 2.21 | 1.00 | 0.98 | 0.78 | 1.76 | 0.78 | 1.38 |
| 4212133048 | 1.14 | 0.88 | 1.00 | 1.43 | 1.00 | 0.79 | 0.80 | 1.26 | 1.00 | 0.96 | 0.91 | 1.19 | 0.91 | 1.08 |
| 4212133422 | 0.60 | 1.66 | 1.00 | 0.85 | 1.00 | 0.71 | 1.13 | 0.89 | 1.00 | 1.00 | 0.68 | 0.89 | 0.68 | 0.60 |
| 4212133604 | 1.51 | 0.66 | 1.00 | 1.01 | 1.00 | 1.56 | 0.57 | 1.75 | 1.00 | 0.97 | 0.86 | 1.76 | 0.86 | 1.52 |
| 4212131978 | 0.05 | 20.61 | 1.00 | 1.69 | 1.00 | 0.98 | 17.78 | 0.06 | 1.00 | 0.97 | 0.86 | 1.85 | 0.86 | 1.60 |
| 4212133878 | 1.18 | 0.84 | 1.00 | 1.10 | 1.00 | 1.65 | 0.92 | 1.08 | 1.00 | 0.97 | 1.09 | 1.60 | 1.09 | 1.75 |
| 4212133871 | 0.49 | 2.06 | 1.00 | 1.18 | 1.00 | 1.19 | 1.76 | 0.57 | 1.00 | 1.03 | 0.86 | 1.68 | 0.86 | 1.44 |
| 4212133601 | 1.77 | 0.57 | 1.00 | 0.93 | 1.00 | 1.44 | 0.49 | 2.05 | 1.00 | 0.98 | 0.86 | 1.52 | 0.86 | 1.32 |
| 4212133423 | 1.13 | 0.89 | 1.00 | 1.25 | 1.00 | 1.57 | 1.19 | 0.84 | 1.00 | 0.99 | 1.34 | 1.45 | 1.34 | 1.94 |
| 4212133264 | 0.82 | 1.22 | 1.00 | 0.88 | 1.00 | 0.69 | 0.59 | 1.71 | 1.00 | 0.94 | 0.48 | 1.19 | 0.48 | 0.57 |
| 4212134163 | 0.96 | 1.05 | 1.00 | 0.79 | 1.00 | 0.91 | 0.97 | 1.03 | 1.00 | 0.99 | 0.92 | 0.77 | 0.92 | 0.71 |
| 4212134198 | 0.98 | 1.02 | 1.00 | 1.00 | 1.00 | 2.02 | 1.00 | 1.00 | 1.00 | 0.93 | 0.97 | 1.94 | 0.97 | 1.88 |
| 4212134020 | 2.98 | 0.34 | 1.00 | 0.68 | 1.00 | 2.31 | 0.87 | 1.15 | 1.00 | 0.99 | 2.58 | 0.60 | 2.58 | 1.55 |
| 4212133939 | 1.98 | 0.51 | 1.00 | 0.57 | 1.00 | 4.82 | 0.73 | 1.36 | 1.00 | 0.93 | 1.45 | 1.76 | 1.45 | 2.56 |

Table 21—Summary of the scaling factors for the wells in BDF in the case study GSA.

Looking more closely to some of the wells in Table 20, we can see they were first produced between 2008 and 2012. The only well producing since 2003 is underlined in Table 21. Compared to the rest of the group, this well is also different because it has more fractures stages for a much smaller lateral length. Based on its completion design, this wells would not be chosen as an analog in because it is older and it has a smaller stage spacing. However our analysis demonstrates how it is possible to rescale this well to the same typical production profile on Fig. 87. The match of the oldest well on the type curve yields a very low permeability (16nd) and a fracture half-length close to the group's average. With such a low permeability, the well is only able to sustain its production based on its large number of fractures that increase the contacted surface area with the matrix. Taking all the known and estimated properties into account, we see that the well has a time scaling factor smaller than 1 and a cumulative scaling factor greater than 1. As we demonstrated previously in the development of the scaling factors, a scaling factor smaller than one means that the wells has to be scaled down to match the average typical profile. A TSF smaller than 1 also means the well does not have an strong depletion efficiency (permeability and fracture spacing) compared to the reference well, which also means that it takes a longer time for the well to reach the end of linear flow and deplete its SRV. In the case of the cumulative factor, scaling the well down means that the well has a greater stimulated volume or a greater drawdown compared to the reference well. Because the oldest well has both a time scaling factor smaller than 1 and a cumulative scaling factor larger than one, it is clear that this well is less performant compared to the group's average. Finally, this result makes sense because the older wells have smaller lateral length and the completion technology that is also probably less performant in 2003 than 2010. As we demonstrated with this example, the two factors are used to characterize and quantify the performance of a well compared to a group. Applying all the scaling factors calculated and presented in Table 22 to their respective production profiles yields the typical production profile shows in Fig. 87.

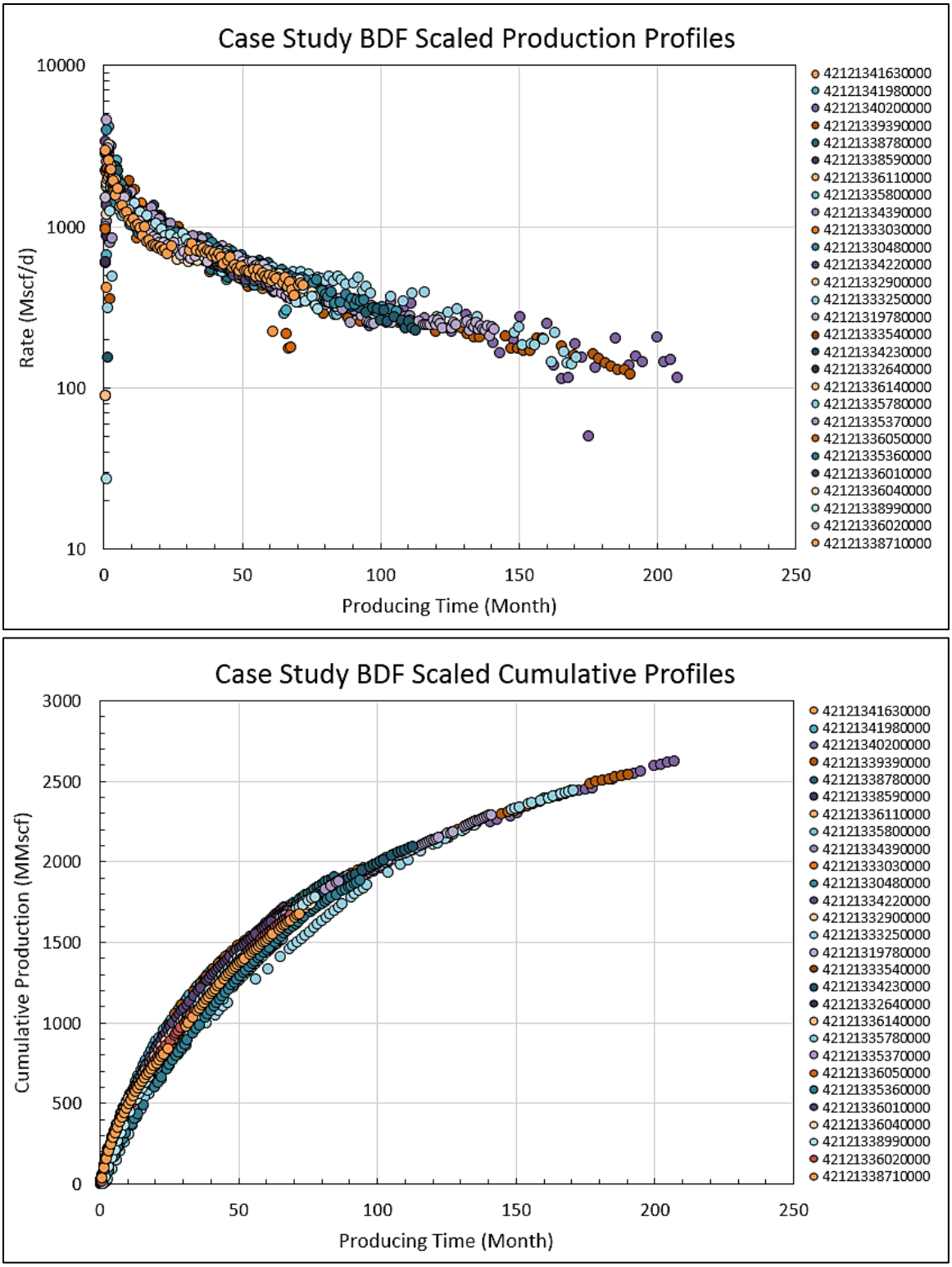


**Fig. 87—Rescaled production of the 28 wells in BDF from the case study GSA, rate-time profiles (top) and cumulative-time profiles (bottom).**

The rescaled production profiles shown on Fig. 87 demonstrates the typical production profile for the base well parameter since they are scaled to the same reference properties. As per step 8.1 of the workflow presented in Fig. 60, we can parametrize this profile and rescale the equations with the scaling factors to forecast production. The time at the end of linear flow for the averaged profile is calculated based on Eq. 26 with the time scaling factor of Table 22 and the time at the end of linear flow of Table 21. **Fig. 88** plots the original and scaled time at the end of linear flow from each profile.

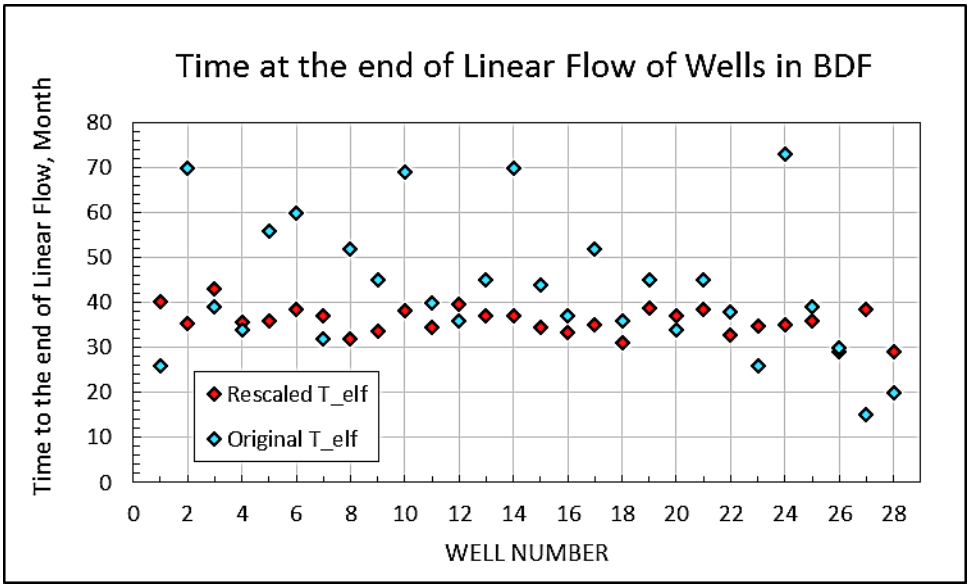


**Fig. 88—Original and scaled time at the end of linear flow of the wells in BDF from the case study GSA.**

The average of time at the end of linear flow for the unscaled profile is 43 months while the average after scaling is 37 months. Originally, the time at the end of linear flow is scattered from 15 to 72 months in the sample of the 28 wells because it represents the permeability and fracture spacing heterogeneity of the sample. Because the time scaling factor is the product of ratios between the well's permeability and fracture spacing to the base well' properties, each production is rescaled (normalized) individually. The scaled time at the end of linear flow

displayed on Fig. 88 shows that the points are centered. **Fig. 89** shows the same data points plotted on a log-probit plot to illustrate how the time scaling factor affects the distribution of the sample.

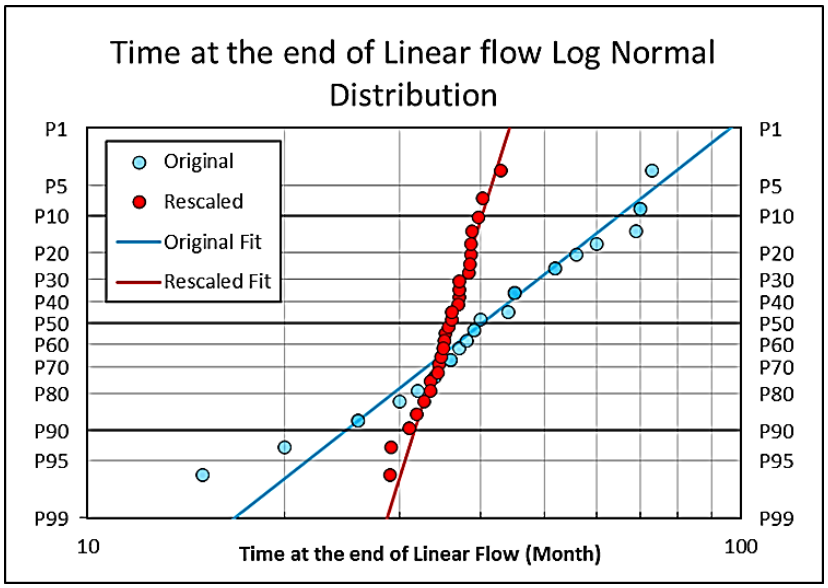


**Fig. 89—Original and rescaled time at the end of linear flow on a lognormal plot**.

Calculating the P10/P90 ratio of the original time at the end of linear flow gives a value of 2.61 whereas the P10/P90 ratio of the rescaled time at the end of linear flow is 1.27. This improvement in P10/P90 ratio combined with the match quality on the cumulative plot presented on Fig. 87 demonstrate how the scaling factors improve the uncertainty of a typical production profile for a set of reservoir and completion properties. Nevertheless, studying the time at the end of linear flow only reflects the heterogeneity in fracture spacing and permeability since they are the parameters that control the time scaling factor.

**Fig. 90** presents the transient behavior of the averaged profile. We see that the transient section of the production profile follows the half slope until 37 to 40 months, after which it starts to deviate towards the unit slope. This observation is in agreement with the average $t_{elf}$ found on Fig. 88. Plotting the production on the log(q)-Np diagnostic plot provides some guidance on how to parametrize the transient section with the composite parametrization.

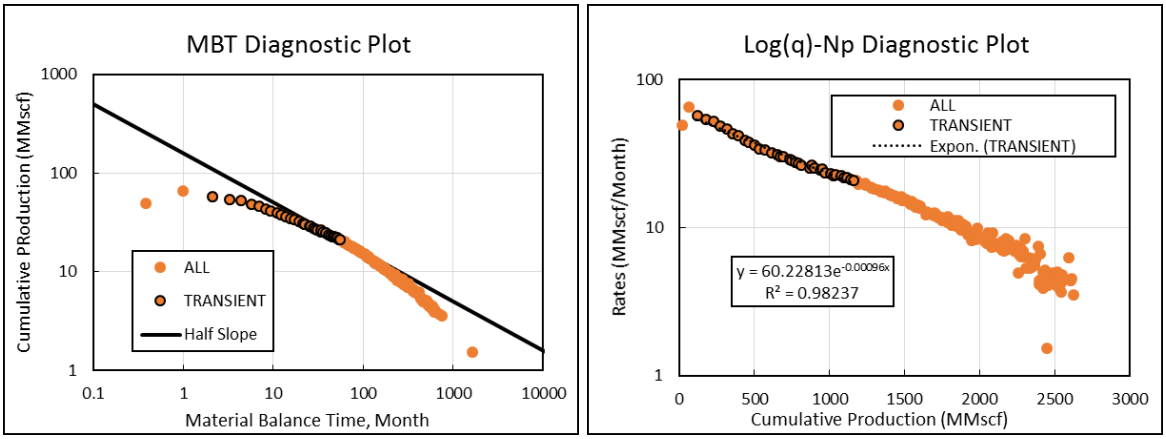


**Fig. 90—Transient diagnostic plot of the averaged profile on the MBT and log(q)-Np plot.**

**Fig. 91** presents the fit of the data with the composite parametrization with the b=1 and b=2 for the transient section of the averaged profile. The parameters used for the case where b=1 are $q_i$ of 55 MMscf/month, $D_i$ of 0.0473 Month$^{-1}$ and ε of 1.006 while appears that the depletion of the group follows a stem with a b factor of 0.6. However, the survivor bias may impact the calculation of the average profile shown in pink and several b values could be risked if the composite parametrization equation is used in a probabilistic model. The fit of the transient section with a b factor of also 2 shows a good fit with the data. The parameters used to parametrize the data are $q_i$ of 150 MMscf/Month, $D_i$ of 0.75 Month$^{-1}$ and ε of 1.78. The equation with b=2 fits better the early rates as shown on the lower plot on the right of Fig. 91. The depletion data seems to follow a depletion stems generated with a b value varying between 0.2 and 0.4.

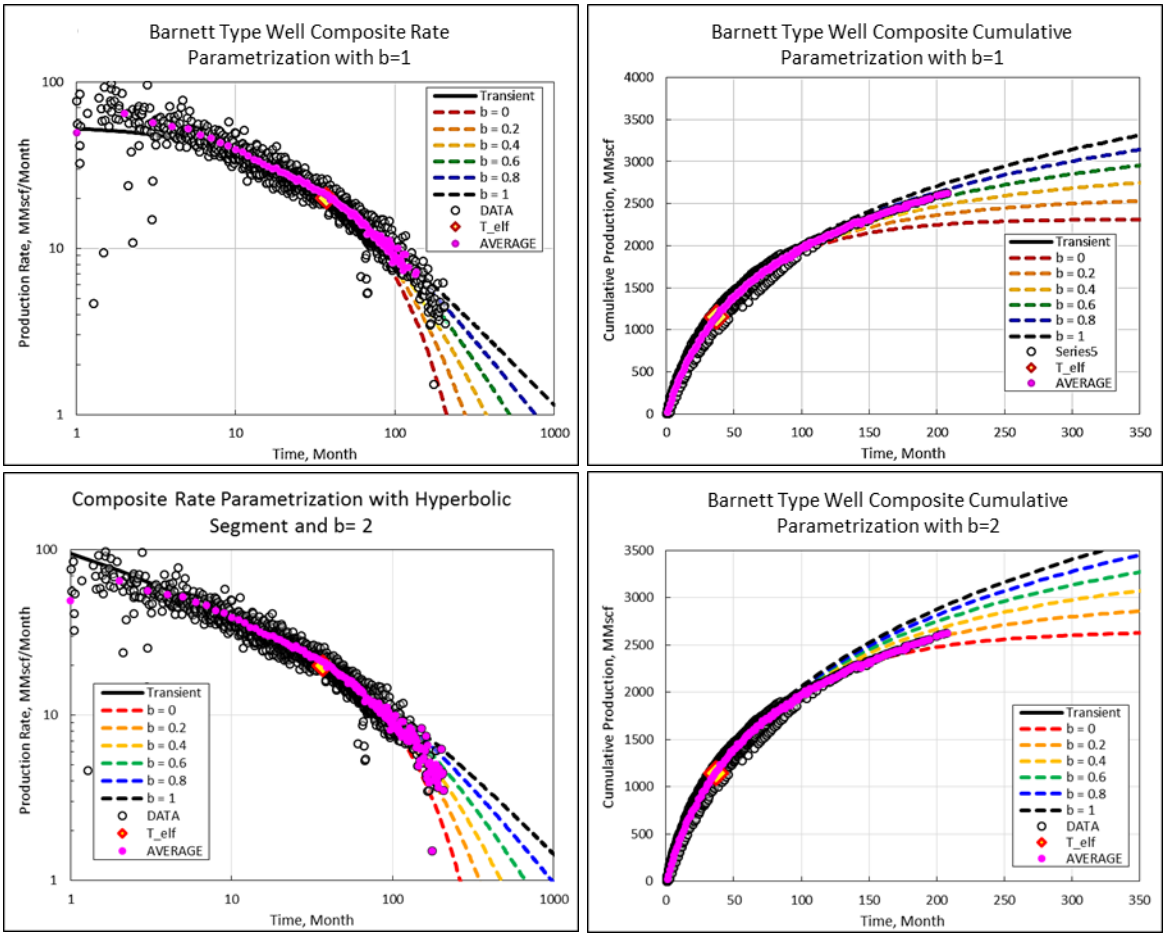


**Fig. 91—Composite parametrization used to forecast the base well and diagnose boundary dominated flow behavior, upper plots show the fit with b=1 where $q_i$= 55 MMscf/month, $D_i$ = 0.0473 $mo^{-1}$, $t_{elf}$ = 37 mo and $\epsilon$ = 1.006 and the depletion b factor of 0.6. The lower plots shows the fit with b=2 with $q_i$= 150 MMscf/mo, $D_i$ = 0.75 $mo^{-1}$, $t_{elf}$ = 37 month and $\epsilon$ = 1.78 and a depletion b factor of 0.3.**

**Fig. 92** shows the type well generated with the time slice method in the solid black line against the type well generated with the scaling factor and the composite parametrization (b=1). Comparing both profiles on the same duration shows the differences at early time. From the start of the production until 70 months, we see that the time slice method generates a well that underestimate the production compared to the group's base well. We calculated more than 17% of difference between the two type wells during the first 25 months of production. A vertical separation was inserted at 70 months to show where the survivor bias starts to influence the shape of the profile generated from the time slice method.

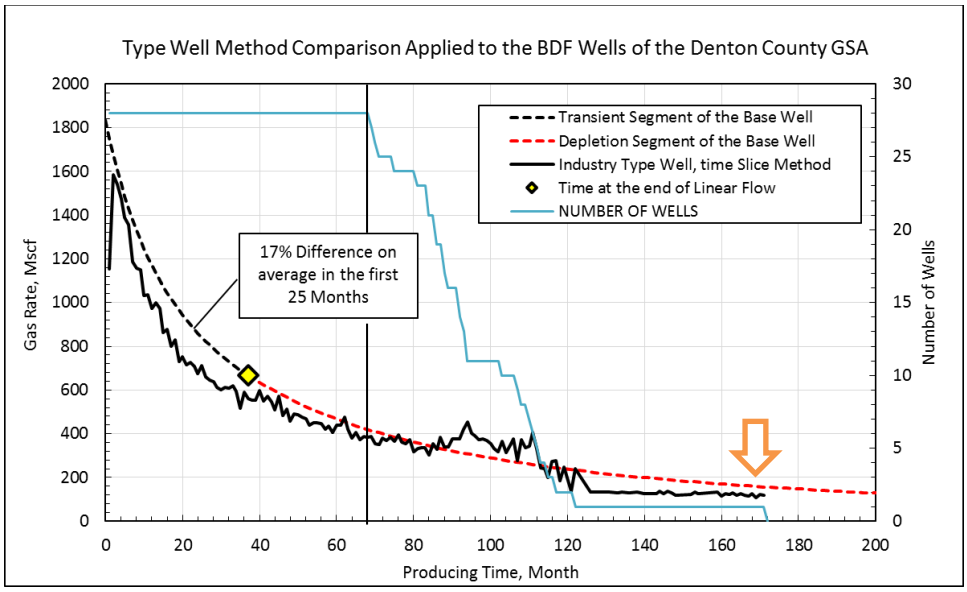


**Fig. 92—Comparison of the base well profile and a common type well generated with the time slice method without re-scaling or normalization for specific parameters.**

Comparing both methods show that the forecast generated with the scaling factors provides a period of "known production" greater than the actual production history, as shown by the green arrow on **Fig.** 93. Furthermore, because all the wells rescale to the same production profile based on the scaling factors, it minimizes the impact of survivor bias and increases the confidence level of this profile.

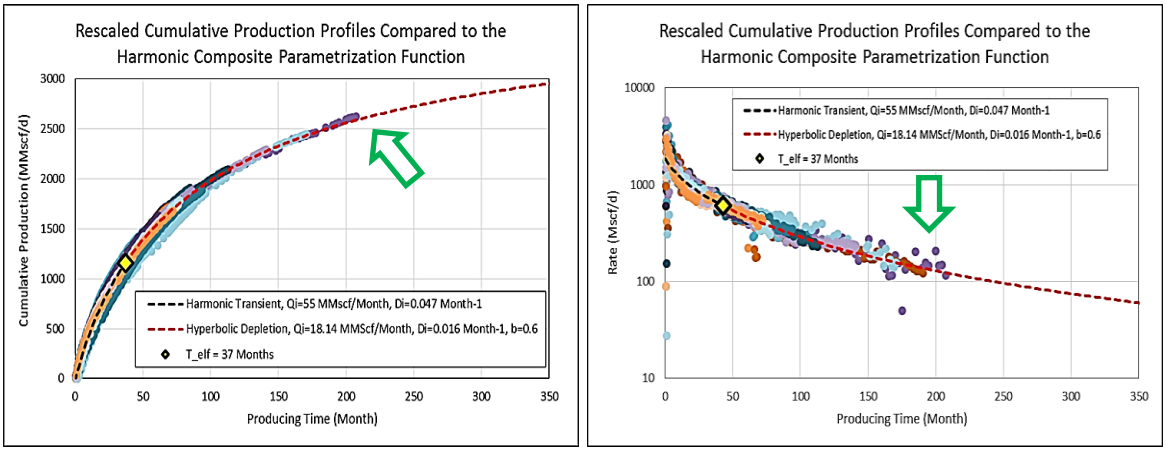


**Fig. 93—Validation of the composite parametrization with rescaled data points.**

In conclusion, we demonstrated that the type wells generated with the time slice methods are less reliable because they are influenced by the survivor bias and they do not take into account the properties' differences between the analogs, especially since they don't normalize on the time. Normalizing the production of the same group to a base well defined by the group's average properties allows to generate a typical well profile with a higher degree of confidence for a period of time usually greater than the maximum producing history. We will show in the next section how to rescale this profile to any set of properties and create type well profiles that can be used to forecast undrilled wells or wells with shorter production history.

## 6.3 Production Forecasting of Well with Short Production History

In this section, we will show how the base well can be utilized to forecast the production of the 28 wells that were used to generate the base well itself. Then, we will apply the methodology explained in step 5.2 to 8.2 to forecast the production of a well flowing in transient flow regime.

### *6.3.1 Forecast of Well in Boundary Dominated Flow Regime*

To forecast production with the base well profile, the new scaling factors are calculated based same relationship presented Table 12. The reference well becomes the well that should be

forecasted instead of the base well. Since the scaling factors of the 28 wells used to build the forecast are already computed in Table 21**,** calculating their inverse give the scaling factors required to scale the base well back on to each profile. This process allows to validate the base well profile to ensure that the typical production fits all the production in the BDF group before it is used to forecast undrilled wells. **Fig. 94** presents how the oldest well, which started its production in 2003, is forecasted from the base well. The white points show the original production, the red points show the rescaled production, with the scaling factors of Table 22. The rescaled production fits the base well profile, illustrated with the solid black line. The yellow diamond shows the last point of the combined rescaled historical production as illustrated by the green arrow on Fig. 90 and it is used to indicate the extent of a high confidence forecast. Finally, the base well profile is rescaled to the type well forecast illustrated with the dotted blue line. The scaling factors required to rescale the base well are the inverse of the original scaling factors used to scale the original production and they are shown in the legend of Fig. 94. The last point of known production allows to forecast the original production up to 242 months based only on the group's production. The production past this point is a forecast based on the composite parametrization and provides less confidence because none of the wells have produced to this extent of time. The colored arrows next to the number were added to Fig. 94 to show the steps of the workflow presented on Fig. 60.

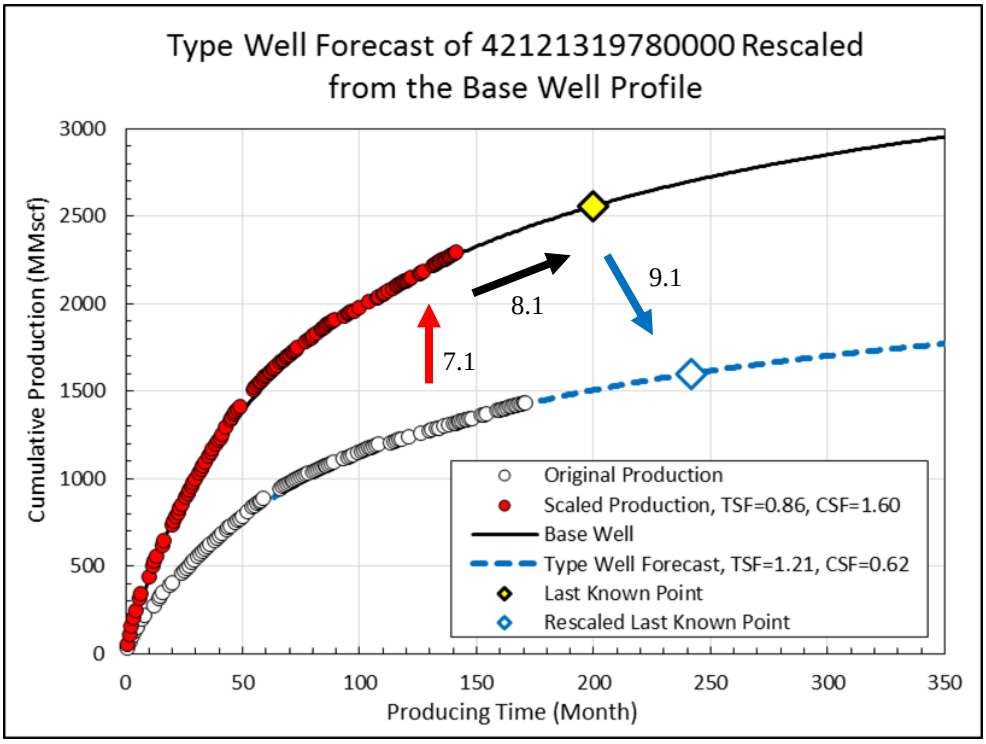


**Fig. 94—Forecast of well 421231978 from the base well of the case study GSA.**

Similar to the example presented on Fig. 94, **Fig. 95** presents a forecast for well 421233303 which was selected to show the limitation of the scaling methodology. As we can see on the plot, the type well forecast does not match exactly on the original production forecast because the scaled production does not match exactly the base well. Hence, this shows how the grouping of the rescaled profiles on Fig. 87 will impact the forecast. In the case of outliers such as the Eagle Ford example presented in section 4.3.2, we can expect a large difference between the forecast and the original production. Nevertheless, the differences from the forecast and the original production can be corrected by adjusting the fit of the production on the modified type curve with trial and error.

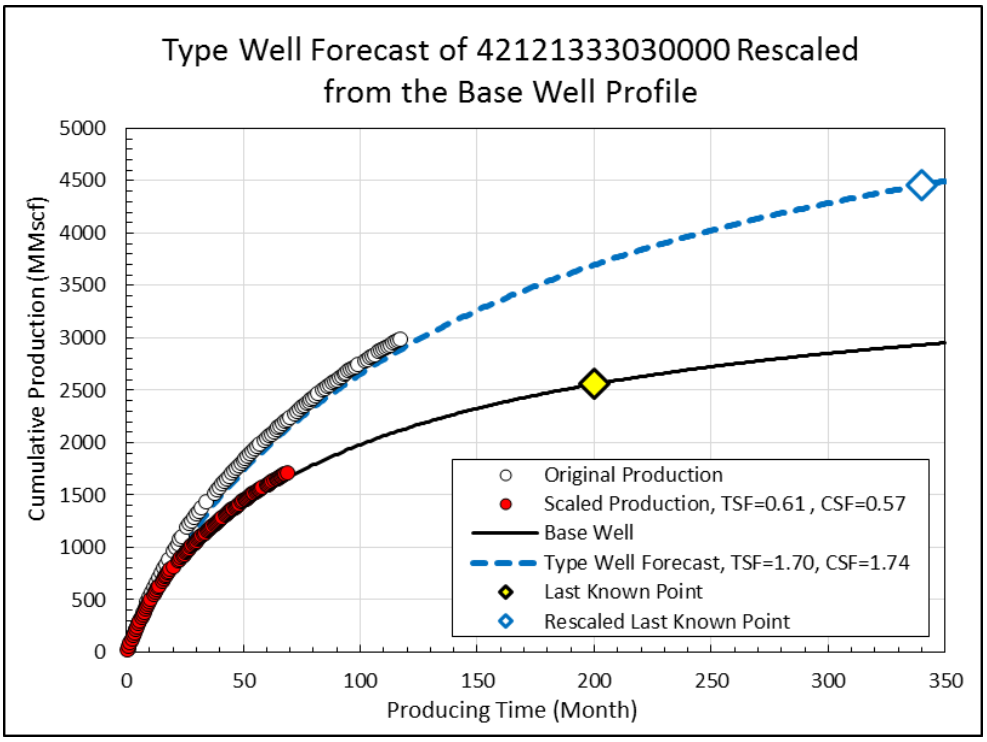


**Fig. 95—Forecast of well 4212133303 from the base well of the case study GSA.**

**Fig. 96** shows the forecast of all the 28 wells diagnosed in boundary dominated flow regime. The upper plot has the forecast that is limited to the last known point of the rescaled production profiles. This forecast is therefore more reliable because it shows how the group's behavior can forecast each well individually. In addition, we see that the better performing wells are forecasted to a much greater time compared to the underperforming wells. This is the effect of the time scaling factor on the time at the end of linear flow and the production history. Indeed, the well presented on Fig. 95 as a smaller permeability than average but it also has a stimulated volume (lateral length and fracture half length) greater than the base well. Hence, this well has large time and cumulative scaling factors that allow to forecast the production to a much longer extent than wells that have a permeability greater than the average, given the same fracture spacing.

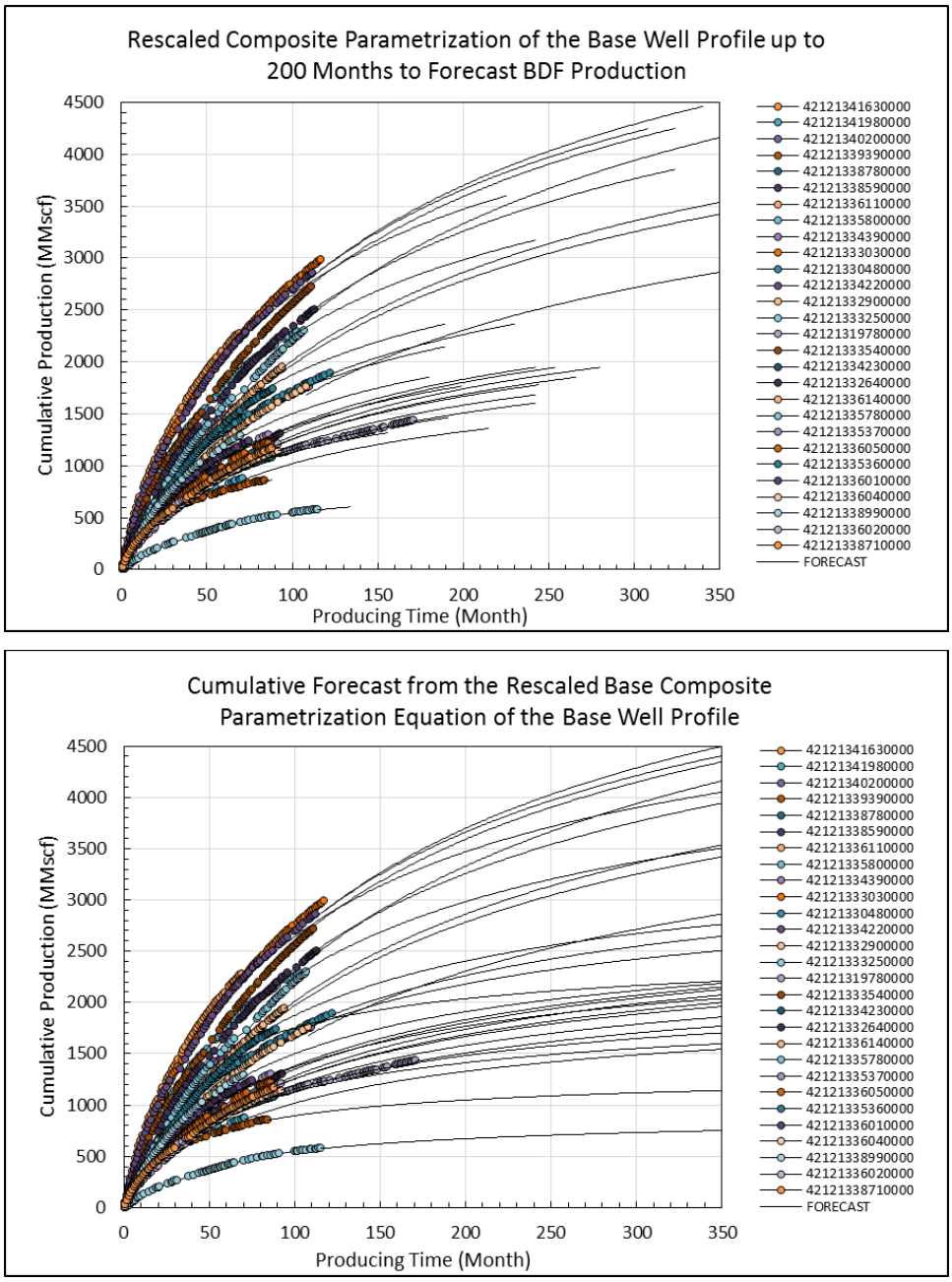


**Fig. 96—Cumulative forecast of the BDF wells in the case study GSA, the upper plot shows the forecast limited to the last point of rescaled historical production and the lower plot shows the unrestricted production forecast.**

Finally, the second plot of Fig. 96 shows the unbounded production forecast of the rescaled composite parametrization equation. Overall, the forecasts match most of the original production within an acceptable range. In summary, this new forecasting technique offers a new alternative that bring more confidence in the forecast because it is analytically related to the reservoir and completion properties of the wells. Finally, this forecasting method is very beneficial if we have wells that quickly reach BDF with a long production history because they increase the duration of "known production".

### *6.3.2 Forecast of Well in Transient Flow Regime*

This sub-section will demonstrate how to forecast the production for a well diagnosed in transient flow regime based on the method suggested in Chapter 5. **Fig. 97** shows the location of a transient well (in red) selected for the analysis.

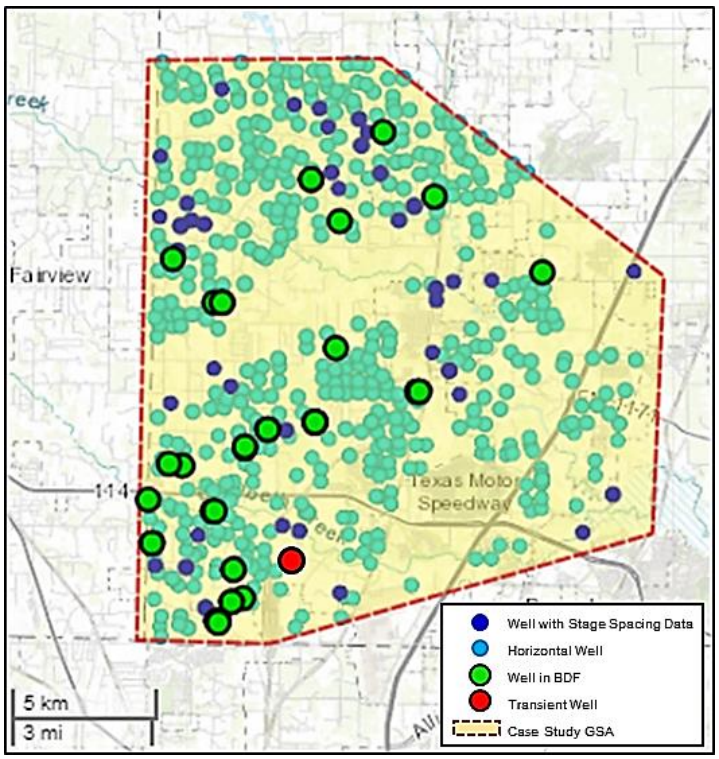


**Fig. 97—Map of the location of the transient well in the case study GSA.**

The chosen well for the analysis is a younger well that has been producing since May 2013. **Table 22** summarizes all the relevant information needed to forecast its production. Compared to the base well generated from the wells in BDF, this transient well has a longer lateral length and a greater fracture spacing. As per the analysis previously conducted, we assumed a 200ft net pay thickness and a pressure gradient of 0.44psi/ft from which we calculated a reservoir pressure and a BHP. Finally, a typical porosity of 6% is used with a gas saturation of 65%.

| **Known Properties** | Value | Units |
|---|---|---|
| Well API# | 42121343360000 | |
| Date of First Production | May-13 | |
| TVD | 7484 | ft |
| Lateral Length | 5628 | ft |
| Proppant Amount | 442000 | lbs |
| Stimulation Volume | 161840 | bbl |
| Gas S. Gravity | 0.6 | |
| Number of Stages | 13 | |
| | | |
| **Assumed Properties** | | |
| Reservoir Temp | 660 | R |
| Gas Saturation | 65 | % |
| Porosity | 6 | % |
| Net pay thickness | 200 | ft |
| Pressure Gradient | 0.44 | psi/ft |
| Total Compressibility | 1.38E-04 | $psi^{-1}$ |
| Gas Viscosity | 0.0227 | cp |
| | | |
| **Calculated Properties** | | |
| Reservoir pressure | 3293 | psia |
| Bottom Hole Pres. | 329 | psia |
| $m(p_i)$ | 688884544 | $psi^2/cp$ |
| $m(p_{wf})$ | 8654623 | $psi^2/cp$ |
| d(m(p)) | 680229921 | $psi^2/cp$ |
| Fracture Spacing | 432.92 | ft |
| Minimum Fracture Half length | 602.76 | ft |
| Maximum Permeability | 271.74 | nD |
| Slope (SQRT(t) | 15030.69 | $cp.days^{-1/2}/psi^2/Mscf$ |

Table 22—Properties used to forecast the production of the transient well 4212134336.

As per step 5.2 and 6.2 of Fig. 60, we determine the $x_f\sqrt{k}$ product of the well in transient flow. As presented in Step 5.3, $x_f\sqrt{k}$ can either be obtained from the square root of time diagnostic plot or by matching the last known data point of the MBT plot to the equivalent rate of the modified type curve. Using Eq. 24 with the data in Table 22, we find a $x_f\sqrt{k}$ of 10.2. **Fig. 98** shows the MBT plot as well as the square root of time plot. Note that only the points lying on the half slope should be fitted to calculate the slope used in Eq. 24 because the other points do not represent the true transient linear flow behavior of the matrix flowing into the fracture.

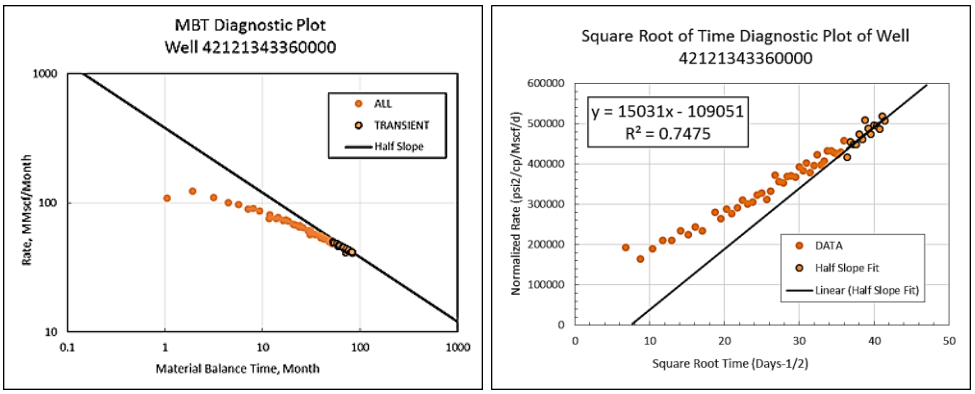


**Fig. 98—Transient diagnostic plot of well 4212134336.**

Fitting the rate-MBT profile on the modified type curve to the most conservative location gives a TMP of 0.0001948 and a RMP of 0.0007022 from which we calculated a maximum permeability of 271 nD and a minimum Fracture half-length of 602 ft. Multiplying both results gives a $x_f\sqrt{k}$ of 9.94 which is very close to the estimate found with the square root of time plot. Combining both methods allows to validate the results. Now that the square root of permeability and the fracture half-length is known, we can rescale the production for the most conservative guess. **Fig. 99** plots the transient production profile compared to the base well profile originally

computed from step 6.2. It is clear that the transient well is over performing the BDF's average profile. This results is not surprising since the lateral length is greater than the average length and the fracture spacing is also wider, which can be an explanation for a greater time until the end of linear flow considering the same permeability.

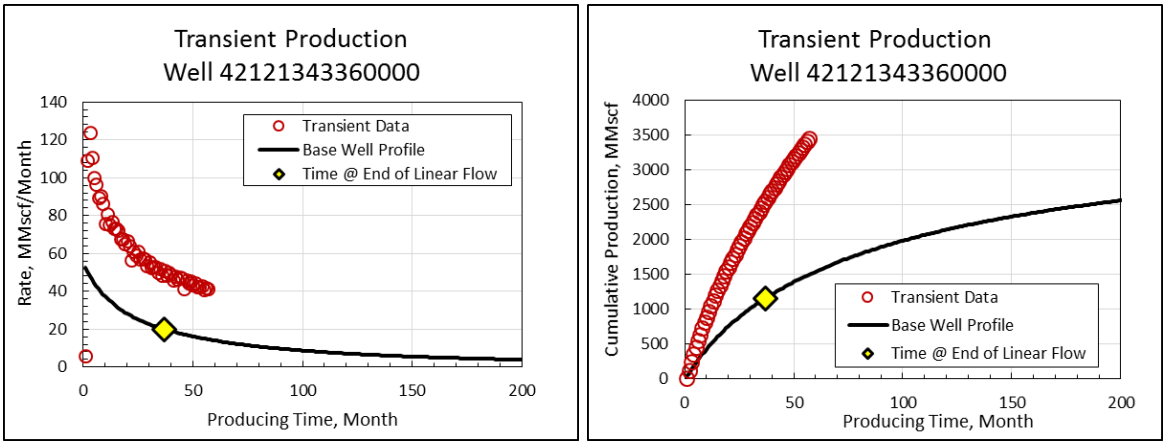


**Fig. 99—Comparison plot of well 4212134336 production profile against the original base well profile.**

The scaling factors required to rescale the base well to the transient well to create a conservative forecast are summarized in **Table 23**. Each scaling factor is calculated based on the relationship presented in Table 12, taking into account that the transient well is the reference well in the calculation. We find a time and a rate scaling factor that are greater than one since the base well is performing not as well as the transient well which is still in transient flow after 58 months of production.

| Parameter | Units | BASE CASE | TRANSIENT | TSF | RSF | CSF |
|---|---|---|---|---|---|---|
| Permeability | nD | 340.12 | 271.74 | 1.25 | 0.80 | 1.00 |
| Fracture Half-Length | ft | 343.36 | 602.76 | 1.00 | 1.76 | 1.76 |
| Lateral Length | ft | 3185.86 | 5628.00 | 1.00 | 1.77 | 1.77 |
| Pseudo-Pressure Drawdown | psi2/cp | 7.03E+08 | 6.80E+08 | 1.00 | 0.97 | 0.97 |
| Fracture Spacing | ft | 383.97 | 432.92 | 1.27 | 0.79 | 1.00 |
| | | | TOTAL | 1.59 | 1.89 | 3.00 |

Table 23—Summary of the scaling factors for the conservative production forecast of well 4212134336

Using the scaling factors of Table 23, the base well profile is rescaled to the transient well parameters. **Fig. 100** presents the transient data and the deterministic type well forecast. It appears from the graph that the base well profile rescale almost perfectly on the transient production data solely based on the scaling factors that were analytically calculated. The forecast following the end of linear flow provides a good level of certainty on the expected production because it is grounded on a strong theoretical development. Note that the time at the end of linear flow also aligns perfectly with the last known production point because the permeability and fracture half-length were selected such that the future production is assumed to transition to the boundary dominated flow regime. The boundary dominated flow regime has a greater decline rate and therefore represents the worst case scenario, or the most conservative case. Other permeability and fracture half-length combination can be chosen probabilistically such that the end of linear flow can occur later in the life of the well. Doing so would maintain higher production rates and a better overall recovery but could also overestimate the real potential of the well.

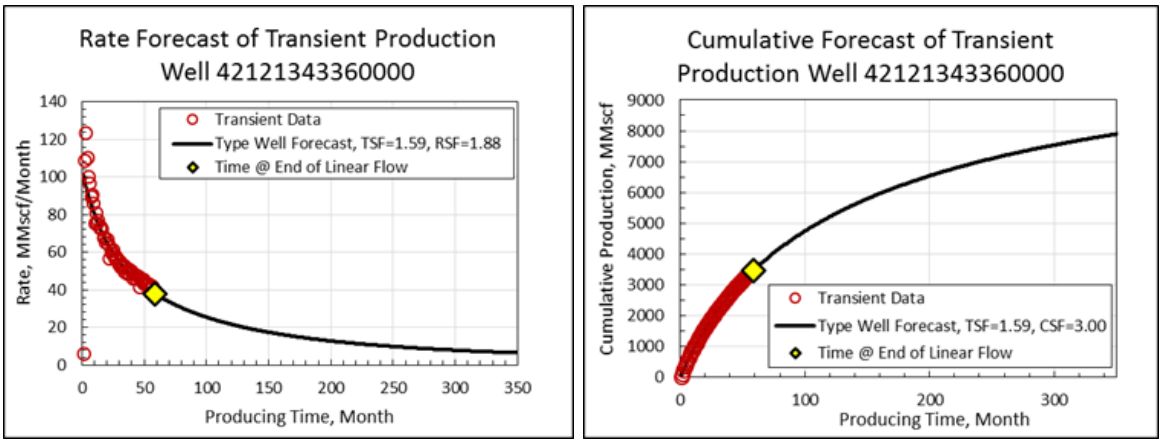


**Fig. 100—Conservative production forecast of transient example, well 4212134336.**

Because there is a fixed relationship between the fracture half-length and the permeability, we are able to *generate a probabilistic production forecast for various permeabilities*. The fracture half-length and the permeability are the two major unknowns of the analytical model. Since the fracture half-length is proportionally related to the permeability with the relationship $x_f\sqrt{k}$, using a probability distribution of the permeability will automatically also give the associated fracture half-length based on a fixed value of $x_f\sqrt{k}$. To carry the probabilistic analysis, we decided to use the permeability distribution found after the diagnostic of the 28 wells in boundary dominated flow. The left plot of **Fig. 101** presents the original permeability histogram with a lognormal distribution drawn above it. Since the transient well has a maximum permeability of 271 nD, most of the distribution from the original BDF permeability distribution is truncated and cannot be used. For the sake of the analysis, a synthetic triangular distribution was designed to represent a realistic permeability distribution. The upper bound of the distribution is also the mode of the data and was chosen at the maximum allowable permeability. This was supported by the fact that the maximum permeability is in the lower half of the original BDF permeability distribution. The lower bound at the distribution was chosen based on a reasonable expectation of the maximum time at the end of linear flow. Assuming a 20 year transient period, the permeability was calculated to be slightly lower than 70nD. Hence, we generated a triangular distribution ranging from 70 to 270 nD with a maximum at 270 nD. The left plot of Fig. 101 shows the distribution and the associated P10, P50

and P90 estimates, respectively estimated at 133.3, 211.5 and 260 nD. The similar procedure can be repeated for each transient well and other permeability distribution, such a uniform or a beta distribution, can be used depending on the available information and the size of the dataset.

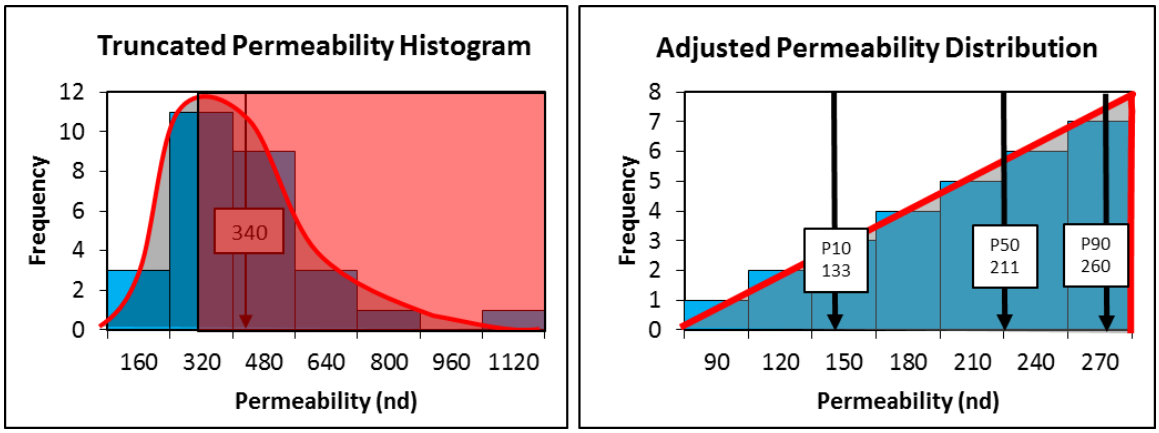


**Fig. 101—Truncated and adjusted permeability distribution of the permeability used to forecast production of the transient example, well 4212134336.**

The fracture half-length was calculated for each permeability with the $x_f\sqrt{k}$ of 9.94. The scaling factor were then generated for each case specifically for each pair of permeability and fracture half length. The results of the calculation are displayed on **Table 24**.

| Parameter | Permeability (nD) | Fracture Half Length (ft) | TSF | RSF | CSF | $T_{ELF}$ (Month) |
|---|---|---|---|---|---|---|
| Minimum | 271 | 603.8 | 1.59 | 1.89 | 3.00 | 58.87 |
| P90 | 260 | 616.5 | 1.66 | 1.85 | 3.07 | 61.53 |
| P50 | 211.5 | 683.5 | 2.04 | 1.67 | 3.40 | 75.64 |
| P10 | 133.3 | 860.9 | 3.24 | 1.32 | 4.29 | 120.01 |
| Maximum | 70 | 1188.1 | 6.18 | 0.96 | 5.92 | 228.54 |

Table 24—Probabilistic scaling factors for the production forecast of transient example, well 4212134336.

Rescaling the base well profile for each probabilistic case gives the results presented on Fig. 94. The profile previously generated from Fig. 100 is labeled on **Fig. 102** as the minimum case since it is the most conservative. We notice that the P90 case is very close to the minimum case as a result of the triangular probability distribution. The percentile forecast is directly related to the chosen permeability distribution since it is the only parameter governing the scaling factors.

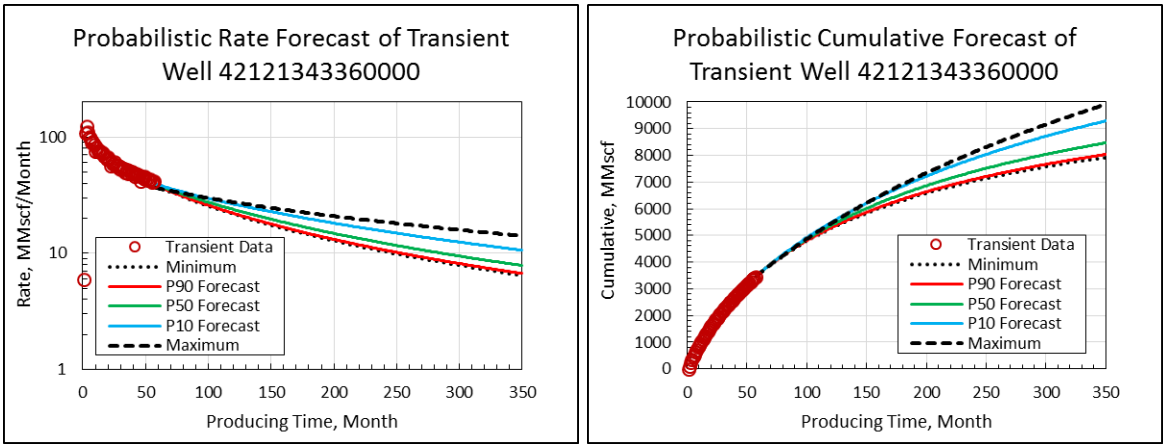


**Fig. 102—Probabilistic forecast of transient example, well 4212134336.**

The large time and cumulative scaling factors of the lowest percentile forecast distorted the cumulative base well profile much more than the rate-time profile. This error is amplified by the difference between the parametric function of the base well and the transient section of the well. Hence, only the rate-time relationship presented on the left plot of Fig. 94 were kept as the original base well. The cumulative profile was generated by integrating the rate-time profile and adding it to the latest cumulative produced volume at 58 months. This is the same process as using a higher epsilon value in the composite parametrization function. Overall, the result of the forecast seems logical and the range provides useful information regarding the expected recovery. Note that the expected production also relies on the assumption that the well will have constant operating conditions and no change in reservoir or completion properties. Infill drilling, re-stimulation and

changing BHP can directly impact the shape of the profile and can be included when forecasting the production of a well over an extended period of time.

In conclusion, we illustrated the step-by-step methodology presented in the workflow on Fig. 60 to deterministically and probabilistically forecast the production of wells flowing in transient regime. This methodology uses the results of the analysis conducted on the wells in BDF in order to rescale the base well profile that characterize a typical reservoir behavior in this GSA. The match of the transient data on the modified type curve provides a useful relationship between the permeability and fracture half-length as $x_f\sqrt{k}$ is constant. Choosing an expected distribution of permeability or fracture half-length allows to generate a probabilistic forecast by rescaling the base well profile after calculating the scaling factors for each case. Such operation do not require much computing power and can be simply performed in a spreadsheet. Finally, the advantage of the composite parametrization is its ability to incorporate the scaling factors directly in the equation, which give the flexibility to forecast any production after calculating the differences between the key parameters. The only limitation of this method depend on the quality of fit of the composite equation on the rescaled production because large scaling factors can distort the forecasted production profile.

### 6.4 Production Forecasting of Undrilled Wells

Forecasting production of undrilled wells can be performed with a Monte Carlo analysis by rescaling the base case profile based on the random sampling of the expected reservoir and completion properties' distribution. The lateral length, stage spacing, well depth, completion technology, drawdown, proppant loading and stimulation volumes are hard input parameters that can be deigned and fixed in the probabilistic estimation. The remaining parameters such as permeability, fracture half-length and net-pay thickness are uncertain and should be modeled based on the results of the modified type curve diagnostic. In this example, we will generate a probabilistic forecast for undrilled wells given a specific lateral length of 4420ft, 11 hydraulic fracture stages and a specific true vertical depth of 8000ft. The results of this probabilistic study

are presented in the form of percentile type wells. The percentile type wells will then be compared with 14 wells of the GSA that share the same characteristics to validate the results.

Because this probabilistic analysis relies on the fit of distributions of reservoir and completions properties and their relationships, we used all the information available in the Denton County to increase the statistical significance of the study. The limited number of well in each GSA led us to consider the parameters' distributions to be homogenous in both GSA. We will not depict any variations between the Denton County GSA and the case study GSA. Based on the number of 126 wells presented on Fig. 82, we then use the 55 wells in BDF and 71 wells in transient flow. As the permeability and fracture half-length is available for the wells in BDF, we also use the most conservative estimate of the permeability and fracture half length of the wells in transient flow regime. The following section will present the data set and the results of the diagnostic of the 126 wells. The distributions of fracture half-lengths, permeability and $x_f\sqrt{k}$ will be studied based on the flow regime and the GSAs, to identify potential biases between the BDF and the transient data. Furthermore, we will investigate the correlations between inputs variables in order to define dependencies to build the probabilistic forecast of an undrilled well.

The histograms of **Fig. 103** illustrate the distributions of the permeability, fracture half-length and $x_f\sqrt{k}$ for the 126 wells in the Denton County. We notice a large discrepancy between the permeability distributions of the wells in BDF with the wells in transient flow regime. 40% of the BDF permeabilities are lower than 300nd whereas all the permeability of the transient wells are below this value. This results is logical with the fact that transient wells have longer time to the end of linear flow since the permeability directly controls the duration of the transient flow regime. Therefore, only the wells with either small stage spacing or very high permeability will reach boundary dominated flow after a short production time. In addition, the transient distribution only illustrates the highest permeabilities as they were recorded based on the most conservative diagnostic. Using only the BDF permeability to forecast undrilled wells would considerably bias the analysis. Using the most conservative distribution of transient permeabilities is acceptable since all the wells were first produced between 2003 and 2013, which means that they have at least 5 years of production, which in turns would be a reasonable assumption for a minimum time at the

end of linear flow. Using the permeability distribution shown by the gray histogram corresponds to a largest possible estimate of the permeability distribution. Given more time of production, the true distribution may appear to be more skewed to the right if the transient permeabilities are lower than the conservative estimate currently used.

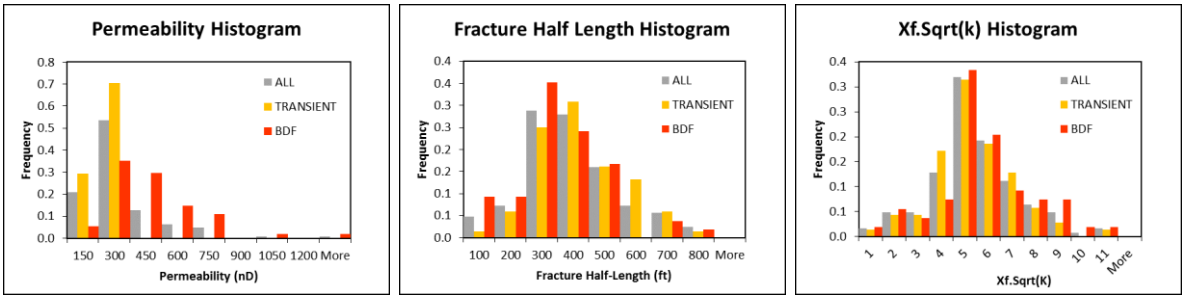


**Fig. 103—Permeability, fracture half-length and $x_f\sqrt{k}$ comparative histograms of the transient and BDF wells from the Denton County GSA.**

The fracture half-length distribution of the wells in boundary dominated flow matches better the distribution of the wells in transient flow regime. It also appears that the fracture half-length is less skewed to the right compared to the permeability distribution. The last distribution of the $x_f\sqrt{k}$ product presented on Fig. 103 has the characteristic shape of a normal distribution. Because we assume that the $x_f\sqrt{k}$ products remains constant during the life of the wells, the grey distribution reflect the true distribution of this parameter and provides a reliable variable which is independent with time.

Now that the distributions and biases have been identified for the fracture half-length and the permeability, **Fig. 104** was prepared to study the correlations between all the input parameters available with the 126 wells. The initial pressure, the amount of proppant, the lateral length, fracture stage spacing and stimulation fluid volumes are presented in the diagonal of the matrix. The Gaussian coefficient generated between each inputs are shown in the upper part of the matrix while the cross-plot of each correlation are presented in the lower half. Only the coefficients greater than +/-0.6 were considered statistically relevant for the sake of the analysis. Only three pairs

revealed to show a correlation. There is an inverse correlation between the permeability and the fracture half-length of +0.62, a stronger correlation between the stimulated volume and the amount of proppant of +0.75. Finally, the strongest correlation relationship occurs between the fracture half-length and the $x_f\sqrt{k}$ with a positive coefficient of almost 0.8.

The correlation between the stimulated volume and the amount of proppant appears to be in agreement with the hydraulic fracture designs as it reflects the need of a minimum amount of fluid to inject a given amount of solid proppants inside the hydraulic fractures. Unfortunately, those two parameters do not seem to correlate directly with other parameters beside the lateral length with a positive correlation coefficient of almost +0.36 and +0.48. Those correlations appear to be intuitively reasonable with assumption that longer wells will have larger stimulation designs. However, the fact that those correlations factors are not high indicates a large heterogeneity between the stimulation design and the lateral length. Finally, the stimulation volumes and the amount of proppant do not provide a useful correlation relationship to rescale the permeability nor the fracture half-length to a specific completion design.

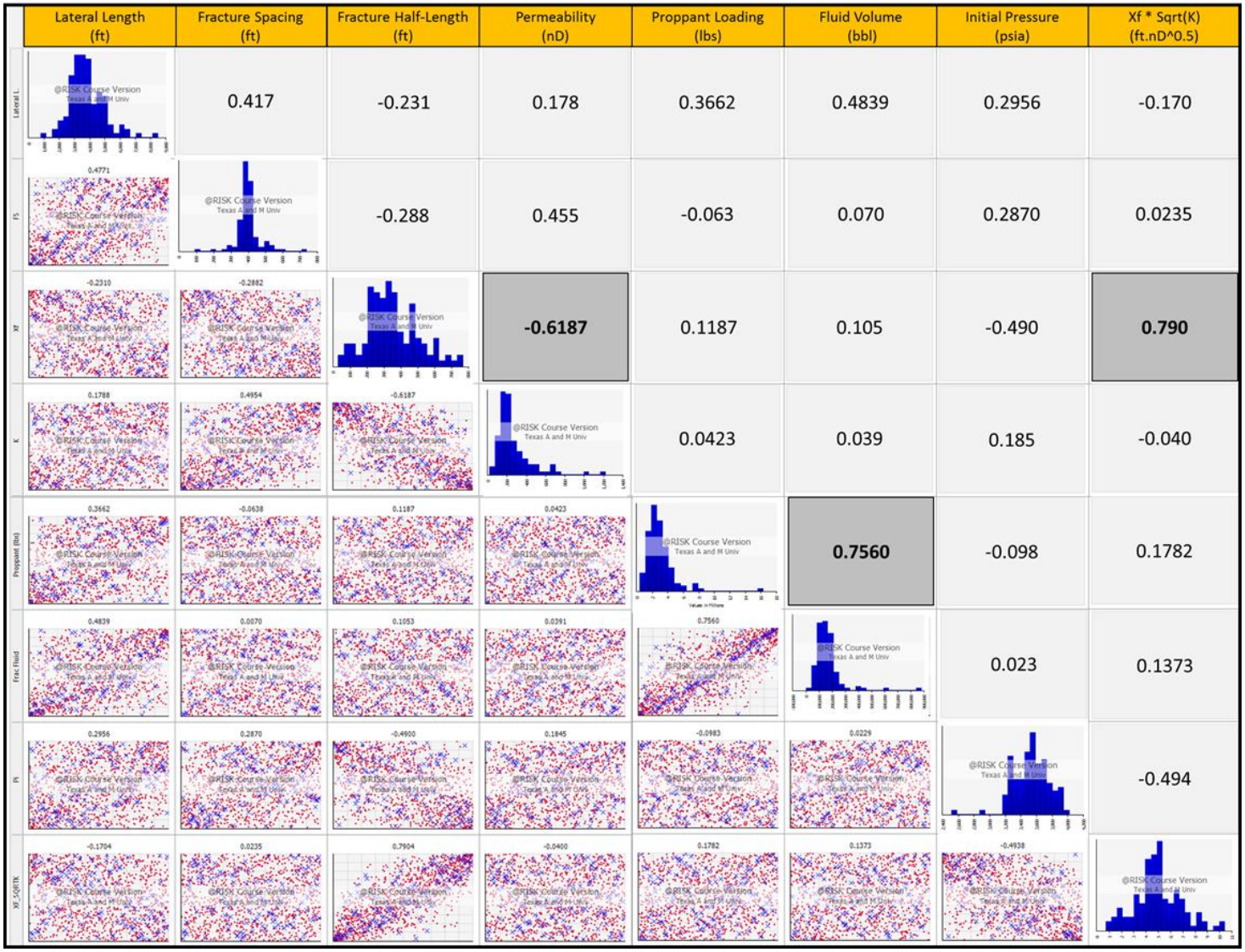


**Fig. 104—Matrix of input parameters with their distribution and correlation coefficients.**

The fact that the $x_f\sqrt{k}$ is highly correlated to the fracture half-length with a positive coefficient of +0.79 provides an interesting insight on this parameter because it demonstrates that the fracture half-length is the dominant parameter in the product. This observation is also emphasized by the fact that the permeability is completely uncorrelated with the $x_f\sqrt{k}$ since it has a coefficient of -0.04 in this dataset. Hence, we see that the fracture half-length product with permeability is a good indicator of the fracture half-length, and therefore could be good indicator of the SRV. As this may be an isolated results, more investigation would be required to validate this observation with other GSA in different resource plays to consider this a reliable indicator of the completion efficiency and the potential EUR of the well.

There is a negative correlation between the permeability and the fracture half-length of +0.62 that indicates wells with a higher permeability have lower fracture half-length. This correlation could be influenced by to the ratio of wells in BDF compared to the wells in transient flow regime. Wells in BDF are generally biased toward the higher permeabilities, lower fracture spacing, and or smaller fracture half-length and lateral length while the transient wells represent the opposite bias. Hence, 55 BDF wells out of the 126 wells may potentially bias this correlation. Nevertheless, given that the $x_f\sqrt{k}$ product remains constant during the life, the mathematical relationship of the $x_f\sqrt{k}$ product reinforce the negative correlation. For instance, as the conservative diagnostic of transient wells are most likely over-estimating permeability, smaller permeabilities would necessitate a higher fracture half-length to honor the constant value given by the diagnostic plot.

Since we previously determined from Fig. 103 that the permeability distribution of the 126 wells was biased by the wells in BDF, it is the least reliable property that would be used for forecasting purposes. An alternative distribution can be generated for the permeability based on the $x_f\sqrt{k}$ relationship. Since the fracture half-length and the $x_f\sqrt{k}$ distributions appears to be highly correlated, a permeability distribution can be generated

from those parameters given a correlation coefficient of 0.8. In order to evaluate the impact of the correlation coefficients identified between the parameters, three distributions of the cumulative production at 300 Months were be generated. The first distribution represents the probabilities using the uncorrelated distributions of fracture half-length and permeability only. The second case uses the same distributions with a negative correlation coefficient of -0.6; and finally, the third case will use the modeled permeability distribution generated from the combination of the fracture half-length and $x_f\sqrt{k}$ given a correlation factor of +0.8. The distributions presented on **Fig. 105** fit of the 126 diagnosed permeabilities, fracture half-length and $x_f\sqrt{k}$ with respectively two lognormal distributions and a normal distribution. While 126 sample can represent a small sample size, it allows to evaluate the range of permeability and fracture half-length of the wells in this GSA.

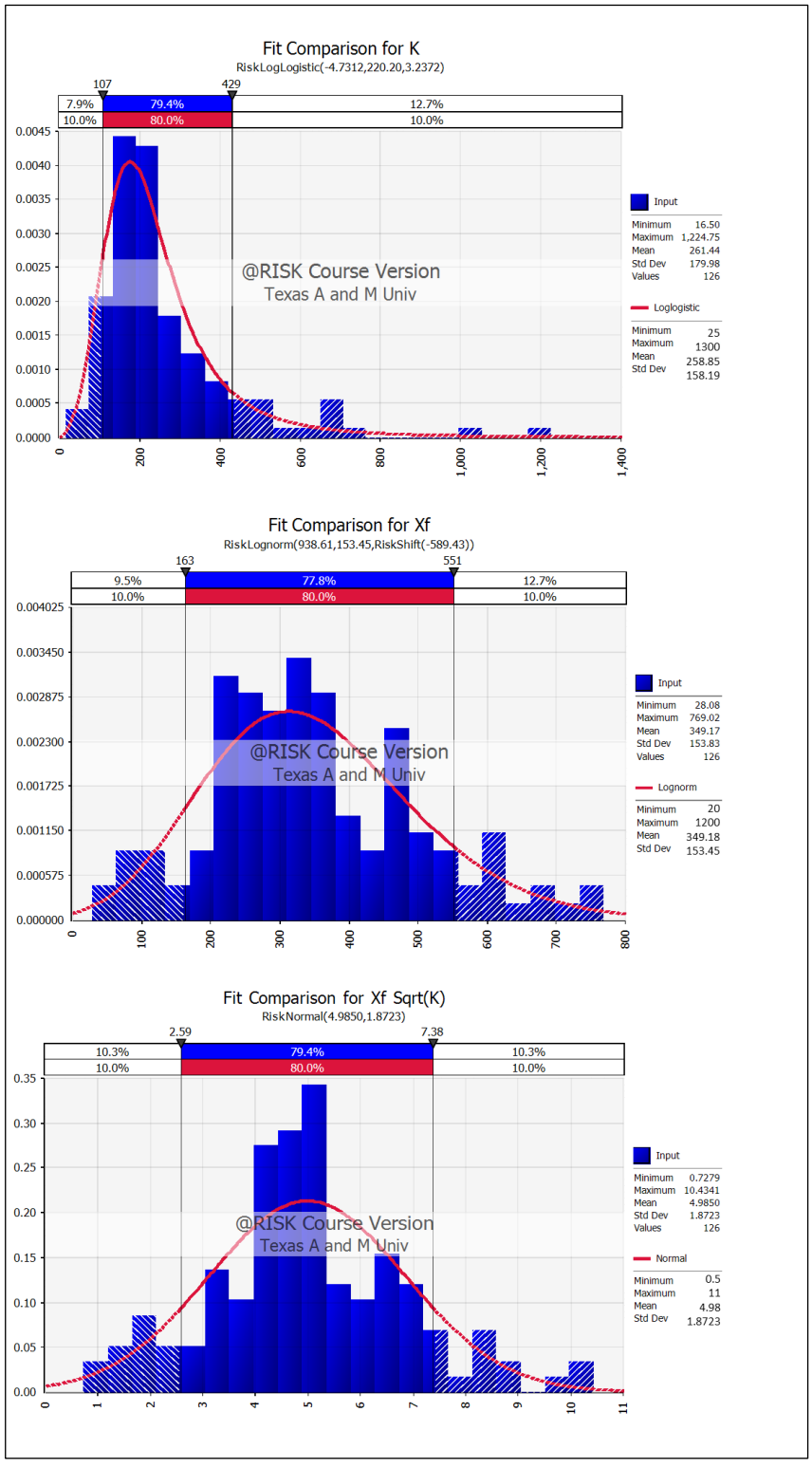


**Fig. 105—Comparison distribution fit with the permeability, fracture half-length and $x_f\sqrt{k}$ dataset from the 126 diagnosed wells of the Denton County GSA.**

The forecast is generated from the composite parametrization, given the two hyperbolic segments. The scaling factors allow to rescale the rate-time and the cumulative-time production at any time for any permeability, fracture half-length and so on. The scaling factors presented in **Table 25** show the fixed parameters that are the lateral length, the well depth and the fracture spacing. The variable parameters are presented with the label "Rnd" since they are randomly sampled from their respective distribution in the Monte Carlo analysis. The "Var" label represents the variable calculated from product of the fixed and variable parameters.

| Parameter | Units | BASE CASE | UNDRILLED | TSF | RSF | CSF |
|---|---|---|---|---|---|---|
| Permeability | nD | 340.12 | Rnd | Rnd | Rnd | 1.00 |
| Fracture Half-Length | Ft | 343.36 | Rnd | 1.00 | Rnd | Rnd |
| Net Pay Thickness | Ft | 200 | 200 | 1.00 | 1.00 | 1.00 |
| Lateral Length | Ft | 3185.86 | 4420 | 1.00 | 1.77 | 1.77 |
| Pseudo-Pressure Drawdown | psi2/cp | 7.03E+08 | 7.60E+08 | 1.00 | 0.97 | 0.97 |
| Fracture Spacing | Ft | 383.97 | 401.25 | 1.09 | 0.92 | 1.00 |
| | | | TOTAL | Var | Var | Var |

Table 25—Scaling factors for the undrilled type well.

**Fig. 106** presents the 3 probability distributions of the cumulative production at 300 months from the simulation with 100,000 runs. For clarity, the outline of the uncorrelated distribution was redrawn. Overall, all the distributions appears to be skewed to the right and could be modeled with a lognormal distribution. We observe that case 2 and case 3, which are the correlated distributions, are very similar as they have almost the same mean around 3570 MMscf and standard deviation of 1340 MMscf. The uncorrelated distribution has a higher mean of 3738 MMScf and a larger standard deviation of 1785 MMscf. The fact that the uncorrelated distribution shows a greater standard deviation reflects the higher uncertainty compared to the correlated distributions. As shown on Fig. 106, 80% confidence interval of the second case (in blue) only covers 66.8% of the uncorrelated distribution. Furthermore, the calculated P10/P90 ratio for the uncorrelated distribution is 3.75, the second case has the smallest ratio of 2.71 and the third case has a ratio of 2.98. The P10/P90 difference between the two correlated cases implies that the

correlation coefficient of -0.6 between the permeability and the fracture half-length leads to a smaller uncertainty than the correlation coefficient of +0.8 when calculating the permeability with the fracture half-length and $x_f\sqrt{k}$. This examples demonstrates that the correlations allow to narrow the confidence interval compared to the uncorrelated parameters. We demonstrated how uncorrelated inputs variable significantly increases the range of uncertainty of the P90 and P10 estimates, which are the reference percentiles for reserve estimation.

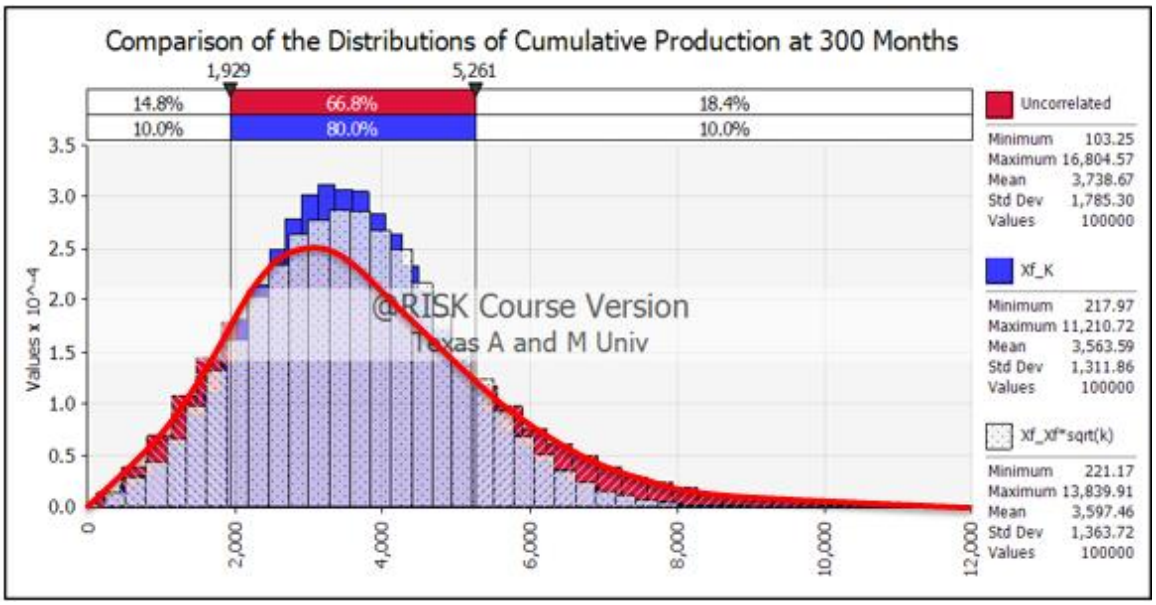


**Fig. 106—Cumulative production at 300 month comparison plot for the undrilled type well.**

Based on the previous results, percentiles type wells can be generated as discrete functions of the percentiles at different times. Similar to the distribution presented on Fig. 106 which is only a time slice at 300 months, the P10, P50 and P90 were simulated with the Monte Carlo analysis for different times in order to simulate a well life of 25 years of production. **Fig. 107** presents the percentile type wells for the 3 cases. As expected, the

blue and the green forecasts are narrower for the entire life of the well, compared to the red forecast which represents the uncorrelated relationships.

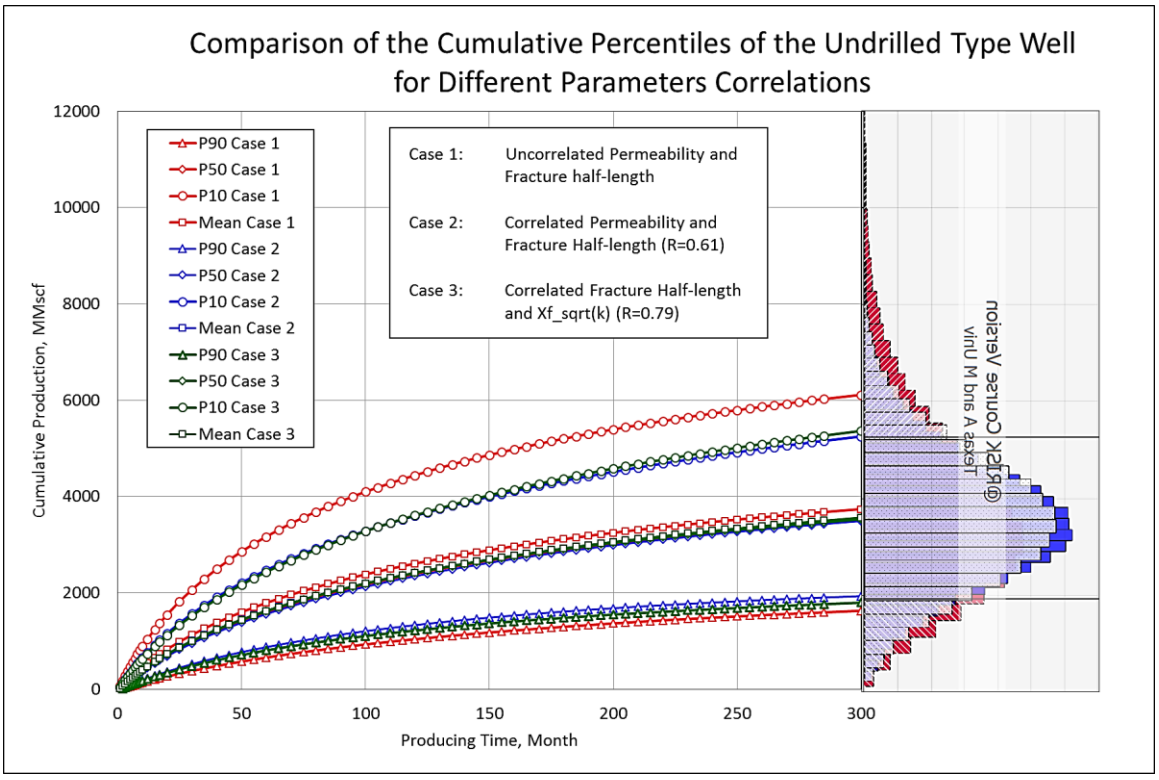


**Fig. 107—Comparison of the cumulative percentiles of the undrilled type well for different parameters and correlation cases.**

By itself, Fig. 107 provides an insightful forecast for the undrilled well given the unique feature that it takes into account physical design parameters. Assuming that the uncertain input parameters' distributions and correlations were known in 2009, we hindcasted this type well forecast to compare with 14 wells that were put in production between 2010 and 2014. None of the 14 wells has been producing in BDF and therefore were used to generate the base well profile presented in section 6.2. Furthermore, the wells

were selected based for their gross perforated interval (Lateral Length), between 4400 and 4450 ft, out of the entire pool of the horizontal wells available in the Denton County, as illustrated in light blue on **Fig. 108**, which shows the geographical distribution of the 126 diagnosed wells and the 14 “undrilled” wells.

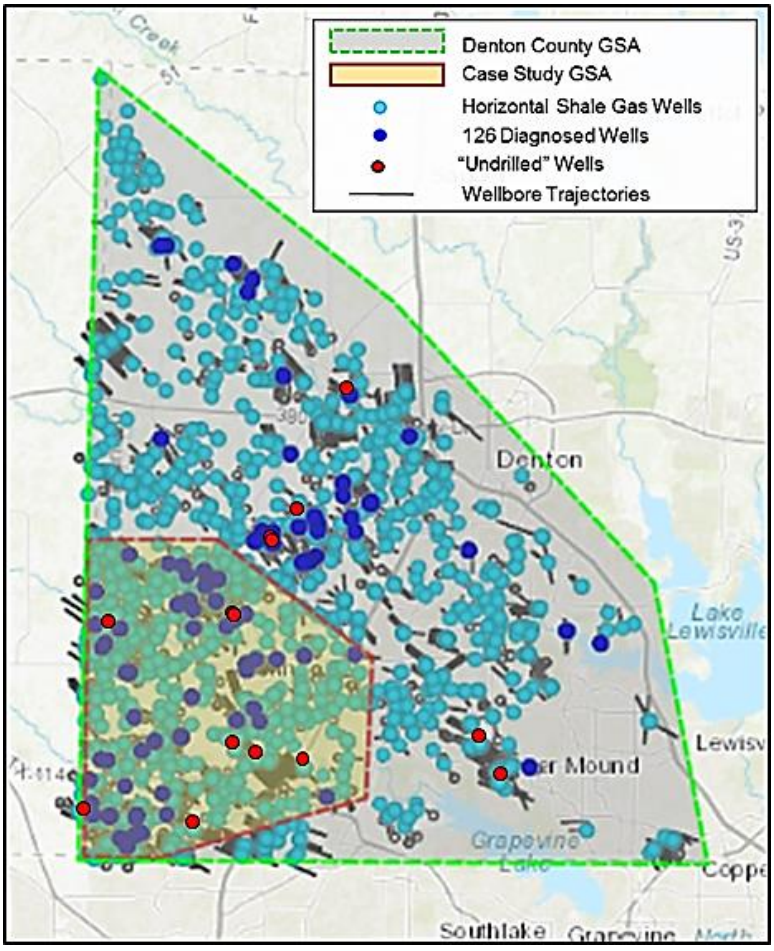


**Fig. 108—Map of the location of the 126 diagnosed wells and the 14 "undrilled" wells.**

**Table 26** presents the available characteristic of the 14 wells selected for this analysis. Only wells 8 to 11, which are underlined in Table 26, are part of the 126 diagnosed wells. Hence, the rest of the wells are completely independent of the distributions of Fig. 105 and were not diagnosed with the modified type curve. Because the number of hydraulic stages were available for only 9 out of the 14 wells, the stimulation volume as well as the proppant information were added to reflect the size of the stimulation design. We purposely kept well 4, shown in red, since it has a smaller reported number of fractures but a similar proppant and fluid design as the underlined wells. The four wells in bold did not have a reported number of stages, and they appear to have a much greater proppant loading compared to the rest of the group. Assuming that the underlined wells feature a fixed amount of proppant per stage, the wells in bold could have a number of hydraulic stages varying from 20 to 40. While those calculated numbers would influence the stage spacing and therefore the production forecast, we purposely kept them in case they could have been fractured with the same number of stages but with a much larger treatment design.

| Well Nº | API Nº | First Prod. Date | True Vertical Depth (ft) | Cum. 50 Months (MMscf) | Stage Number | Stage Spacing (ft) | Total Proppant (lbs) | Total Fluid (bbl) | Months Produced | Perforated Interval ft |
|---|---|---|---|---|---|---|---|---|---|---|
| 1 | 4212133699 | 6/1/2010 | 7915.4 | 1128103 | 11 | 403.0 | 2792325 | 151045 | 94 | 4433 |
| 2 | 4212133900 | 11/1/2010 | 8785.7 | 1299425 | 10 | 442.4 | 4186250 | 219541 | 89 | 4424 |
| **3** | **4212133816** | **1/1/2011** | **7550.73** | **2804778** | **-** | **-** | **9893974** | **195171** | **87** | **4414** |
| **4** | **4249736992** | **3/1/2011** | **7348.62** | **1090872** | **7** | **629.4** | **3827200** | **148380** | **85** | **4406** |
| **5** | **4212133884** | **5/1/2011** | **8217.88** | **1534081** | **-** | **-** | **7702906** | **159000** | **81** | **4419** |
| 6 | 4212133936 | 8/1/2011 | 8351.61 | - | - | - | 5543309 | 114830 | 24 | 4411 |
| 7 | 4212134180 | 1/1/2012 | 8450.88 | 1566789 | 12 | 370.1 | 3420640 | 182581 | 75 | 4441 |
| 8 | 4212134201 | 8/1/2012 | 7956.73 | 963371 | 11 | 401.7 | 2503570 | 139792 | 68 | 4419 |
| 9 | 4212134206 | 8/1/2012 | 8041.85 | 1132780 | 11 | 401.2 | 2503570 | 139792 | 68 | 4414 |
| 10 | 4212134276 | 9/1/2012 | 8098.49 | 1376021 | 11 | 401.2 | 3248000 | 171200 | 67 | 4414 |
| 11 | 4212134277 | 10/1/2012 | 8247.28 | 1502597 | 11 | 401.2 | 3248000 | 171200 | 66 | 4414 |
| **12** | **4212134367** | **3/1/2014** | **7552.49** | **2252038** | **-** | **-** | **6497519** | **271616** | **49** | **4431** |
| 13 | 4212134410 | 3/1/2014 | 7524.67 | 1606110 | 11 | 402.8 | 4228400 | 167691 | 49 | 4431 |
| **14** | **4212134448** | **11/1/2014** | **7688.86** | - | - | - | **6160000** | **118840** | **40** | **4442** |
| | Type Well | - | 8000.00 | - | 11 | 401.81 | - | - | - | 4420 |

Table 26—Undrilled wells characteristics for the validation of the undrilled percentile type well

**Fig. 109** and **Fig**. 110 compare the production profiles of the 14 wells against the percentile type wells illustrated on Fig. 107. Only case 3's forecast was plotted on the graphs in the solid lines as it yields approximately the same results as the second case. The solid line represent the percentile type wells issued from the correlations between inputs and the dotted line are the type wells for the uncorrelated inputs. Before analyzing the results, it should be remembered that the probabilistic/percentile type wells are the likelihood of performing a certain rate or cumulative production at a given time. In the case of the rate-time relationship, the rate at a given time is usually governed by the flow regime and the pressure drawdown. Percentile type wells can only be realistic if a constant BHP is maintained, but since some of the wells have had shut-in or produced at different drawdown, this may limit the interpretation of the results. Finally, the cumulative production at a given month depends on the previous month's cumulative production and the rate of the current month. In the case of a long ramp-up period or many outliers in the

data, some well may not be comparable to the cumulative percentile type well as it would be assumed that the wells wouldn't have produced under the same reservoir behavior during its entire production history.

The analysis of the 14 wells presented in Fig. 109 and Fig. 110 will be performed as a group but the production of some of the wells will be discussed individually to showcase the types of interpretations that can be performed with the analytical scaling factors. The main observation from Fig. 110 is that all of the wells fit inside the forecasted P10 and P90 range, except for wells number 3, 12 and 14 that are above the $10^{th}$ percentile of the correlated forecast. The remaining wells are grouped inside the correlated P10-P90 window, which is a positive validation of the forecast. As for the cumulative plot, Fig. 109 also indicates that the monthly rates of the 14 wells fall in the 80% confidence interval. Since none of the outliers were removed from the profile, most of the data points falling under the P90 rate forecast could be considered as outliers.

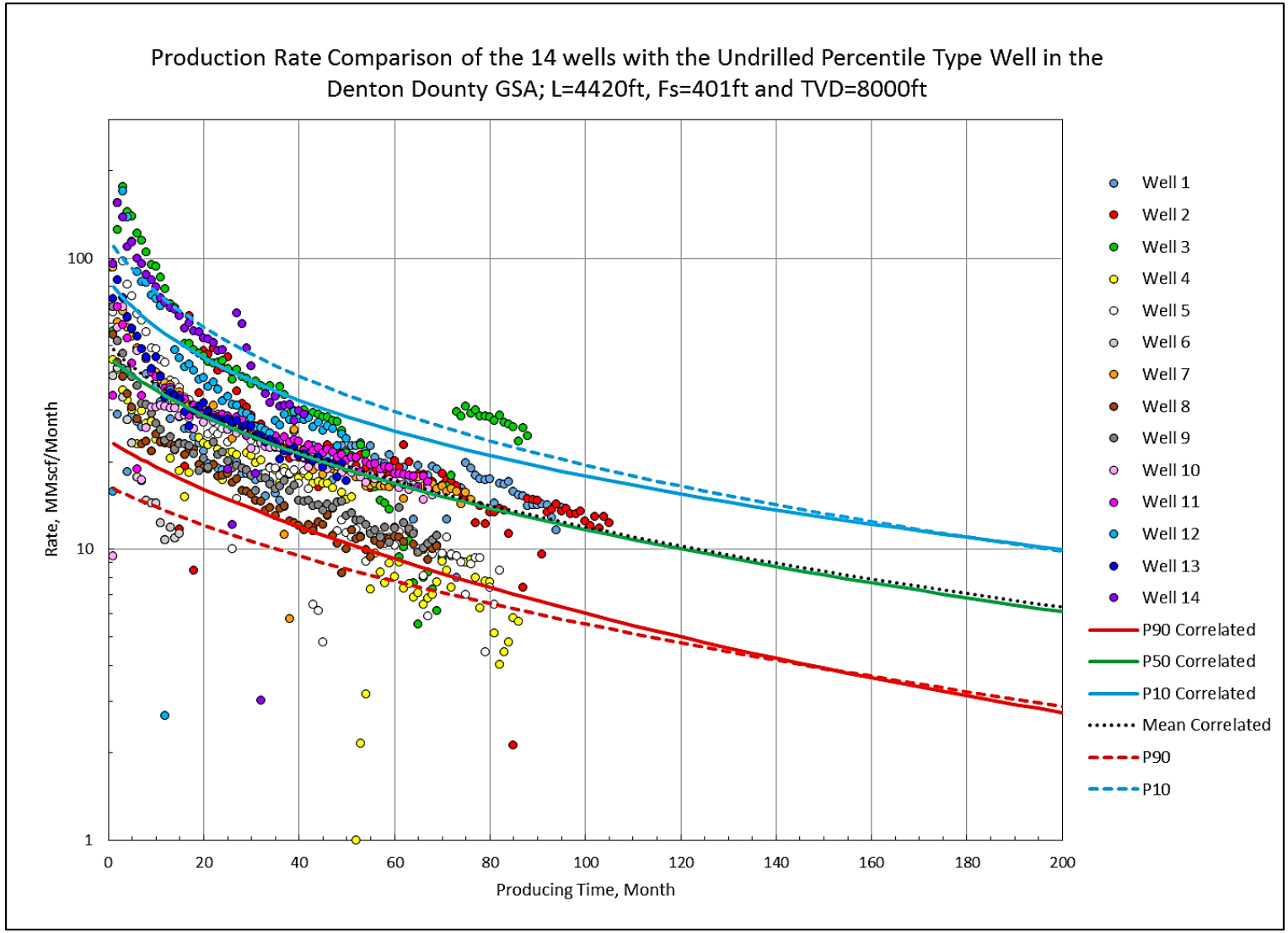


**Fig. 109—Rate-time profiles comparison of the 14 wells with the undrilled percentile type well in the Denton County GSA; L=4420ft, Fs=401ft, TVD=8000ft.**

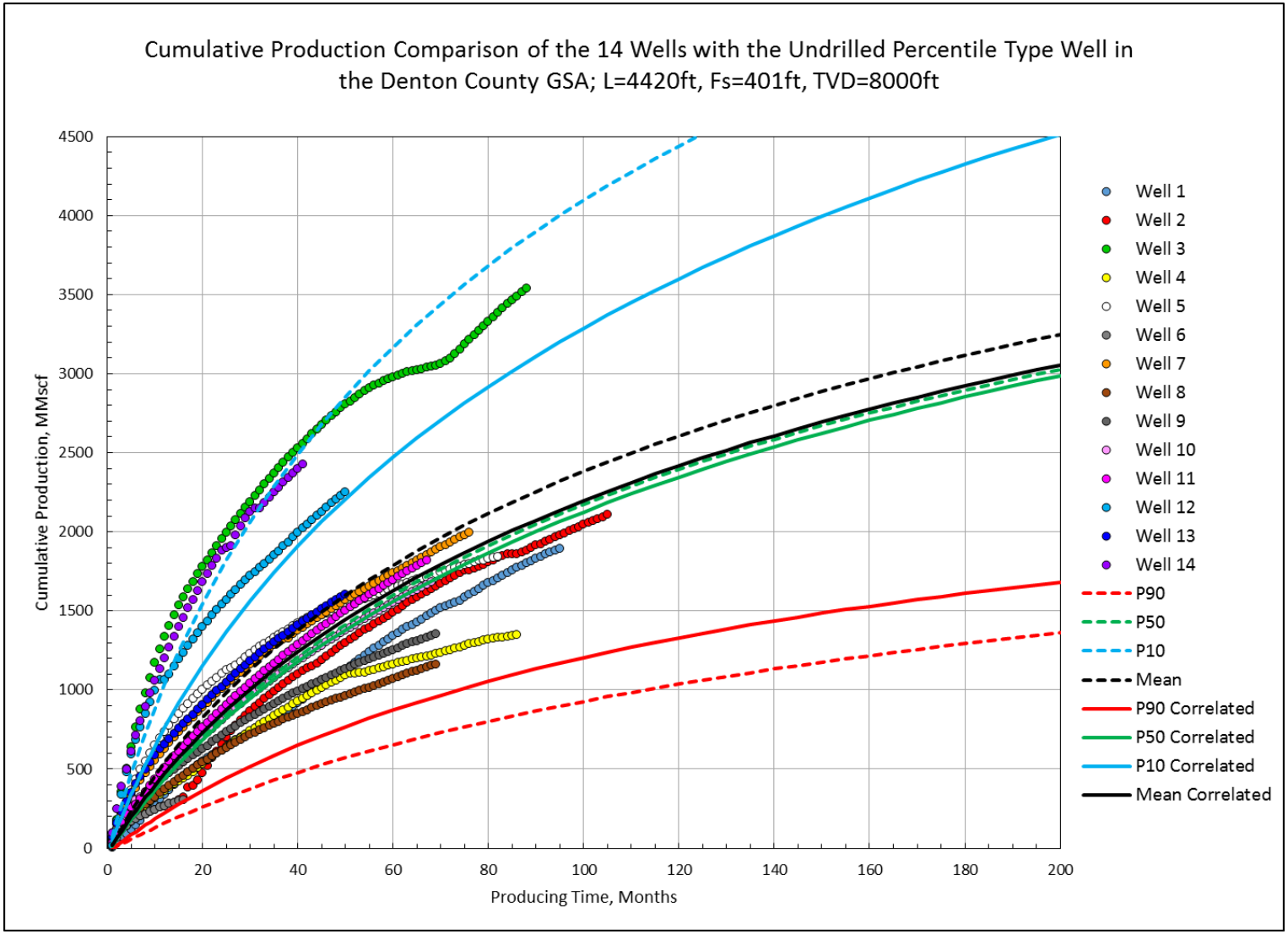


**Fig. 110—Cumulative-time production comparison of the 14 wells with the undrilled percentile type well in the Denton County GSA; L=4420ft, Fs=401ft, TVD=8000ft.**

It appears that the 3 profiles that are over-performing the type well forecast are also the wells that have an unknown number of hydraulic fracture stages and a larger stimulation designs. This observation could validate the assumptions that those have more fracture stages. In fact, the difference in fracture spacing between two wells relates to an increase by a power of two in the time scaling factors, as presented in Table 12. In the case that the fracture spacing would be reduced by two, the time scaling factor would be divided by 4 and the rate scaling factor multiplied by 4. This makes the fracture spacing a very sensitive parameter in the analytical scaling factor theory and represents a major source of uncertainty in the estimation of permeability if it is unkown. Assuming that they have 22 stages (instead of 11) because the stimulation designs are so large, we normalized the three profiles by applying a time scaling factor of 4, in order to compare them to undrilled type well. **Fig. 111** shows the results of this time adjustment; and the rescaled profiles fall in the P50-P90 windows of the forecast. While the number of stages will remain unknown, the possibility that the three wells have a smaller stage spacing is coherent with the observations made on Fig. 111.

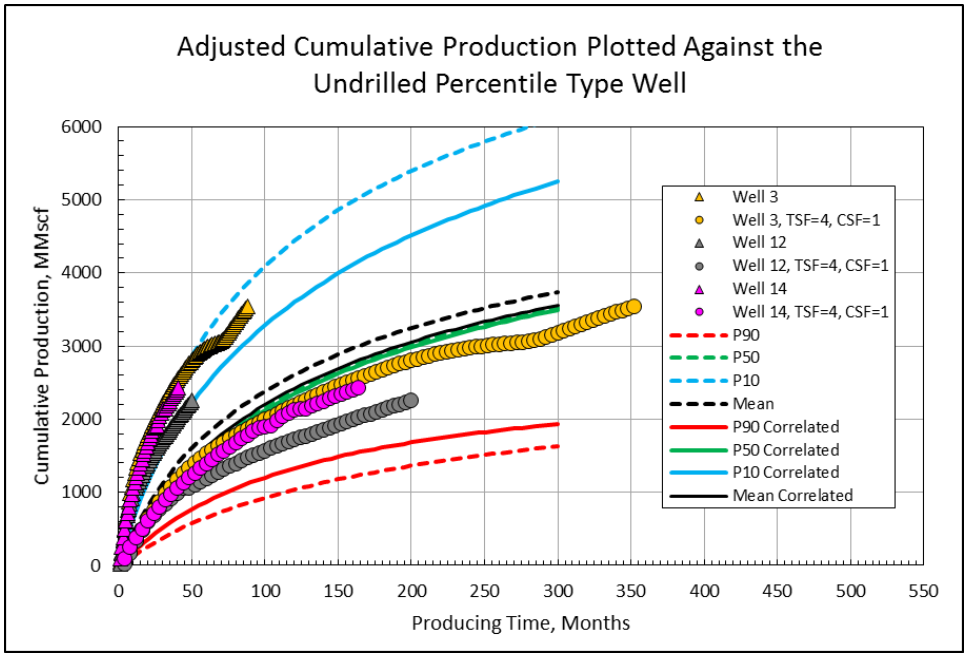


**Fig. 111—Adjusted cumulative production of wells with unknown fracture spacing plotted against the undrilled percentile type wells.**

On the opposite side of the group, four wells were identified as underperforming: number 1, 4, 8 and 9. Their performance could be explained by the fact that well 1, 8 and 9 have a lighter proppant loading compared to well 6 an 7 for the same stage spacing. Finally, well 4 have a similar proppant loading compared to 6 and 7 but it only has 7 fracture stages instead of 11. Combining both observations lead to a strong correlation between the proppant loading and the performance of the wells. **Fig. 112** confirms this observation as there is a positive $R^2$ coefficient of 0.72 between the proppant loading and the cumulative production at 50 months of production. However, we did not observe a correlation between input parameters on Fig. 104. As the cumulative production at a given time can both changed by the time and the cumulative scaling factors, the proppant loading can have a combined impact on more than one parameter that govern those scaling factors. If this correlation is true for the 126 wells previously studied, a multivariate analysis could be performed to study these correlations.

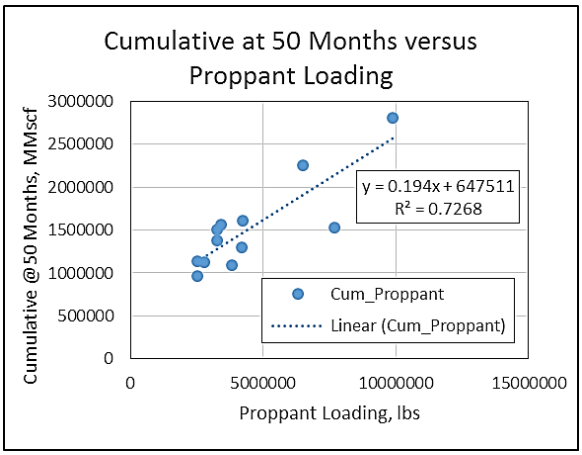


**Fig. 112—Cumulative production of the 14 "undrilled" wells at 50 months versus proppant loading.**

Finally, the remaining wells; 2, 5, 7, 10, 11 and 13 are very well grouped around the mean and the P50 percentile type wells. This observation validates the forecast as 6 out of 11 similar

wells fall exactly on the P50 with a +/- 10% accuracy. As prescribed by McLane and Gouveia (2015), the sequential aggregation plot presented in their paper is an excellent tool to validate our undrilled type well forecast. For this case study, we chose to plot and compare the cumulative production at 40$^{th}$ month because 13 out of the 14 wells reached this stage of production. The aggregation plots were generated for the uncorrelated and the correlated type wells, which are presented in **Fig. 113**.

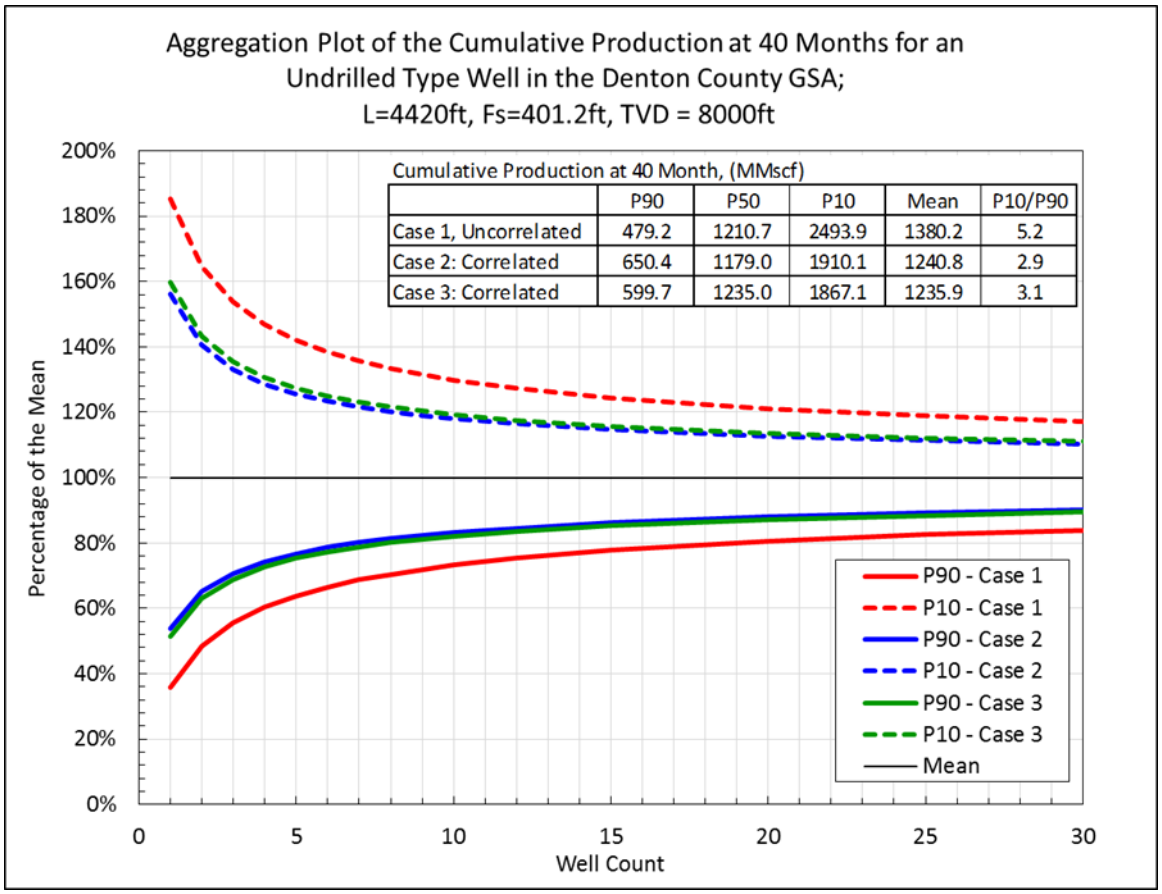


**Fig. 113—Aggregation curves for the undrilled type well in the Denton County GSA.**

Based on the method detailed by McLane and Gouveia (2015), a sequential aggregation plot can be generated at 40 months of production from Fig. 113. **Fig. 114** presents the sequential

aggregation plot for the undrilled type well based on the forecast of the second case, for which the permeability and the fracture half-length are correlated. We present 14 wells in yellow diamonds, and also plotted the 11 wells (in pink) by eliminating the 3 wells with a suspected higher number of fractures. It appears that the probabilistic distributions generated by the Monte Carlo analysis is valid as the incremental cumulative production of 11 wells, which is the conservative case, stays in the P10 and P90 window. As shown below, the sequential accumulation plot provides a good validation tool of the forecast of undrilled wells and it can be performed at any time based on the available data.

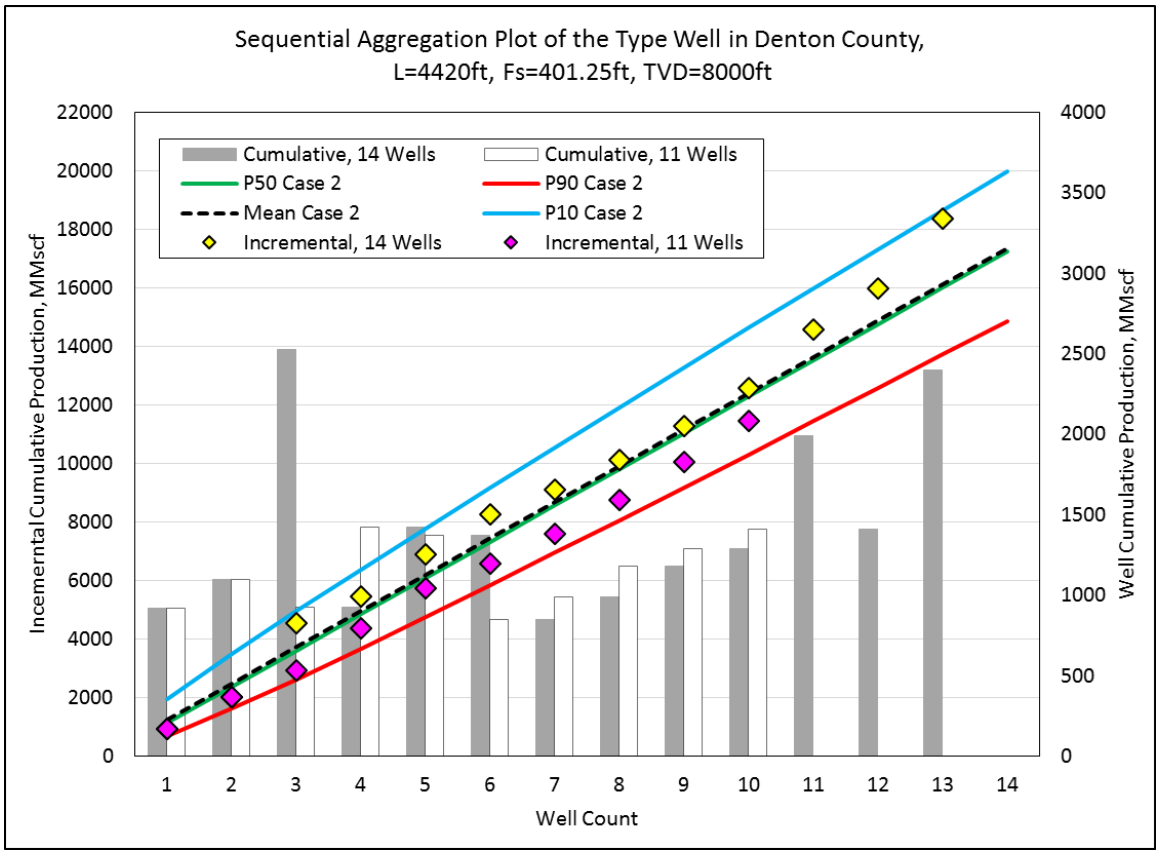


**Fig. 114—Sequential aggregation plot of the undrilled of the Denton County GSA.**

The remaining discussion will address how an irregular production history can affect the diagnostic when using percentile type wells. For instance, well 4 colored in yellow, had a steady production located in the correlated P50-P90 window until 50 months as indicated on Fig. 109. However, the monthly production became unstable and mostly below the P90 rates for the remaining time of its production history. This sudden change in production may indicate operational issues or reflect some Non-producing time (NPT) not reported in monthly sale volumes. As mentioned earlier, the best practice is to always plot the production against producing time, and not calendar time, when using the analytical scaling factors. For instance, if the well only produced 2.16 MMscf in 3 days over the 53th month of production, while it was shut-in during the remaining 28 days, it would still be reported as 1 months of production in calendar time while it would be only 0.1 months in producing times. This observation directly addresses the limitations of publically available data. Not correcting the calendar time will also impact the cumulative production diagnostic. As illustrated on Fig. 110, the slope of the cumulative production of well 4 changes after 50 months. Because the cumulative production plot carries the history of production, if the well would perform in the future to the equivalent of P50 rates, its cumulative profile would be lower and be diagnosed at a lower cumulative percentile. The same observation can be done with well 3 between $70^{th}$ to $90^{th}$ months of production: the rate percentile is lower than the 10% percentile while the cumulative percentile is higher. To a certain extent, the cumulative and rate profiles can only be in agreement if they follow relatively closely the same type well percentile performance during their entire production history. For instance, well 11 is a good example as illustrated on Fig. 109 and Fig. 110 in magenta. This theory provides useful insights for production analysis and forecasting. If a production profiles consistently follows one percentile of the type well profiles, we validate that it aligns with the typical behavior identified in this GSA, and can be accurately forecasted in the range of certainty determined by the last known point of production of the Base Well. However, this would happen in only rare cases as the production is reported in calendar days and the wells are not usually not flowing under the same operating conditions during their entire life.

In summary, the percentile type wells illustrate the confidence of achieving either a rate or a cumulative production at any given time, assuming a steady production conditions. The analytical scaling factors provide a rigorous methodology to generate percentile type wells with a Monte Carlo analysis based on the uncertainty of the parameters. This technique allows to use and test different correlations between input parameters and their associated uncertainty. Furthermore, this method allows to use the estimated features of a GSA to create specific forecasts. This integrated process proves to be much trustworthy than the empirical averaging of analogous profile. In fact, characterizing the range of permeability and fracture half-length of a GSA is similar to the work performed in conventional workflows when building a reservoir model. Henceforth, it provides a robust workflow to estimate the statistical parameters such as P90, P50, P10 and P10/P90 for reserve evaluation. The example of the 14 wells shows a very good agreement between the data and the forecast, and validates that the forecasted percentiles could be used for production forecasting and reserve estimation in resource plays. Finally, the percentile type wells can be potentially used as good tools to investigate the behavior of the well, given that both the cumulative and rate plots are plotted to compare the data.

Finally, this methodology can easily be combined with an economical model in order to calculate the NPV of an undrilled well and choose the most optimal design to achieve an economical target. Moreover, the tools developed to implement the workflow (graphical type curve match, outlier detection tool, composite parametrization, scaling factors and Monte Carlo simulations) were coded and performed in a spreadsheet software.

# CHAPTER VII

# SUMMARY, CONCLUSIONS, AND RECOMMENDATIONS FOR FUTURE WORK

## 7.1 Summary

- The objective of the work presented in Chapter 3 was to propose an analytical scaling solution applicable to most of unconventional horizontal multi fractured wells.
  - We derived a modified analytical solutions from the commonly-used Wattenbarger type curve for horizontal wells exhibiting transient linear flow followed by boundary-dominated flow.
  - We validated the modified analytical model with ten different shale gas plays in the world by validating the characteristic geometrical shape of the type curve on the rate-MBT log-log plot.
- The objective of the work presented in Chapter 4 was to establish a set of scaling factors for each key parameters used in the modified type curve based on the simulation of an analytical model.
  - We demonstrated that scaling factors are mathematically related to difference of matrix permeability, net pay thickness, fracture half length, fracture spacing, and lateral length, while we approximated a scaling relationship for the difference in pseudo-pressure drawdown. Those relationships are summarized in Table 12.
  - We applied the scaling factor to normalize the production of 10 wells for each play in the Haynesville, Eagle Ford, Marcellus and Barnett resource plays.
  - We demonstrated that scaling the production profiles to a common set of properties allows to capture a typical production profile.
- The objective of the work presented in Chapter 5 was to propose an integrated workflow to generate type wells from publically available information in a GSA.
  - We recommended to fit the production profiles of HMFW to the modified type curve in order to diagnose flow regimes, reservoir and completion parameters
  - We suggested to separate the production profiles of a GSA into three groups based on their flow regime characteristics

- We suggested to create a type well profile by scaling the production of all the wells in BDF to a "base well" defined by the respective average of the properties diagnosed with the modified type curve
- We suggested to rescale the base well profile into a deterministic type well given a specific set of reservoir and completion parameters, which can also be used to forecast production
- We presented a methodology to create a probabilistic type well forecast for wells flowing in transient flow based on their value of $x_f\sqrt{k}$
- We presented a methodology to create a probabilistic type well for undrilled wells defined by a specific set of reservoir and completion properties based on the correlations between the key inputs parameters of a GSA

- The objective of the work performed in Chapter 6 was to illustrate the workflow presented in Chapter 5 with a data set of 179 horizontal shale gas well from the Denton county in the Barnett Shale.
  - Sorted 179 production profiles of a GSA into three groups based on their flow regime characteristics
  - We fitted the production profiles of 126 HMFW to the modified type curve in order to diagnose flow regimes, reservoir and completion parameters
  - We created a Base well profile from the wells BDF
  - We forecasted the production of 28 wells in BDF by rescaling the base well profile
  - We demonstrated the methodology to create a probabilistic type well forecast for a well in transient flow regime
  - We diagnose the correlations between the input parameters of the 126 wells
  - We generated a probabilistic type well for an undrilled wells and validated the forecast with 14 analogs using the sequential aggregation plot
- In the Appendices, we presented some of the derivations and to tools developed to facilitate the implementation of the workflow presented in Chapter 5.
  - We developed an outlier detection tool to improve the fit of production data to the modified type curve, and in turn the diagnostic of flow regime
  - We presented the composite parametrization as a way to fit a modified hyperbolic to the cumulative-time and rate-time profiles.

## 7.2 Conclusions

The high-level conclusions of this research are:

- The production profiles of HMFW in resource plays follow the same production behavior characterized by an analytical model modified from the Wattenbarger linear flow model
- We demonstrated and analytically derived a set scaling factors for each properties of the analytical model to be used to normalize production profiles of MFHW.
- We successfully presented a methodology that analytically generates type wells and production forecasts for specific reservoir and completion parameters, which circumvent the main limitations of the current industry's practices

Further conclusions related to the three points above are presented into the following sections, in order to address the work performed with the modified analytical model, the scaling factors and the new type well workflow.

*Modified Analytical Model:*

- The modified type curve allows to diagnose two reservoir and completion properties present in the dimensionless equations. The major unknowns of the model are generally the matrix permeability and the fracture half-length and they also respectively define the reservoir and completion's performance of the model. Other properties such as the net pay thickness is also a major unknown that governs the stimulated volume. Choosing a net-pay thickness directly impacts the calculation of the fracture half-length as the production of the two must remain equal to honor the match of the dimensionless equation. Assumptions of properties such as the net-pay, the porosity or the compressibility will affect the calculated permeability and fracture half-length. Choosing a consistent value for those parameters, if they are unknown, allows to normalize the estimated results, which in turn allows and improves the comparison of multiple wells in a GSA.
- We successfully used the modified analytical model to match the rate-MBT of publicly available production although they are not corrected for producing time and for varying BHP. Only the wells with large discontinuities in their production history did not provide a reliable

match to the type curve. Using publically available data to diagnose an effective permeability and fracture half-length provide *key performance indicators* that can be used to scale production.

- An assumption of the number of fractures (assumed to be the number of hydraulic stages or clusters in Appendix K) is required to calculate a permeability. If the number of fractures is unknown, the group $F_s^2/k$ can characterize the depletion potential of the well and can act as a key performance indicator. A large value of $F_s^2/k$ indicate a well that will deplete less efficiently, which limits the recovery of the hydrocarbons in time.

*Scaling Factors:*

- The analytical scaling factors rigorously accounts for the different of the modified analytical model's properties to normalize the production to a reference well. We demonstrated the impact of each properties on the production profile as either a vertical and horizontal shift on a log-log plot. The shift is proportional to the ratio between the two properties and correspond to a constant that multiplies to time, rate or cumulative variable.
- We define the scaling factor as a constant that multiplies the time, rate or cumulative variable as a way to normalize production. The match points when fitting a dimensionless curve to a production profile are also scaling factors, as they rescale the production profile to the equivalent location of the dimensionless type curve when plotted on the same graph.
- The scaling factors equations are governed by the dimensionless equations as demonstrated in Appendix B. *Therefore, the properties in the dimensionless equations of other analytical models for different flow geometries and fluid types can provide scaling factors* when the analytical model can be matched to the production history.
- The scaling factor for drawdown is only valid in transient flow regime because the drawdown is calculated based on the initial reservoir pressure and a constant BHP. However, the drawdown in boundary dominated flow is calculated based on the average reservoir pressure which varies based on the material balance. As the drawdown scaling factor does not account for the change in average reservoir pressure in boundary dominated flow, we expect a variation between the rescaled and the true profile in boundary dominated flow.

- The difference between the rate scaling factor and the cumulative scaling factor is due to the integration of time of the rates to generate the cumulative. The rate scaling factor is the quotient of the cumulative scaling factor and the time scaling factor.
- The time scaling factor only rescale for the permeability and fracture spacing, which is in agreement with the distance of investigation equation in linear flow. Similarly, based on the properties studied, the cumulative scaling factor only rescale for the parameters that govern the total stimulated volume and the drawdown in the transient region. In other term, the cumulative scaling factors scale the EUR and the time scaling factor scale the duration of flow regimes
- We demonstrated in Appendix D that the scaling factors are related to the ratio of the Arps constants, assuming that a hyperbolic segment with the same b factor can model a segment of the data.

*Type Well Workflow*

- Rescaling the production profiles of 10 wells in different plays to the average properties of the group showed that their production profiles depict a common reservoir behavior.
- Normalizing production with the rate and time scaling factors allows to account for the difference in properties and provides a rigorous tool to create a type well profile for a specific set of reservoir and completion parameters.
- Averaging the production of wells with different properties does not provide a type well forecast specific to a set of reservoir and completion properties. As shown on Fig. 92, comparing the industry type wells (time slice) and the base well profile shows a large difference at early time. Since type wells are used to characterize the value of an asset, the time slice method should not be used as it is empirical and it does not provide a reliable estimation of an expected well design.
- The production profiles should be scaled **both on rate and time**, to honor the scaling factor relationship. A difference in permeability and fracture spacing require to normalize the time on both the rate and the cumulative profile. To this point, none of the sources presented in the

literature review considered normalizing the production profile on time. We concluded that the production profiles have to be treated as a multi-dimensional problem.

- Scaling underperforming wells with small $t_{elf}$ can improve the duration of a forecast
- Scaling factors normalize the production to a common profile, which reduces the impact of the survivor bias. As several authors suggested to avoid forecasting the average but rather average the forecast, this recommendation does not apply as we do not need to forecast wells to identify a typical behavior. Using the forecast can bias the typical production; instead, we suggest to forecast the average of the normalized profiles.
- $x_f\sqrt{k}$ can be used to forecast wells in transient flow regime because the mathematical relationship bounds the two unknown parameters. We also found that the fracture half-length is the dominant variable in the Barnett shale case study.
- The combination of the scaling factors, the composite parametrization and the GSA properties allow to analytically generate percentile type wells from a Monte Carlo simulation. This technique can also incorporate correlations between input parameters and their associated uncertainty. This integrated process proves to be much trustworthy than the empirical averaging of analogous profile. In fact, characterizing the range of permeability and fracture half-length of a GSA is similar to the work performed in conventional workflows when building a reservoir model. Henceforth, it provides a robust workflow to estimate the statistical parameters such as P90, P50, P10 and P10/P90 for reserve evaluation.

### 7.3 Recommendations

The following list summarizes some of the elements that were not addressed in this workflow:

- Differences in completion design
- Operatorship
- Skin Effect
- Adsorption
- Non-Darcy Flow
- Multi-phase flow
- Variation in PVT

The main recommendation for the application of this workflow is to understand the limitation of the data. Based on this, an analysis with daily rates and pressures can only improve the characteristic and diagnostic of the analysis. The biggest limitation in this research was the access to stage number, in order to compute the permeability. Using more accurate data will improve the accuracy of the match on the modified type curve and when normalizing the production history

We recommend to use the scaling factors to investigate the change in operating conditions during the life of the well, as in changes in artificial lift, fracture interferences, re-stimulation treatments, choke management, and other workover operations. Since those affect the model's properties, they can be scaled to show the most recent set of properties. In addition, we should keep in mind that the cumulative production has a memory, which should be considered when scaling multiple segments of the same profiles.

We suggest to further investigate how the fit of the Arps' decline curves can be used to quantify the change in reservoir and completion properties during the life of the well. Such analysis would require high frequency data, pressure history and a complete history of the interventions on the well and its neighbors.

In the effort to forecast production probabilistically, more work should be performed to investigate the effect of certain technologies on the permeability and Xf distributions. We believe the technology or the fracture design can be studied from those distributions and should be used to forecast the production more accurately. Similarly, more work should be performed on the correlations between the secondary input variables with the primary input variables presented in Section 5.4. The production performances (IR, IP, EUR, CUM) are technically only an outcome that is directly correlated to the input variables via the scaling factors. Since most of the profiles are rescaled based on input variables, the evaluators should focus on the relationships between well designs, stimulation technologies or operatorships against the fracture half length, the effective permeability, the net pay thickness.

As the integrated workflow presented in this research was only illustrated with gas wells, the examples in the Appendices J and K demonstrate its applicability to other fluid types. Furthermore, derivation of scaling factors is also for vertical wells and reservoir geometries.

Related to the previous recommendation, some should investigate how the distributions of properties of different well geometries compare to the horizontal wells. This could bring more insights in the effort to characterize a GSA if key performance indicators of vertical wells **may be** correlated to the horizontal wells. Because vertical wells have longer production history, they could improve production forecasting of other wells in the same GSA.

Above all, the outcome of this research on scaling factors provides an appropriate foundation to investigate the peculiar features of unconventional GSA in resources plays such that it can be combined with an economical model in order to calculate the NPV of an undrilled well and choose the most optimal design to achieve a target.

# REFERENCES


Agarwal, R.G., Gardner, D.C., Kleinsteiber, S.W. et al. 1998. Analyzing Well Production Data Using Combined Type Curve and Decline Curve Analysis Concepts. SPE Annual Technical Conference and Exhibition, New Orleans, Louisiana, 1998/1/1/. 10.2118/49222-MS.

Agnia, A., Alkouh, A., Wattenbarger, R.A. 2012. Bias in Rate-Transient Analysis Methods: Shale Gas Wells. SPE Annual Technical Conference and Exhibition, San Antonio, Texas, USA, 2012/1/1/. 10.2118/159710-MS.

Al-Hussainy, R., Ramey, H.J., Jr., Crawford, P.B. 1966. The Flow of Real Gases Through Porous Media. 10.2118/1243-A-PA.

Ambrose, R. J., Hartman, R. C., Diaz Campos, M., Akkutlu, I. Y., & Sondergeld, C. (2010, January 1). New Pore-scale Considerations for Shale Gas in Place Calculations. Society of Petroleum Engineers. doi:10.2118/131772-MS

Anderson, D.M., Mattar, L. 2007. An Improved Pseudo-Time for Gas Reservoirs With Significant Transient Flow. 10.2118/07-07-05.

Arps, J.J. 1945. Analysis of Decline Curves. 10.2118/945228-G.

Aziz, Khalid & Mattar, L & C.M. Ko, Stephen & Brar, G.S.. (1976). Use of Pressure, Pressure-Squared Or Pseudo-Pressure In the Analysis of Transient Pressure Drawdown Data From Gas Wells. Journal of Canadian Petroleum Technology - J CAN PETROL TECHNOL. 15. 10.2118/76-02-06.

Bowker, K.A. 2007. Barnett Shale gas production, Fort Worth Basin: Issues and discussion. *AAPG Bulletin* **91** (4): 523-53310.1306/06190606018.

Chaudhary, N.L., Lee, W.J. 2016a. Detecting and Removing Outliers in Production Data to Enhance Production Forecasting. 2016/5/10/. 10.2118/179958-MS.

Chaudhary, N.L., Lee, W.J. 2016b. An Enhanced Method to Correct Rate Data for Variations in Bottom-Hole Pressure. 2016/5/10/. 10.2118/179959-MS.

Clarkson, C.R. 2013. Production data analysis of unconventional gas wells: Review of theory and best practices. *International Journal of Coal Geology* **109–110**: 101-146https://doi.org/10.1016/j.coal.2013.01.002.

DrillingInfo. 2018. *US DATA SETS*. DrillingInfo (Reprint).

Duong, A.N. 2010. An Unconventional Rate Decline Approach for Tight and Fracture-Dominated Gas Wells. 2010/1/1/. 10.2118/137748-MS.

EIA. 2018. *Total Dry Gas Production*, 01/09/2018 (Reprint). https://www.eia.gov/outlooks/steo/data/browser/#/?v=15.

Fetkovich, M.J. 1980. Decline Curve Analysis Using Type Curves. 10.2118/4629-PA.

Fetkovich, M.J., Vienot, M.E., Bradley, M.D. et al. 1987. Decline Curve Analysis Using Type Curves: Case Histories. 10.2118/13169-PA.

Freeborn, R., Russell, B. 2016. Creating More-Representative Type Wells. 10.2118/175967-PA.

Freeborn, R., Russell, B., Keinick, W.E. 2012. Creating Analogs, Fact and Fiction. 2012/1/1/. 10.2118/162630-MS.

Fulford, D.S., Blasingame, T.A. 2013. Evaluation of Time-Rate Performance of Shale Wells using the Transient Hyperbolic Relation. 2013/11/5/. 10.2118/167242-MS.

Fulford, D.S., Bowie, B., Berry, M.E. et al. 2016. Machine Learning as a Reliable Technology for Evaluating Time/Rate Performance of Unconventional Wells. 10.2118/174784-PA.

Groulx, B. 2015. *Understanding Type-well Curve Complexities & analytic Techniques*: Reservoir, Evaluation, and Production Optimization Luncheon (Reprint). https://www.verdazo.com/wp-content/uploads/2016/03/VISAGE-SPE-Presentation-2015-12-01-Calgary.pdf.

PseudoPressure.xls, 2007. Burlington, Gulf Professional Publishing, http://booksite.elsevier.com/9780750682701/solutions/PseudoPressure.xls.

Hartman, R.C., Ambrose, R.J., Akkutlu, I.Y. et al. 2011. Shale Gas-in-Place Calculations Part II - Multicomponent Gas Adsorption Effects. North American Unconventional Gas Conference and Exhibition, The Woodlands, Texas, USA, 2011/1/1/. 10.2118/144097-MS.

Holdaway, K. 2014. *Harness Oil and Gas Big Data with Analytics : Optimize Exploration and Production with Data Driven Models*. Somerset, UNITED STATES, John Wiley & Sons, Incorporated (Reprint). http://ebookcentral.proquest.com/lib/tamucs/detail.action?docID=1686621.

Ibrahim, M.H., Wattenbarger, R.A. 2006. Analysis of Rate Dependence in Transient Linear Flow in Tight Gas Wells. Abu Dhabi International Petroleum Exhibition and Conference, Abu Dhabi, UAE, 2006/1/1/. 10.2118/100836-MS.

IHS. Hybrid Model Theory, http://www.fekete.com/SAN/WebHelp/FeketeHarmony/Harmony_WebHelp/Content/HTML_Files/Reference_Material/Analysis_Method_Theory/Hybrid_Model_Theory.htm#Hybrid_model_pseudo-press-def.

Ilk, D., Rushing, J.A., Perego, A.D. et al. 2008. Exponential vs. Hyperbolic Decline in Tight Gas Sands: Understanding the Origin and Implications for Reserve Estimates Using Arps' Decline Curves. 2008/1/1/. 10.2118/116731-MS.

Jarvie. 2012. Shale resource systems for oil and gas: Part 1—Shale-gas resource systems. *J. A. Breyer* (Shale reservoirs—Giant resources for the 21st century: AAPG Memoir 97): 69–8710.1306/13321446M973489.

Lacayo, J., Lee, J. 2014. Pressure Normalization of Production Rates Improves Forecasting Results. SPE Unconventional Resources Conference, The Woodlands, Texas, USA, 2014/4/1/. 10.2118/168974-MS.

Mattar, L., Rushing, J.A., Anderson, D.M. 2006. Production Data Analysis - Challenges, Pitfalls, Diagnostics. 2006/1/1/. 10.2118/102048-MS.

McLane, M., Gouveia, J. 2015. Validating Analog Production Type Curves for Resource Plays. 2015/9/2/. 10.2118/175527-MS.

Miller, P., Frechette, N., Kellett, K.D. 2017. Building Type Wells for Appraisal of Unconventional Resource Plays. 2017/2/15/. 10.2118/185053-MS.

Ozkan, E., Brown, M.L., Raghavan, R. et al. 2011. Comparison of Fractured-Horizontal-Well Performance in Tight Sand and Shale Reservoirs. 10.2118/121290-PA.

Palacio, J.C., Blasingame, T.A. 1993. UNAVAILABLE - Decline-Curve Analysis With Type Curves - Analysis of Gas Well Production Data. Low Permeability Reservoirs Symposium, Denver, Colorado, 1993/1/1/. 10.2118/25909-MS.

Pollastro, R.M. 2007. Total petroleum system assessment of undiscovered resources in the giant Barnett Shale continuous (unconventional) gas accumulation, Fort Worth Basin, Texas. *American Association of Petroleum Geologists Bulletin* **91** (4): 551-57810.1306/06200606007.

Russell, B., Freeborn, R. 2012. A Practical Guide to Unconventional Petroleum Evaluation. 2012/1/1/. 10.2118/158867-MS.

Russell, B., Freeborn, R. 2013. A Practical Guide to Unconventional Petroleum Evaluation Part 2. 2013/11/5/. 10.2118/167215-MS.

SPEE. 2011. *Guidelines for the Practical Evaluation of Undeveloped Reserves in Resource Plays*: Monograph 3 (Reprint). www.spee.com.

SPEE, ed. 2016. *Estimating Ultimate Recovery of Developed Wells in Low-Permeability Reservoirs*: Monograph 4.

Spivey, J.P., Lee, J. 2013. *Applied well test interpretation. John P. Spivey, W. John Lee*: SPE textbook series: v. 13, Richardson, Tex. : Society of Petroleum Engineers, [2013]

(Reprint). http://lib-ezproxy.tamu.edu:2048/login?url=http://search.ebscohost.com/login.aspx?direct=true&db=cat03318a&AN=tamug.4714250&site=eds-live.

Valko, P.P., Lee, W.J. 2010. A Better Way To Forecast Production From Unconventional Gas Wells. 2010/1/1/. 10.2118/134231-MS.

Voneiff, G., Sadeghi, S., Bastian, P. et al. 2014. Probabilistic Forecasting of Horizontal Well Performance in Unconventional Reservoirs Using Publicly-Available Completion Data. SPE Unconventional Resources Conference, The Woodlands, Texas, USA, 2014/4/1/. 10.2118/168978-MS.

Wattenbarger, R.A., El-Banbi, A.H., Villegas, M.E. et al. 1998. Production Analysis of Linear Flow Into Fractured Tight Gas Wells. 1998/1/1/. 10.2118/39931-MS.

Wright, J.D.W. 2015. *Oil and Gas Property Evaluation*, Thompson Wright Associates (Reprint). https://books.google.com/books?id=1eGRngEACAAJ.

Xiong, H., Gao, S., Li, H. 2017. Generate Type Well Performance Curves by Combining Multi-Segment Decline Models and Calibrated Numerical Simulation Models for UR Wells in Permian Basin. SPE/AAPG/SEG Unconventional Resources Technology Conference, Austin, Texas, USA, 2017/7/24/. 10.15530/URTEC-2017-2668394.

Yu, S., Gouveia, J. 2015. Normalization of Analog Horizontal Wells for Type Curve Generation in Tight Gas Plays. SP 1 E/CSUR Unconventional Resources Conference, Calgary, Alberta, Canada, 2015/10/20/.0.2118/175888-MS.

# APPENDIX A: DEVELOPMENT OF THE SOLUTION FOR THE MODIFIED ANALYTICAL MODEL

Recalling Eq. 2 and 3 characterizing the linear flow into a fracture from Wattenbarger et al. (1998):

$$\frac{1}{q_D} = \frac{kh\left[m(p_i) - m(p_{wf})\right]}{1424 q_g T} \quad \text{A1}$$

$$t_{Dye} = \frac{0.00633kt}{(\emptyset \mu c_t)_i y_e^2} \quad \text{A2}$$

Multiplying Eq. A1 by the quotient of $y_e$ divided by $x_e$ on both sides, we express the solution for the dimensionless type curve shown in Fig. 9 where $x_e$ was replaced by $x_f$ since the fracture extends to the limit of the reservoir.

$$\left(\frac{y_e}{x_f}\right) q_D = \left(\frac{y_e}{x_f}\right) \frac{1424 q_g T}{kh\left[m(p_i) - m(p_{wf})\right]} \quad \text{A3}$$

Recalling Eq. 7, we can express the flow from a single fracture $q_g$ as:

$$q_g = \frac{F_s}{L_w} * q_t \quad \text{A4}$$

Substituting Eq. A4 and Eq. 8 into Eq. A3, we get:

$$\left(\frac{F_s}{2x_f}\right) q_D = \left(\frac{F_s}{x_f}\right) \frac{1424\, T F_s q_t}{2khL_w\left[m(p_i) - m(p_{wf})\right]} \quad \text{A5}$$

Simplifying Eq. A5 and combining the terms on the LHS we get:

$$\left(\frac{F_s}{x_f}\right) q_D = \left(\frac{F_s^2}{x_f}\right) \frac{1424\, T q_t}{khL_w\left[m(p_i) - m(p_{wf})\right]} \quad \text{A6}$$

Finally, substituting Eq. 8 into Eq. A2, we get the dimensionless time $t_{DF_s}$ for the modified analytical model presented in Fig. 8:

$$t_{DF_s} = \frac{0.02532kt}{(\emptyset \mu c_t)_i F_s^2} \quad \text{A7}$$

Note that since $F_s$ is equal to twice the value of $y_e$, we can write the following relationship:

$$2\left(\frac{y_e}{x_e}\right) q_D = \left(\frac{F_s}{x_f}\right) q_D \quad \text{A8}$$

Therefore, since the dimensionless rate as a function of fracture spacing is twice greater than the dimensionless expression of the dimensionless rate as a function of $y_e$, the modified type curve must therefore greater than the original type curve due to the change of units. Fig. 115 shows both type curves plotted against their respective axis.

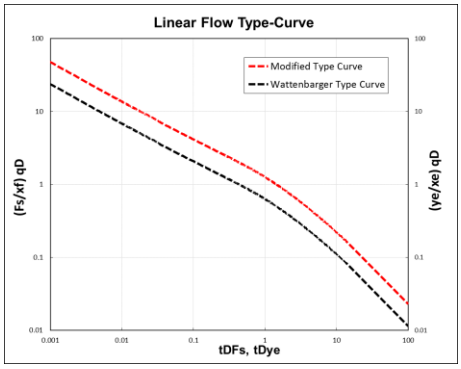


**Fig. 115—Linear Flow Type Curve Comparison**

In conclusion, we presented the working equations for an analytical model that was modified from the original Wattenbarger linear flow model in order to account for multiple fractures connected with an horizontal well.

## APPENDIX B: SCALING FACTORS AND TYPE CURVE MATCH POINT RELTIONSHIP

The rate and time match points relationship required to overlay a production profiles to a dimensionless solution of the modified analytical model is given by the Eq. 9 and 10:

$$\left(\frac{F_s}{x_f}\right)q_D = \left(\frac{{F_s}^2}{k}\right)\frac{1424\,T\,q_t}{x_f h L_w\left[m(p_i)-m(p_{wf})\right]} \quad \text{B1}$$

$$t_{DF_s} = \left(\frac{k}{F_s^2}\right)\frac{0.02532}{(\emptyset\mu c_t)_i}t_{mb} \quad \text{B2}$$

Let us define two different profiles with different fracture and reservoir properties. Since each profile is different, we can write Eqs. B3 to B6 such that we express the dimensionless term of the equation as a function of the parameters of each models.

$$\left(\frac{F_s}{x_f}\right)q_D = q_1\left(\frac{{F_{s1}}^2}{k_1}\right)\frac{1424\,T}{x_{f1}h_1L_1\Delta m(p)_1} \quad \text{B3}$$

$$t_{DF_s} = t_1\left(\frac{k_1}{F_{s1}^2}\right)\frac{0.02532}{(\emptyset\mu c_t)_i} \quad \text{B4}$$

$$\left(\frac{F_s}{x_f}\right)q_D = q_2\left(\frac{{F_{s2}}^2}{k_2}\right)\frac{1424\,T}{x_{f2}h_2L_2\Delta m(p)_2} \quad \text{B5}$$

$$t_{DF_s} = t_2\left(\frac{k_2}{F_{s2}^2}\right)\frac{0.02532}{(\emptyset\mu c_t)_i} \quad \text{B6}$$

Equating Eq. B3 and B5 as well as B4 and B6 we get:

$$q_1\left(\frac{{F_{s1}}^2}{k_1}\right)\frac{1424\,T}{x_{f1}h_1L_1\Delta m(p)_1} = q_2\left(\frac{{F_{s2}}^2}{k_2}\right)\frac{1424\,T}{x_{f2}h_2L_2\Delta m(p)_2} \quad \text{B7}$$

$$t_1\left(\frac{k_1}{F_{s1}^2}\right)\frac{0.02532}{(\emptyset\mu c_t)_i} = t_2\left(\frac{k_2}{F_{s2}^2}\right)\frac{0.02532}{(\emptyset\mu c_t)_i} \quad \text{B8}$$

Rearranging the rate and time on the LHS of the equation and canceling terms based on the assumption of similar temperature and $(\emptyset\mu c_t)_i$ we get:

$$\frac{q_1}{q_2} = \left(\frac{{F_{s1}}^2}{{F_{s2}}^2}\right)\left(\frac{k_2}{k_1}\right)\left(\frac{x_{f2}}{x_{f1}}\right)\left(\frac{h_2}{h_1}\right)\left(\frac{L_2}{L_1}\right)\left(\frac{\Delta m(p)_2}{\Delta m(p)_1}\right) \quad \text{B9}$$

$$\frac{t_1}{t_2} = \left(\frac{{F_{s2}}^2}{{F_{s1}}^2}\right)\left(\frac{k_1}{k_2}\right) \quad \text{B10}$$

Recall the rate match point and the time match point presented in Eq. 11 and 12 of the analytical model, we can define a different set of match point based on Eq. B9 and B10 in the same fashion where the profile labeled number 2 will be matched on the profile labeled number 1. Eq. B11 to B12 show the match points required to shift production profile 2 onto production profile 1.

$$QM = \left(\frac{F_{s1}}{F_{s2}}\right)^2\left(\frac{k_2}{k_1}\right)\left(\frac{x_{f2}}{x_{f1}}\right)\left(\frac{h_2}{h_1}\right)\left(\frac{L_2}{L_1}\right)\left(\frac{\Delta m(p)_2}{\Delta m(p)_1}\right) = \text{RSF} \quad \text{B11}$$

$$TM = \left(\frac{F_{s2}}{F_{s1}}\right)^2\left(\frac{k_1}{k_2}\right) = \text{TSF} \quad \text{B12}$$

The rate match point and the time match point equation is the product of the scaling factor relationships summarized in Table 12 and demonstrated in Table 14. We can also express QM and TM as RSF and TSF given by Eq. 21 and 22.

In conclusion, comparing Eq. B11 and B12 to Eq. 21 and 22, this appendix demonstrates that the scaling factors relationships empirically found in chapter 4 are mathematically demonstrated by the dimensionless Eq. 9 and 10 (B1 and B2 in this appendix) when matching a profile onto another one.

# APPENDIX C: DERIVATION OF THE RATE SCALING FACTOR WITH HYPERBOLIC EQUATIONS

Arps (1945) proposed relations for flow rate and cumulative production such that it can be expressed by the hyperbolic equation, as shown by Eq. C1 and C2 where the b factor is a constant varying such that 0<b<1. The exponential equation is given for a b value of 0 and the harmonic decline curve is given for a b value of 1.

$$N_p(t) = \frac{q_i}{(1-b)D_i}[1-(1+bD_it)^{1-1/b}] \quad \text{C1}$$

$$q(t) = \frac{q_i}{(1+bD_it)^{1/b}} \quad \text{C2}$$

Based on the RSF, TSF and CSF equations developed in Chapter 4, if we assume that a hyperbolic equation fits a segment of a profile, it means that we should be able to rescale a decline curve to another profile. The objective of this appendix is to derive the RSF of the rate-time hyperbolic equation based on the cumulative-time equation in which we included the scaling factors. Dividing the TSF and CSF to the time variable and the cumulative variable respectively, we get Eq. C3:

$$\frac{N_p(t)}{CSF} = \frac{q_i}{(1-b)D_i}\left[1-\left(1+\frac{bD_it}{TSF}\right)^{1-1/b}\right] \quad \text{C3}$$

Since the rate-time profile is the derivative of the cumulative-time profile, we can write Eq. C4:

$$q(t) = \frac{d}{dt}\,N_p(t) \quad \text{C4}$$

Inserting Eq. C3 into Eq. C4 we get:

$$q(t) = \frac{d}{dt}\left(\frac{CSF*q_i}{(1-b)D_i}\left[1-\left(1+\frac{bD_it}{TSF}\right)^{1-\frac{1}{b}}\right]\right) \quad \text{C5}$$

Removing the constant term of Eq. C5, we can simplify to:

$$q(t) = \frac{CSF*q_i}{(1-b)D_i}\frac{d}{dt}\left(1+\frac{bD_it}{TSF}\right)^{1-\frac{1}{b}} \quad \text{C6}$$

Apply the power rule such that $[u(x)^n]' = n*u(x)^{n-1}*u'(x)$ where $[u(x)^n]' = \frac{d}{dt}\left(1+\frac{bD_it}{TSF}\right)^{1-\frac{1}{b}}$

$$q(t) = \frac{-CSF*q_i}{(1-b)D_i}\left(1-\frac{1}{b}\right)*\left(1+\frac{bD_it}{TSF}\right)^{-\frac{1}{b}}*\left(\frac{bD_i}{TSF}\right) \quad \text{C7}$$

Re-writing Eq. C5 and simplifying the numerator with the b and the negative sign:

$$q(t) = \frac{CSF*q_i(1-b)(D_i)}{TSF(1-b)D_i\left(1+\frac{bD_it}{TSF}\right)^{-\frac{1}{b}}} \quad \text{C8}$$

Simplifying the RHS of the equation:

$$q(t) = \frac{CSF*q_i}{TSF\left(1+\frac{bD_it}{TSF}\right)^{-\frac{1}{b}}} \quad \text{C9}$$

Based on the Eq. 13 and 14 which state that the TSF and the RSF are inversely proportional for the permeability and fracture spacing parameters, we can write the following equation as combination of Eq. 21 to 23:

$$RSF = \frac{CSF}{TSF} \quad \text{C10}$$

Plugging Eq. C8 into Eq. C7 yields:

$$q(t) = \frac{RSF*q_i}{\left(1+\frac{bD_it}{TSF}\right)^{-\frac{1}{b}}} \quad \text{C11}$$

Multiplying RSF on both side give the rate-time relationship of the hyperbolic decline with the correct arrangement of scaling factors:

$$\frac{q(t)}{RSF} = \frac{q_i}{\left(1+\frac{bD_it}{TSF}\right)^{-\frac{1}{b}}} \quad \text{C12}$$

The steps from Eq. C3 to C10 demonstrate the relationship between the CSF and the RSF, which is caused by the derivation process between the cumulative-time and the rate-time equation. In conclusion, this derivation theoretically validates the empirical relationship between the rate, time and cumulative scaling factors. Finally, it provides a useful method to combine scaling factors and decline curve equations.

# APPENDIX D: DERIVATION OF THE SCALING FACTORS WITH ARPS PARAMETERS

We demonstrated that scaling factors are reliable to rescale rate-time and cumulative-time profiles. We observe those profiles can be parametrized with common decline curve equations, so we investigate the relationship between the scaling factors and Arp's decline curve parameters in this appendix.

In order to do so, an appropriate decline curve equation shall be chosen as it should fit a large extent of the profiles. The modified hyperbolic has been very popular since it fits the production profiles with several segments, but it would be too complex to use as the time at which the segment change needs to be consistent with the TSF that we are trying to solve for. Instead, we recommend to use only one segment with a fixed b factor. This segment should be chosen in order to fit as much of the production as possible in the history of the base well. In the work carried in this research, we decided to use the harmonic equation (b=1), because it has been observed on a log(q)-Np plot that most of the shale gas wells had approximately a linear behavior until an advanced state in BDF. In this appendix, we present two production profiles that were fitted with a harmonic equation. However, as derived in Appendix C, the scaling factors are coupled with the physical properties, and the objective is to relate them to the constants of the equations.

The following equation describe the rate equation with the harmonic decline (b=1) as a function of time and the scaling factors:

$$q(t) = \frac{RSF * q_i}{1 + \frac{D_i t}{TSF}} \quad \text{D1}$$

Rearranging such that the time scaling factor does not multiply directly the time variable we get:

$$q(t) = \frac{RSF * q_i}{\frac{D_i}{TSF}(\frac{TSF}{D_i} + t)} \quad \text{D2}$$

Simplifying the scaling factors since RSF=CSF/TSF we get:

$$q(t) = \frac{CSF * \frac{q_i}{D_i}}{(\frac{TSF}{D_i} + t)} \quad \text{D3}$$

Simplifying the constant terms by substituting m and a, such that $m=q_i/D_i$ and $a=1/D_i$, we get:

$$q(t) = \frac{CSF * m}{(TSF * a + t)} \quad \text{D4}$$

Integrating and solving for the initial condition such that $N_p(t=0)=0$ to express the cumulative production as a function of a and m:

$$Np(t) = CSF * m * [\ln(TSF * a + t) - \ln(TSF * a)] \quad \text{D5}$$

Comparing Eq. D4 and D5 to the original Eq. C9 and C3 from Appendix C, we managed to multiply the time scaling factor to the constant a, (the inverse of the decline) and the cumulative scaling factor to constant m (the initial rate divided by the initial decline). This derivations shows that instead of multiplying the time and the rate variables, as originally performed in chapter 4 when normalizing the analytical results, we can multiply the constants of the decline curve equations. The following equations present how the scaling factors actually represent the relative difference between two different profiles.

Assuming that two different profiles were parametrized with the harmonic equation, their rate-time equations could be expressed based on Eq. D4 without scaling factors. The subscripts in the following equations are used to differentiate the parameters of the first profile with the second.

$$q_1(t) = m_1/(t + a_1)$$

$$q_2(t) = m_2/(t + a_2)$$

Since the scaling factors allows us to rescale the production such that $q_1(t) = q_2(t)$ at any given time, the CSF and TSF can be used such that the second profile matches the parameters of the first one:

$$q_1(t) = CSF * m_2/(x + TSF * a_2)$$

If:

$$CSF = m_1/m_2$$

And

$$TSF = a_1/a_2$$

We can further bring back the original decline curve parameters in the equation such that we can express the scaling factors as the initial rate and the initial decline:

$$CSF = \frac{q_1 D_2}{q_2 D_1}$$

And

$$TSF = \frac{D_2}{D_1}$$

This derivation demonstrates that the cumulative scaling factor and the time scaling factors can be expressed as the ratio of the decline curve parameters. Furthermore, the rate scaling factor can be expressed such that:

$$RSF = \frac{CSF}{TSF} = \frac{q_1 D_2}{q_2 D_1} * \frac{D_1}{D_2} = \frac{q_1}{q_2}$$

As this derivation was performed only for the harmonic case, plugging the RSF and the TSF into Eq. C10 also demonstrates that it can rescale any hyperbolic equations if the b factor is the same:

$$\frac{q_1(t)}{RSF} = \frac{q_1}{\left(1 + \frac{bD_1 t}{TSF}\right)^{-\frac{1}{b}}} = q_2(t)$$

In summary, we demonstrated that the scaling factors previously defined as the ratio of physical properties such as the permeability, fracture half-length and so on **is also** the ratio of the initial rate and the initial decline of the Arps equations, **assuming that they fit the data.** This demonstration also puts in perspective that the "empirical" nature of the initial rates and the declines of Aprs' decline curves are related to analytical scaling factors, and therefore physical properties of the analytical model. Finally, Arps decline parameters are directly scalable with the scaling factors.

$$CSF = \frac{q_1 D_2}{q_2 D_1} = \left(\frac{x_{f2}}{x_{f1}}\right)\left(\frac{h_2}{h_1}\right)\left(\frac{L_2}{L_1}\right)\left(\frac{\Delta m(p)_2}{\Delta m(p)_1}\right)$$

$$TSF = \frac{D_2}{D_1} = \left(\frac{F_{s2}}{F_{s1}}\right)^2 \left(\frac{k_1}{k_2}\right)$$

# APPENDIX E: DEVELOPMENT OF THE OUTLIER REMOVAL METHOD

This appendix presents the development of a new outlier detection tool for the production rates of unconventional resource plays for rate transient analysis, decline curve analysis and type curve matching. Given that most of the publicly available production data in the US is reported based on a monthly sales volumes and allocated production, outlier detection tools can be used to reflect a more reliable reservoir behavior from the production data that is biased by the low-frequency and inaccurate reporting. Furthermore, monthly produced volumes may be reported without the non-productive time. This potentially creates more outliers when computing the daily rate based on the number of days in a month instead of the producing days. Finally, as the reporting requirement depends State's policies, this method should only be applied to the production of a single well and not a lease with multiple wells.

Unconventional resources plays by nature are characterized with extremely low hydraulic conductivities, which hold the free hydrocarbons (non-sorbed) in place and prevent any hydrodynamic migration. Resources plays require extensive stimulations to create artificial fractures and improve the flow pattern from the formation to the reservoir in order to produce at economic rates. The reservoir fluids flow towards the wellbore via the fractures based on the pressure drawdown applied between the reservoir pressure and the BHP. Assuming no hydrodynamic supports in the matrix and a constant operating BHP, one should expect high initial production rates followed by a declining production in time. Discarding other complex fracture clean-up and heterogeneity, produced volumes at a given time should always be lower than the previous month when depleting a closed boundary reservoir. As this theoretical principle applies for rate-time data, it also applies to the MBT since the rates are proportional to the total produced volume and the rate themselves. The methodology we present takes advantage of this logic to correlate the sorted ranks of time and the MBT for each rate to identify the outliers. An objective function combined with a tolerance function are presented to differentiate the outliers from the data. The methodology was developed in a Microsoft Excel spreadsheet and can be easily automated and integrated in production analysis workflows.

**Fig. 116** shows outlier detection theory on the case of a harmonic decline. For each rate, we associate a time rank based on the order of production. We also assign a MBT rank after sorting all the MBTs from smallest to largest. We can therefore associate a time rank and a material time rank for each rate. In the following example, the production does not have any outliers, the time rank matches exactly the MBT rank. Hence, all the points on the rank cross plot fall on a unit line.

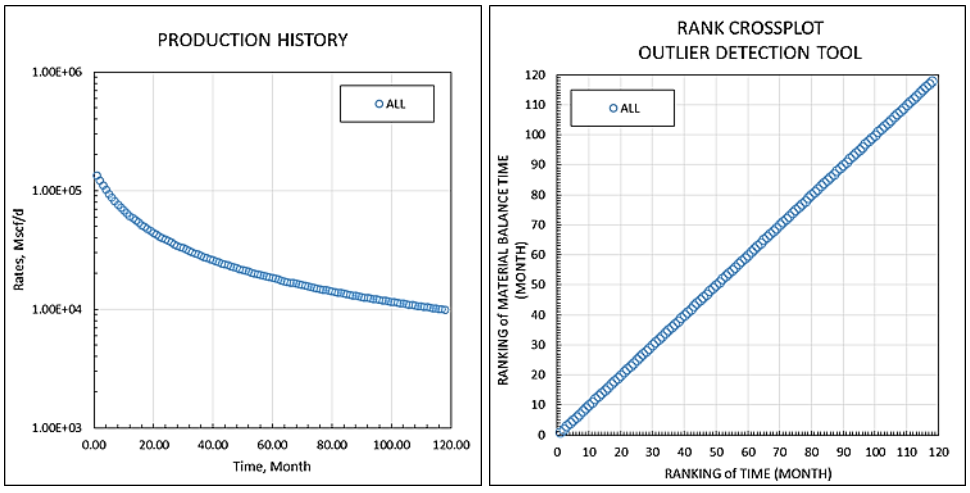


**Fig. 116—Harmonic decline, no outlier**

Based on the previous examples, an outlier with a smaller production rate (equivalent to the rate at 30 months) is introduced at the 10th month of production as shown in the left plot of **Fig. 117**. The MBT is re-calculated based on the outlier and after assigning the time and MBT ranks, we see that this rate actually ranks has the 21th smallest MBT. Based on his rank, we can see the impact of the outlier on the rank cross plot. We see that the MBT ranks are deviated downward from the unit slope line from the 10th to the 20st month due to the presence of the outliers.

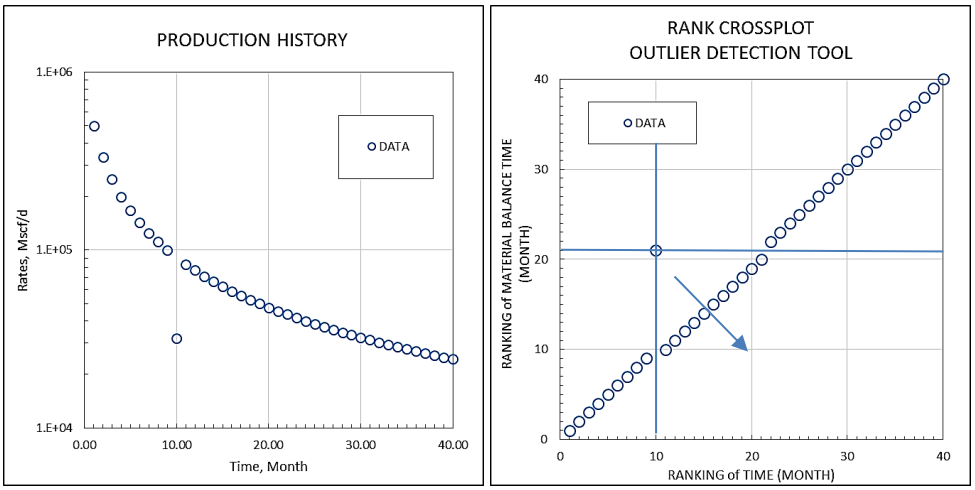


**Fig. 117—Harmonic decline with a smaller outlier at t=10 mo.**

In the same manner, we introduced an outlier at the 30th month with a much larger production rate, which is equivalent to the rate after 10 months of production. Based on the observation of Fig. 118, we see that a greater outlier has the opposite impact on other MBT ranks, as it deviates the ranks upward.

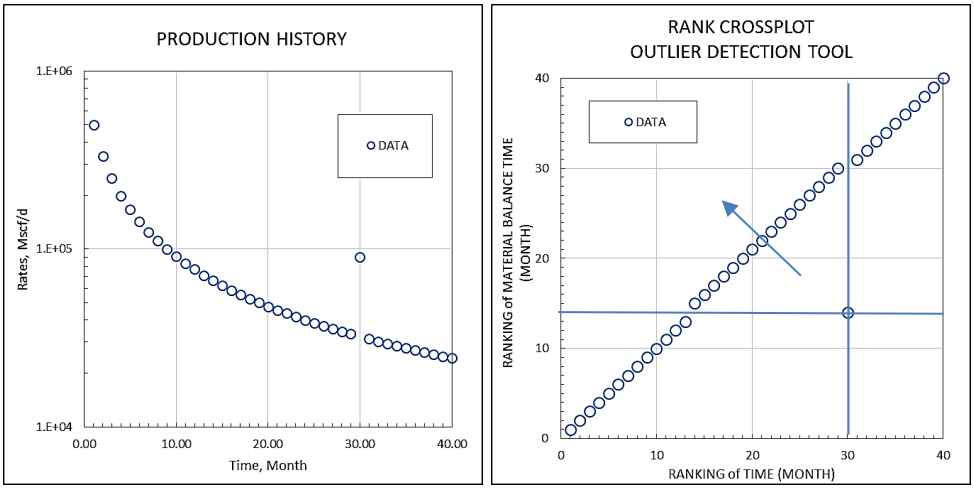


**Fig. 118—Harmonic decline with higher outlier at t=30 mo.**

From the previous observations, we can imagine an objective function $O(R_t)$ that should follow the rightful "path" on the rank cross plot by taking into account the outlier's effect. In the case of no outliers, the objective function would always increase by one after each time rank such that it follows the unit slope line. To shift the ranks upward we must increase the objective function by two MBT ranks. In the same way, we shift the rank down by maintaining the objective function to the previous MBT rank instead of increasing it by one. Since we do not know which point is an outlier and at what rank, we define the following relationship: $R_{mbt} > O(R_{t-1}) + 1$ to increase the objective function and $R_{mbt} < O(R_{t-1}) + 1$ to decrease it. **Fig. 119** shows one smaller and greater outlier respectively located at the beginning and the end of the production profile. We can see how the objective function is generated. For instance, at

T = 7, $R_T$ = 7 and $R_{MBT}$ = 12 and $O(R_{t-1}) = 6$, hence we increase the objective function by two because $12 > 6 + 1$. Similarly at T = 13, $R_T$ = 13 and $R_{MBT}$ = 13 and $O(R_{t-1}) = 11$. There, we increase the objective function because $13 > 11 + 1$. We also see that the objective function is adjusted when $R_{mbt} < O(R_{t-1}) + 1$ at T=8 and T=32. However, there is a limitation with this the larger outliers because we increase the objective function by two at T=7 while it should be decreased in order to go through the point (8,7).

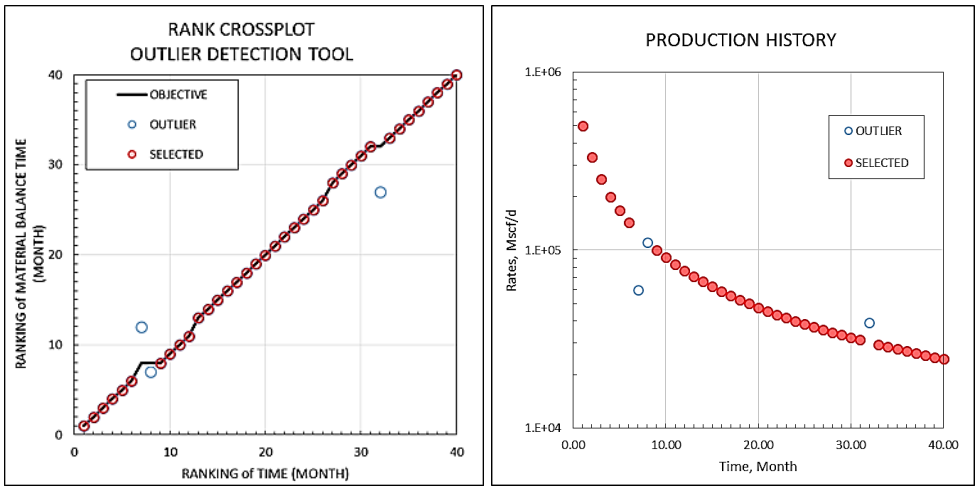


**Fig. 119—Harmonic decline with two outliers located at t=7 and t=32 mo.**

Since the objective function does not follow exactly all the right points, we propose another rule that would optimize the selection of points when $R_{mbt} < O(R_{t-1}) + 1$ such that $O(R_t) = O(R_{t-1}) - 1$ when $R_{mbt-1} > O(R_{t-2}) + 1$. **Fig. 120** shows the result when implementing the new rule in order to correct the objective function. Indeed, at T=8, $R_T$ = 8 and $R_{MBT}$ = 7 and $O(R_{t-1}) = 8$, so we reduce the objective function by 1 such that $O(R_t) = 7$ since $R_{mbt-1} > O(R_{t-2}) + 1$ as $R_{mbt-1} = 12$ and $O(R_{t-2}) = 6$. The results shown on the figure proves that all the correct points are selected based on the objective function designed above.

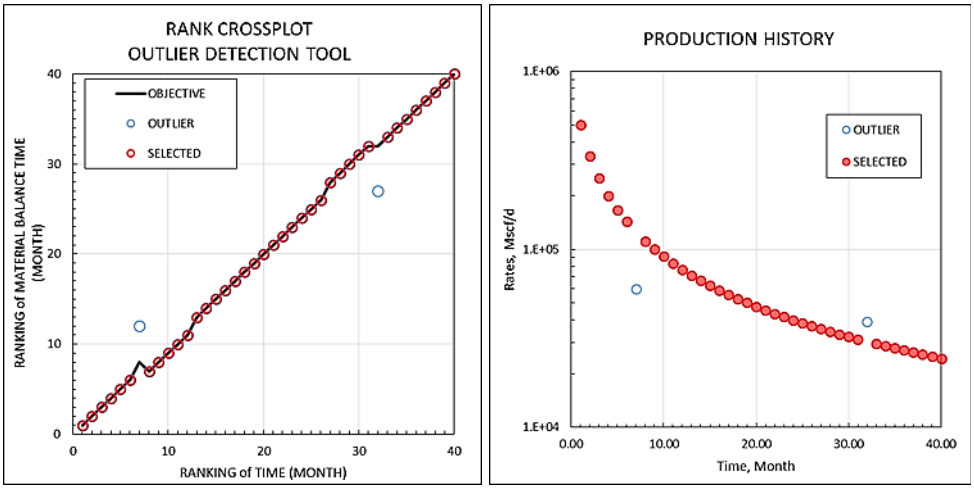


**Fig. 120—Harmonic decline with two outliers at t=7 and t=32 mo, combined with improved objective function.**

The following equations summarize the proposed objective function demonstrated in the previous examples. It is important to note that this methodology was developed based on the impact of one outlier only, but other objective functions and mathematical relationships may prove to be more reliable.

$$O(R_{t=1}) = 1$$

$$O(R_t) = \begin{cases} O(R_{t-1}) + 2 & if \quad R_{mbt} > O(R_{t-1}) + 1 \\ O(R_{t-1}) + 1 & if \quad R_{mbt} = O(R_{t-1}) + 1 \\ O(R_{t-1}) & if \quad R_{mbt} < O(R_{t-1}) + 1 \\ O(R_{t-1}) - 1 & if \quad R_{mbt-1} < O(R_{t-2}) + 1 \ and \ R_{mbt} < O(R_{t-1}) + 1 \end{cases}$$

Now that we defined the objective function, we shall test the efficiency of the objective function when multiple outliers are added, and more specifically next to each other. **Fig. 121** shows eight outliers located at different times. The first five outliers represents a hypothetical case where the production was limited to 20,000Mscf/D, and the last three represent a mistake in the allocation calculation. In both cases, the outliers do not reflect the reservoir behavior as they represent either human intervention or reporting errors. The objective function identified the eight points as outliers as displayed in green on the left plot. However, we see that the objective function rejected more points than the number of outliers, as shown in the red circles. Based on the equation developed above, the objective function can only increase by either a maximum slope of two or decrease by a minimum slope of one. We can see on the left plot that the objective function slope can only reach valid points with a horizontal line from the 11$^{th}$ month until the 20$^{th}$ points. The upside of this method is that it detects outliers, while it also excludes more points if the data is too noisy. Nevertheless, curve fitting the selected points of the right plot would provide a perfect match with the original model.

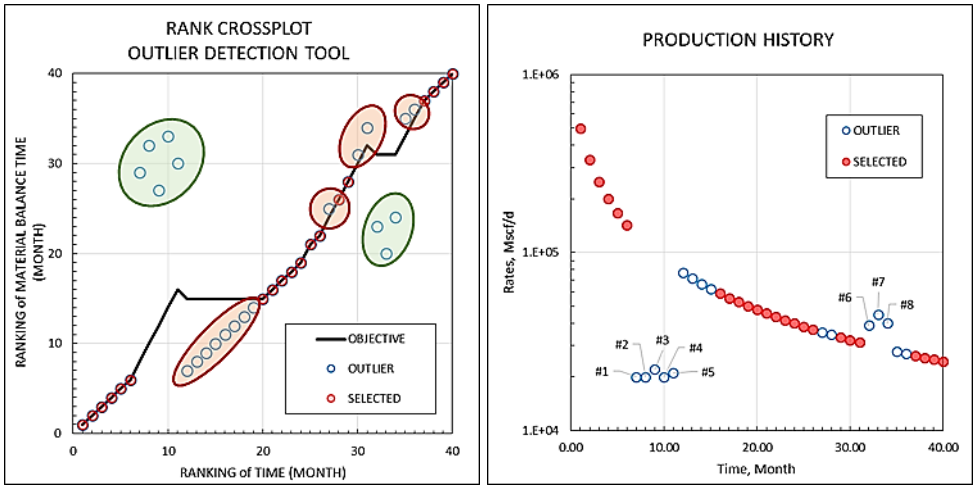


**Fig. 121—Objective function applied on harmonic decline with multiple outliers.**

Given that production data are usually noisy and considered unreliable, the objective function could be allowed a tolerance range in which the points in the rank cross-plot would be considered valid data points while the others are considered as outliers. The tolerance function $Tol$ can be a constant or an equation as a function of the time rank. The outliers are defined when the MBT rank is either greater or lower than the Min and Max functions given by the equation below.

$$Min(R_t) = O(R_t) - Tol(R_t)$$
$$Max(R_t) = O(R_t) + Tol(R_t)$$

**Fig. 122** illustrates two possible tolerance functions. The left plot displays a constant tolerance function set to the value four. The second method presented is a variable tolerance calculated based on the total rank and a tolerance value. In this case, the total rank is 40 and a final tolerance is 4, such that they are used into the equation displayed on the figure to create a triangular tolerance range around the objective function. We found the triangular method particularly useful with very long unconventional shale production history since they usually have higher decline at the beginning of the production life. Indeed, when the production decline is stronger, there is most likely less interferences between the MBT rank and the time rank, and the objective function can detect outliers while it does not

exclude too many other points. On the opposite, at later times we usually observe a much smaller production decline, which combined with noise, can limit the selection of the objective function. The final tolerance term allows to control how many ranks above and below the objective function can be considered appropriate for curve fitting. On the right plot, the tolerance is rounded to the nearest integer at T=30 based on the equation displayed on the figure such that Tol(30) = 4*30/40 = 3. In both cases, we see that the tolerance allows accept more valid points.

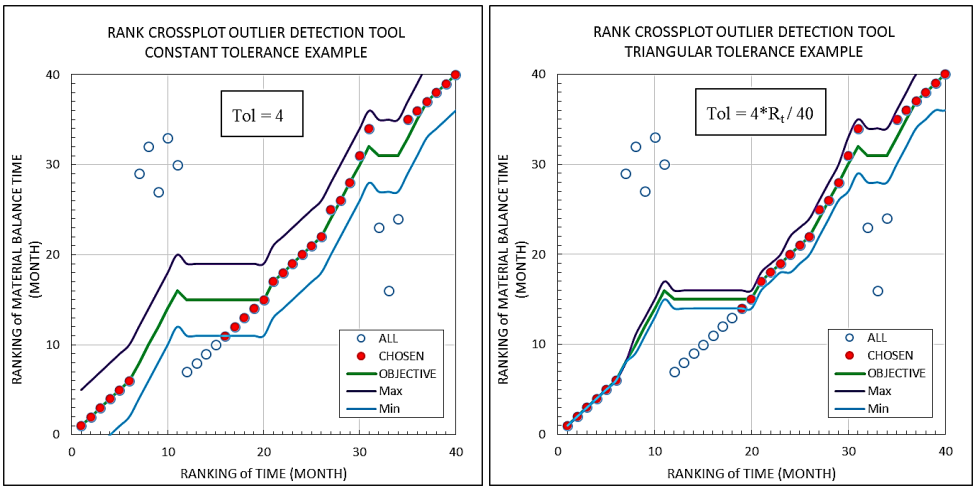


**Fig. 122—Comparison of the constant tolerance function with the triangular tolerance function on the harmonic decline with 8 outliers.**

The last point to be addressed in this methodology is the case when a well does not have a continuous production decline. In fact, conditions of production vary during the life of a well as it may be shut-in for an extended period of time, re-stimulated or the artificial lift design may also change. Such operating condition may change the reservoir and completion characteristics and can lead to new transient behaviors. We refer to a COC as a Constant Operation Condition period of time when there is a rather continuous production with a monotonous decline. **Fig. 123** shows a synthetic well that was re-stimulated after should 30 months of production. The black dotted box shows where the rates of both segments overlap while the MBT is still calculated based on the total produced volumes. None of the segments contain outliers they both show two reservoir behaviors.

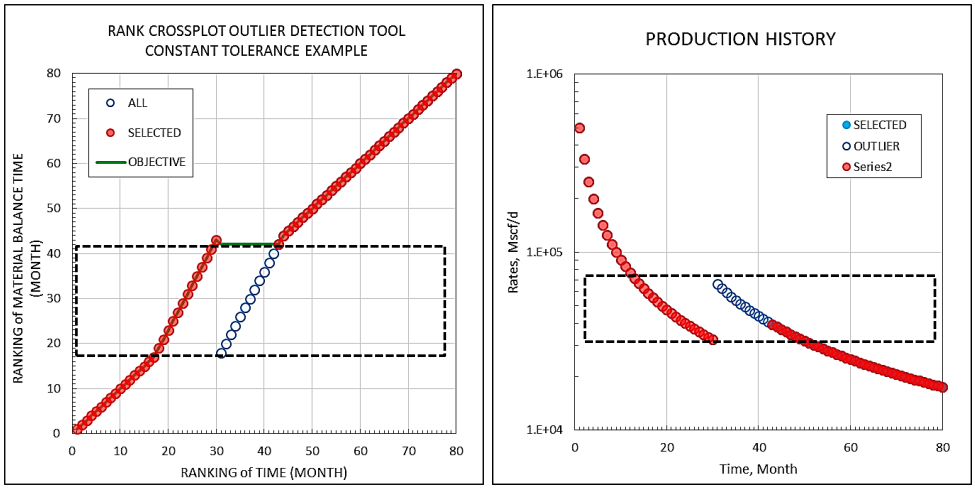


**Fig. 123—Objective function applied on a multi-segmented harmonic decline.**

In order to remediate with this issue, we suggest to treat both segments separately to detect outliers. The time rank should remain the same but the MBT ranks should be allocated after sorting the MBTs separately. In the previous case, the MBT ranks would be given to the rate from the beginning to the 30$^{th}$ month of production after sorting the

MBTs. Then, the remaining MBT ranks from 30 to 80 are given based on the sorted MBTs of the second segments. **Fig. 124** shows the results after sorting the MBTs separately between segment 1 in red and segment 2 in blue.

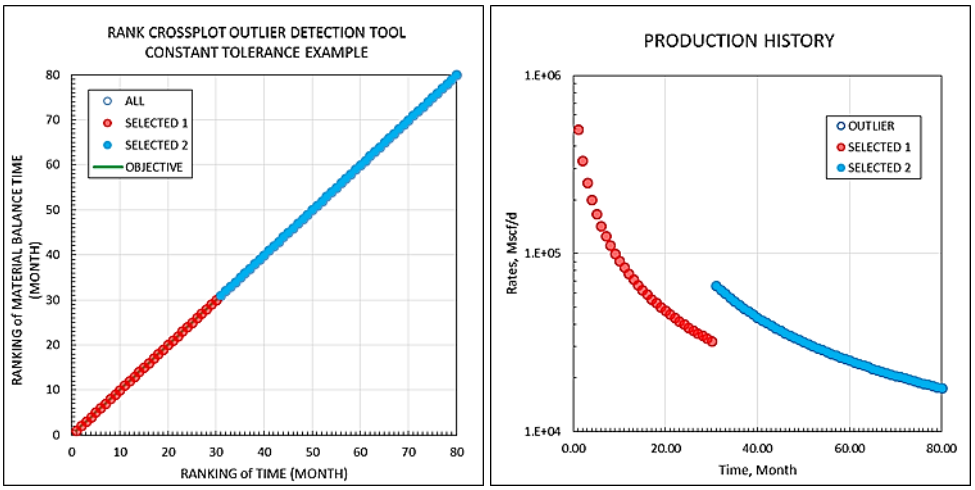


**Fig. 124—Segmented objective function applied to a multi-segmented harmonic decline.**

The following workflow explains how to implement this new outlier detection tool. **Fig. 125** following the workflow illustrates a simplified example of spreadsheet table and the associated production and rank cross plot. One outlier was purposely set at the 6th month of production and a change in operating condition was also added after the 14th month of production.

1. Compile the production data (Rate, Cumulative and Time) in order to compute the MBT for each rate. Use Producing time if available instead of calendar time in column 3 and 4.
2. Define segments of constant operating condition based on the well's production history. The change in constant operating condition is located after the 14th month of production in the next example and is illustrated by the change in color and separated with a horizontal line.
3. Sort the MBTs from the smallest to largest for each segments and assign a MBT rank, $R_{mbt}$, to the associated rate in the 7th column. Assign a time rank, $R_t$, to each rate based on the chronological order of production in the 6th column. The sorted MBT is located in column 5. The discontinuity in MBT between the two segments shows how the MBT are sorted from the smallest to the greatest in each segment.
4. Plot the MBT rank on the y-axis against the time rank on the x-axis for each rates on a cross plot and apply the objective function and the tolerance to determine the outliers that lie outside of the minimum and the maximum tolerance function.

| TIME Month | Rate Mcf/D | CUM MMcf | *MBT (Month)* | *SORTED MBT* | **TIME RANK** | **MBT RANK** | OBJECTIVE - | TOLERANCE - | OUTLIER *(Y/N)* |
|---|---|---|---|---|---|---|---|---|---|
| 1 | 500000 | 500 | *1.00* | 1.00 | **1** | **1** | 1 | 0 | NO |
| 2 | 333333.3 | 833.3333 | *2.50* | 2.50 | **2** | **2** | 2 | 0 | NO |
| 3 | 250000 | 1083.333 | *4.33* | 4.33 | **3** | **3** | 3 | 0 | NO |
| 4 | 200000 | 1283.333 | *6.42* | 6.42 | **4** | **4** | 4 | 0 | NO |
| 5 | 166666.7 | 1450 | *8.70* | 8.70 | **5** | **5** | 5 | 0 | NO |
| 6 | 75000 | 1525 | *20.33* | 13.20 | **6** | **9** | 6 | 0 | YES |
| 7 | 125000 | 1650 | *13.20* | 15.85 | **7** | **6** | 7 | 0 | NO |
| 8 | 111111.1 | 1761.111 | *15.85* | 18.61 | **8** | **7** | 8 | 0 | NO |
| 9 | 100000 | 1861.111 | *18.61* | 20.33 | **9** | **8** | 9 | 0 | NO |
| 10 | 90909.09 | 1952.02 | *21.47* | 21.47 | **10** | **10** | 10 | 1 | NO |
| 11 | 83333.33 | 2035.354 | *24.42* | 24.42 | **11** | **11** | 11 | 1 | NO |
| 12 | 76923.08 | 2112.277 | *27.46* | 27.46 | **12** | **12** | 12 | 1 | NO |
| 13 | 71428.57 | 2183.705 | *30.57* | 30.57 | **13** | **13** | 13 | 1 | NO |
| 14 | 66666.67 | 2250.372 | *33.76* | 33.76 | **14** | **14** | 14 | 1 | NO |
| 15 | 94339.62 | 2344.711 | *24.85* | 24.85 | **15** | **15** | 15 | 1 | NO |
| 16 | 89285.71 | 2433.997 | *27.26* | 27.26 | **16** | **16** | 16 | 1 | NO |
| 17 | 84745.76 | 2518.743 | *29.72* | 29.72 | **17** | **17** | 17 | 1 | NO |
| 18 | 80645.16 | 2599.388 | *32.23* | 32.23 | **18** | **18** | 18 | 1 | NO |
| 19 | 76923.08 | 2676.311 | *34.79* | 34.79 | **19** | **19** | 19 | 1 | NO |
| 20 | 73529.41 | 2749.841 | *37.40* | 37.40 | **20** | **20** | 20 | 1 | NO |

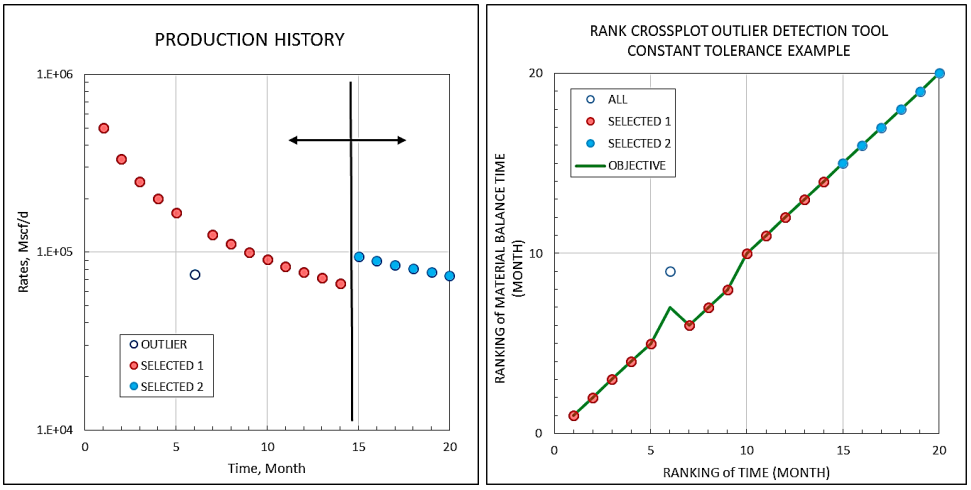


**Fig. 125—Outlier detection tool example on a synthetic production profile with one outlier and one change in operating condition.**

In conclusion, we presented a methodology that allows to identify outliers by comparing the time rank with the MBT rank. We developed an objective function that allows to take into account the relative shift in ranks by identifying outliers. We also demonstrated that the quality of the data will impair the objective function if the data is too noisy. A tolerance function was presented to bring more flexibility in the data selection process. Finally, this methodology proved to be more efficient if the user defines constant operating condition, especially if the rates history overlaps during the production. The following section will present several examples.

Example 1:

The production profile illustrated in **Fig. 126** was taken from SPE 179958-MS and shows the production from a Barnett shale well. We can see that the selected data seems to be lie on a unique decline, while there an apparent change of operating conditions after 14 months and 84 months of production.

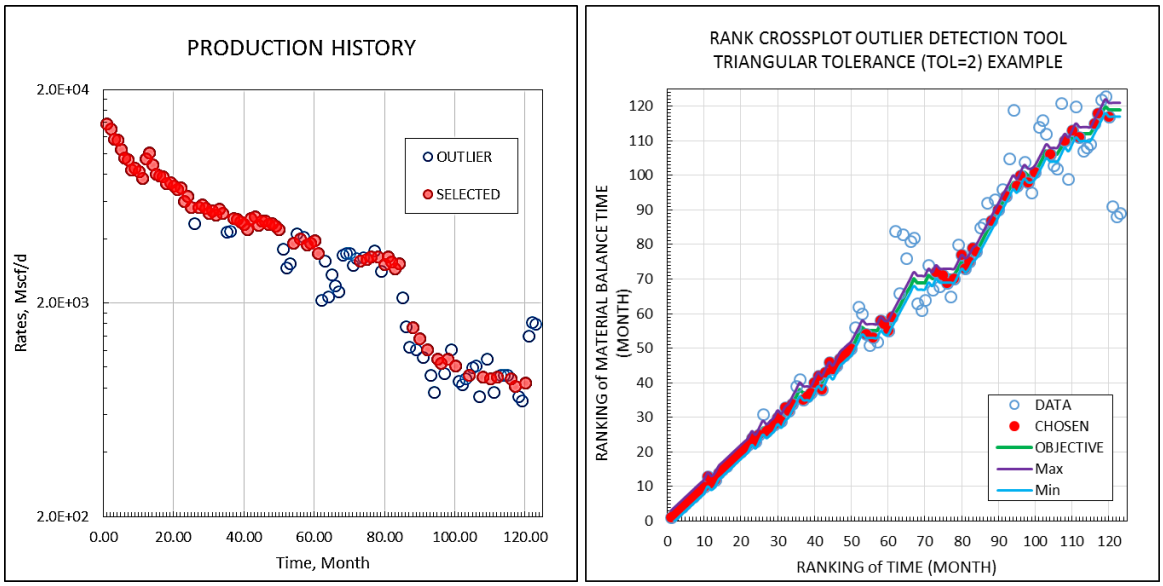


**Fig. 126—Outlier detection example modified from SPE-179958-MS.**

The detection tool applied on the rank cross-plot with a triangular tolerance fixed at two provides a narrow range that discard the main outliers of the production profile as seen on the left. Furthermore, the selected rates after the 85$^{th}$ months appear to highlight the reservoir behavior, although the data is very noisy. Compared to the methodology presented in SPE-179958-MS, more points are remove with the outlier detection tool. The advantage of our outlier detection tool is the confidence on the points selected in red, as the method was derived by studying the impact of outliers on the ranks. Finally, the points selected in our method appear to provide more guidance to fit the data, even though the results are dependent on the tolerance function, the presence of more than one COC and the overall quality of the data.

Example 2:

The well presented on **Fig. 127** is located in the Johnson County and produced from the Barnett Shale formation between 2004 and 2012. The well was selected for its rather noisy production profile, making it hard to identify the reservoir behavior and the potential fit of a decline curve. Applying the outlier detection tool with a triangular tolerance set a 3 provides a selection of points that appear in to highlight a continuous decline on the production history.

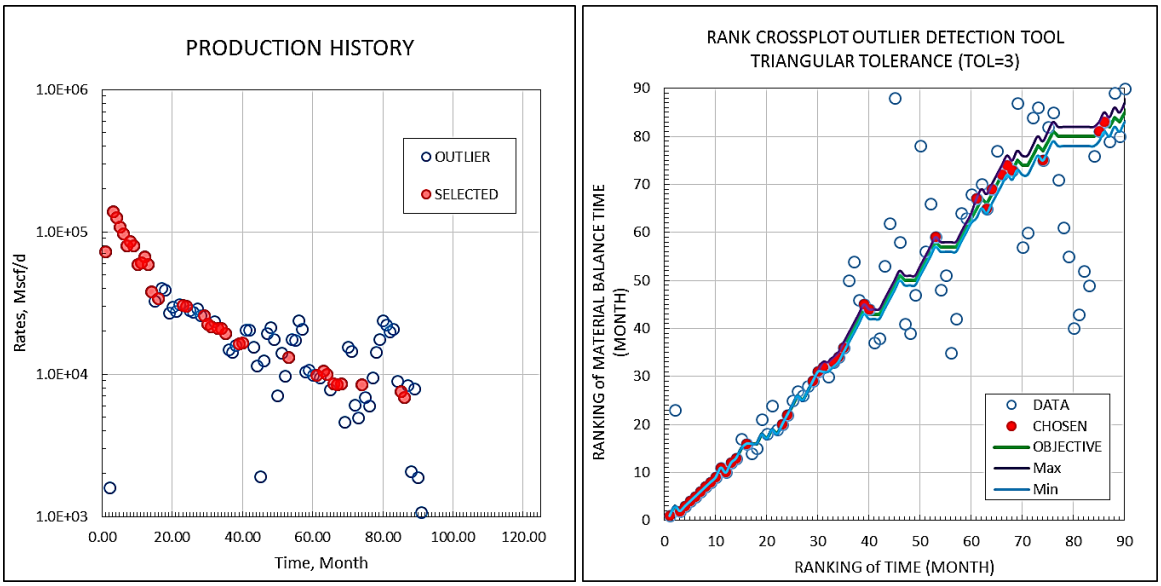


**Fig. 127—Outlier detection example 2.**

Example 3:

This last example demonstrates a rather smooth decline with a few outliers at the end of the profile as shown on **Fig. 128**. It also illustrates the limitation of the method as it selected one rate at 25 months that appears to be an outlier with its neighbors. As previously discussed, a larger number of outliers next to each others can limit the objectivity of the objective function. Since it is limited by a maximum slope of +2 and -1,it results in a selection of a few wrong points in the same time as it discards valid data points until the profiles stabilize back.

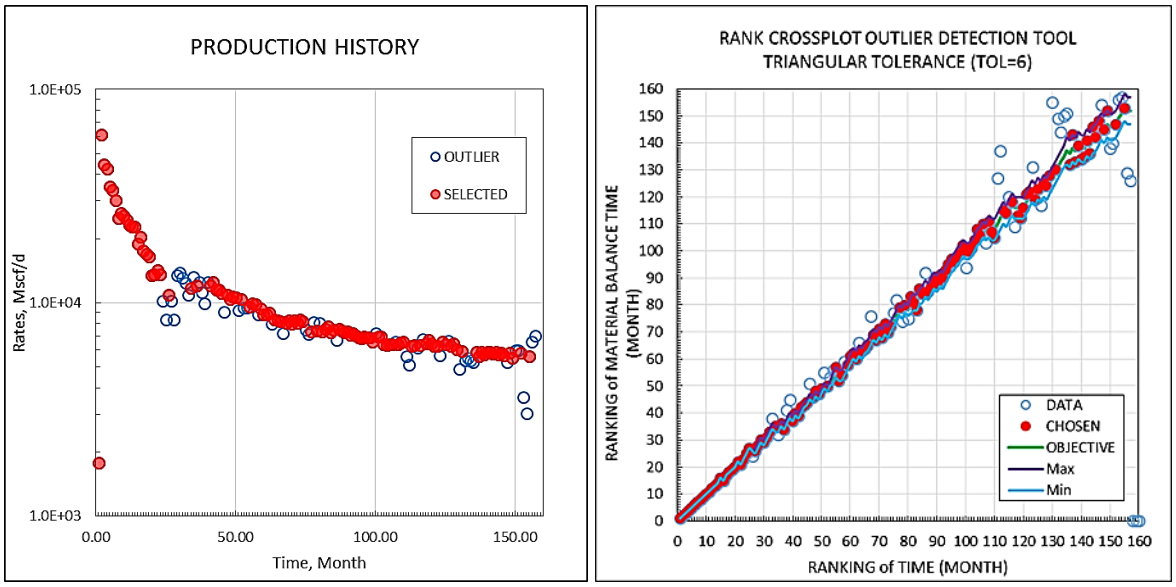


**Fig. 128—Outlier detection example 3 with a continuous segment.**

In conclusion, this methodology was developed based on the observation of outliers and provides a new technique that can be easily integrated in production analysis workflows.

# APPENDIX F: DERIVATION OF THE SQUARE ROOT TIME PLOT DIAGNOSTIC EQUATION FOR THE MODIFIED ANALYTICAL MODEL

Spivey and Lee (2013) give the solution of the transient linear flow toward a fracture place under constant pressure drawdown, which summarized by Eq. F1. We note that the solution can be linearized when the inverse of the rate is plotted against the square root of the real time.

$$\frac{[\Delta m(p)]}{q_D} = m_{sl}\sqrt{t} + b' \qquad (F1)$$

In Eq. F1, $m_{sl}$ is the slope of straight line on the square root of time plot, which can be used to solve for the $A_{cm}\sqrt{k}$ product, where $A_{cm}$ is the total fracture cross sectional area during linear flow. Ibrahim and Wattenbarger (2006) proposed Eq. F2 as a solution for linear flow.

$$A_{cm}\sqrt{k} = f_{cp}\frac{1262T}{m_{sl}}\sqrt{\frac{1}{\mu\emptyset c_t}} \qquad (F2)$$

Because they found that the level of drawdown influences the slope of the square root of time plot, they proposed an empirical correction factor $f_{cp}$. The correction factor is given by Eq. F3 as a function of the dimensionless drawdown:

$$f_{cp} = 1 - 0.0852D_D - 0.0857\,D_D^2 \qquad (F3)$$

Where the dimensionless drawdown is given by Eq. F4:

$$D_D = \frac{[m(p_i) - m(p_{wf})]}{m(p_i)} = \frac{[\Delta m(p)]}{m(p_i)} \qquad (F4)$$

In a horizontal well with multiple vertical fractures, the total fracture area $A_{cm}$ is the contacted hydraulic fracture area. Based on the modified analytical model, $A_{cm}$ is given by Eq. F5:

$$A_{cm} = 4\,x_f\,h\,n_f \qquad (F5)$$

Substituting the Eq. F5 into Eq. F2, we can express the fracture half-length and permeability product with Eq. F6:

$$x_f\sqrt{k} = f_{cp}\frac{1262T}{4hn_f m_{sl}}\sqrt{\frac{1}{\mu\emptyset c_t}} \qquad (F6)$$

Rearranging Eq. F6, we get:

$$x_f\sqrt{k} = f_{cp}\frac{315.5F_s}{hLm_{sl}}\frac{T}{\sqrt{(\mu\emptyset c_t)_i}} \qquad (F7)$$

Replacing the correction factor with Eq. 12 we get the permeability as a function of the drawdown:

$$x_f\sqrt{k} = \left(1 - 0.0852\frac{[\Delta m(p)]}{m(p_i)} - 0.0857\,\frac{[\Delta m(p)]^2}{m(p_i)^2}\right)\frac{315.5F_s}{hLm_{sl}}\frac{T}{\sqrt{(\mu\emptyset c_t)_i}} \qquad (F8)$$

In conclusion, Eq. F8 provides the working equation that can be used to diagnose the $x_f\sqrt{k}$ based on the slope and t

# APPENDIX G: DERIVATION OF THE MODIFIED HARMONIC EQUATION TO FIT TRANSIENT HISTORY OF COMPOSITE PARAMETRIZATION

Starting from the rate-time harmonic decline curve given by Eq. G1:

$$q(t) = \frac{q_i}{(1 + D_i t)} \qquad (G1)$$

Rearrange Eq. G1 by dividing by $D_i$

$$q(t) = \frac{q_i}{D_i} * \frac{1}{(\frac{1}{D_i} + t)} \qquad (G2)$$

Integrate Eq. G2 to find the cumulative production:

$$N_p(t) = \frac{q_i}{D_i} * \ln\left(t + \frac{1}{D_i}\right) + C \qquad (G3)$$

Solve for C based on initial conditions as $N_p(0) = 0$

$$C = -\frac{q_i}{D_i} * \ln\left(\frac{1}{D_i}\right) \qquad (G4)$$

However, the harmonic profile is most likely not fitting the entire transient period of the rate-time profile especially due to either a higher decline of the rate or the production build-up during the ramp-up period. Hence, we suggest to multiply C by a correction factor $\epsilon$ to account for the mismatch at early time in the rate-time profile. Multiplying $\epsilon$ to G4 and inserting into G3 yield Eq. G5:

$$N_p(t) = \frac{q_i}{D_i}\left[\ln\left(t + \frac{1}{D_i}\right) - \epsilon \ln\left(\frac{1}{D_i}\right)\right] \qquad (G5)$$

In order to solve for the constant terms of Eq. G5, developed two methods:

**METHOD 1: The log(q)-Np Plot**

The harmonic decline plots as a straight line on the log(q)-Np graph based on the following equation:

$$q = q_i exp\left[-\frac{D_i}{q_i} N_p\right]$$

Hence, one can use an exponential trend line fit function in a spreadsheet to fit the linear portion of the curve and determine $q_i$ and $D_i$. Then, the correction factor $\epsilon$ is then either found withy trial and error in order to overlay the cumulative profile.

**METHOD 2: The Initial Decline Coefficient Transformation**

Eq. G5 can be linearized such that:

$$y = mx + a$$

Where:

$$y = N_p(t)$$
$$x = \ln\left(t + \frac{1}{D_i}\right)$$
$$m = \frac{q_i}{D_i}$$
$$a = -\epsilon \frac{q_i}{D_i} \ln\left(\frac{1}{D_i}\right)$$

Given a known function y, which is the discrete profile to be matched, a spreadsheet application can used to determine the optimal $D_i$ that provides the most linear transformation of the data. The given value of m and a are used to solve for $q_i$ and $\epsilon$.

Example:

This example shows a sample well producing in transient up to 20 months of production. We see that the log(q)-Np diagnostic plot is almost linear, which means that we can fit a section of the history with an harmonic model. The trendline equation shown on figure gives us a value for the initial rate: 156.65 and we can calculate the initial decline: 0.002*156.65 = 0.3133

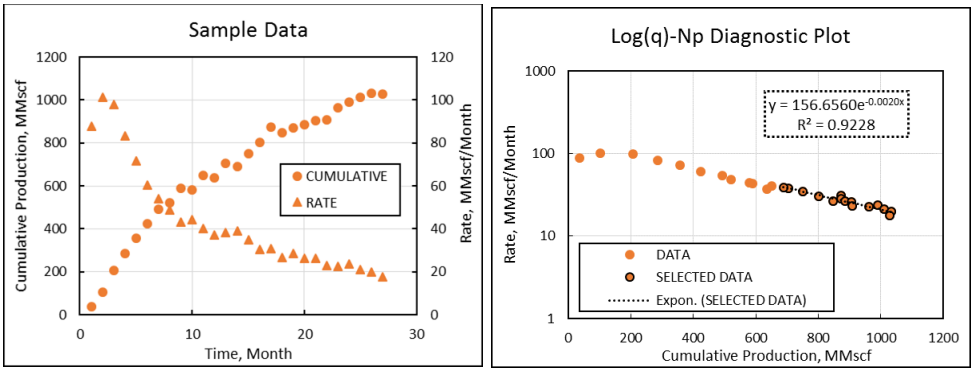


Based on the parameters diagnosed above, we can generate a harmonic profile for the cumulative and the rate profile:

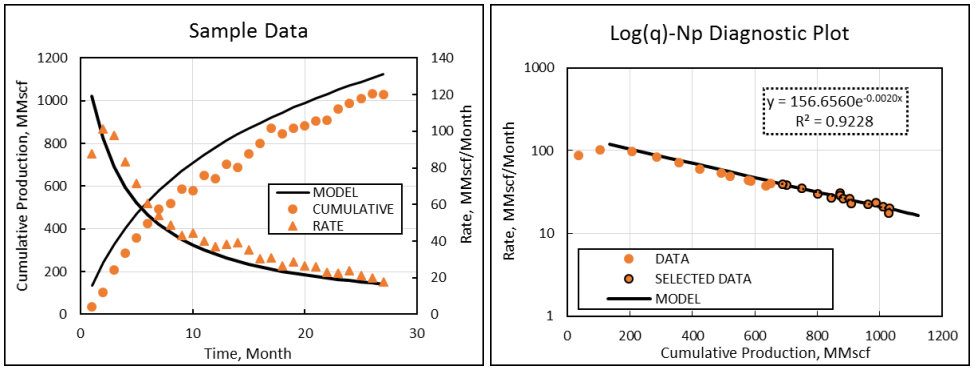


In order to match the model with the cumulative profile, can use the epsilon constant to shift the model down by using a value of 1.15:

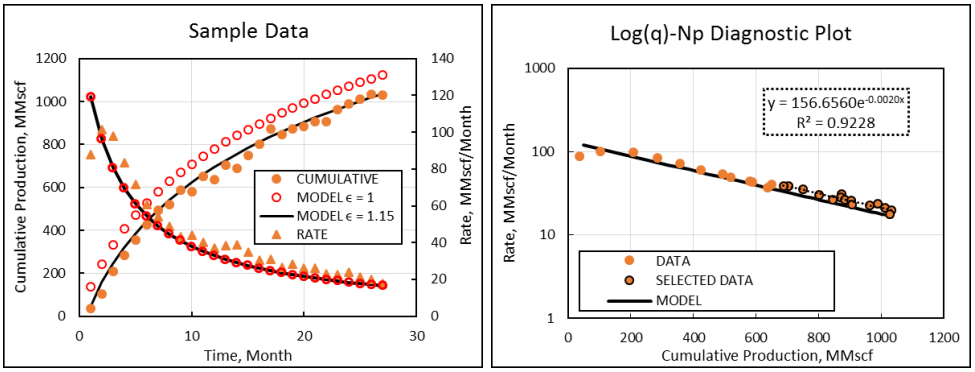


As we can see on the last figure, cumulative-time profile changed while the rate-time profile did not change because the constant epsilon disappear in the derivative form of the cumulative production. While Epsilon allows to correct the cumulative profile in this methodology, it allows to identify a proper Qi and Di for the match. Based on observations, wells with a long ramp-up period will have an epsilon greater than one because there is missing production. Wells with rates very higher than the harmonic model will have an epsilon value smaller than 1.

# APPENDIX H: DERIVATION OF THE HYPERBOLIC EQUATION WITH B=2 TO FIT TRANSIENT HISTORY OF THE COMPOSITE PARAMETRIZATION

Starting from the rate-time hyperbolic decline curve given by Eq. H1:

$$q(t) = \frac{q_i}{(1 + bD_i t)^{1/b}} \qquad (H1)$$

Since the transient period is expected to be following a negative unit slope on the rate-MBT plot, it also means that it can be modeled with a b factor equal to two. Replacing b by 2 and integrating Eq. H1 to find the cumulative production:

$$N_p(t) = \frac{q_i}{D_i}\sqrt{2D_i t + 1} + C \qquad (H2)$$

Solve for C based on initial conditions as $N_p(0) = 0$:

$$C = -\frac{q_i}{D_i} \qquad (H3)$$

However, the profile is most likely not fitting the entire transient period of the rate-time profile especially due to either a higher decline of the rate or the production build-up during the ramp-up period. Hence, we suggest to multiply C by a correction factor $\epsilon$ to account for the mismatch at early time in the rate-time profile. Multiplying $\epsilon$ to H3 and inserting into H3 yield Eq. H4:

$$N_p(t) = \frac{q_i}{D_i}\left[\sqrt{2D_i t + 1} - \epsilon\right] \qquad (H4)$$

The diagnostic plot method: **The Np-(1/q)** allows to identify the region where the flow follows a hyperbolic segment. Furthermore, we can find a combination of qi and Di when the entire curve follows the decline. However, only a segment of the profile matches the hyperbolic curve, a value of epsilon obtained by trial and error process can be used to match the cumulative and the rate history.

The Np-1/q plot was found as diagnostic plot based on the following derivation : Rearranging Eq. H1 with b=2 we can write:

$$\sqrt{2D_i t + 1} = \frac{q_i}{q(t)} \qquad (H5)$$

Substituting Eq. H5 in Eq. H2 we get:

$$N_p(t) = \frac{q_i}{D_i}\left[\frac{q_i}{q(t)} - 1\right] \qquad (H6)$$

Eq. H6 can be linearized such that:

$$y = mx + a$$

Where:

$$y = N_p(t)$$
$$x = \frac{1}{q(t)}$$
$$m = \frac{{q_i}^2}{D_i}$$
$$a = -\frac{q_i}{D_i}$$

Based on this observation, a and m provides a solution for Qi and Di.

$$q_i = -\frac{m}{a}$$
$$D_i = \frac{m}{a^2}$$

Note that when the production does not match at early time, the cumulative is biased by the previous production and values derived by the two equation from the constants of the Np-1/q plot will not fit exactly the data. Example 1 shows a good fit while Example 2 shows the limitation of this method. An epsilon can be also used to fit the cumulative when the rate profiles matches.

Example 1:

The first example is based on a well that has been producing in transient flow regime for more than 12 years in the Barnett Shale. The Welll API# is 422513026 and was also used in Appendix E. The following figure shows the rates and cumulative production history as well as the MBT time plot.

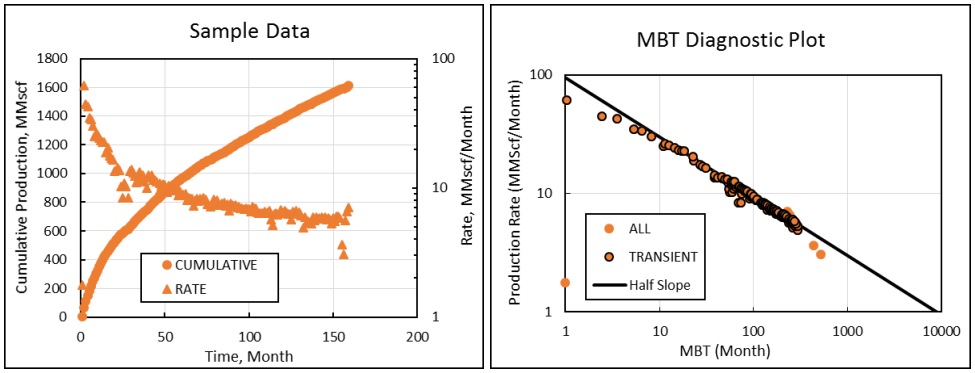


We can see from the half slope line on the diagnostic plot that most of the production is in transient linear flow. Since most of the data points fall on the line, we should expect a good fit with the hyperbolic parametrization for a b value of 2 and an epsilon of 1. The following figure shows the Cumulative-rate inverse plot where we can clearly fit a linear regression to the data points.

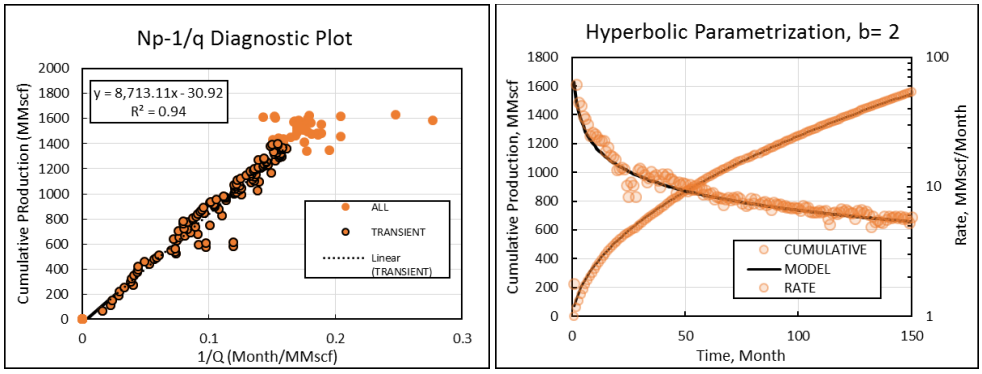


From the slope and the intercept of the linear fit of the data on the plot above, we can calculate the Qi and Di parameters required as presented in the method, using an epsilon of 1. In this case, Qi = 281.75 MMscf/Month (8713.9/30.92) and Di = ($8713.9/30.92^2$). Implementing the two parameters in the parametrization yield the following fit in black with an epsilon value of 1 as shown on the above right plot. Hence, in a nearly perfect case as this one, the hyperbolic parametrization with a b factor of 2 works and the diagnostic tool allows to easily identify the initial rate and decline parameters.

Example 2:

The second example is more complex because the first data points do not follow exactly the hyperbolic decline. It was chosen based on most of the wells encountered in this research. This well produced in transient for approximatively 17 months after transitioning into boundary dominated flow. The following figures show the production history of the well along with the rate-MBT diagnostic plot.

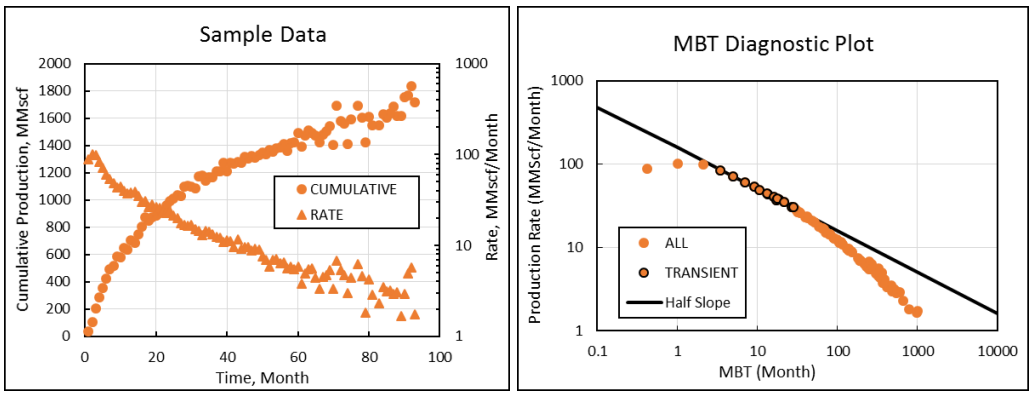


Based on the diagnosed points in transient linear flow as depicted above on the right plot, we can read the slope and intercept of the selected points on the Np-1/q plot below. Based on the slope of 26039.9 and the intercept of -8.08, we calculate qi and Di such that qi = 3224 (26039.9/8.07) and Di = 400 (3224/8.07). The following figures show the diagnostic plot and the generated model over the transient region:

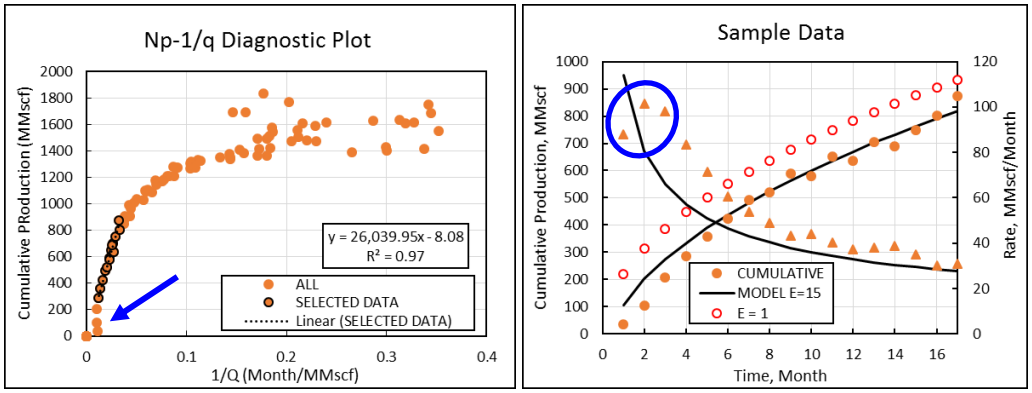


We see that in this case, the black line does not fit the production after the 4th month of production. This illustrate perfectly the limitation of the Np-1/q plot. Nevertheless, the epsilon constant is used to shift the cumulative-time model down by using a value of 15. While the constant epsilon allows to correct the cumulative profile in this methodology, it unfortunately does not change the rate-time profile. Based on those observations, wells with a long ramp-up period will have an epsilon greater than one, the wells with a stronger production than the model will have an epsilon value smaller than 1.

In conclusion, the Np-1/q plot is good to diagnose the region that fits a hyperbolic segment with a b of two, but it does not provide a rigorous method to estimate the initial rates and initial decline. Trial and error on Qi and Di can allow to adjust the rate-time profile, and a value of epsilon then permits to shift the cumulative vertically. Note that large values of epsilon will impact the early time as it deviates from the initial boundary condition of Np(t=0)=0. Hence, it is not recommended to rescale profiles that were parametrized with large epsilons as it will bias the forecast when large scaling factors are used.

# APPENDIX I: EQUATIONS OF THE DEPLETION SEGMENT OF THE COMPOSITE PARAMETRIZATION

Based on the parametrization of the transient segment with the equation provided in Appendix G, we can calculate the Initial decline, rate and cumulative to be used in the harmonic, hyperbolic and exponential decline curves based on the following equations. Note that the superscript indicates either the first or the second segment.

**HARMONIC b = 1**

$$q_i^2 = \frac{q_i^1}{1 + D_i^1 t_{elf}}$$

$$N_{p_i}{}^2 = \frac{q_i^1}{D_i^1}\left[\ln\left(t_{elf} + \frac{1}{D_i^1}\right) - \epsilon\ln\left(\frac{1}{D_i^1}\right)\right]$$

$$D_i^2 = \frac{D_i^1}{1 + D_i^1 t_{elf}}$$

**HYPERBOLIC b = 2**

$$q_i^2 = \frac{q_i^1}{(1 + 2D_i^1 t_{elf})^{0.5}}$$

$$N_{p_i}{}^2 = \frac{q_i^1}{D_i^1}\left[\sqrt{2D_i^1 t_{elf}} - \epsilon\right]$$

$$D_i^2 = \frac{D_i^1}{1 + 2D_i^1 t_{elf}}$$

The cumulative-time and rate-time harmonic stem equations for $t \geq t_{elf}$ are:

$$N_p(t) = N_{p_i}{}^2 + \frac{q_i^2}{D_i^2}\left[\ln\left(1 + D_i^2(t - t_{elf})\right)\right]$$

$$q(t) = \frac{q_i^2}{1 + D_i^2(t - t_{elf})}$$

The cumulative-time and rate-time exponential stem equations for $t \geq t_{elf}$ are:

$$N_p(t,b) = N_{p_i}{}^2 + \frac{q_i^2}{D_i^2}\left[1 - \text{EXP}\left(-D_i^2(t - t_{elf})\right)\right]$$

$$q(t) = q_i^2\,\text{EXP}\left(-D_i^2(t - t_{elf})\right)$$

The cumulative-time and rate-time hyperbolic stem equations for $t \geq t_{elf}$ are:

$$N_p(t,b) = N_{p_i}{}^2 + \frac{q_i^2}{(1-b)D_i^2}\left[1 - \left(1 + bD_i^2(t - t_{elf})\right)^{1-\frac{1}{b}}\right]$$

$$q(t,b) = \frac{q_i^2}{\left(1 + bD_i^2(t - t_{elf})\right)^{\frac{1}{b}}}$$

In conclusion, this appendix presents how we suggest to compute the 2nd segment of the composite parametrization model.

# APPENDIX J: CASE STUDY – HOWARD COUNTY, MIDLAND BASIN TIGHT OIL

The objective of the case study presented in this Appendix is to show how the analytical scaling methodology applies to oil wells producing from tight/shale reservoirs. As the Barnett shale case study was prepared to apply the type well workflow and forecasting methods presented on Fig. 60. In this study, we will only generate the type well from the wells in BDF from step 1 to step 8.1 of the workflow.

The Midland basin was selected for this case study because it has been extensively developed in the past 5 years among other resources plays in the US. The Midland basin was deposited in the Paleozoic era and more specifically in the lower and middle Permian period. The largest hydrocarbon bearing formations of the midland basin are the Spraberry and Wolfcamp. Those formations were simultaneously deposited in an anaerobic environments with organic-rich carbonate and clastic sediments, creating a mix of conventional and unconventional reservoirs. The GSA selected for this case study is located in the north-east side of the basin, delimited by the geographical boundaries of the Howard County in Texas, as presented on **Fig. 129**.

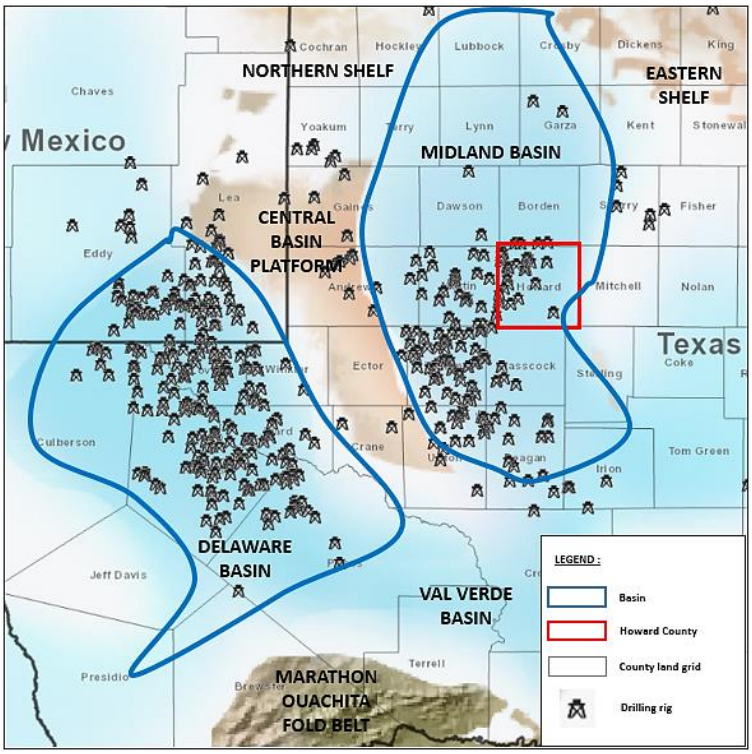


**Fig. 129—Location of the Howard County shown on a paleo geographic map of the early Permian period with current drilling activities.**

A set of 144 actively producing horizontal oil wells from the Wolfcamp and Spraberry formations was selected for the analysis, as displayed on **Fig. 130**.The total vertical depth of the lateral section varies between 7000 and 8500 ft and the average gross perforated interval is 7845 ft. Most of the wells were first produced between the 2013 and 2017. Only monthly produced volume were used for the analysis and the number of hydraulic stages is unknown for most of the wells.

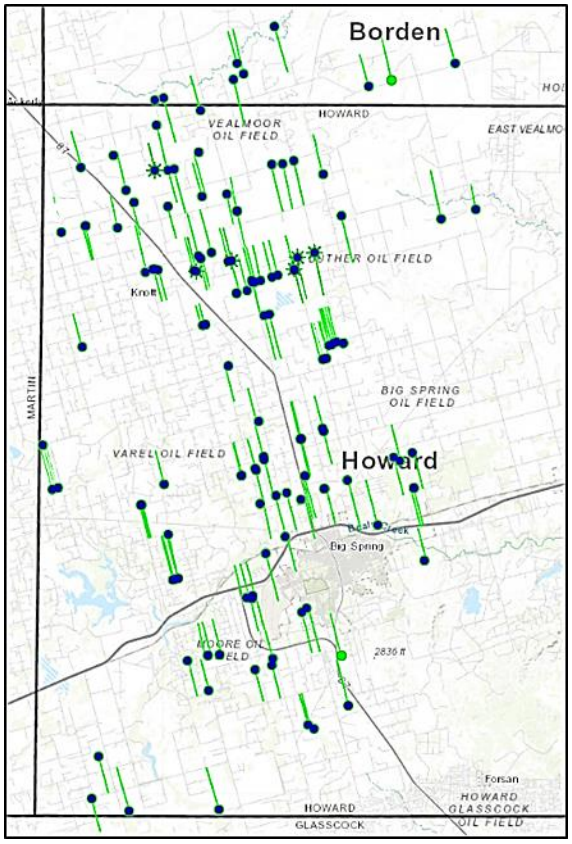


**Fig. 130—Location of the 144 wells of the Midland basin Case Study.**

Based on the defined GSA, the production data was treated according to step 2 to 4 as described in Fig. 60. The wells were organized into the three different groups based on the flow regime diagnostic on the rate-MBT plot. As presented on **Fig. 131**, there was a total number of 80 wells in BDF, 38 wells in transient and 26 wells with short and discontinuous production history.

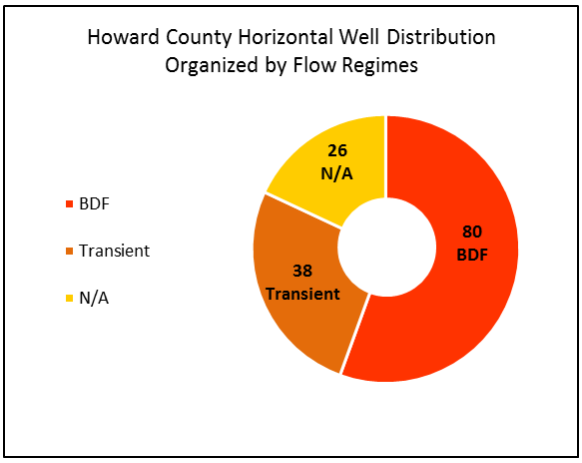


**Fig. 131—Distribution of the Howard county wells by flow regime.**

In order to perform the type curve match and the diagnostic of the reservoir and completion parameters, we used the equations for a single liquid fluid flowing into the wellbore through the fracture network. Eq. J-1 and J-2 were used with Fig. 9 as opposed to Eqs. 11 and 12 which were developed for the gas case.

$$QM = \frac{\left(\frac{F_s}{x_f}\right) q_D}{q_t} = \left(\frac{F_s^2}{k}\right) \frac{141.2 B \mu}{x_f h L_w [p_i - p_{wf}]} \tag{J-1}$$

$$TM = \frac{t_{DF_s}}{t_{mb}} = \left(\frac{k}{F_s^2}\right) \frac{0.02532}{(\emptyset \mu c_t)_i} \tag{J-2}$$

An oil formation volume factor of 1.35 was used for all the wells, same as a viscosity of 0.5 cp, a porosity of 10% and a total compressibility of 1.85E-05psi$^{-1}$. The initial reservoir pressure was calculated based on the reported TVD of the lateral section with a pressure gradient of 0.465 psi/ft. The BHP was calculated as $0.1p_i$ for all the wells. The four histograms presented on **Fig. 132** show the distribution of the gross lateral length, total vertical depth, fracture half-length and permeability of the 80 wells diagnosed in BDF. Since the number of hydraulic stages was unknown for the wells of this GSA, we assumed that the wells were completed with a stage spacing of 200 ft, with a fracture height of 200 ft. Based on this assumption, the number of fractures was automatically calculated. As per the equations used with the time match point for each rate-MBT profiles, the diagnosed permeability is proportionally biased by our assumption. Nevertheless, the ratio $F_s^2/k$ remains representative of the well performance independently of our assumption. Similarly, the fracture half-length is proportionally biased by our assumption of a common net-pay thickness. Hence, the permeability and fracture half-length distributions presented on Fig. 132 are not the real distributions, but they give a good idea of the wells' parameters, as if the wells were normalized based on realistic assumptions. Overall, we find an average permeability of 4.5 µD and an average fracture half-length of 55 ft which are reasonable for oil wells producing in tight/shaly formations in the midland

basin. Finally, given the fracture spacing, we find that the permeability is lognormally distributed on a range of 1 to 20 µD and the fracture half-length is more normally distributed on a range of 20 to 100 ft.

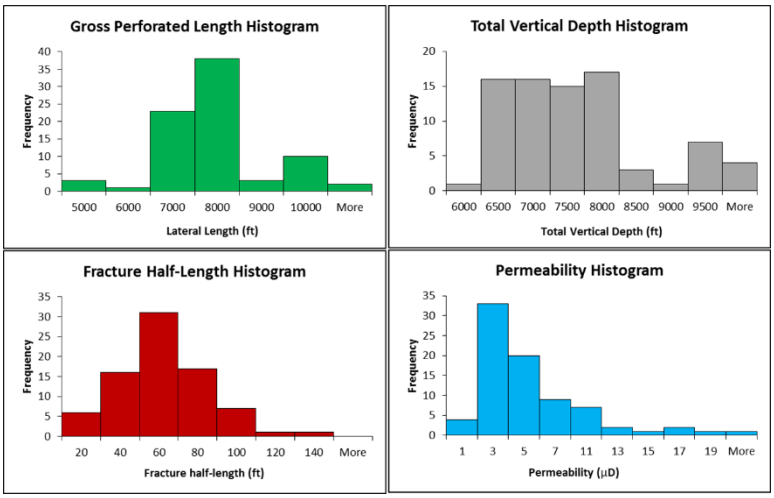


**Fig. 132—Statistics of the 80 wells in BDF from the Howard county GSA.**

The performance of the 80 wells diagnosed in boundary dominated flow is shown in grey on Fig. 133. We see that there is a large array of performances among the wells varying from 50 000 bbl up to 300 000 bbl of cumulative oil production after 20 months of production. Due to the large number of wells in BDF, we decided to select 15 wells shown in red on **Fig. 133**. The 15 wells were used in this case study to create a type well with the analytical scaling factors according to the workflow presented on Fig. 60. To maintain a representative selection of our GSA, 5 out of the 15 wells have been first producing since 2017, another 5 were selected because they have been producing since 2016 and the last 5 wells produced since 2015.

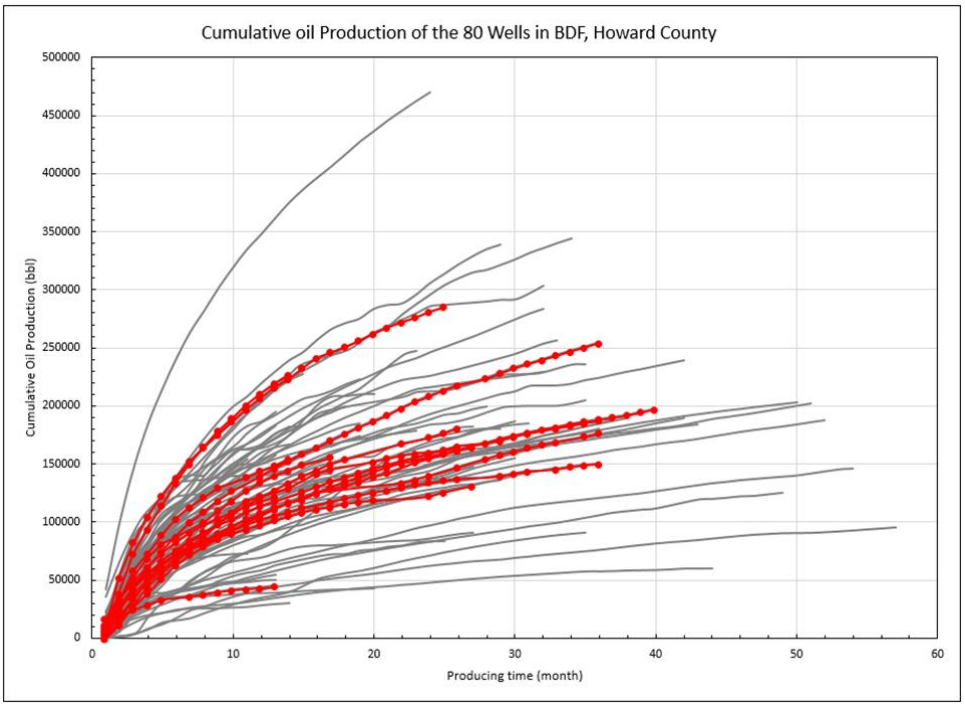


**Fig. 133—Cumulative production of the 80 wells in BDF (in grey) and the 15 wells selected for the type well study (in red).**

**Table 27** presents the results of the type curve diagnostic of the 15 wells selected for the type well construction. The last row shows the parameters used to generate the base well profile. **Table 28** shows the scaling factors computed for each parameter based on the analytical scaling factors presented in Table 12.

| Well API Number | First Prod. | Lateral Lengt | Stage Number | Fracutre Spacing | Well Depth | Net Pay | Proppant Loading | Frac Fluid | Initial Pressure | Flowing Pressure | P.P. Drawdown | TM | QM | Xf | K |
|---|---|---|---|---|---|---|---|---|---|---|---|---|---|---|---|
| | MM-YY | (ft) | | (ft) | (ft) | (ft) | (lbs) | (bbls) | (psia) | (psia) | (psia^2/cp) | (10-3) | (10-3) | (ft) | (μD) |
| 4222738837 | May-17 | 10315 | 52 | 200.0 | 7345 | 200 | #N/A | #N/A | 3415.4 | 341.5 | 3074 | 2.05 | 1.63 | 62.02 | 3.0 |
| 4222738692 | May-17 | 7663 | 38 | 200.0 | 7610 | 200 | 1.3E+07 | 1.3E+07 | 3538.7 | 353.9 | 3185 | 7.06 | 3.52 | 10.88 | 10.2 |
| 4222738939 | Feb-17 | 4156 | 21 | 200.0 | 7864 | 200 | 1.3E+07 | 1.1E+07 | 3656.8 | 365.7 | 3291 | 2.11 | 2.43 | 94.07 | 3.1 |
| 4222738845 | May-17 | 7802 | 39 | 200.0 | 7300 | 200 | 1.5E+07 | 1.8E+07 | 3394.5 | 339.5 | 3055 | 2.81 | 2.00 | 49.28 | 4.1 |
| 4222738940 | Jun-17 | 6752 | 34 | 200.0 | 7709 | 200 | 9.2E+06 | 1.2E+07 | 3584.7 | 358.5 | 3226 | 3.19 | 2.31 | 41.12 | 4.6 |
| 4222738693 | Apr-16 | 6508 | 33 | 200.0 | 7003 | 200 | #N/A | #N/A | 3256.4 | 325.6 | 2931 | 1.44 | 3.72 | 64.40 | 2.1 |
| 4222738646 | Apr-16 | 7656 | 38 | 200.0 | 7529 | 200 | 1.5E+07 | 1.9E+07 | 3501.0 | 350.1 | 3151 | 1.19 | 3.62 | 63.70 | 1.7 |
| 4222738640 | Mar-16 | 7590 | 38 | 200.0 | 7257 | 200 | 1.1E+07 | 1.2E+07 | 3374.5 | 337.5 | 3037 | 1.99 | 3.77 | 38.08 | 2.9 |
| 4222738738 | May-16 | 6600 | 33 | 200.0 | 8030 | 200 | 1.2E+07 | 1.0E+07 | 3734.0 | 373.4 | 3361 | 2.45 | 2.54 | 47.84 | 3.5 |
| 4222738722 | Jun-16 | 7435 | 37 | 200.0 | 7826 | 200 | 1.4E+07 | 1.4E+07 | 3639.1 | 363.9 | 3275 | 1.84 | 1.78 | 82.59 | 2.7 |
| 4222738535 | Jul-15 | 9333 | 47 | 200.0 | 7785 | 200 | 1.3E+07 | 1.5E+07 | 3619.9 | 362.0 | 3258 | 0.87 | 4.99 | 49.62 | 1.3 |
| 4222738492 | Jul-15 | 7803 | 39 | 200.0 | 7687 | 200 | #N/A | 1.1E+05 | 3574.5 | 357.4 | 3217 | 1.01 | 3.44 | 75.33 | 1.5 |
| 4222738456 | Jun-15 | 6954 | 35 | 200.0 | 7904 | 200 | 1.2E+07 | 8.7E+06 | 3675.4 | 367.5 | 3308 | 1.62 | 4.03 | 43.89 | 2.3 |
| 4222738245 | Mar-15 | 6950 | 35 | 200.0 | 7732 | 200 | 1.4E+07 | 1.1E+07 | 3595.5 | 359.6 | 3236 | 0.77 | 5.30 | 71.87 | 1.1 |
| 4222738454 | Jun-15 | 7107 | 36 | 200.0 | 7991 | 200 | 1.0E+07 | 8.6E+06 | 3716.0 | 371.6 | 3344 | 0.94 | 4.66 | 63.22 | 1.4 |
| Base Well | | 7375 | - | 200.0 | - | 200 | - | - | - | - | 3197 | - | - | 57.19 | 3.0 |

**Table 27—Parameters of the 15 wells in BDF.**

| Well API No | Permeability | | Lateral Length | | Fracture Half Length | | Fracture Spacing | | Pseudo-Drawdown | | Rate-Time | | Cumulative-Time | |
|---|---|---|---|---|---|---|---|---|---|---|---|---|---|---|
| | TSF | RSF | TSF | RSF | TSF | RSF | TSF | RSF | TSF | RSF | TSF | RSF | TSF | CSF |
| 4222738837 | 0.98 | 1.02 | 1.00 | 0.71 | 1.00 | 0.92 | 1.00 | 1.00 | 1.00 | 1.04 | 0.98 | 0.70 | 0.98 | 0.69 |
| 4222738692 | 3.38 | 0.30 | 1.00 | 0.96 | 1.00 | 5.26 | 1.00 | 1.00 | 1.00 | 1.00 | 3.38 | 1.50 | 3.38 | 5.08 |
| 4222738939 | 1.01 | 0.99 | 1.00 | 1.77 | 1.00 | 0.61 | 1.00 | 1.00 | 1.00 | 0.97 | 1.01 | 1.04 | 1.01 | 1.05 |
| 4222738845 | 1.34 | 0.74 | 1.00 | 0.95 | 1.00 | 1.16 | 1.00 | 1.00 | 1.00 | 1.05 | 1.34 | 0.85 | 1.34 | 1.15 |
| 4222738940 | 1.52 | 0.66 | 1.00 | 1.09 | 1.00 | 1.39 | 1.00 | 1.00 | 1.00 | 0.99 | 1.52 | 0.99 | 1.52 | 1.51 |
| 4222738693 | 0.69 | 1.45 | 1.00 | 1.13 | 1.00 | 0.89 | 1.00 | 1.00 | 1.00 | 1.09 | 0.69 | 1.59 | 0.69 | 1.10 |
| 4222738646 | 0.57 | 1.76 | 1.00 | 0.96 | 1.00 | 0.90 | 1.00 | 1.00 | 1.00 | 1.01 | 0.57 | 1.55 | 0.57 | 0.88 |
| 4222738640 | 0.95 | 1.05 | 1.00 | 0.97 | 1.00 | 1.50 | 1.00 | 1.00 | 1.00 | 1.05 | 0.95 | 1.61 | 0.95 | 1.54 |
| 4222738738 | 1.17 | 0.85 | 1.00 | 1.12 | 1.00 | 1.20 | 1.00 | 1.00 | 1.00 | 0.95 | 1.17 | 1.09 | 1.17 | 1.27 |
| 4222738722 | 0.88 | 1.13 | 1.00 | 0.99 | 1.00 | 0.69 | 1.00 | 1.00 | 1.00 | 0.98 | 0.88 | 0.76 | 0.88 | 0.67 |
| 4222738535 | 0.42 | 2.39 | 1.00 | 0.79 | 1.00 | 1.15 | 1.00 | 1.00 | 1.00 | 0.98 | 0.42 | 2.13 | 0.42 | 0.89 |
| 4222738492 | 0.48 | 2.06 | 1.00 | 0.95 | 1.00 | 0.76 | 1.00 | 1.00 | 1.00 | 0.99 | 0.48 | 1.47 | 0.48 | 0.71 |
| 4222738456 | 0.78 | 1.29 | 1.00 | 1.06 | 1.00 | 1.30 | 1.00 | 1.00 | 1.00 | 0.97 | 0.78 | 1.72 | 0.78 | 1.34 |
| 4222738245 | 0.37 | 2.72 | 1.00 | 1.06 | 1.00 | 0.80 | 1.00 | 1.00 | 1.00 | 0.99 | 0.37 | 2.26 | 0.37 | 0.83 |
| 4222738454 | 0.45 | 2.22 | 1.00 | 1.04 | 1.00 | 0.90 | 1.00 | 1.00 | 1.00 | 0.96 | 0.45 | 1.99 | 0.45 | 0.90 |

**Table 28—Scaling factors for the 15 wells in BDF.**

The scaling factors presented in **Table 28** were used to rescale the 15 production profile as shown on **Fig. 134.** Similar to the case study in the Barnett shale, Fig. 134 demonstrates that the production of HMFW producing from oil bearing formations can be rescaled analytically. Looking at the rescaled cumulative-time profile, we demonstrate that there is a characteristic production profile for a specific set of reservoir and completion parameters. The grouping of the 15 wells around a common decline shows how the analytical scaling factors can be used on monthly produced volume to generate type wells forecasts. Based on the results presented on Fig. 134, one could carry the same analysis performed on the Barnett shale case

study in order to forecast undrilled wells and wells in transient flow regime. Because we do not have access to stage spacing information, we decided not to perform this analysis as the permeability's and fracture half-length distributions do not represent the real potential of the field.

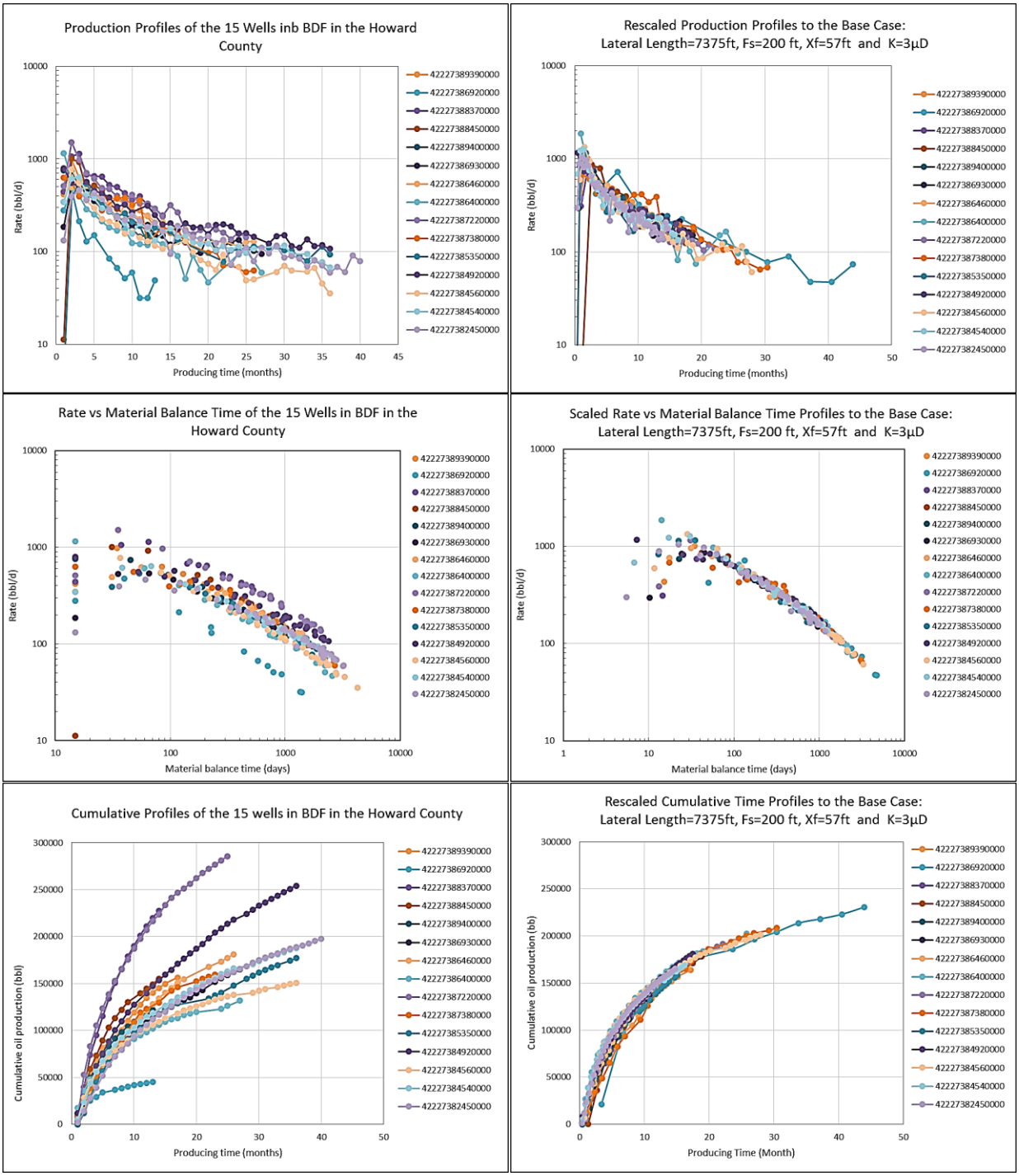


**Fig. 134—Production profiles before (left) and after (right) the application of the analytical scaling factors.**

In conclusion, we demonstrated that both oil and gas wells production follow the characteristic shape of the Wattenbarger type curve. It also shows how the multiple fractures networks govern the production behavior in a resource play at the scale of a monthly produced volumes. And while this type of information is known to be unreliable due to the limitations presented in Chapter 2, we nevertheless demonstrated that it can be used to characterize flow regimes over a period as short as 1 years as demonstrated in this appendix. Finally, we demonstrated that publically available data is compatible with the analytical scaling factors. The combination of both provides a powerful set of tools applicable to oil and gas wells that can be used to:

- Characterize the performances of wells in a resource play
- Generate type wells for a specific set of reservoir and completion properties
- Deterministically forecast wells with short production history
- Probabilistically forecast undrilled wells

# APPENDIX K: CASE STUDY – EAGLE FORD, SHALE CONDENSATE

The objective of this case study is to show how the analytical scaling factors apply to high frequency rate/pressure data of 3 wells in the Eagle Ford Shale. We successfully generated a typical well profile and were able to characterize the performance of the wells with the estimated properties from the modified type curve. We also demonstrate pressure corrected rates improves the match on the type curve.

The 3 wells presented in this analysis produce from the condensate region in Webb County in the Eagle Ford shale at an average depth of 8500 ft. The information available to study the well is presented in **Table 29** and **Table** 30.

**Table 29—Properties of the 3 wells of the Eagle Ford case study.**

| | Well 1 | Well 2 | Well 3 |
|---|---|---|---|
| Lateral length, ft | 7200 | 7100 | 4382 |
| Stage Count | 45 | 71 | 44 |
| Clusters/Stg | 8 | 5 | 5 |
| Average BHP, psi | 1000 | 1500 | 1200 |
| Proppant, lbs | 14,155,906 | 14,190,222 | 18,842,408 |
| Fluid, bbls | 617,974 | 621,639 | 412,870 |
| Proppant density, lbs/ft | 1960 | 1998 | 4300 |
| Fluid Density, bbls/ft | 86 | 88 | 94 |
| Gas Gravity | 0.76 | 0.73 | 0.75 |
| Oil API | 62.1 | 69.8 | 59.8 |
| Oil SG | 0.73 | 0.70 | 0.74 |
| Molecular Weight | 111.91 | 97.77 | 116.96 |
| Gas equivalent, SCF/stb | 868.63 | 956.26 | 841.08 |
| Average condensate yield, STB/MMscf | 50 | 35 | 50 |
| Well stream gravity | 0.89 | 0.82 | 0.88 |
| Gas viscosity | 0.041 | 0.037 | 0.041 |
| Gas compressibility | 6.4E-05 | 7.0E-05 | 6.5E-05 |
| Water compressibility | 2.7E-06 | 2.7E-06 | 2.7E-06 |
| Total compressibility | 6.0E-05 | 6.5E-05 | 6.0E-05 |

**Table 30—Reservoir properties of the Eagle Ford case study.**

| | | |
|---|---|---|
| Rock compressibility | 4.51E-06 | $Psi^{-1}$ |
| Porosity | 12 | % |
| Initial Reservoir Pressure | 6600 | psia |
| Swi | 0.15 | % |
| Sgi | 0.85 | % |
| Soi | 0 | % |
| Reservoir Temperature | 225 | $^{o}F$ |

The average BHP and condensate yields were determined by selecting a representative value on the production history as shown on Fig. 135. The water to gas ratio was observed to be stable enough to be assumed constant for all the wells. To match the production data, we assumed that all the produced fluids are in the gas phase at reservoir condition. Based on those assumptions, we calculated the gas equivalent volume of produced condensate, the combined gas gravity (wellstream), the gas compressibility and the associated viscosity at reservoir condition as presented in Table 29. We neglected the presence of the water, which is under liquid phase at initial reservoir conditions. In order to fit the data onto the diagnostic plot presented on Fig. 9, a specific workflow shown on Fig. 136 was prepared to obtain the pressure corrected gas equivalent rates vs. their MBT.

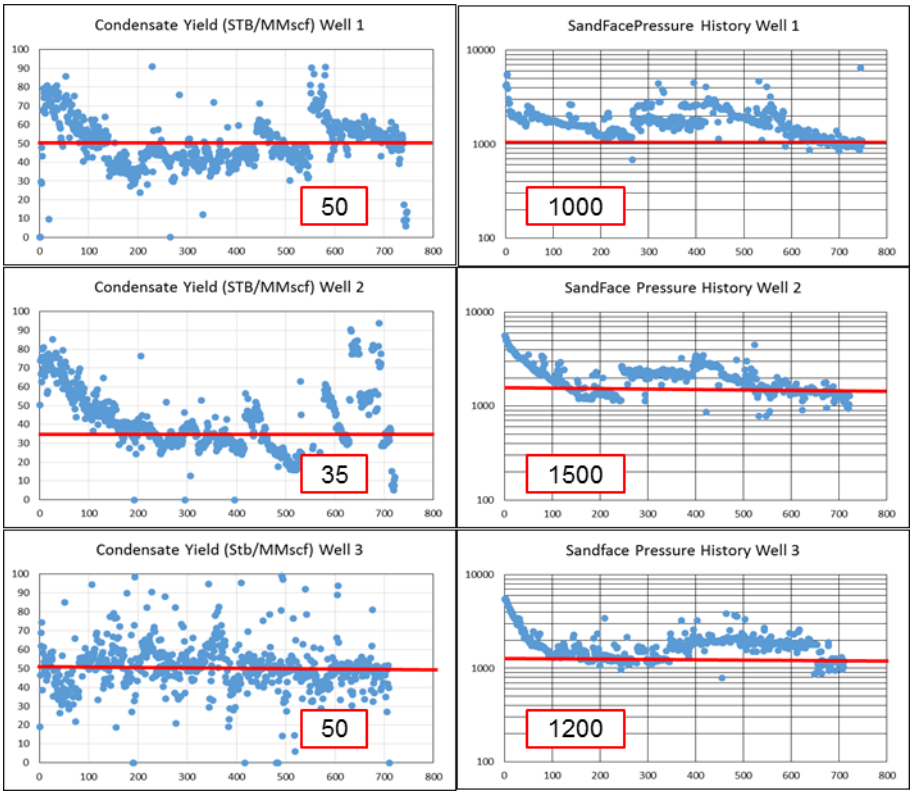


**Fig. 135—Condensate yield and sand-face pressure history of the 3 Eagle Ford wells.**

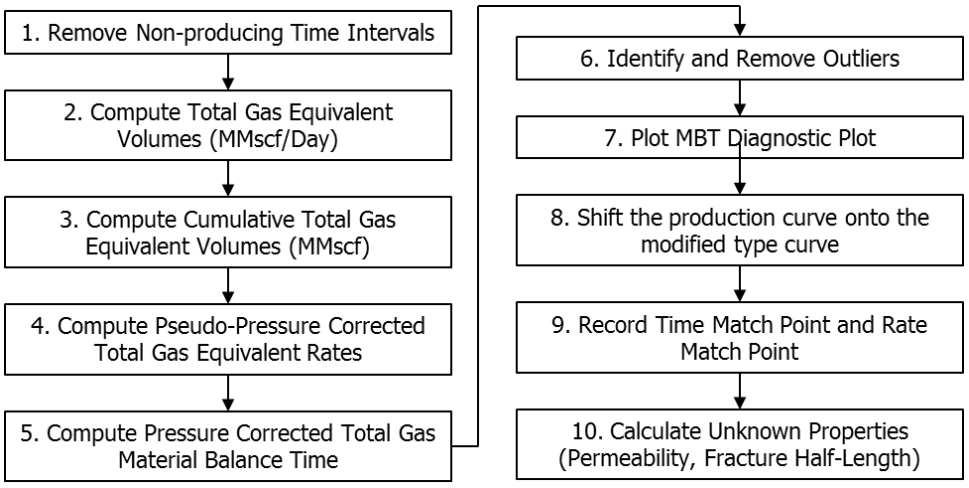


**Fig. 136—Production analysis and workflow for gas condensate.**

**Fig. 137**Fig. **139** present how the pressure correction proposed by Lacayo and Lee (2014) affects the gas rates on the material balance time plot. We notice the most of the early points are significantly normalized

to higher rates as the sand-face pressure takes time to stabilize to the average pressure. This improves the fit of the data on a negative half-slope as illustrated with the dotted lines on each figure. Finally, we see that each well transition from a negative half-slope to a negative unit with time.

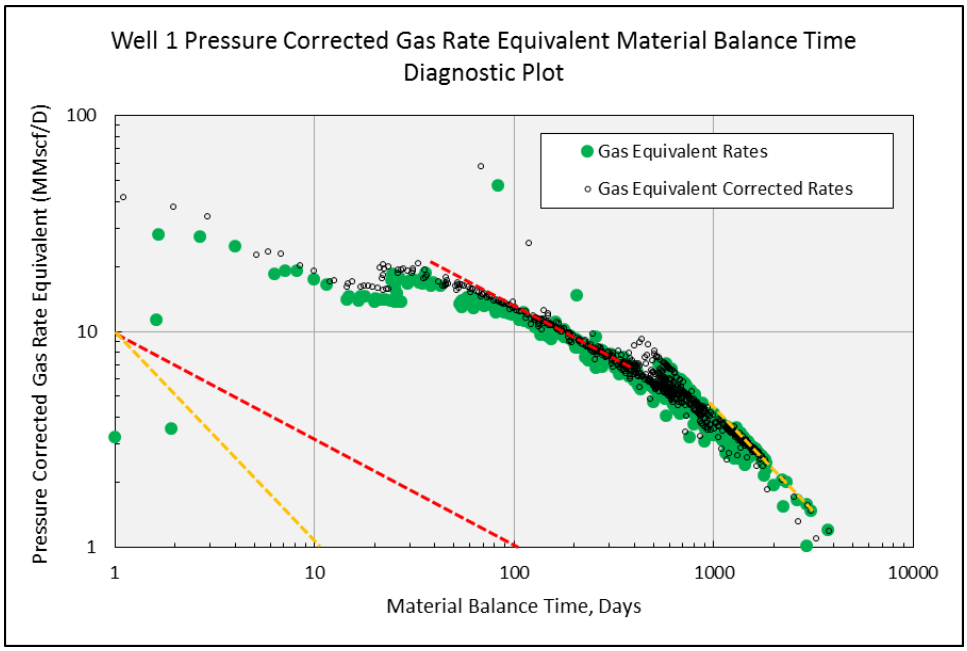


**Fig. 137—Well 1 gas equivalent rate vs. MBT diagnostic plot.**

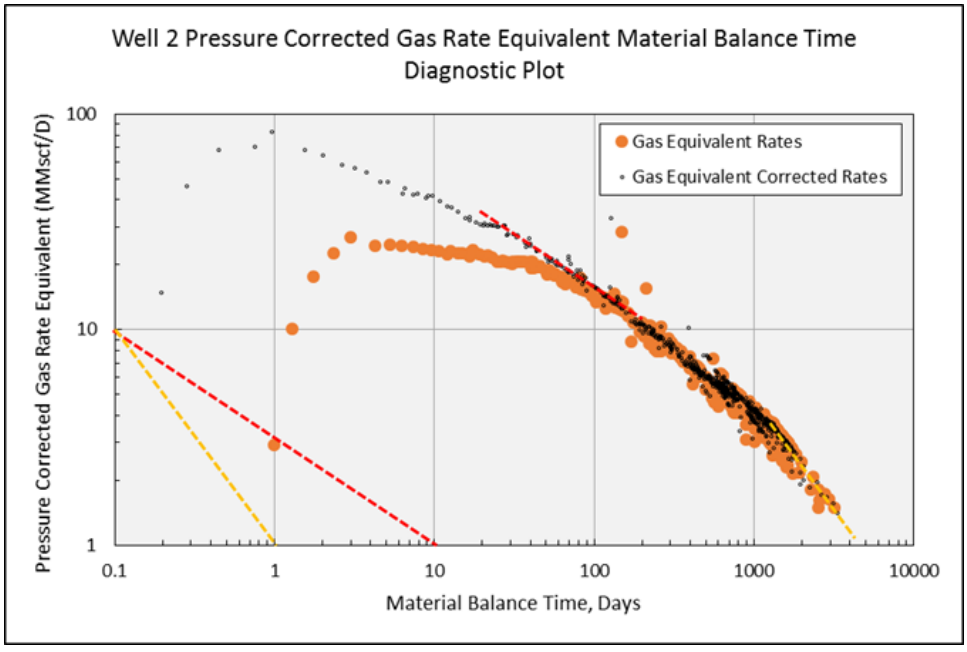


**Fig. 138—Well 2 gas equivalent rate vs. MBT diagnostic plot.**

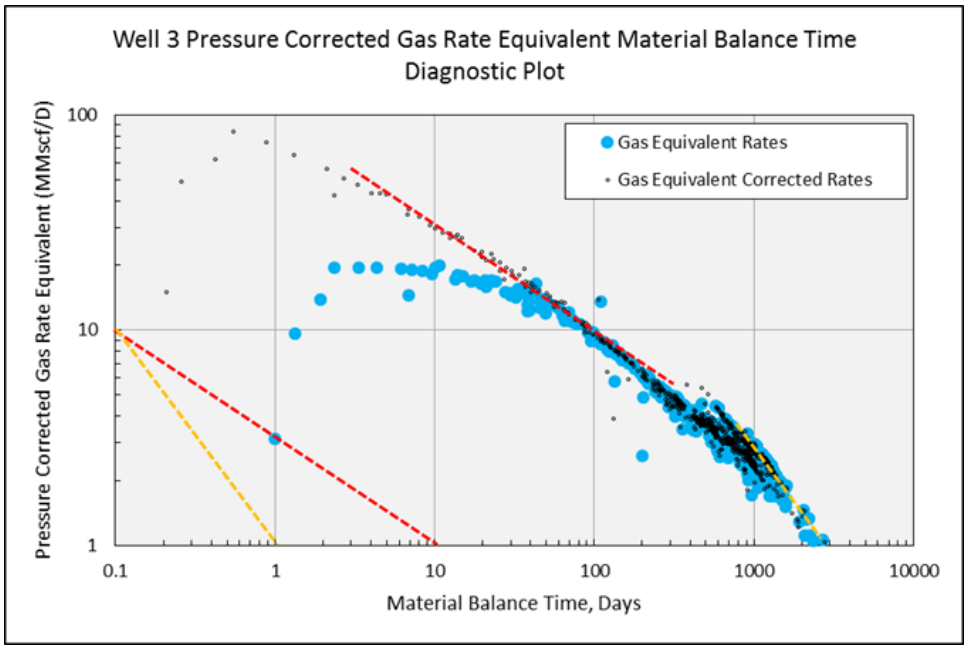


**Fig. 139—Well 3 gas equivalent rate vs. MBT diagnostic plot.**

As we can observe on Fig. 137Fig. 139, it appears that several sections of the production could be fitted with a negative unit slope on well 1 and 3. We identified 5 different producing regions and plotted them on the rate-MBT plot with their respective colors as shown on **Fig. 140**. It appears that each segment falls on a negative unit slope line, and most of them cannot match the trend of segment 1. Those examples illustrate very well the challenges discussed in Section 5.5. While the data can match multiple locations on the type curve, it becomes a potential source of error when estimating the permeability and the fracture half-length. Referring to the scaling factor theory, which implies that a horizontal or vertical displacement is correlated to a change in property, the shift of the production profile could be explained by a change in fracture half-length of permeability with time. This interpretation requires further study because such effects can be demonstrated analytically, but it is outside of the scope of this research.

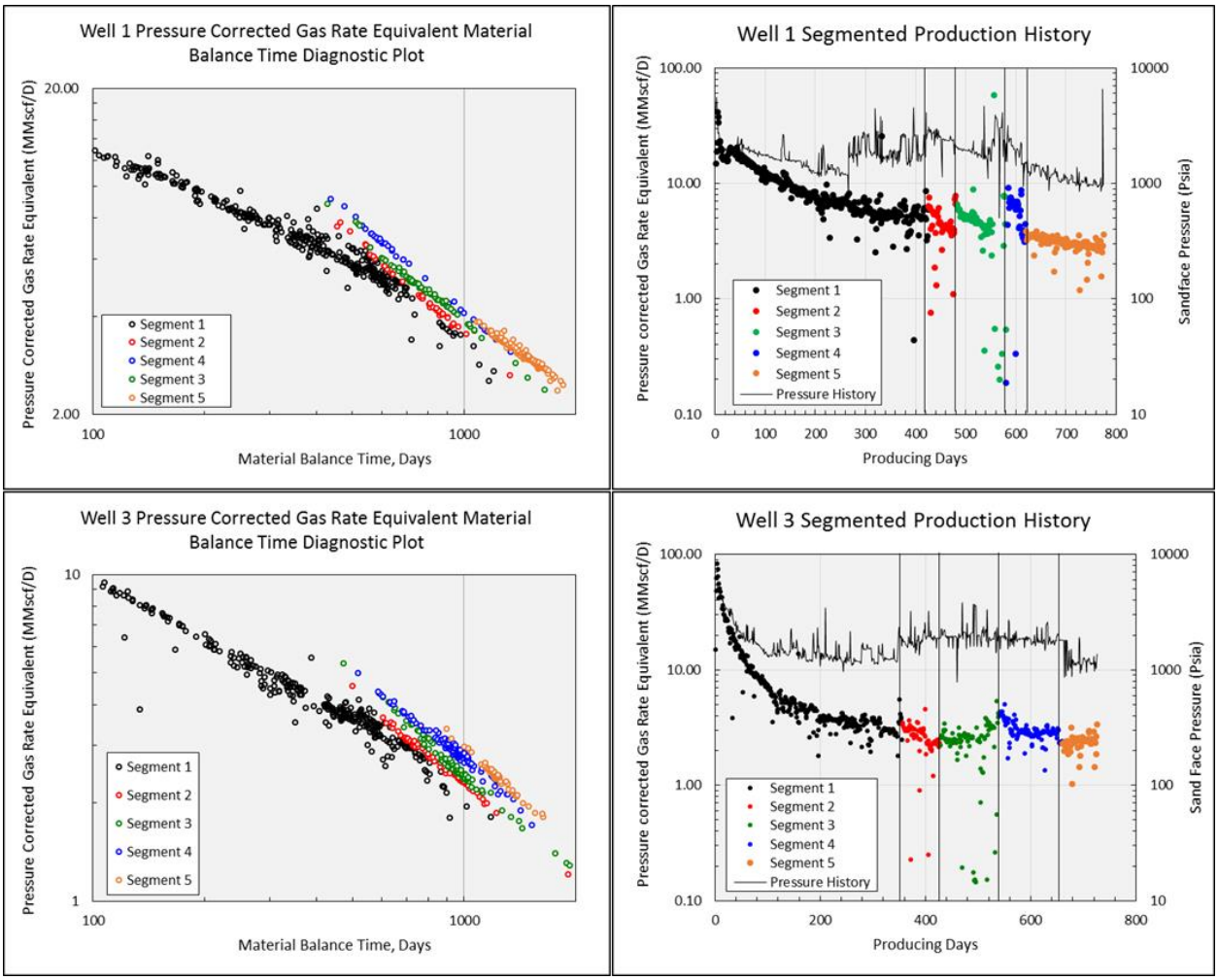


**Fig. 140—Comparison of the production profile with multiple segments on the MBT diagnostic plot.**

Based on the observations made on the previous figures, we present the match of the 3 profiles on the modified type curve as shown on **Fig. 141**. From the right plots, we see that the 3 profiles align properly on the type curve, expect for well 3 where we suggested a second match in green. This alternate match was performed by shifting the production down, as indicated by the arrow. This shift on the type curve keeps the same permeability, but increases the fracture half-length. As demonstrated with the 5 segments, the discontinuities present different matches on the type curve.

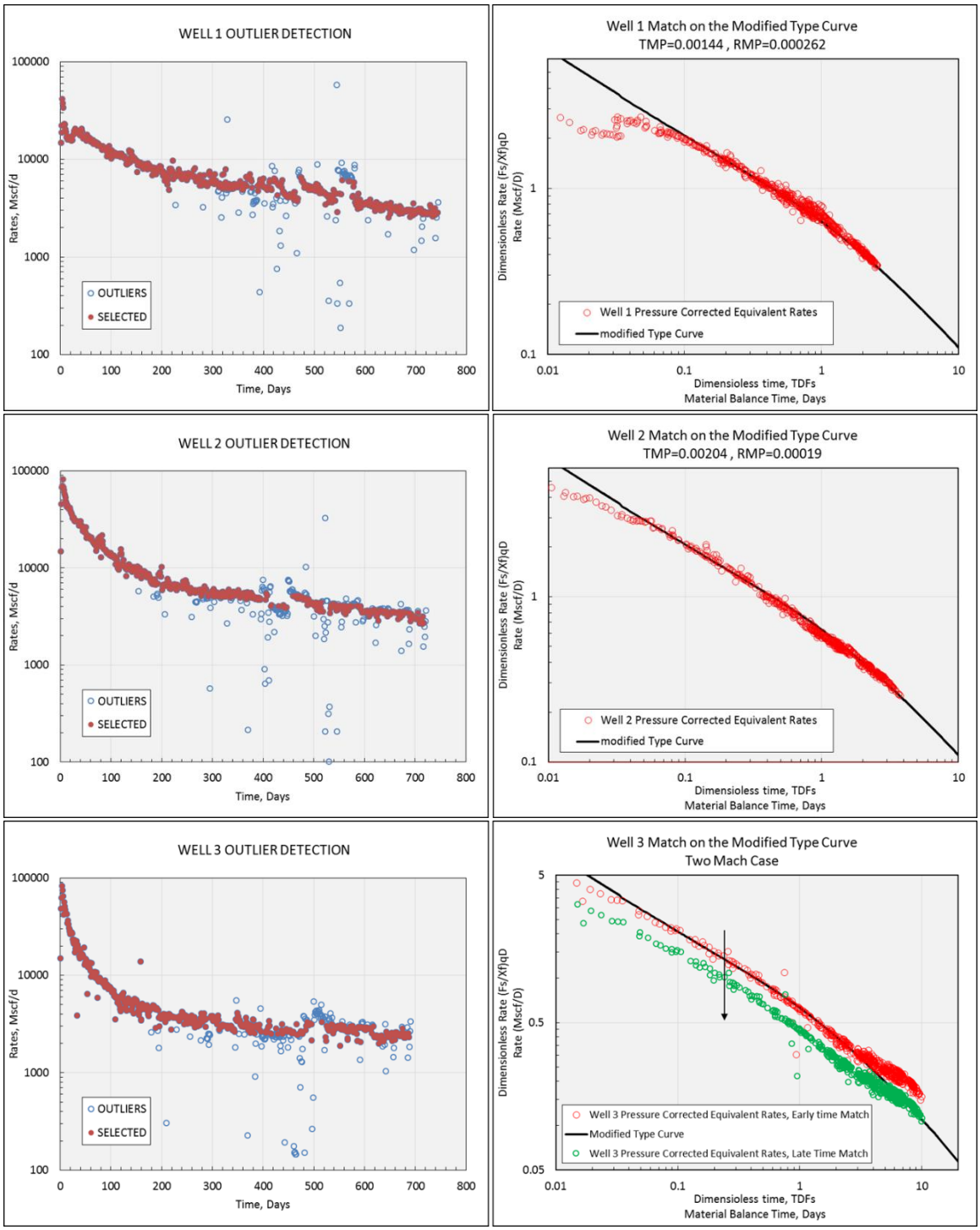


**Fig. 141—Outlier detection and match of the production data on the modified type curve.**

The results from the match on the type curve are presented on **Table 31**. We calculated the permeability based on the original assumption that we create one fracture per hydraulic stage. Since the cluster spacing is also available, we computed the permeability assuming one fracture per cluster. Because all the wells

have the same cluster spacing, it normalizes the calculated permeabilities and demonstrates that a greater stage number could have induced a better permeability when comparing well 1 and 2. Looking at the results of well 3, we find that it has the highest permeability for both assumptions. Beside fracture the assumptions, we recommend to study the value of $\boldsymbol{F_s^2/k}$ as a good performance indicator for the depletion of the well. In general, it is economically preferable to deplete the SRV as fast as possible. This can be achieved with either a large permeability or a small fracture spacing, which yields a small value of $\boldsymbol{F_s^2/k}$ in both cases. Therefore, based on this value we see that well 3 over performs the other wells.

**Table 31—Summary of the known and estimated properties of the Eagle Ford case study**

| | Well 1 | Well 2 | Well 3 |
|---|---|---|---|
| Lateral Length (ft) | 7221 | 7102 | 4382 |
| Stage Count | 45 | 71 | 44 |
| Clusters/Stg | 8 | 5 | 5 |
| Cluster Spacing (ft) | 20.05 | 20 | 19.9 |
| Permeability [Stage] (nD) | 366.6 | 197.94 | 653.51 |
| Permeability [Cluster] (nD) | 5.685 | 7.914 | 26.15 |
| $F_s^2/k$ | 70.35 | 50.54 | 15.17 |
| Fracture Half-length (ft) | 230 | 233.62 | 134.26 - 188.9 |
| Drawdown (Psi) | 5600 | 5100 | 5400 |

As we demonstrated that well 3 depletes better than wells 1 and 2, we however see that it underperforms in term of cumulative production on **Fig. 142**. This performance is due to the size of its SRV. Assuming the same net pay thickness for all the well, we estimate that well 3 has a SRV almost 4 times smaller than wells 1 and 2. Overall, well 3 depleted a smaller volume more efficiently than the other wells that have a greater SRV's and lower permeabilities.

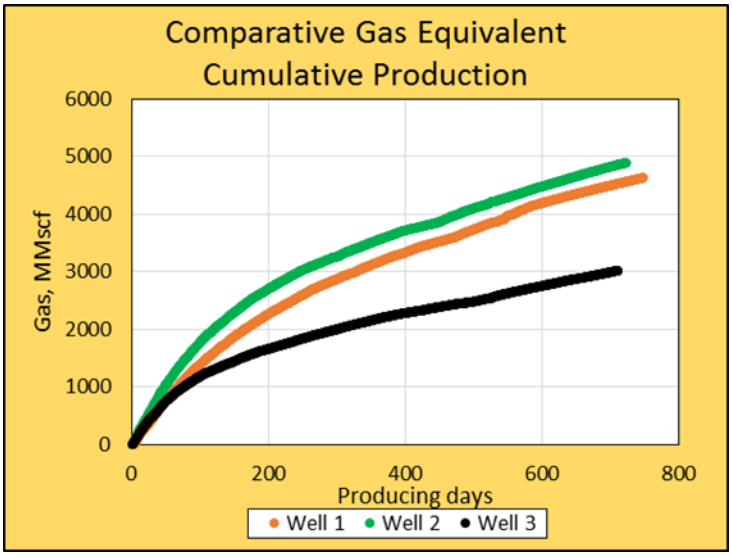


**Fig. 142—Comparison of the cumulative gas equivalent production.**

Based on the diagnostic provided above, we generate a type well for the group by calculating the average of each properties. Similar to the workflow presented on Fig. 60, the averages are associated to the base well profile. The scaling factors required to scale the wells are calculated with the equations of Table 12 and shown on Table 32.

**Table 32—Base well properties and scaling factors of the Eagle Ford case study.**

| | Well 1 | Well 2 | Well 3 | Base Well | Well 1 | | Well 2 | | Well 3 | |
|---|---|---|---|---|---|---|---|---|---|---|
| | | | | | TSF | RSF | TSF | RSF | TSF | RSF |
| Permeability (nD) | 366.6 | 197.94 | 653.51 | 406.02 | 0.90 | 1.11 | 0.49 | 2.05 | 1.61 | 0.62 |
| Fracture Half-length (ft) | 230 | 233.62 | 134.6 | 199.41 | 1.00 | 0.87 | 1.00 | 0.85 | 1.00 | 1.49 |
| Lateral Length (ft) | 7221 | 7102 | 4382 | 6235 | 1.00 | 0.86 | 1.00 | 0.88 | 1.00 | 1.42 |
| Pseudo Pressure Drawdown | 1.57E+09 | 1.56E+09 | 1.53E+09 | 1.56E+09 | 1.00 | 0.99 | 1.00 | 1.00 | 1.00 | 1.02 |
| Fracture Spacing (ft) | 160.47 | 100.03 | 99.59 | 120.03 | 0.56 | 1.79 | 1.44 | 0.69 | 1.45 | 0.69 |
| | | | | TOTAL : | 0.50 | 1.47 | 0.70 | 1.06 | 2.34 | 0.92 |

The 3 rate-time and cumulative-time profiles rescaled to the base well are displayed **Fig. 143.** We see that the 3 profiles rescale almost perfectly on the same production behavior. Interestingly, we see that well 3 has a much longer production history compared to wells 1 and 2 after scaling. This implies that it is a much deeper depletion stage, which is coherent with the observations previously made on the $F_s^2/k$ ratio and the SRV. Looking at the time scaling factors of the 3 wells, see that well 3 has a greater than 1 while the other wells have a value lower than 1. In fact, we understand that well 3 reached BDF much quicker than the other wells because it has a better permeability and a smaller SRV.

Looking at the bottom right plot of Fig. 140 automatically shows how well 3 can be used to forecast wells 1 and 2. Finally, we plotted in red what we would use as a type well for this group. We see that the decline at the end of the production of well 3 is not continuous since the rates increases after 1200 days. This shows the same issue that was pointed on the different segments of Fig. 140. Hence, we recognize that is a change in operating conditions (such as fracture interference) and we recommend to discard this section of the well for forecasting purposes.

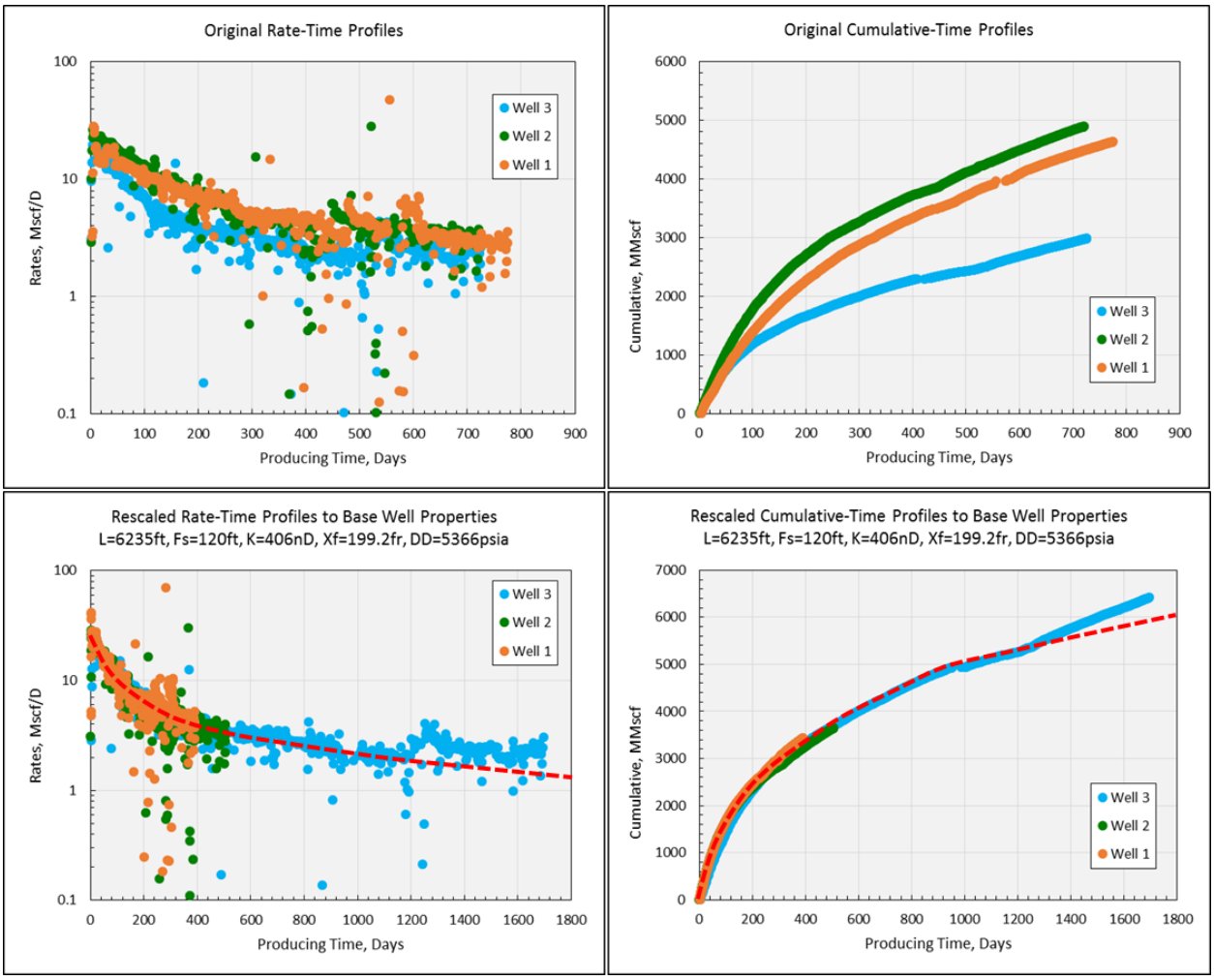


**Fig. 143—Original and scaled production of the 3 condensate wells from the Eagle Ford shale.**

In conclusion, the 3 wells successfully demonstrated the same production behavior when rescaled based on the properties diagnosed with the modified type curve. This demonstrates another application of the analytical scaling factors and the type well workflow to a different kind of well (condensate). We confirm that high frequency rates and pressure are more accurate to properly identify the change in flow regimes and match accurately a type curve. However, we observed some issues when matching the type curve with profiles that have discontinuous segments. Finally, we demonstrated how the ratio $F_s^2/k$ work independently of the fracture assumptions and how we can use it to assess the depletion performance of a well.